Université de Liège

Faculté des Sciences

Dynamique du carbone inorganique dans la banquise côtière arctique et échanges air-glace de CO_2

Inorganic carbon dynamics in coastal arctic sea ice and related air-ice CO_2 exchanges

Dissertation présentée par

Geilfus Nicolas-Xavier

En vue de l'obtention du grade de Docteur en Sciences

Avril 2011

Remerciements

Je souhaiterais remercier le Dr. Bruno Delille pour l'ensemble du temps qu'il m'a consacré, sa patience, son enseignement constant sur des sujets les plus divers et pour m'avoir entrainé sur tous les océans du globe. Merci pour la confiance que tu m'as donnée, de m'avoir laissé apprendre au travers de mes erreurs. J'ai eu beaucoup de chance d'avoir pu travailler avec un tel expert du CO_2 et je suis heureux d'avoir pu être ton premier «doctorant».

Je souhaiterais ensuite remercier le Pr. Jean-Louis Tison qui m'a «éveillé» pendant ma licence en géographie et qui m'a transmis sa passion des pôles. Travailler à tes côtés a été extrêmement enrichissant et cela dès mes premiers pas à l'ULB (cela fait déjà si longtemps…). Merci pour cette énergie inépuisable qui te caractérise, qui fait que même dans les situations les plus difficiles, on a toujours envie de donner le meilleur de soi. Et merci de m'avoir fait «expatrier» en Principauté pour me faire plonger en océanologie. Grâce à cela, j'ai pu en apprendre bien davantage sur un milieu qui m'a toujours fasciné.

Merci aussi au Dr. Alberto Borges de m'avoir accueilli au sein de l'Unité d'Océanographie Chimique et pour ses conseils avisés.

J'aimerais également remercier Tim Papakyriakou pour ses relectures et conseils lors de la rédaction des différentes publications qui composent ce travail, pour son aide logistique, financière et scientifique lors des différentes missions de terrains. Ainsi que Gehard Dieckmann et Gernot Nehrke pour leur accueil dans leur laboratoire de l'AWI et le partage de leur expertise sur ces fameux cristaux de carbonate de calcium qu'on a tant cherché.

Saïda, un immense merci. Sans toi, il n'y aurait pas eu de mémoire de géographie, de mémoire d'océanologie, pas de thèse… Et notre labo de glaciologie ne serait pas ce qu'il est. Merci pour tes innombrables coups de mains, ta bonne humeur perpétuelle,…, et… de ne jamais partir en vacances, ou jamais trop longtemps pour éviter qu'on soit tous perdu ! Merci !

Une pensée à l'ensemble de mes camarades et amis (qui se reconnaîtront, j'en suis sûr) de l'ULB et l'ULg avec qui j'ai eu la chance de partager des expériences inoubliables, que ce soit par -30°C perdu au milieu de l'océan, +30°C sous un soleil radieux… ou

dans un bureau. Une pensée spéciale à Gauthier, avec qui j'aurais partagé quasiment toutes mes aventures polaires et ce, malgré les différentes tentatives d'assassinat par accident de motoneige. Merci d'avoir partagé l'excitation de la recherche de petits cristaux de carbonate de calcium avec moi, d'y avoir consacré un temps fou.

Et pour finir, merci à toute ma famille d'avoir été là, et de m'avoir permis de réaliser tout cela, merci à Jean François pour son support logistique en informatique, gracieusement prêté par Studiotech® Belgium SA-NV (www.studiotech.be).

Aurélie, qui partage ma vie, merci d'être parvenue à me supporter pendant ces longues années, de m'avoir encouragé, soutenu, relu,… Merci pour tout.

Merci à Microsoft® pour ces…. longs, très longs moments de…. solitude devant l'ordinateur…

Ce travail a été rendu possible grâce à une bourse d'étude octroyée par le Fonds pour la Recherche en Industrie Agro-alimentaires (F.R.I.A.), au soutien du projet ARC SIBClim financé par la Communauté Française de Belgique, de la Politique Scientifique Fédérale à travers le projet BELCANTO III (contrat SD/CA/03A), et des projets FNRS/FRFC «Biogéochimie des glaces de mer dans les océans polaires: implication sur les échanges de gaz à effets climatique et les variations climatiques d'origine naturelle anthropique – une contribution à l'Année Polaire Internationale (2007-2008)» (convention 2.4649.07) et «Suivi annuel des flux air-glace-mer de CO_2 au-dessus de la banquise arctique: une contribution à l'Année Polaire Internationale» (convention 2.4584.09).

Les co-promoteurs de ce travail sont le Dr. A. Borges et le Pr. J.-L. Tison (ULB)

Les membres du jury sont les Pr. J.M. Bouquegneau (Président), Dr. B. Delille, Dr. G. Dieckmann (Alfred Wegener Institut, Allemagne), Dr. B. Heinesch, Dr. M. Vancoppenolle (UCL).

Abstract

Arctic Ocean contributes to the global oceanic uptake of CO_2 by about 5% to 14% in taking up from 66 to 199 TgC yr^{-1}. However, the role of the marine cryosphere was ignored because it is considered as an impermeable barrier, impeding the gas exchanges between the ocean and the atmosphere [*Bates and Mathis*, 2009]. However, a growing body of evidence suggests that gases exchange could occur between sea ice and the atmosphere. In this context, two arctic surveys were carried out in the framework of the International Polar Year (IPY). From there, we present a snapshot of the partial pressure of CO_2 (pCO_2) dynamics firstly during the initial sea ice growth and secondly from early spring to the beginning of the summer.

We confirmed previous laboratory measurement findings that growing young sea ice acts as a source of CO_2 to the atmosphere by measuring CO_2 efflux from the ice (4 to 10 mmol m^{-2} d^{-1}). We also confirmed the precipitation of calcium carbonate as ikaite in the frost flowers and throughout the ice and its negligible role on the effluxes of CO_2. In early spring, supersaturations in CO_2 (up to 1834 µatm) were observed in sea ice as consequence of concentration of solutes in brines, $CaCO_3$ precipitation and microbial respiration. As the summer draw near, brine shifts to a marked undersaturation (down to almost 0 µatm) because of the brine dilution by ice meltwater, dissolution of $CaCO_3$ and photosynthesis during the sympagic algal bloom. Out of the winter, soon as the ice becomes permeable, CO_2 fluxes were observed: (i) from the ice to the atmosphere, as the brine were supersaturated, (ii) from the atmosphere to the ice, as brine shift to an undersaturation. Temperature appears to be the main driver of the pCO_2 dynamics within sea ice. It mainly controls the saturation state of the brine (where others processes may be added, *e.g.*, $CaCO_3$ precipitation, primary production) and thus, the concentration gradient of CO_2 between sea ice and the atmosphere. It also controls the brine volume and so the brine connectivity, allowing the gas exchanges between sea ice and the atmosphere.

We also present a new analytical method to measure the pCO_2 of the bulk sea ice. This method, based on equilibration between an ice sample and a standard gas, was successfully applied on both artificial and natural sea ice. However, this method is only applicable for permeable sea ice (*i.e.,* brine volume > 5% [*Golden et al.,* 1998; 2007]) to allow the equilibration between the ice and the standard gas.

Résumé

La contribution de l'Océan Arctique au puits océanique global de CO_2 est estimée entre 5 et 14%, soit une absorption de 66 à 199 TgC an^{-1}. Toutefois, le rôle de la banquise est ignoré parce qu'elle est considérée comme une barrière imperméable, empêchant les échanges de gaz entre l'océan et l'atmosphère [*Bates and Mathis,* 2009]. Cependant, de nombreuses études mettent en évidence que de tels échanges peuvent avoir lieu. Dans cette optique, deux études de la dynamique de la pression partielle en CO_2 (pCO_2) ont été réalisées en Arctique, sur de la glace de mer côtière, dans le cadre de l'Année Polaire Internationale (API). Premièrement, lors de la croissance initial de la banquise et deuxièmement depuis la sortie de l'hiver jusqu'au début de l'été.

Nous confirmons les précédents travaux de laboratoire suggérant qu'une jeune glace de mer en croissance agit comme une source de CO_2 vers l'atmosphère (de 4 à 10 mmol m^{-2} jr^{-1}). Nous confirmons également la précipitation de carbonate de calcium en tant qu'ikaite au sein de la banquise et son rôle minime sur le relargage de CO_2. Au début du printemps, une sursaturation en CO_2 (jusque 1834 µatm) a été observée dans la glace, comme conséquence de la concentration des solutés dans les saumures, de la précipitation de $CaCO_3$ et de la respiration microbienne. A l'approche de l'été, les saumures deviennent sous-saturées en CO_2 (jusqu'à ~ 0 µatm) suite à leur dilution par l'eau de fonte de la glace, la dissolution du $CaCO_3$ et la photosynthèse. À la sortie de l'hiver, dès que la glace devient perméable (volume de saumure > 5%), des flux de CO_2 sont observés, d'abord vers l'atmosphère (suite à la sursaturation des saumures) ensuite vers la glace (une fois les saumures sous-saturées). La température semble être le facteur principal de la dynamique de la pCO_2 au sein de la banquise. Celle-ci contrôle (i) l'état de saturation des saumures (auxquels d'autres processus peuvent s'ajouter comme la précipitation de $CaCO_3$ ou la production primaire), et donc le gradient de concentration en CO_2 entre la glace et l'atmosphère, (ii) le volume de saumure et par conséquent la capacité qu'a la glace à avoir des échanges avec l'atmosphère.

Nous présentons également une nouvelle méthode d'analyse pour mesurer la pCO_2 de la glace de mer. Celle-ci est basée sur l'équilibration d'échantillons de glace avec un gaz standard et a été appliquée avec succès sur des glaces artificielles et naturelles. Cependant, elle n'est applicable que pour des glaces perméables, afin d'assurer une équilibration optimale entre l'échantillon et le standard gazeux.

Contents

CHAPTER I: INTRODUCTION 5

1. Oceans and sea ice in the global change context 7

2. Chemistry of the carbonate system 12
2.1 Partial pressure 12
2.2 Fugacity 13
2.3 Solubility 14
2.4 Dissociation of carbonic acid and equilibrium constants 15
2.5 Dissolved Inorganic Carbon 16
2.6 Bjerrum plot 16
2.7 pH scales 17
2.7.1. NBS scale 18
2.7.2. Free scale 18
2.7.3. Total scale 19
2.7.4. Seawater scale 19
2.8 Total Alkalinity 20
2.9 Inorganic carbon dynamics 23
2.9.1. Abiotic processes 23
2.9.1.1. Temperature 23
2.9.1.2. Salinity 24
2.9.1.3. Water masses mixing 25
2.9.1.4. CO_2 exchanges 25
2.9.1.5. Calcium carbonate 25
2.9.2. Biological processes 27
2.9.2.1. Oxic processes 27
2.9.2.1.1. Photosynthesis 27
2.9.2.1.2. Respiration 27
2.9.2.2. Anoxic processes 27
2.9.2.2.1. Denitrification 28
2.9.2.2.2. Manganese (IV) reduction 28
2.9.2.2.3. Iron (III) reduction 28
2.9.2.2.4. Sulfatoreduction 28
2.9.2.2.5. Methanogenesis 28
2.9.3. Quantification 28

3. Sea ice 31
3.1 Sea ice structure and composition 31
3.2 Water conditions for sea ice formation 34
3.3 Sea ice classification 35
3.3.1. Textural classification 36
3.3.2. Genetic classification 36
3.3.2.1. Thermodynamic formation 36
3.3.2.2. Frazil formation 36
3.3.2.2.1. Transition layer 38
3.3.2.2.2. Congelation ice 38
3.3.2.2.3. Snow ice 39

3.3.2.2.4. Superimposed ice 39
3.3.2.2.5. Platelet ice 40
3.3.2.2.6. Multiyear ice 41
3.3.2.3. Dynamic formation 41
3.3.3. Classification based on ice location 42
3.4 Sea ice salinity 42
3.4.1. Initial salt entrapment 43
3.4.1.1. Constitutional supercooling and dendritic growth 45
3.4.1.2. Chemical fractionation in the boundary layer 46
3.4.2. Desalination processes 47
3.4.2.1. Brine pocket migration 48
3.4.2.2. Brine expulsion 49
3.4.2.3. Gravity drainage 49
3.4.2.4. Brine flushing 50
3.4.3. Brine inclusions 51
3.4.4. Brine volume and brine salinity 52
3.4.5. Mean salinity and salinity profile 54
3.5 Gas volume within sea ice 56
3.5.1. Syngenetic processes 57
3.5.2. Epigenetic processes 58
3.5.3. Exogenetic processes 59
3.5.4. Gas composition 59
3.5.5. Potential gas transport 60

4. Carbon dioxide dynamics within sea ice: state of the art 62
4.1 CO_2 fluxes measurements 62
4.1.1. Accumulation chamber vs. Eddy correlation 62
4.1.2. Published studies 63
4.1.3. Summary 67
4.2 Brine pCO_2 68
4.2.1. Biotic processes 68
4.2.2. Abiotic processes 69
4.3 Synthesis 73

5. Aims 75

CHAPTER II: FIRST ESTIMATES OF THE CONTRIBUTION OF $CACO_3$ PRECIPITATION TO THE RELEASE OF CO_2 TO THE ATMOSPHERE DURING YOUNG SEA ICE GROWTH 77

Foreword 78

Abstract 79

1. Introduction 79

2. Methods 83

3. Results 87
3.1 Sea ice properties 87

3.2 Carbonate system 89
3.3 Air-ice CO_2 fluxes 91
3.4 Precipitation of minerals 91

4. Discussion 94

5. Conclusions 99

6. Acknowledgements 100

CHAPTER III: PCO_2 DYNAMICS AND RELATED AIR-ICE CO_2 FLUXES IN THE ARCTIC COASTAL ZONE (AMUNDSEN GULF, BEAUFORT SEA) 101

Foreword 102

Abstract 104

1. Introduction 104

2. Study site, material and methods 108

3. Results 111
3.1 Background measurements 111
3.2 Inorganic carbon 114
3.3 CO_2 fluxes 117

4. Discussion 118
4.1 Effects of primary production 118
4.2 Effects of $CaCO_3$ precipitation, dissolution 119
4.3 Effects of temperature and salinity 120
4.4 Under-ice melt ponds 122
4.5 Inter-hemisphere comparison 122
4.6 Air-ice CO_2 fluxes 123

5. Conclusions 126

6. Acknowledgments 126

CHAPTER IV: TOWARDS A METHOD FOR HIGH RESOLUTION MEASUREMENTS OF THE PARTIAL PRESSURE OF CO_2 WITHIN BULK SEA ICE 129

Foreword 130

Abstract 131

1. Introduction 131

2. Materials and methods 134
2.1 General principle of the pCO_2 analytical procedure 135

2.2 Synthesis of standard artificial sea ice....135
2.2.1. Salinity of artificial ice....136
2.2.2. Thin sections....136
2.3 Natural sea ice sampling....137
2.4 Ice pCO_2....137
2.4.1. Dedicated container for pCO_2 measurements in sea ice samples....137
2.4.2. Vacuum line and gas chromatograph....138
2.4.3. Temperature equilibrium....139
2.4.4. pCO_2 analysis....140

3. Results and discussion....141
3.1 Standard artificial sea ice properties....141
3.1.1. Thin sections....141
3.1.2. Salinity....141
3.2 Time required for temperature adjustment....143
3.3 pCO_2 measurements in standard sea ice....145
3.4 Influence of the headspace volume:ice volume ratio....147
3.5 pCO_2 measurement in arctic sea ice....149

4. Conclusions....153

5. Acknowledgments....154

CHAPTER V: CONCLUSIONS....155

1. Context....157

2. Summary of processes controlling sea ice inorganic carbon dynamics....158

3. New analytical method....161

4. Annual cycle....163

5. Impact of sea ice changes to the overall uptake of CO_2 by the Arctic Ocean....166

6. Perspectives....167

REFERENCES....169

LIST OF PUBLICATIONS....185

1. Publications....187

2. Others....187

ANNEXE....189

Chapter I: Introduction

Sea ice observed from the bridge during the CFL cruise.

1. Oceans and sea ice in the global change context

The *Intergovernmental Panel on Climate Change* (IPCC) defines climate change as "*a change in the state of the climate that can be identified by changes in the mean and/or the variability of its properties and that persists for an extended period, typically decades or longer. It refers to any change in climate over time, whether due to natural variability or as a result of human activity*". According to the *IPCC* [2007], the warming of the climate system is obvious as the observed global average air and ocean temperature increases, snow and ice melt, the sea level rises, the precipitation raises and the arctic sea ice shrinks.

Climate change is driven by changes in the atmospheric concentration of greenhouse gases (GHGs) and aerosols, but also by changes in land use (*i.e.*, deforestation) and solar radiation which alter the energy balance of the climate system [*IPCC*, 2007]. Next to water vapor, carbon dioxide (CO_2) is the most important anthropogenic greenhouse gas [*Zeebe R.E. and Wolf-Gladrow*, 2001]. *Luthi et al.* [2008] compiled and presented CO_2 concentration measured in air trapped in ice cores from several sites in Antarctica. In the last 800 kyr, atmospheric CO_2 concentration was strongly coupled with the antarctic air temperature. The CO_2 concentration ranged from 180 ppm during glacial age to 280 ppm during interglacial age, with a maximal fluctuation of 100 ppm over the 800 kyr before present (Fig. I.1).

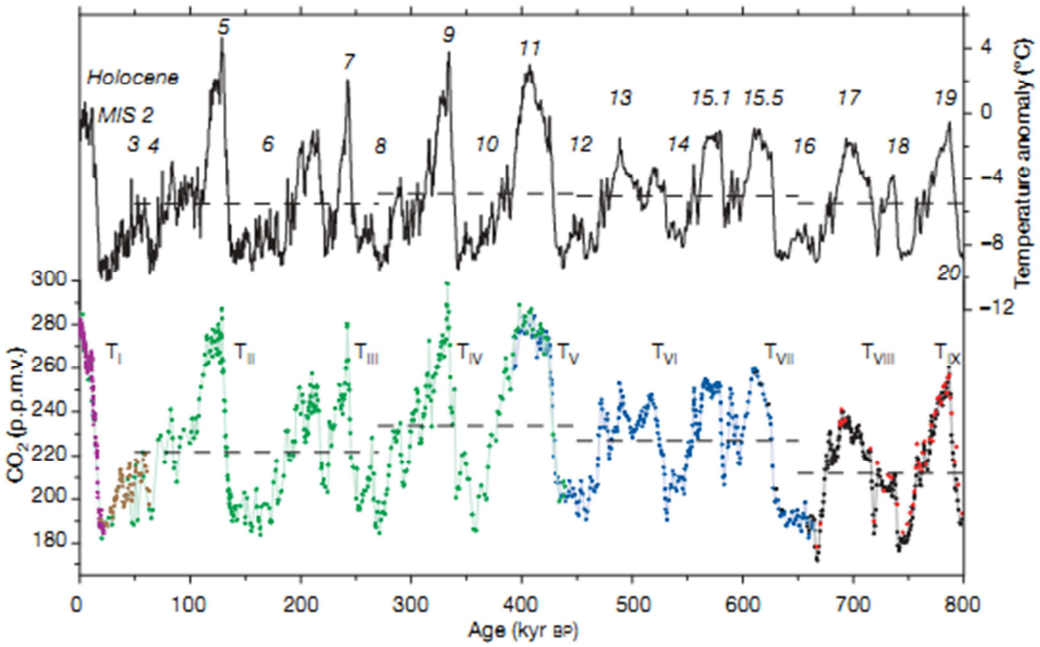

Figure I.1: Compilation of CO_2 records from EPICA, Vostok and Taylor Dome and temperature anomaly from EPICA, over the 800 kyr before present. The dashed line represents the mean values of temperature and CO_2 for the different time periods [*Luthi et al.*, 2008].

Since the beginning of the industrial period in the late 18th century until now (so-called the anthropocene period), large quantities of anthropogenic CO_2 were released to the atmosphere. The global atmospheric concentration of CO_2 increases from a pre-industrial value of about 280 ppm to 379 ppm in 2005 [*IPCC*, 2007] and up to 391.8 ppm in February 2011 (Fig. I.2).

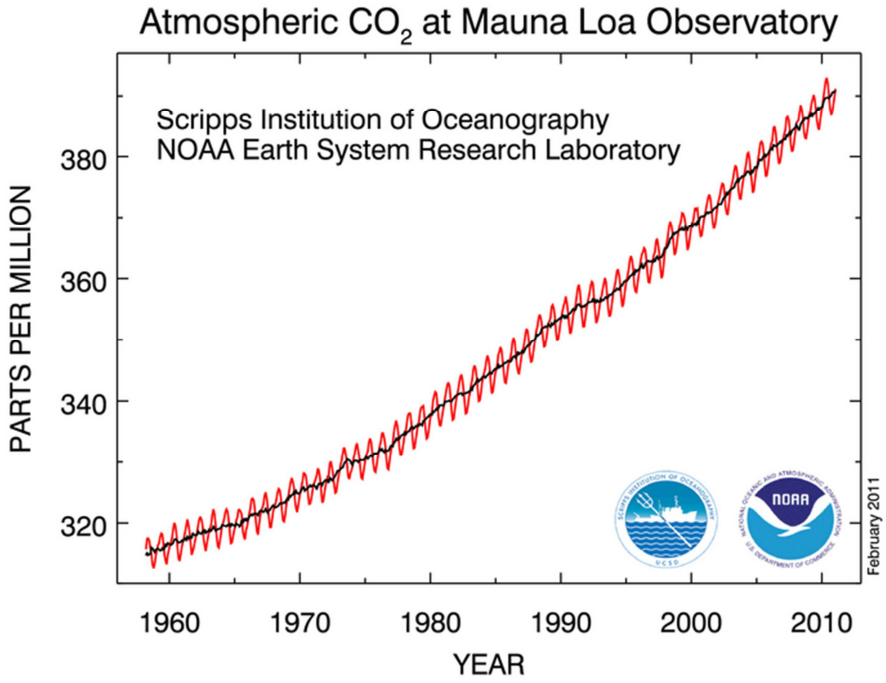

Figure I.2: Monthly mean atmospheric CO_2 concentration measured at Mauna Loa Observatory, Hawaii (http://www.esrl.noaa.gov/gmd/ccgg/trends/).

The annual CO_2 concentration growth rate was larger during the last decade than it was since the beginning of continuous direct atmospheric measurements [*IPCC*, 2007]. Global atmospheric concentrations of CO_2 have increased markedly as a result of human activities since 1750 and now far exceed pre-industrial values determined from ice core spanning many thousands of years. The combined radiative forcing due to increases of GHGs, including CO_2, and its rate of increase during the anthropocene have been unprecedented in more than 10000 years. The CO_2 radiative forcing increased by 20% from 1995 to 2005, the largest change for any decade in at least the last 200 years. Therefore, the *IPCC* [2007] argued, with very high confidence (>90%), that the global average effect of human activities since 1750 has been warmed the atmosphere with a mean radiative forcing of +1.6 W m^{-2}. This corresponds to an increase of ~0.6°C for the last century.

Global oceans play a crucial role in the global carbon cycle. Indeed, they are the largest reservoir of CO_2 that equilibrates with the atmosphere and regulates its concentration

[*Sigman and Boyle*, 2000; *Sigman et al.*, 2010]. Oceans CO_2 uptake is assessed to 1.4 PgC yr^{-1} to be compared to the annual anthropogenic emission of CO_2 of about 7 PgC yr^{-1}. According to *Sabine et al.* [2004], the oceanic sink accounts for ~48% of the anthropogenic CO_2 emissions.

The exchange of CO_2 between the atmosphere and the ocean depends upon the gradient between the natural reservoirs and biological activity, the so-called "solubility pump" and "biological pump", respectively (Fig. I.3).

The "solubility pump" is directly due to the CO_2 solubility into seawater. The efficiency of this pump is related to seawater temperature and salinity (*cf.*, Ch. I.2.3.). CO_2 is more soluble in cold and saline waters. Atmospheric CO_2 sequestration into the ocean is therefore controlled by the formation of cold, dense water masses (due to sea ice formation) at high latitudes. As these water masses sink into the deep-ocean, CO_2 is sequestered from the atmosphere up to 1000 years in deep waters.

The "biological pump" transforms CO_2 to biogenic carbon and transports it from the euphotic layer below the pycnocline, to the deep oceans. CO_2 is taken up by photosynthesizing organisms which require light and nutrients for their growth. The net effect on CO_2 budget of the transfer of organic carbon from the surface layer to the deep water is called the "organic carbon pump". In addition to the "organic carbon pump", several marine organisms produce calcium carbonate structures. The biogenic calcification in seawater produces CO_2 (*cf.*, Ch. I.2.9). This mechanism is called "carbonate counter pump". The global production of $CaCO_3$ is estimated to range between 0.4 PgC yr^{-1} to 1.8 PgC yr^{-1} [*Berelson et al.*, 2007]. A fraction of this $CaCO_3$ reaches the seafloor (0.6 PgC yr^{-1}), is dissolved (0.4 PgC yr^{-1}) or is buried (0.1 PgC yr^{-1}) into the sediments.

Sea ice affects the atmosphere and the ocean, and therefore the climate in many ways. For example, as sea ice is an insulating medium, it limits the flux of heat between the ocean and the atmosphere. Owing to sea ice high albedo, a high fraction of solar radiation is directly reflected to the atmosphere and therefore not absorbed by the ocean. Sea ice controls the thermohaline circulation through the production of deep water during its formation and the stratification of the surface waters during the melt period [*Dieckmann and Hellmer*, 2010; *Weeks*, 2010].

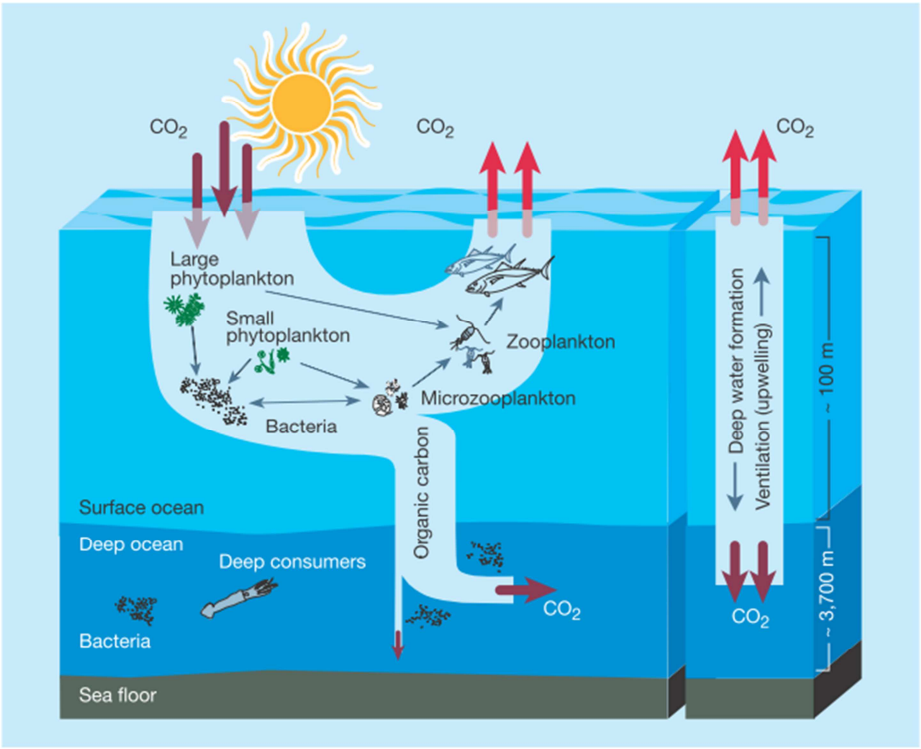

Figure I.3: Sketch of the "biological pump" (left) and the "solubility pump" (right) [*Chisholm*, 2000].

According to the *IPPC* [2007], observations show a consistent picture of surface warming and reduction of all components of the cryosphere, with the exception of antarctic sea ice. Indeed, the global temperature increased of 0.75°C during the last century. As a result the arctic sea ice surface has shrunk of -3.8 ±0.2% per decade while the trend of antarctic sea ice is positive with a slight increase of +1.2 ±0.2% per decade. This positive trend for antarctic sea ice during a scenario of global warming has actually been predicted even if the mechanism that causes this positive trend is not yet understood [*Comiso*, 2010]. In the Arctic, it must be noted that, while the overall surface of sea ice cover decreased, a large shift from multiyear to first year sea ice is also reported, so that both surface and thickness are reduced [*Nghiem et al.*, 2007; *Rothrock et al.*, 2008]. Sea ice retreat is one of the main forcing of change in polar oceans physics and ecosystem functioning in the next decades.

Global and regional budgets of air-sea CO_2 exchange have ignored ice-covered regions [*Tison et al.*, 2002; *Bates and Mathis*, 2009] relying instead on the assumption that a sea-ice cover is impermeable to gases. Presently, a growing body of recent researches challenges this assumption, as large fluxes of CO_2 have been reported on sea ice during the winter [*Heinesch et al.*, 2009; *Miller et al.*, 2011] and spring [*Semiletov et al.*, 2004; *Zemmelink et al.*, 2006; *Delille et al.*, 2007; *Nomura et al.*, 2010b; *Nomura et al.*,

2010a; *Papakyriakou and Miller*, 2011]. In the same time, it was highlighted how complex is the inorganic carbon dynamics in sea ice [*Papadimitriou et al.*, 2004; *Delille et al.*, 2007; *Rysgaard et al.*, 2007; 2009; *Munro et al.*, 2010], providing the need for further investigation. This is crucial to better understand this problematic to be able to incorporate it in global and regional models involved in assessing the oceanic CO_2 uptake. Especially as sea ice covers is one of the largest biomes on earth with a global extension ranging from 16.6 10^6 km^2 to 27.5 10^6 km^2 that corresponds to up to 7% of the earth's surface [*Comiso*, 2010].

2. Chemistry of the carbonate system

This part is mainly inspired from the book "*CO_2 in seawater: equilibrium, kinetics, isotopes*" from *R. Zeebe* and *D. Wolf-Gladrow* [2001].

Carbon dioxide (CO_2) is the fifth most abundant gas in the earth's atmosphere (after nitrogen, oxygen, argon and water vapor) and it is the most abundant greenhouse gas after the water vapor. In contrast to nitrogen and oxygen, most CO_2 of the combined atmosphere – ocean system is dissolved in water (98%), because this gas is not simply dissolved in water like other gases, but it reacts with water to form bicarbonate (HCO_3^-) and carbonate (CO_3^{2-}) ions. A fourth form, H_2CO_3, co-exists with CO_2. But as CO_2 and H_2CO_3 forms are not analytically separable and since the H_2CO_3 concentration is much lower than that one of CO_2 (<0.3%), these two forms are usually noted by CO_2. The concentration of these different ions depends on thermodynamical equilibriums which are related to salinity, temperature and pressure.

2.1 Partial pressure

The CO_2 partial pressure assigned to a seawater sample refers to the partial pressure of CO_2 in the gas phase that is in equilibrium with that seawater. Once the pCO_2, or more precisely the fugacity fCO_2, was determined, we can use the Henry's law to calculate the concentration of dissolved CO_2 in solution. We can also calculate the differences in pCO_2 between the ocean (or sea ice) and the atmosphere and use the difference to estimate the net air-sea (or sea ice) gas CO_2 flux [*Delille*, 2006; *Delille et al.*, 2007; *Takahashi et al.*, 2009; *Nomura et al.*, 2010b; 2010a].

The mole fraction, *x*, of CO_2 (or any gas) is the number of moles of CO_2 divided by the total number of moles of all components in the sample, usually in µmol mol^{-1}:

$$x_{CO_2} = \frac{n_{CO_2}}{\sum_i n_i} \qquad \text{(I.2.1)}$$

The partial pressure of CO_2 (or any gases) is proportional to its mole fraction:

$$pCO_2 = x_{CO_2}.p \qquad \text{(I.2.2)}$$

where *p* is the total pressure of the mixture. The widely used unit of partial pressure is atmosphere (atm). At a given mole fraction, the pCO_2 will depend on the atmospheric pressure. If the mole fraction is determined in dry air, the calculated pCO_2 of 2 samples

with the same mole fraction depends on the local *in situ* humidity because the partial pressure of H_2O contributes to the local pressure. The conversion of pCO_2 in dry air to pCO_2 in wet air (or saturated in water vapor) is made according to:

$$pCO_{2(wet\ air)} = pCO_{2(dry\ air)}\left(1 - VP(H_2O)\right) \qquad \text{(I.2.3)}$$

where $VP(H_2O)$ is the water pressure vapor in atm, which can be computed from the relationship proposed by *Weiss and Price* [1980] as recommended by *Kortzinger et al.* [2000]:

$$ln\left(VP(H_2O)\right) = 24.4543 - 67.4509\frac{100}{T_K} - 4.8489ln\frac{T_K}{100} - 0.000544 \times S \qquad \text{(I.2.4)}$$

where S corresponds to salinity and T_K to the absolute temperature.

The partial pressure of CO_2 of a seawater sample is usually determined by equilibrating a large volume of seawater with a small volume of gas. Because pCO_2 varies strongly with temperature (*e.g., Copin-Montégut* [1988]), corrections have to be applied in order to calculate pCO_2 at the *in situ* conditions.

2.2 Fugacity

According to *Weiss* [1974] "*In most natural applications which do not require accuracies greater than ~0.7%, the fugacity…. may be taken as equal to the partial pressure*".

Partial pressure is a concept appropriate for ideal gases. According to Dalton's law, the total pressure of an ideal gas mixture is given by the sum of the partial pressures of the gases, where the partial pressure of a perfect gas is the pressure it would exert if it occupied the container alone. The chemical potential of gas species i, μ_i, is, for ideal gas:

$$\mu_i = \mu_i^0 + RTlnp_i \qquad \text{(I.2.5)}$$

where μ_i^0 is the standard potential, R is the gas constant, T is the absolute temperature and p_i is the partial pressure. For real gases, Dalton's law is an approximation and the chemical potential is strictly given by:

$$\mu_i = \mu_i^0 + RTlnf_i \qquad \text{(I.2.6)}$$

where f_i is the fugacity of gas species i.

Fugacity approaches the partial pressure in the limit of infinitely dilute mixtures. For very accurate calculations, the fCO_2 can be used instead of pCO_2. The fugacity can be calculated from its partial pressure:

$$fCO_2 = pCO_2 . exp\left(p\frac{B+2\delta}{RT}\right) \quad \text{(I.2.7)}$$

where fCO_2 and pCO_2 are in µatm, the total pressure, p, is in Pa (1 atm = 101325 Pa), the first virial coefficient of CO_2, B, and parameter δ are in $m^3\ mol^{-1}$, R = 8.314 J K^{-1} is the gas constant and the absolute temperature, T, is in K. B was determined by Weiss [1974]:

$$B(m^3 mol^{-1}) = (-1636.75 + 12.0408T - 3.27957.10^{-2}T^2 + 3.16528.10^{-5}T^3).10^{-6} \quad \text{(I.2.8)}$$

The parameter δ is the cross virial coefficient:

$$\delta(m^3 mol^{-1}) = (57.7 - 0.118T).10^{-6} \quad \text{(I.2.9)}$$

2.3 Solubility

In thermodynamic equilibrium with gaseous carbon dioxide ($CO_{2(g)}$), the concentration of $CO_{2(aq)}$ is given by Henry's law with K_0 being the solubility coefficient of $CO_{2(g)}$ in seawater:

$$CO_{2(g)} \overset{K_0}{\Leftrightarrow} CO_{2(aq)} \quad \text{(I.2.10)}$$

The pCO_2 of a seawater sample refers to the partial pressure of CO_2 in the gas phase that is in equilibrium with that sample. The equation I.2.10 can be rewritten as:

$$pCO_2 = \frac{[CO_2]}{K_0} \quad \text{(I.2.11)}$$

K_0 can be estimated in mol kg^{-1} atm^{-1} according to *Weiss* [1974]:

$$lnK_0 = -60.2409 + 93.4517\frac{100}{T_K} + 23.3585\, ln(0.01T_K) + S[0.023517 - 0.00023656T_K + 0.0047036(0.01(T_K)^2] \quad \text{(I.2.12)}$$

where S corresponds to salinity and T_K to the absolute temperature.

The solubility of CO_2 in seawater (or brine) also depends on the Bunsen coefficient, β. It is defined as the volume of gas (in standard condition, STP: P = 1 atm and T = 0°C) absorbed per unit volume of solution, at the temperature of the measurements, when the total pressure is at 1 atm.

According to *Weiss* [1974], β is formulated as:

$$\beta_{CO_2} = Q_{CO_2}^{-1} V_{CO_2}^{*} \rho N exp\left(\frac{-\bar{v}_{CO_2}}{RT}\right) \quad \text{(I.2.13)}$$

where Q_{CO_2} is a modified Henry's law constant and a function only of the temperature and the nature of the gas. $V_{CO_2}^{*}$ is the volume of one mole of the real gas at STP, ρ is the density of the solution, N is the number of moles in a unit weight of solvent, P is the pressure, in atm, R is the gas constant. By comparing β calculated for different gases (Table I.2.1), the CO_2 coefficient appears to be significantly larger to the others, which means that CO_2 is the most "soluble".

	Gas	**Bunsen coefficient (10^{-3} mol kg^{-1} atm^{-1})**	**Solubility STP (mol kg-1)**
Wiesenburg and Guinasso [1979]	H_2	0.788	0.45 x 10^{-9}
Wiesenburg and Guinasso [1979]	CO	1.245	0.14 x 10^{-9}
Benson and Krause[1984]	O_2	1.67	347.9 x 10^{-6}
Wiesenburg and Guinasso [1979]	CH_4	1.935	2.71 x 10^{-9}
Weiss [1974]	CO_2	62.87	21.83 x 10^{-6}

Table I.2.1: Bunsen coefficient and solubility for seawater at S = 35, calculated at 0°C.

Existing thermodynamic relationships indicate that the solubility of gases in seawater in equilibrium with air increases as temperatures drops, while the increases in salinity has the opposite effect (*i.e.*, decreases gas solubility) [*Thomas and Papadimitriou*, 2003].

2.4 Dissociation of carbonic acid and equilibrium constants

In standard seawater conditions, the carbonate species are related by the following equilibrium:

$$CO_{2(aq)} + H_2O \Leftrightarrow H_2CO_3 \overset{K_1}{\Leftrightarrow} HCO_3^- + H^+ \overset{K_2}{\Leftrightarrow} CO_3^{2-} + 2H^+ \quad \text{(I.2.14)}$$

where K_1 and K_2 are equilibrium constants, referred respectively as the first and second dissociation constants of the carbonate system.

$$K_1 = \frac{a_{H^+} a_{HCO_3^-}}{a_{CO_2}} \quad \text{(I.2.15)}$$

$$K_2 = \frac{a_{H^+} a_{CO_3^{2-}}}{a_{HCO_3^-}} \quad \text{(I.2.16)}$$

However, only the activity of H^+ and total concentrations of the other quantities can be directly measured. Therefore, the equations should be rewritten using apparent equilibrium constants with molal concentrations rather than activities. Activities are

valid for a single media, like seawater (characterized by high ionic strength). These apparent equilibrium constants K_1^* and K_2^* are applicable only for the pH scale and ionic strength for which these were determined:

$$K_1^* = \frac{[HCO_3^-][H^+]}{[CO_2]} \quad \text{(I.2.17)}$$

$$K_2^* = \frac{[CO_3^{2-}][H^+]}{[HCO_3^-]} \quad \text{(I.2.18)}$$

K_1^* and K_2^* are given in mol kg^{-1} according to *Mehrbach et al.* [1973] refitted by *Dickson and Millero* [1987] on the total pH scale:

$$pK_1^* = \frac{3670.7}{T_K} - 62.008 + 9.7944 ln T_K - 0.0118 \times S + 0.000116 \times S^2 \quad \text{(I.2.19)}$$

$$pK_2^* = \frac{1394.7}{T_K} + 4.777 - 0.0184 \times S + 0.000118 \times S^2 \quad \text{(I.2.20)}$$

where S and T_K correspond to the salinity and the absolute temperature, respectively. These estimations are considered as the optimal dissociation constant for the carbonate system computations [*Wanninkhof et al.,* 1999].

2.5 Dissolved Inorganic Carbon

The sum of the dissolved forms CO_2, HCO_3^-, CO_3^{2-} is called dissolved inorganic carbon or DIC, in µmol kg^{-1}of seawater:

$$\mathrm{DIC} = \sum \mathrm{CO_2} = [\mathrm{CO_2}] + [\mathrm{HCO_3^-}] + [\mathrm{CO_3^{2-}}] \quad \text{(I.2.21)}$$

2.6 Bjerrum plot

The plot of Bjerrum (Fig. I.2.1) represents the logarithm of the concentration of CO_2, HCO_3^- and CO_3^{2-} versus pH. We considered typical arctic condition of seawater (S=33) in equilibrium with the atmosphere (pCO_2 = 390 µatm, pH = 8.04) at a temperature of 2°C. Then, the concentration of CO_2, HCO_3^- and CO_3^{2-} accounts for, respectively, 1.08%, 94.4% and 4.52% of the total pool of inorganic carbon, DIC = 2139 µmol kg^{-1} and the total alkalinity, TA = 2262.5 µmol kg^{-1} (TA is defined below). DIC is mainly present as HCO_3^- and CO_2 are present only in small concentrations.

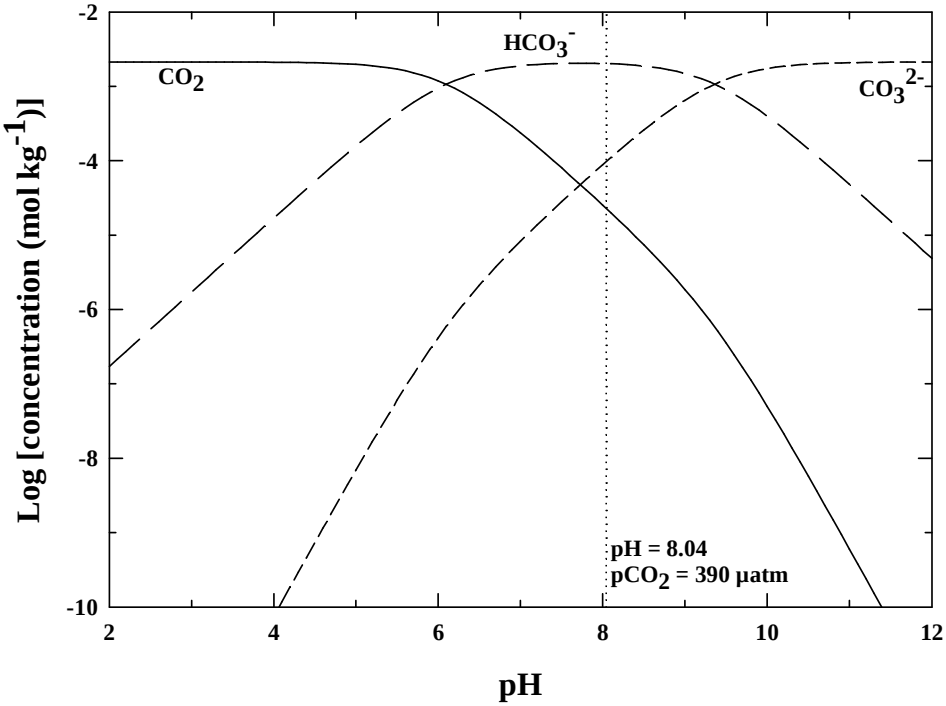

Figure I.2.1: Bjerrum plot showing the changes of CO_2, HCO_3^- and CO_3^{2-} in typical conditions of arctic surface waters (S = 33, T = 2°C, P = 1 atm, DIC = 2139 µmol kg^{-1}). The vertical dotted line corresponds to the equilibrium with the atmosphere.

Bjerrum plot exhibits the intricate link between pH and the relative proportion of the carbonate species in the ocean. The carbonate system is the natural buffer for the seawater pH.

2.7 pH scales

The conventional definition of pH is:

$$pH = -log[H^+] \qquad \text{(I.2.22)}$$

This equation is not useful while studying seawater since free protons do not exist in any significant amount in this media [*Dickson*, 1984]. Indeed, these protons are bonded to water molecules to form an H_3O^+ ion among other hydrates. Furthermore, protons are also complexed with other ions, mainly sulfates (SO_4^{2-}) and fluoride (F^-) ions. Subsequently, the proton activity (a_{H^+}) should be used instead of concentration:

$$pH_a = -loga_{H^+} \qquad \text{(I.2.23)}$$

However, it is not always possible to measure pH according to equation I.2.23. Individual ion activities cannot be determined experimentally since the concentration of a single ion cannot be varied independently because electroneutrality is required.

Therefore, four other operational definitions of pH were proposed: NBS scale, free scale, total scale and the seawater scale.

2.7.1. NBS scale

The NBS scale is defined by a series of standard buffer solutions with assigned pH values close to the best estimates of $-log a_{H^+}$. pH_{NBS} is close but not identical to pH_a.

$$pH_{NBS} \approx pH_a \tag{I.2.24}$$

The reference state for pH_a and pH_{NBS} is the infinite dilute solution, *i.e.*, as we dilute a solution, the distance between solutes increases and in the limit of infinite dilution, the solutes are infinitely far apart. The activity coefficient of H^+ approaches -1 when $[H^+]$ approaches 0 in pure water.

NBS standard buffer solutions have very low ionic strength (~0.1) while seawater has high ionic strength (~0.7). The use of NBS buffers in pH measurements using electrodes in seawater is therefore not recommended. Indeed, the large difference in ionic strength between the buffer and the seawater causes significant changes in the liquid junction potential[1] between calibration and sample measurement.

The use of NBS scale is not recommended for seawater measurements, but is appropriate for pH measurements in fresh and brackish waters, in particular in estuarine systems [*Frankignoulle and Borges*, 2001].

2.7.2. Free scale

The pH calculated in the free scale can be defined by:

$$pH_F = -\log[H^+]_F \tag{I.2.25}$$

This scale takes into account the "free" protons. However, in seawater, protons interact with sulfate ions according to:

$$H^+ + SO_4^{2-} \overset{K_S^*}{\Leftrightarrow} HSO_4^- \tag{I.2.26}$$

where K_S^* is the dissociation constant of HSO_4^-.

[1] The liquid junction potential is the electric potential difference between the solution in the electrode and the measurement solution. Ideally it depends only on the composition of the electrode solution and measurement solution. In reality, however, it also depends on the practical design of the liquid junction.

So that the total hydrogen concentration, $[H^+]_T$, is:

$$[H^+]_T = [H^+]_F + [HSO_4^-] \qquad \text{(I.2.27)}$$

Analytically, only $[H^+]_T$ can be determined [*Dickson,* 1993].

$$[H^+]_F = [H^+]_T - [HSO_4^-] = [H^+]_T \left(1 + \frac{[SO_4^{2-}]}{K_S^*}\right)^{-1} \qquad \text{(I.2.28)}$$

The use of the free scale requires an accurate value of K_S^* in seawater, which is difficult to obtain.

2.7.3. Total scale

This scale includes the effect of sulfate ion in its definition and therefore circumvents the problem of determining K_S^*:

$$pH_T = -log([H^+]_F + [HSO_4^-]) = -log[H^+]_T \qquad \text{(I.2.29)}$$

In this scale, the activity coefficient approaches 1 when $[H^+]_F + [HSO_4^-]$ approaches 0 in the ionic medium. This pH scale is the most widely used for pH measurements in seawater. A useful set of buffer standards was proposed in artificial seawater containing sulphate ions, whose assigned pH values was accurately determined on the "total scale" [*Dickson,* 1993]. Furthermore, a set of consistent apparent dissociation constants were accurately determined on this pH scale based on similar artificial seawater composition as the buffer proposed by *Dickson* [1993].

2.7.4. Seawater scale

If the medium additionally contains fluoride ions (F^-), a more accurate scale takes them into account:

$$H^+ + F^- \overset{K_F^*}{\Leftrightarrow} HF \qquad \text{(I.2.30)}$$

The total hydrogen ion concentration in this pH scale is therefore:

$$[H^+]_{SWS} = [H^+]_F + [HSO_4^-] + [HF] \qquad \text{(I.2.31)}$$

This leads to the definition of the seawater scale:

$$pH_{SWS} = -log([H^+]_F + [HSO_4^-] + [HF]) \qquad \text{(I.2.32)}$$

The difference between the total scale and the seawater scale therefore simply arises from the fact that whether the medium on which the scale is based contains fluoride

ions or not. However, this difference is small (typically 0.001) because $[HSO_4^-]$ is much larger than $[H^+]$ in seawater.

There are formulas to convert the different scales between them. However, the best approach is to avoid such conversion and to use consistent sets of pH scale, buffers and dissociation constants. In the present study, we used the "total" pH scale using buffers proposed by *Dickson* [*1993*] with apparent dissociation constants from *Mehrbach et al.* [1973] refitted by *Dickson and Millero* [1987] since they have been estimated to be the optimal apparent dissociation constants for seawater [*Wanninkhof et al.*, 1999].

2.8 Total Alkalinity

The current widely accepted definition of total alkalinity, TA, was given by *Dickson* [1981] as "*the number of moles of hydrogen ion equivalent to the excess of proton acceptors over proton donors in one kilogram of sample*". Where proton acceptors describe the bases formed by weak acids with a dissociation constant of $K \leq 10^{-4.5}$ at 25°C and zero ionic strength and where proton donors describe acids with $K > 10^{-4.5}$.

In seawater, TA is defined, in µmol kg^{-1}, as:

$$TA = [HCO_3^-] + 2[CO_3^{2-}] + [B(OH)_4^-] + [OH^-] + [HPO_4^{2-}] + 2[PO_4^{3-}] + [H_3SiO_4^-] + [NH_3] + [HS^-] - [H^+]_F - [HSO_4^-] - [HF] - [H_3PO_4] \quad \text{(I.2.33)}$$

where $[H^+]_F$ is the free concentration of protons.

The total alkalinity of a sample according to equation I.2.33 is determined with the following method. The sample is titrated with a strong acid, usually HCl, and the equivalence point is determined by following the decrease of pH. During this work, the equivalence point was determined using the Gran function [*Gran*, 1952]. The equivalence point of the titration generally occurs around pH = 4.3 and corresponds to the endpoint of the titration of the carbonic acid, as carbonic acid is the dominant weak acid-base system in seawater (see Bjerrum plot, Fig. I.2.1).

According to Dickson's definition, bases formed from weak acids with $pK \geq 4.5$ are to be considered as proton acceptors, while acids with $pK < 4.5$ are to be considered as proton donors. This definition unambiguously separates proton acceptors from proton donors. The figure I.2.2 illustrates this separation by the vertical dashed line at pH = 4.5 for the acid-base systems included in equation I.2.33. This figure provides an overview

of the main acid-base systems present in seawater and, in addition, gives an overview of their relative concentrations in the course of the titration.

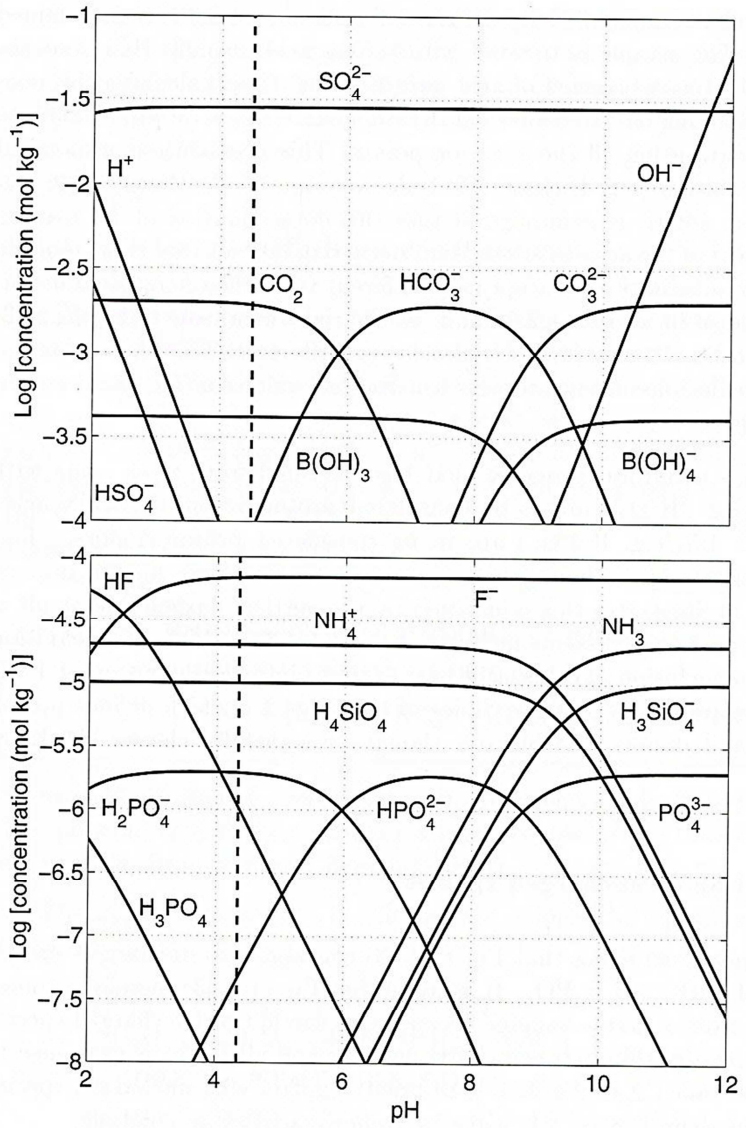

Figure I.2.2: Extended Bjerrum plot showing the acid-base systems relevant to TA in seawater. The vertical dashed line at pH = 4.5 indicates species to be considered as proton donors and acceptors [*Zeebe R.E. and Wolf-Gladrow*, 2001].

According to figure I.2.2, carbonic acid and boric acid (in addition to water itself) are the most important acid-base systems in seawater. A good approximation of TA, namely the practical alkalinity (PA) is therefore given by accounting only the contribution of these two acids and water.

The contribution of carbonic acid is denoted as carbonate alkalinity (CA) which is a useful and simple approach of alkalinity:

$$CA = [HCO_3^-] + 2[CO_3^{2-}] \qquad \text{(I.2.34)}$$

The contribution of boric acid to PA, the borate alkalinity, $[B(OH)_4^-]$, can be derived from:

$$B(OH)_3 + H_2O \overset{K_B}{\Leftrightarrow} B(OH)_4^- + H^+ \quad \text{(I.2.35)}$$

where K_B is the dissociation constant of boric acid, depending on salinity and temperature. The concentration of total borate (B_t) is conservative and a function of salinity.

$$B_t = \left[B(OH)_3\right] + [B(OH)_4^-] \quad \text{(I.2.36)}$$

It comes:

$$[B(OH)_4^-] = \frac{B_t \times K_B}{[H^+] + B_t} \quad \text{(I.2.37)}$$

This expression can be readily computed from temperature, pH and salinity. The contribution of water to PA can be expressed as:

$$water\ alkalinity = [OH^-] - [H^+]_F \quad \text{(I.2.38)}$$

Hence the practical alkalinity (PA) can be expressed as:

$$PA = [HCO_3^-] + 2[CO_3^{2-}] + [B(OH)_4^-] + [OH^-] - [H^+]_F \quad \text{(I.2.39)}$$

According to the Dittmar principle (or rule of constant proportion), the relative concentration of the major ions in seawater is constant. Hence, their concentrations are conservative, which is useful in, for example, the use of TA as water mass tracer in addition to salinity. Taking into account the most abundant ions in seawater and electroneutrality principle, it comes:

$$[Na^{2+}] + 2[Mg^{2+}] + 2[Ca^{2+}] + [K^+] + \cdots + [H^+]_F - [Cl^-] - 2[SO_4^{2-}] - [NO_3^-] - [HCO_3^-] - 2[CO_3^{2-}] - [B(OH)_4^-] - [OH^-] - \cdots = 0 \quad \text{(I.2.40)}$$

We can write the equation with the cations and anions of strong bases and acids, which are completely dissociated and therefore not affected by pH, on the left:

$$[Na^{2+}] + 2[Mg^{2+}] + 2[Ca^{2+}] + [K^+] + \cdots - [Cl^-] - 2[SO_4^{2-}] - [NO_3^-] - \cdots = [HCO_3^-] + 2[CO_3^{2-}] + [B(OH)_4^-] + [OH^-] - [H^+]_F + [minor\ components] = TA \quad \text{(I.2.41)}$$

The relative concentrations on the left do not depend on equilibrium constants and are not affected either by pH or temperature. Therefore the right hand side, *i.e.,* TA, is also conservative.

Above equations are used for the quantitative description of the carbonate system in seawater. The two equilibrium conditions (Eq. I.2.17 and I.2.18), the mass balance for total inorganic carbon (Eq. I.2.21) and the charge balance (Eq. I.2.33) constitute 4 equations with 6 unknown variables. As a result, when only 2 variables are known, the system is determined and all the other components can be calculated. Only $[CO_2]$, $[H^+]$, DIC and TA can be measured directly.

2.9 Inorganic carbon dynamics

As mentioned before, the carbonate system can be influenced by abiotic processes like changes in temperature and salinity or by mixing of waters masses and precipitation/dissolution of calcium carbonate. Biological processes also influence the inorganic carbon dynamics through the biologically mediated precipitation/dissolution of calcium carbonate and oxic and anoxic processes.

2.9.1. Abiotic processes

2.9.1.1. Temperature

Temperature changes affect the pCO_2 through the dissociation constants K_1 and K_2 and the coefficient of solubility, K_0. This effect can be calculated using the algorithms of *Copin-Montégut* [1988]. These algorithms are used to correct pCO_2 measurements or to remove temperature effects on pCO_2 changes. pCO_2, at given temperature *t*, can be calculated from $pCO_{2,i}$ at a given temperature *i* according to:

$$ln(pCO_2) = \frac{a_t}{a_{t_i}} ln(\frac{pCO_{2_i}}{b_{t_i}}) + ln(b_t) \qquad \text{(I.2.42)}$$

with:

$$a_t = 1 - ((1090 + 7 \times S) \times 10^{-6}) \times t \qquad \text{(I.2.43)}$$

$$b_t = 1 - \left((3695 + 9 \times S) \times 10^{-5}\right) \times t + \left((389 + 2.2 \times S) \times 10^{-6}\right) \times t^2 + ((0.34 - 0.124 \times S) \times 10^{-6})t^3 \qquad \text{(I.2.44)}$$

where *t* is the temperature (°C) and *S* the salinity.

During our field sampling, this correction was always applied to the direct brine pCO_2 measurements to ensure a correct pCO_2 value at the *in situ* temperature.

2.9.1.2. Salinity

The dissociations constants depend on salinity. This effect, as well as the temperature effect, is illustrated in the figure I.2.3. A shift in the pK^* value leads to a shift in the relative proportions of CO_2, HCO_3^- and CO_3^{2-} at a given pH.

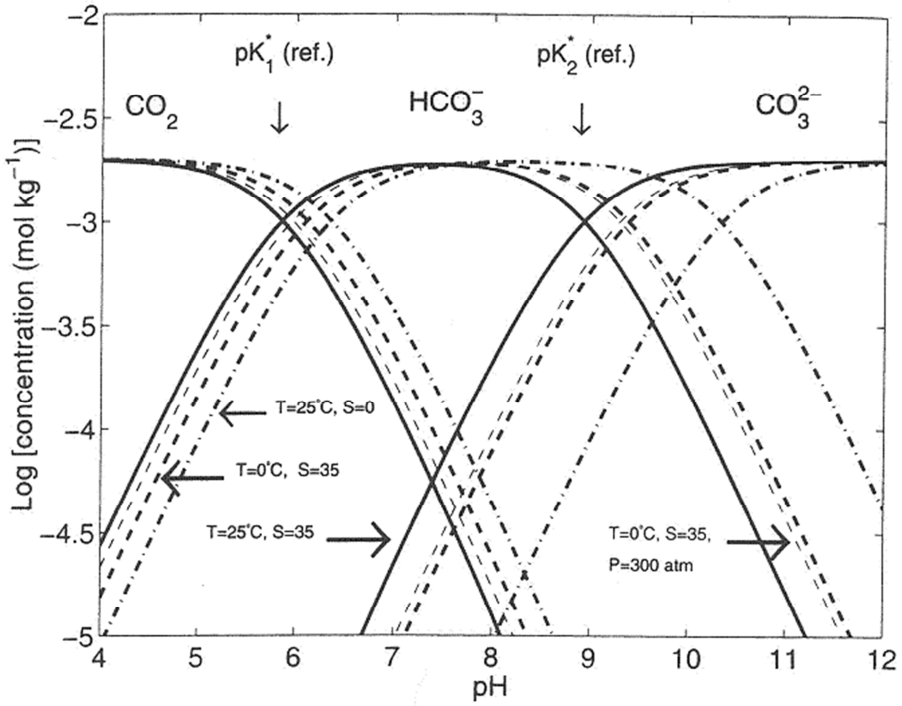

Figure I.2.3: Illustration of the effect of temperature, pressure and salinity on pK_1* and pK_2*. The reference case (solid line) is T = 25°C, S = 35, P = 1 atm. DIC = 2 mmol kg^{-1} in all cases.

Also salinity effect has a large influence on the inorganic carbon dynamics, due to related changes in solutes concentration. This is of a significant importance in sea ice, where salinity changes are enhanced compared to the water column. During the sea ice growth, brine salinity could reach values above 100 while, during the sea ice melt, brine salinity could decrease down to 0. Effect of salinity changes on the carbonate system can be estimated since both TA and DIC are conservative, *i.e.,* proportional to salinity. It is possible to decipher the salinity effect on TA and DIC from other physical and biogeochemical processes by using the normalized TA and DIC at a constant salinity (usually 35, denoted TA_{35} and DIC_{35}) according to:

$$TA_{35} = \frac{TA \times 35}{S} \qquad \text{(I.2.45)}$$

$$DIC_{35} = \frac{DIC \times 35}{S} \qquad \text{(I.2.46)}$$

where TA and DIC are given at the salinity *S*.

These equations are commonly used to normalize TA and DIC, although these assume a 0 value for both TA and DIC in freshwater, which is un-realistic. A more complex normalization procedure is proposed by *Friis et al.* [2003] that takes into account TA end-member ($TA_{S=0}$) different from zero, according to the equation:

$$TA_{35} = \frac{TA_{measured} - TA_{S=0}}{S_{measured}} \times 35 + TA_{S=0} \qquad \text{(I.2.47)}$$

2.9.1.3. Water masses mixing

Any mixing of water masses either due to advection, upwelling or vertical mixing, affects significantly the pCO_2 and the carbonate system speciation. These effects can be estimated from TA and DIC which are conservative through mixing processes.

2.9.1.4. CO_2 exchanges

An increase of the CO_2 leads to an increase of DIC but it does not change TA because the charge balance is not affected.

Many processes affecting the carbonate system in the ocean are best described by considering the change of DIC and TA that is associated with them. On the figure I.2.4, the mains open ocean processes affecting the carbonate system are described considering their change on DIC and TA.

2.9.1.5. Calcium carbonate

The precipitation of calcium carbonate ($CaCO_3$) in standard seawater conditions is described by:

$$Ca^{2+} + 2HCO_3^- \Leftrightarrow CaCO_3 + CO_2 + H_2O \qquad \text{(I.2.48)}$$

The formation of $CaCO_3$ decreases both DIC and TA. For each mole of $CaCO_3$ precipitated, one mole of C and one mole of Ca^{2+} ions are taken up which leads to a decrease of DIC and TA in a ratio of 1: 2 (Fig. I.2.4). As a result, the system shifts to higher CO_2 level and lower pH. Dissolution of $CaCO_3$ corresponds to the reverse of the equation Eq. I.2.48. Production of $CaCO_3$ can be biologically mediated by organisms which produce calcitic or aragonitic shells and skeletons. The major calcite producers in the open ocean are coccolithophorids and foraminiferas.

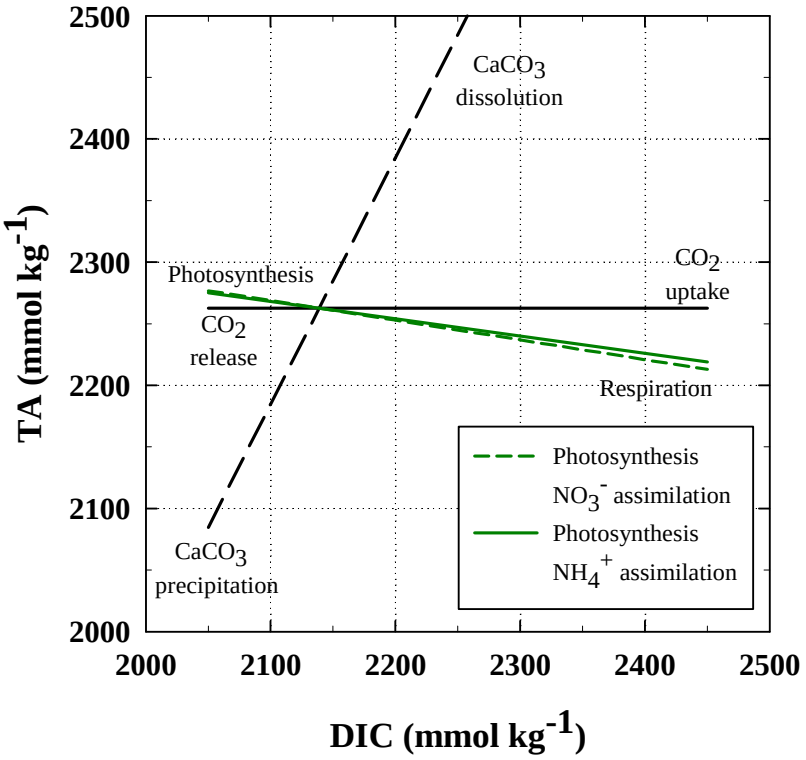

Figure I.2.4: Effects of precipitation of $CaCO_3$, photosynthesis and CO_2 exchanges on DIC and TA. The initial conditions are typical conditions found in arctic surfaces waters (S = 33, T = 2°C, P = 1 atm) in equilibrium with the atmosphere (pCO_2 = 390 µatm, pH = 8.04) with a DIC of 2139 µmol kg^{-1} and a TA of 2262.5 µmol kg^{-1}.

This precipitation can also be induced as a result of thermodynamic equilibrium, depending on the saturation state of seawater (Ω):

$$\Omega = \frac{[Ca^{2+}]_{sw} \times [CO_3^{2-}]_{sw}}{K_{sp}^*} \qquad \text{(I.2.49)}$$

Where $[Ca^{2+}]_{sw}$ and $[CO_3^{2-}]_{sw}$ are the concentration of Ca^{2+} and CO_3^{2-} in seawater respectively and K_{sp}^* is the solubility product at the *in situ* conditions of temperature, salinity and pressure. A Ω > 1 corresponds to supersaturation, whereas Ω < 1 corresponds to undersaturation. In the open ocean, $[Ca^{2+}]$ variations are rather small and closely related to variations in salinity. Ω is therefore mainly determined by the carbonate ion concentration.

Calcite is the dominant polymorph of calcium carbonate, aragonite and vaterite are two other anhydrous crystalline polymorphs while amorphous monohydrate calcium carbonate and hexahydrate calcium carbonate (*e.g.*, ikaite) are hydrated forms of calcium carbonate.

2.9.2. Biological processes

2.9.2.1. Oxic processes

2.9.2.1.1. Photosynthesis

According to the classical Redfield-Ketchum-Richards (RKR) reaction of biosynthesis [*Redfield et al.*, 1963]:

$$106CO_2 + 16NO_3^- + H_2PO_4^- + 17H^+ + 122H_2O \rightarrow (CH_2O)_{106}(NH_3)_{16}H_3PO_4 + 138O_2 \quad \text{(I.2.50)}$$

One mole of H^+ is consumed for each mole of NO_3^- or $H_2PO_4^-$ consumed through biosynthesis, increasing TA by one mole. Thus, photosynthesis reduces DIC and pCO_2 and slightly increases TA (Fig. I.2.4).

2.9.2.1.2. Respiration

Aerobic respiration corresponds to the reverse of the equation I.2.50. It involves a complete recycling of nitrogen in first instance. It induces an increase in DIC and pCO_2 and a decrease in TA (Fig. I.2.4).

If the assimilation of NO_3^-, as predicted by the RKR equation, is replaced by the assimilation of NH_4^+, photosynthesis decreases TA (by H^+ production) according to:

$$R{\sim}OH + NH_4^+ \leftrightarrow R - NH_2 + H^+ + H_2O \quad \text{(I.2.51)}$$

where *R*~ represents organic matter. The equation I.2.51 is the reverse equation of the ammonification which then increases TA.

Nitrification decreases TA due to H^+ production according to:

$$NH_4^+ + 2O_2 \Leftrightarrow NO_3^- + 2H^+ + H_2O \quad \text{(I.2.52)}$$

The complete recycling of nitrogen involves both ammonification and nitrification and leads to a net production of H^+ and thus a decrease in TA. It corresponds, eventually to the equation I.2.50.

2.9.2.2. Anoxic processes

When O_2 concentration comes to exhaustion, a series of anoxic reactions can occur depending on the availability of electron acceptors and the free enthalpy of the corresponding oxidation reactions. The following reactions are sorted according to their

free enthalpy. The first equation has the highest free enthalpy and then occurs preferentially. The term CH_2O represents the organic matter.

2.9.2.2.1. Denitrification

$$5CH_2O + 4NO_3^- + 4H^+ \rightarrow 5CO_2 + 7H_2O + 2N_2 \quad \text{(I.2.53)}$$

2.9.2.2.2. Manganese (IV) reduction

$$CH_2O + 2MnO_2 + 4H^+ \rightarrow CO_2 + 3H_2O + 2Mn^+ \quad \text{(I.2.54)}$$

2.9.2.2.3. Iron (III) reduction

$$CH_2O + 2Fe_2O_3 + 8H^+ \rightarrow CO_2 + 5H_2O + 4Fe^{2+} \quad \text{(I.2.55)}$$

2.9.2.2.4. Sulfatoreduction

$$2CH_2O + SO_4^{2-} + 2H^+ \rightarrow 2CO_2 + 2H_2O + H_2S \quad \text{(I.2.56)}$$

2.9.2.2.5. Methanogenesis

$$2CH_2O \rightarrow CO_2 + CH_4 \quad \text{(I.2.57)}$$

All of these processes, with the exception of methanogenesis, consume H^+ and therefore increase TA. These occur mainly in sediments and due to the large abundance of SO_4^{2-} in seawater, sulphato-reduction is one of the main anaerobic diagenetic organic matter pathway.

2.9.3. Quantification

Quantitative examples of all processes affecting carbonate system are provided in the table I.2.2 and their effects on TA and DIC are shown in figure I.2.5. The initial conditions are the typical conditions found in arctic surface waters (S = 33, T = 2°C, P = 1 atm) in equilibrium with the atmosphere (pCO_2 = 390 µatm, pH = 8.04) with a DIC of 2139 µmol kg^{-1} and a TA of 2262.5 µmol kg^{-1}. CO_2 speciation was calculated using the CO2sys.xls package [*Pelletier et al.,* 1998], the CO_2 acidity constants of *Mehrbach et al.* [1973] refitted by *Dickson and Millero* [1987], the CO_2 solubility coefficient of *Weiss* [1974], the SO_4^{2-} dissociation constant of *Dickson* [1990a], the borate acidity constant of *Dickson* [1990b] while the total borate molality was calculated using the

Uppström [1974] ratio to chlorinity. pCO_2 changes related to water masses mixing involves mechanisms beyond the scope of the table.

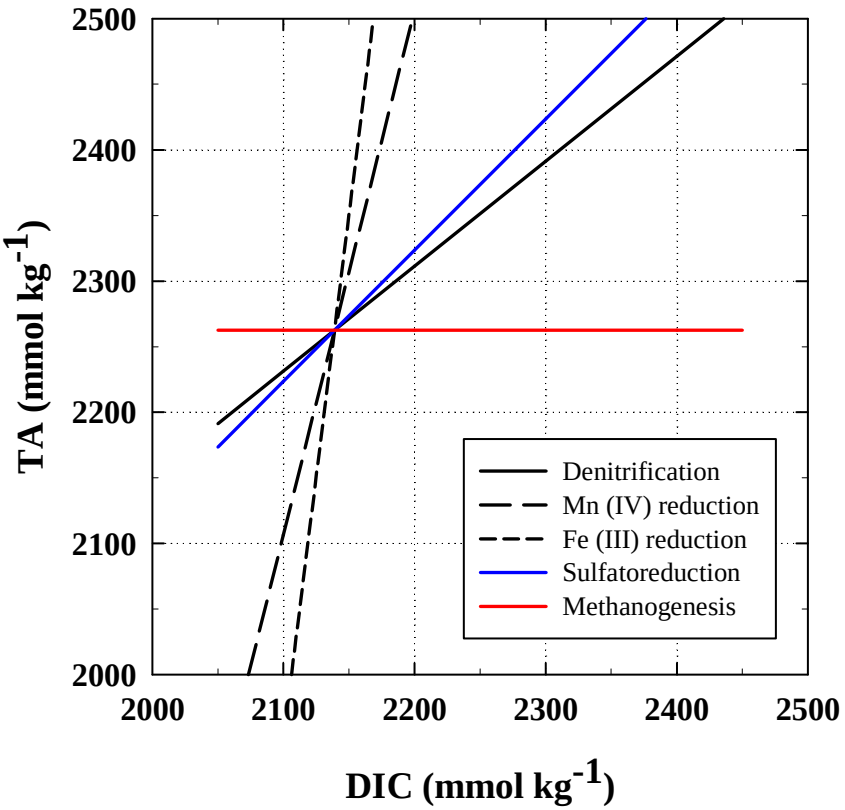

Figure I.2.5: Effects of different processes on DIC and TA (with the exception of precipitation of $CaCO_3$, gas exchange and photosynthesis that are provided in Figure I.2.4). The initial conditions are typical conditions found in arctic surfaces waters (S = 33, T = 2°C, P = 1 atm) in equilibrium with the atmosphere (pCO_2 = 390 µatm, pH = 8.04) with a DIC of 2139 µmol kg^{-1} and a TA of 2262.5 µmol kg^{-1}.

		Processes	Quantitative example	ΔDIC (µmol kg^{-1})	ΔTA (µmol kg^{-1})	ΔpCO_2 (µatm)
Abiotic		T (°C)↗	+1°C	0	0	+19.41
		S ↗	+1 of salinity	+64.81	+68.56	+17.91
		Mixing of water masses	Conservative			
		Uptake of CO_2 from atmosphere	Seawater in equilibrium with an atmosphere at 400 µatm	+3.53	0	+10
		$CaCO_3$ precipitation	Precipitation of 10 µmol of $CaCO_3$	-10	-20	+13.59
Biotic	Oxic	Photosynthesis by NO_3^- assimilation	Synthesis of 10 µmol of organic matter*	-10	+1.6	-30.09
		Photosynthesis by NH_4^+ assimilation	Synthesis of 10 µmol of organic matter*	-10	+1.4	-29.65
		Ammonification	Involving 10 µmol of organic matter*	0	+1.5	-3.72
		Nitrification	Involving 10 µmol of organic matter*	0	+3	-7.41
	Anoxic	Denitrification	Degradation of 10 µmol of organic matter*	+10	+8	+7.81
		Mn (IV) reduction	Degradation of 10 µmol of organic matter*	+10	+40	-63.11
		Fe (III) reduction	Degradation of 10 µmol of organic matter*	+10	+80	-127.37
		Sulfatoreduction	Degradation of 10 µmol of organic matter*	+10	+10	+22.72
		Methanogenesis	Degradation of 10 µmol of organic matter*	+5	0	+14.26

Table I.2.2: Main physical and biogeochemical processes and their interactions with pCO_2 and the carbonate system.

3. Sea ice

Sea ice is a thin, fragile, dynamic and solid layer that is formed by the congelation of seawater. The buildup of the sea ice cover, however, results from the combination of thermodynamic processes (heat exchanges with the atmosphere above and the seawater below) and dynamic processes (resulting from mechanical interactions of the individual ice plates driven by surface winds and ocean currents). Sea ice can be considered as a porous solid, constituted of a matrix of pure ice containing liquid and gaseous inclusions. Hence, the "mushy layer" concept is put forward by some authors [*Wettlaufer et al.*, 2000; *Feltham et al.*, 2006; *Notz and Worster*, 2009] in comparison with processes occurring during solidification of other materials (salt, metals). Sea ice properties have been described in details, among others, by *Weeks and Ackley* [1982], *Eicken* [2003] and *Thomas and Dieckmann* [2003].

3.1 Sea ice structure and composition

Structure of sea ice crystals shows, as for most ice forms at the Earth surface, a hexagonal symmetry. Each atom of oxygen is located at the center of a tetrahedron with four other oxygen atoms located at each of the apices. This highly regular network of oxygen atoms is bonded together by a series of hydrogen bonds. The oxygen atoms are concentrated close to a series of parallel planes that are referred to as the basal planes. The direction perpendicular to these planes is referred to as the principal hexagonal or "*c*-axis" (symmetry 6). The "*a*-axis" (symmetry 2) line up with the plane of the fastest growing ice while the "*c*-axis" is the optical axis of the crystal (Fig. I.3.1).

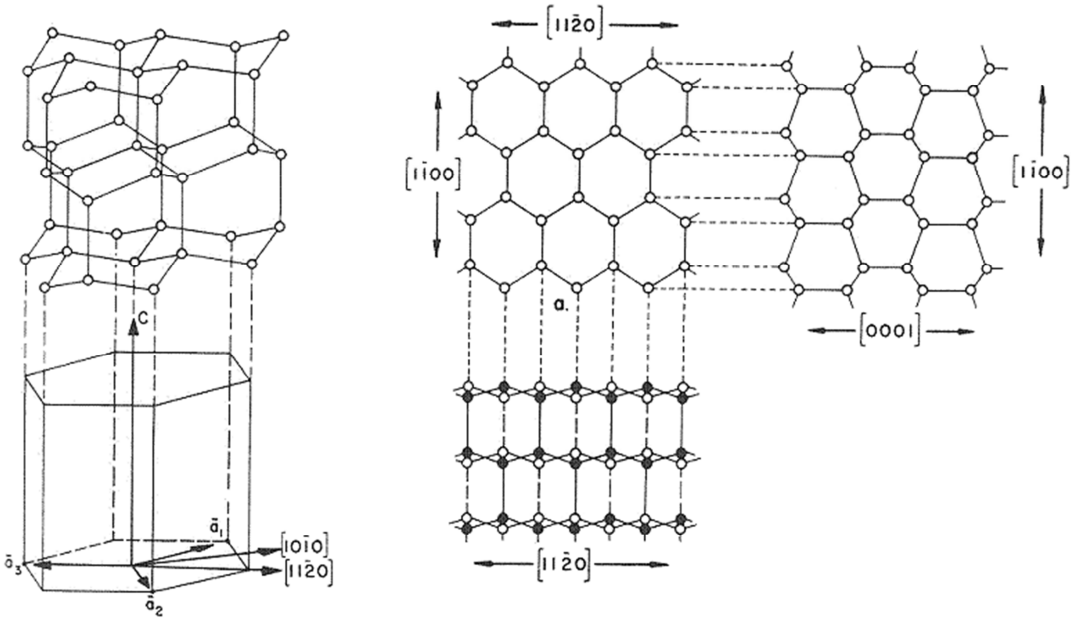

Figure I.3.1: Positions of the oxygen atoms in ice as viewed from several different angles. In the middle diagram the view is parallel to the *c*-axis and in the diagram on the right it is perpendicular to the *c*-axis [*Weeks and Ackley*, 1982].

The low density of the ice is the result of the tetrahedral coordination of every water molecule by hydrogen bonds resulting in a very open structure.

As sea ice is formed of seawater solution essentially, all the solute are rejected back into the liquid or melt. As more ice forms with temperature decreasing gradually, the melt that coexists in equilibrium with the ice becomes saltier. With cooling, ice forms and the remaining brine becomes more saline. As cooling continues, different solid salts also precipitate from the brine. The phase diagram [*Assur*, 1958] specifies the composition of the different phases (ice, brine, solid salts) that coexist at different temperatures and pressures. The figure I.3.2 represents the phase diagram for standard sea ice, which is defined as sea ice of such composition that its meltwater will have the same relative concentrations of ions (to each other) as normal seawater.

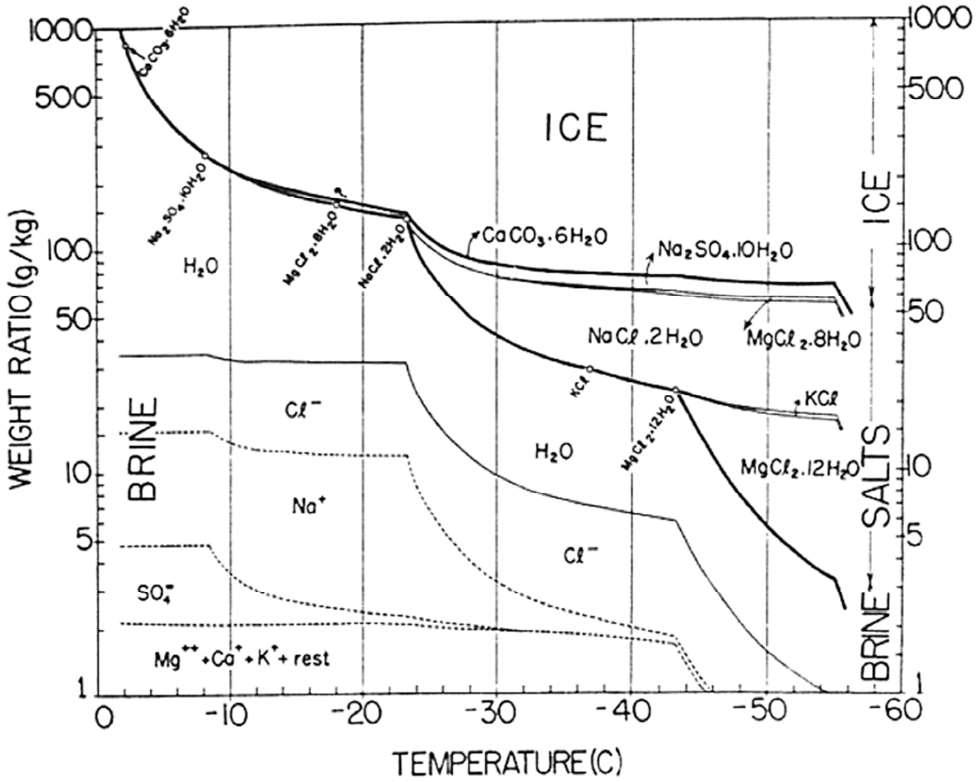

Figure I.3.2: Phase diagram of sea ice. The different curves indicate the mass fraction of solid ice (top), salts (middle) and liquid brine (bottom) present in a closed volume of ideal seawater at different temperatures [*Assur*, 1958].

Sea ice composition can be determined in this diagram. Sea ice is mainly formed of pure ice, brine (the composition of which depends of the ice temperature) and solid salts precipitated from brine. The relative proportion of these three elements depends on the ice temperature (Table I.3.1, for 1 kg of standard sea ice with a salinity of 34.325).

	-10°C		**-30°C**	
Ice	768 g		917 g	
Solid salt	4.2 g		43.4 g	
Brine	228 g		39.5 g	
	water fraction	195 g		30 g**
	*ions fraction**	32 g		10 g**

Table I.3.1. Relative proportion of ice, solid salt and brine at-10°C and -30°C.
*including Cl^-, Na^+, SO_4^{2-}, Mg^{2+}, Ca^{2+}, K^+…
**estimates from the figure I.3.2.

The initial temperatures of crystallization of the various solid salts believed to be present in natural sea ice are given in table I.3.2.

Salt composition	Mineral name	Crystal system	Density (mg/m^3)	T of initial salt formation in brine (°C)
$CaCO_3.6H_20$	Ikaite	Monoclinic	1.771	-2.2
$Na_2SO_4.10H_2O$	Mirabilite	Monoclinic	1.49	-8.2
$MgCl_2.8H_2O$				-18
$NaCl.2H_2O$	Hydrohalite	Monoclinic	1.61	-22.9
KCl	Sylvite	Hexoctahedral	1.99	-36.8
$MgCl_2.12H_2O$		Monoclinic		-43.2
$CaCl_2.6H_20$	Antarcticite	Trapezohedral	1.71	≤-55

Table I.3.2: Sequential precipitations of salts within sea ice, adapted from *Weeks and Ackley* [1982].

It should be noted that some differences may exist between this theoretical diagram and the real state of the ice. Brine pocket may form, isolating portions of brine and solid salts, thereby changing the sequence of possible reactions between theses phases and the ice. Sea ice can also age with brine drainage taking place with potentially some of the solid salts remaining behind within the ice. This process would result in the enrichment of ions that are associated to the solid salt previously formed in the ice.

3.2 Water conditions for sea ice formation

Seawater has, on average, a salinity of about 35. As the rate of decrease of the freezing point (T_g) of water, with an increasing salinity, is lower than the rate of decrease of its temperature of maximum density ($T_{\rho max}$), $T_{\rho max}$ becomes lower than T_g for a salinity higher than 24.695 (Fig. I.3.3). This property creates an unstable vertical density distribution, causing convective mixing, as seawater cools down to being above its freezing point, while cooled down from the atmosphere, will start a thermohaline convection (overturning of colder surface water which is in turn replaced by warmer water displaced at depth) until the entire upper layer stirred by wind, waves and thermohaline mixing (mixed layer) reach the freezing point. Once the entire water column reaches the freezing point, additional cooling allows the water column to be supercooled and ice crystals appear.

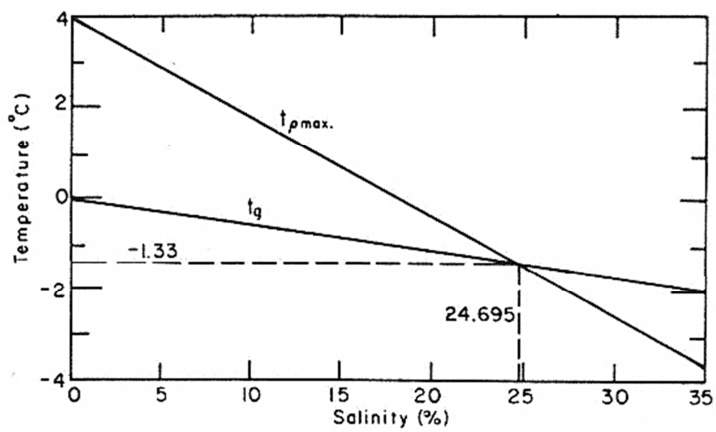

Figure I.3.3: Temperature of the density maximum $T_{\rho max}$ and of the freezing point T_g for seawater of different salinities [*Weeks and Ackley*, 1982].

3.3 Sea ice classification

Depending on location and environmental conditions, sea ice may be formed from several processes which will result in different textures characteristics. Sea ice may therefore be classified according to its texture (morphology), genetic process or place of formation. This is summarized by *Eicken* [2003] and shown in figure I.3.4 for the textural and genetic types.

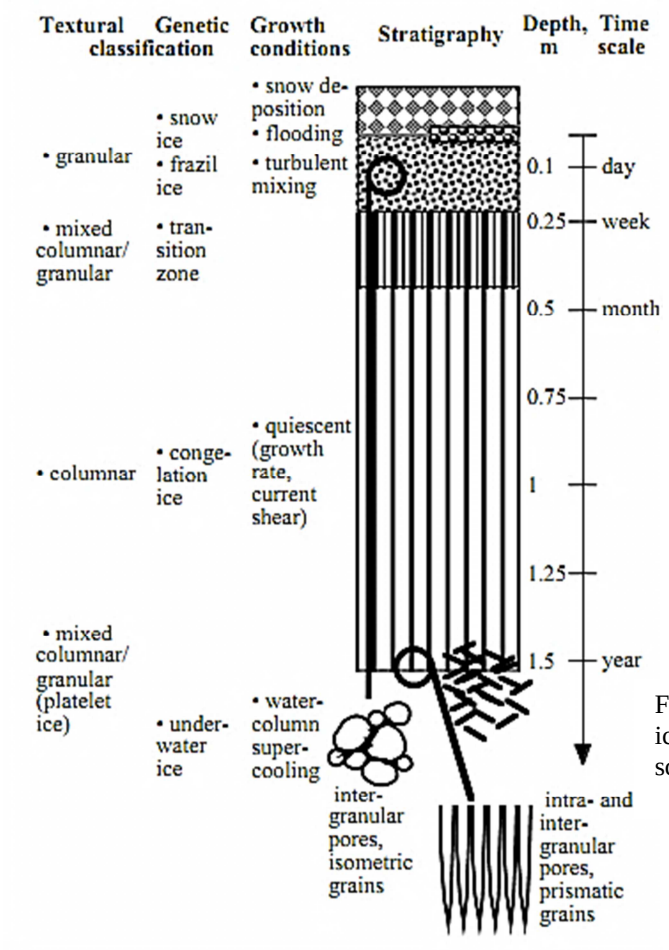

Figure I.3.4: Schematic summarizing the main ice textures, growth conditions and times scales for first-year sea ice [*Eicken*, 2003].

3.3.1. Textural classification

Different sea ice categories are distinguished according to their texture.

- Columnar ice is made of large, vertically elongated crystals with intracrystalline substructures. It is unanimously recognized as the unequivocal signature of congelation ice resulting from direct freezing of seawater, at the bottom of the ice floe, for example [*Tison et al.*, 1998].
- Granular ice is made of equigranular crystals. The crystals size (from millimeter to centimeter scale) and shape depend on the mode of ice formation [*Tison et al.*, 1998].
- Intermediate columnar / granular ice is made of slightly elongated grains. The grains are indented and interlocked. Grains exhibit planar, smooth vertical boundaries and highly indented, irregular horizontal ones. They result from congelation of supercooled seawater at the advancing ice-water interface [*Eicken and Lange*, 1989].
- Platelet ice is predominantly made of elongated acicular grains both in vertical and horizontal thin sections. The platelet facies generally occurs as a mix of platelet-congelation facies with a wide range between the two components [*Tison et al.*, 1998].

3.3.2. Genetic classification

3.3.2.1. Thermodynamic formation

The first type of sea ice formation is associated to thermodynamic processes such as the cooling of seawater by the atmosphere above, the mixing of seawater masses of different properties or pressure changes in a given water masses.

3.3.2.2. Frazil formation

Ice crystals formed in seawater take the shape of needles, spicules or platelets, often intertwined into aggregates and are known as frazil ice. Individual crystals are typically a few millimeters to a few tens millimeters across and less than a millimeter in thickness [*Weeks and Ackley*, 1982]. These crystals are formed at the surface of the seawater or within the water mass. They are less dense than seawater and thus raise and accumulate

at the surface or at the bottom of a pre-existing ice column. Their accumulation in a uniform layer of frazil ice crystals is called grease ice.

Several mechanisms are responsible for frazil ice formation. The most important is due to turbulence induced by wind and waves in surface seawater. This process mainly occurs in leads or polynyas[2] [*Lange et al.*, 1989; *Jeffries and Weeks*, 1992]. Under calm weather conditions, the grease ice layer quickly consolidates into a solid ice cover with randomly oriented ice crystals (granular texture). This process occurs before the transition to the columnar ice. With significant wave action, the frazil collects to form rounded discs collectively called "pancake ice". Pancake sizes range from a few tens centimeters to a few meters [*Perovich and Gow*, 1996]. The pancakes continually collide and separate resulting into characteristic elevated rims. With ongoing freezing the pancakes adhere into a continuous ice sheet. Once a solid surface layer has formed, further ice growth typically commences through congelation at the ice-water interface. This whole process is referred to by *Lange et al.* [1989] as the "pancake cycle" (Fig. I.3.5).

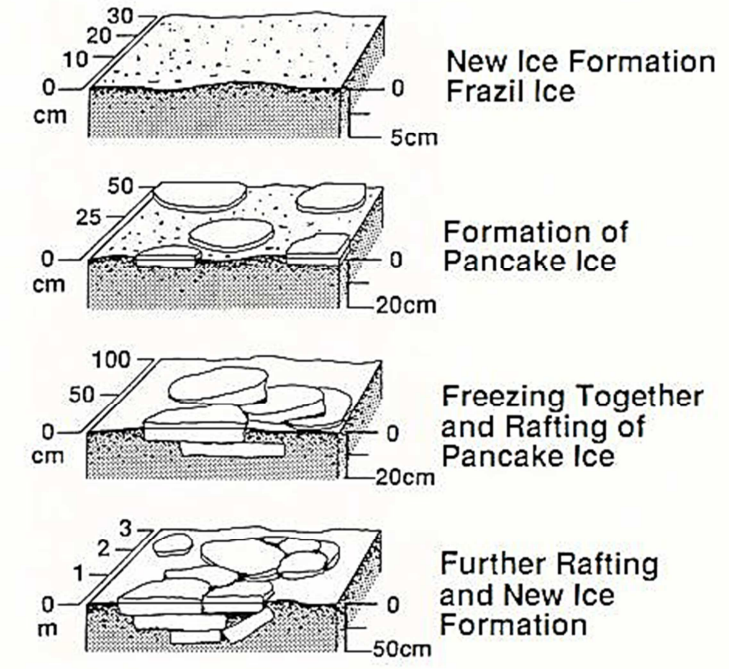

Figure I.3.5: Schematic representation of the "pancake cycle" [*Lange et al.*, 1989].

[2] According to *Weeks* [2010], the definition of polynyas and flaw leads is somewhat ambiguous. Both refer to areas of open water (and thin ice) in a region and season where one would otherwise expect thicker ice. The *World Meteorological Organization* [1985] defines a lead as being any fracture or passage through sea ice that is navigable by surface vessels. However, once a lead forms, open water will only exist for a short time before an ice cover starts to form converting open leads into refrozen leads. Polynyas are areas of persistent open water. They are larger than lead and reoccurs in a similar location annually due to regional characteristics.

3.3.2.2.1. Transition layer

Once a continuous ice cover is formed, the water column is separated from the atmosphere. The latent heat needed to freeze the water will be extracted through the ice. The growth rate is determined by the temperature gradient in the ice and by the heat capacity of the ice. Moreover, the ice crystals with a more horizontal *c*-axis orientation have a slight growth advantage. Therefore, further ice growth results in geometric selection towards columnar ice crystals with their *c*-axis in the horizontal plane and an increase of their size with depth. This transition occurs within a few centimeters thick transition zone that forms the so called intermediate granular/columnar ice or transition layer (Fig. I.3.6).

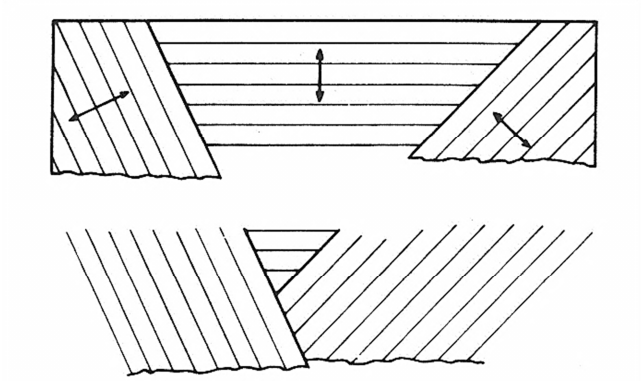

Figure I.3.6: Schematic diagram showing the process of geometric selection. The arrows indicate the direction of the c-axes [*Weeks and Ackley,* 1982].

3.3.2.2.2. Congelation ice

Below the transition layer in sea ice, the ice has all the characteristics of the columnar texture type. It possesses a strong crystal elongation parallel to the direction of heat loss, a pronounced crystal orientation and a gradual increase in grain size over crystals closer to the cold source [*Weeks,* 2010]. In this type of ice, all crystals have the *c*-axis oriented within a few degree of the horizontal plane.

According to *Eicken and Lange* [1989], three wind controlled ice formation regimes may be distinguished. For wind speeds < 3m/s, a continuous sheet of columnar ice with little deformation (< 10% rafted) is developed. For wind speed ranging between 3 m/s and 10 m/s, the ice cover is more highly rafted and ridged (25% - 30%) and shows an intermediate columnar/granular texture with features common to both ice types. Finally, for wind speed > 10 m/s, the ice cover is mainly rafted and ridged (> 50%) and formation of granular ice predominates.

Following the *World Meteorological Organization* [1985], new ice is a weakly or non-consolidated collection of ice crystals which usually include frazil ice and grease ice. Once consolidated, nilas (0 – 10 cm) is formed, which is further classified into dark nilas (0 – 5 cm) and light nilas (5 – 10 cm). When sea ice sheet becomes thicker than 10 cm, the ice is classified as young ice. Young ice includes grey ice (10 – 15 cm) and grey-white ice (15 – 30 cm). Recently formed sea ice thicker than 30 cm is called first year sea ice. A special case is the pancake ice which is formed as a result of wave action. Based only on thickness, pancake ice may be classified as belonging to either nilas or young sea ice types [*Ehn et al.,* 2007].

In complement to the most frequent frazil – congelation sea ice growth process described above, it is also other sea ice types such as "snow ice", "superimposed ice" or "platelet ice" for the most known.

3.3.2.2.3. Snow ice

A thick snow cover depresses the ice surface below the water level, so that seawater floods the ice surface and subsequently refreezes together with the water-saturated snow. This is called the "flood-freeze cycling" [*Fritsen et al.,* 1998]. The resulting "snow ice" has a fine granular texture with polygonal crystals (sharp linear crystal contours) with no interlocking grains. This type of ice is often quite porous [*Eicken,* 2003] and can only be distinguished from granular ice of frazil origin by its negative $\delta^{18}O$, because of the significant contribution of ^{18}O depleted snow crystals [*Lange et al.,* 1990].

In the Arctic, snow thickness is rarely high enough to allow surface flooding and snow ice formation. In Antarctica, however, an overall thinner ice cover and higher snow accumulation rates result in widespread occurrence of this phenomenon, with more than 50 % of the surface flooded in some areas [*Eicken,* 2003].

3.3.2.2.4. Superimposed ice

Superimposed ice formation occurs during summer when the snow melts internally and percolating meltwater refreezes either in the snow or at the snow-ice interface when the temperature gradients within snow and ice are negative, *e.g.,* the ice is colder than the freezing temperature of freshwater [*Haas et al.,* 2001; *Nicolaus et al.,* 2003; 2009]. Superimposed ice can form layers of a few decimeters in thickness in Antarctica while

in the Arctic superimposed ice usually rapidly deteriorates after formation due to strong surface ablation [*Nicolaus et al.,* 2003]. The typical superimposed ice texture is isometric grains with planar boundaries. The grain-size often decreases with depth [*Haas et al.,* 2001].

3.3.2.2.5. Platelet ice

Platelet ice is formed through consolidation of an ice platelet layer underneath the solid sea ice cover. The highly disorganized texture with crystals extending in all directions results from the freezing of voids in between randomly oriented platelets. The network of loose ice platelets determines the morphology and orientation of crystals grown in the voids [*Eicken and Lange,* 1989].

The growth of platelet ice is attributed to unrestrained frazil ice nucleation and growth resulting from adiabatic supercooling in ascending Ice Shelf Water (ISW) but also by growth and accumulation of plate-like frazil ice directly to the bottom of an existing ice sheet from an adiabatically supercooled water mass [*Eicken and Lange*, 1989; *Gow et al.*, 1998; *Tison et al.*, 1998].

The formation of the ISW is linked to the Deep Thermohaline Convection (DTC) (Fig. I.3.7). As sea ice is formed, salt are partly rejected into the underlying water, increasing its density. This water called High Salinity Shelf Water (HSSW), denser and at its freezing point, sinks to form the DTC. During its adiabatic sink, its freezing point decreases due to increasing pressure. A part of the HSSW sinks beneath the ice shelf and reaches the grounding line when it melts meteoric ice in the basal part of the ice shelf. The mixing between this meltwater and the HSSW forms the ISW. This water is less salty, so less dense. Therefore it resurfaces adiabatically ahead of the ice shelf and, with the decrease of the pressure, becomes supercooled. As a result, frazil crystals grow from thermodynamic adjustments. These crystals are less dense than the ISW and thus slowly float up to the surface and grow as platelet crystals [*Jacobs et al.,* 1992].

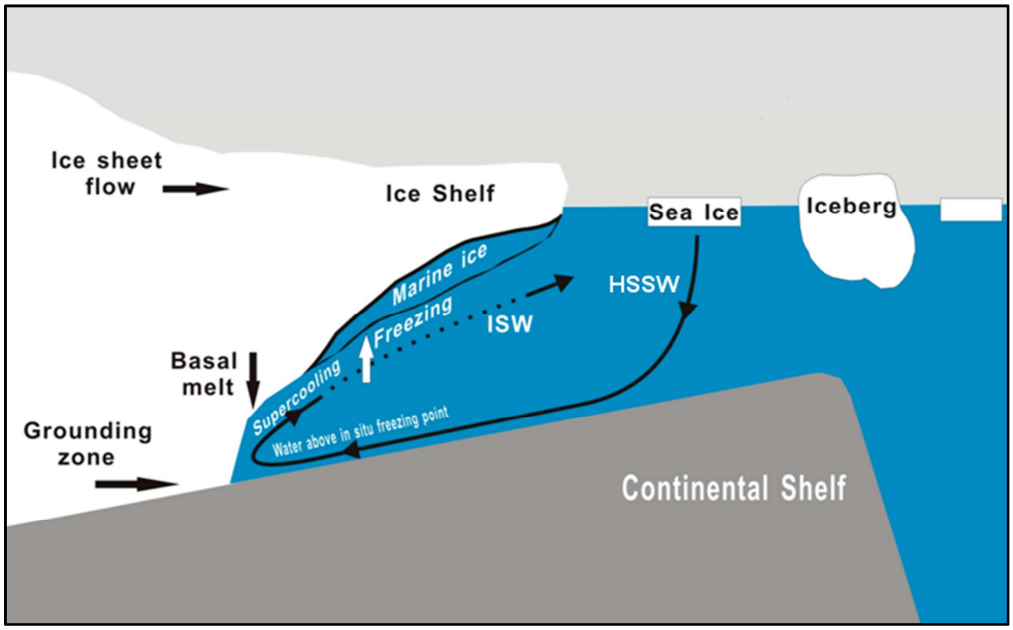

Figure I.3.7: Sketch summarizing the Deep thermohaline Convection (DTC), resulting in Ice Shelf Water (ISW) production and frazil / marine ice formation, adapted from *Jacobs et al.* [1992].

3.3.2.2.6. Multiyear ice

During the summer melt season, the first year sea ice undergoes profound changes as it eventually survives into multiyear ice. As the snow cover melts, the ice surface begins to melt as well. Concurrently, the interior of the ice warms up due to the absorption of solar radiation and conduction, causing an increase in brine volume. Subsequent increase of the hydraulic head of the brine network results on the flushing of the surface meltwater and brine drainage in the ice, leading to significant desalination [*Weeks and Ackley*, 1982; *Perovich and Gow*, 1996]. Over time, with dynamic and thermodynamic contributions, the ice surface develops surface relief. The later combines depressed ovens where melt ponds can form and raises areas called hummocks. Hummocks are well above freeboard, facilitating brine drainage. As drainage occurs, brine pockets are transformed into air bubbles, resulting in bubbly ice with a lower density [*Perovich and Gow*, 1996].

3.3.2.3. Dynamic formation

The main external parameter controlling the dynamic ice growth is the wind speed, which also determines the hydrodynamic conditions of the upper water column. As mentioned above, *Eicken and Lange* [1989] recognized 3 distinct regimes of sea ice formation and development for wind speed in the ranges < 3 m s^{-1}, 3-10 m s^{-1} and > 10 m s^{-1}.

For a wind speed less than 3 m s^{-1}, generally a thin layer of frazil ice will form at the surface. Once the ice cover is established, ice growing downward is columnar ice. With a wind speed ranging from 3m s^{-1} to 10 m s^{-1}, the new ice cover breaks up in the vicinity of open water areas due to wave action and the amount of rafting (superposition of individual ice plates) increases significantly. Ices up to about 0.3 m in thickness are more susceptible to rafting, while thicker ice tends to be ridged in the process of compressional deformation. If the wind speed is higher than 10 m s^{-1}, the ice rides up against the pack ice boundary or against larger, more inert floes. Swell generated by the wind causes surrounding floes to break up and decrease in size.

3.3.3. Classification based on ice location

Two types of sea ice may be distinguished based on their distance to the coast. Landfast ice is formed along the coast, attached to the shoreline, generally in quiet conditions. Pack ice is any sea ice formed in the open sea. Pack ice can shoal on the coast to become landfast ice and conversely landfast ice can disintegrate and drift into the open ocean area.

Landfast ice is mainly made up of congelation ice because of the relatively calm conditions dominating during its formation. Nevertheless, landfast ice may contain a variable proportion of frazil ice or platelet ice [*Eicken and Lange,* 1989*; Lange et al.,* 1989]. As pack ice is formed in open sea, the conditions of formation are more dynamics. Therefore, this type of ice is formed through the “pancake cycle” and may contain a large proportion of frazil ice. Only at a late stage, congelation ice may develop. The dynamical and thermodynamical conditions prevailing in the area where pack ice is formed determines the relative importance of the different ice types and ice texture.

3.4 Sea ice salinity

Temperature and salinity of the ice are the prime variables governing not only the phase fractions (*cf.,* Ch. I.3.1.) but also a whole host of other physic-chemical properties. The thermodynamic coupling between these two variables is a key aspect of sea ice since any temperature change directly affects the porosity and pore microstructure of the ice as well as the salinity and chemical composition of the brine. The *in situ* brine volume fraction and other properties derive from the bulk salinity of an ice sample and from its

in situ temperature. The latter can be measured by inserting a temperature probe into freshly drilled holes in a core or measured from sensors frozen into the ice. To measure the salinity, an ice core is divided into section and melted in the lab. Salinity is derived from electrolytical conductivity measurements.

According to *Cox and Weeks* [1983], sea ice salinity, S_{ice}, is defined as:

$$S_{ice} = \frac{M_{salt}}{M_{ice}+M_{brine}+M_{solid\ salt}} \times 1000 \qquad \text{(I.3.1)}$$

where M_{salt}, M_{ice}, M_{brine}, $M_{solid\ salt}$ corresponds to the mass of salt (solid and dissolved), brine and solid salt, respectively.

According to the phase diagram of *Assur* [1958], the mass of solid salt is insignificant, at least during the first step of the ice formation. The equation I.3.1. becomes:

$$S_{ice} = \frac{M_{salt}}{M_{ice}+M_{brine}} \times 1000 \qquad \text{(I.3.2)}$$

Salinity may be expressed in ‰ or in practical salinity unit (psu) as defined by UNESCO [1978]. The practical salinity scale (pss) assumes constant seawater composition (ideal salinity) and is based on conductivity ratios measured in the salinity interval from 1 to 42. Since bulk salinity of sea ice and brine are often well above these values, and given the varying chemical composition of ice and brine, salinities of sea ice and brine may be quoted in ‰ as based on measurements of electrolyte conductivity of melted samples. Assuming standard seawater composition, for practical purposes, concentrations in ‰ and psu can be assumed to coincide between 1‰ and 42‰ [*Eicken*, 2003]. Nevertheless, according to the equations I.3.1. and I.3.2., salinity is defined by a ratio of same units numbers. Therefore, salinity is defined by a "pure" number, without unit.

3.4.1. Initial salt entrapment

During sea ice growth, salt becomes entrapped in the ice phase, largely in the form of liquid inclusions located along the boundaries between the ice plates. As ice grows and the ice-water interface advances downward into the melt, salt and ions are rejected from the ice. The salt rejected at the advancing interface, increases the salinity of a thin layer ranging from a few millimeters to a few centimeters in thickness, called "boundary layer" [*Lake and Lewis*, 1970]. In this layer, salt is transported by diffusion only, from the ice-water interface towards the bulk water reservoir. It results in a gradient in salt

concentrations. Therefore, in the case of thermodynamic equilibrium, the interface is always at the salinity-driven melting-freezing point, an increase in salt concentration going along with a drop in temperature relative to the underlying seawater.

However, the diffusive heat transport from the water column (warmer) to the interface (colder) is faster than the transport of salt away from the interface (roughly by an order of magnitude). As a result, a thin layer ahead of the interface is cooled but has not yet received influx of salt from above. This layer is said to be constitutionally supercooled since salt concentration and temperature are at a mismatch with respect to the local freezing point, figure I.3.9, [*Weeks and Ackley*, 1982; *Eicken*, 2003].

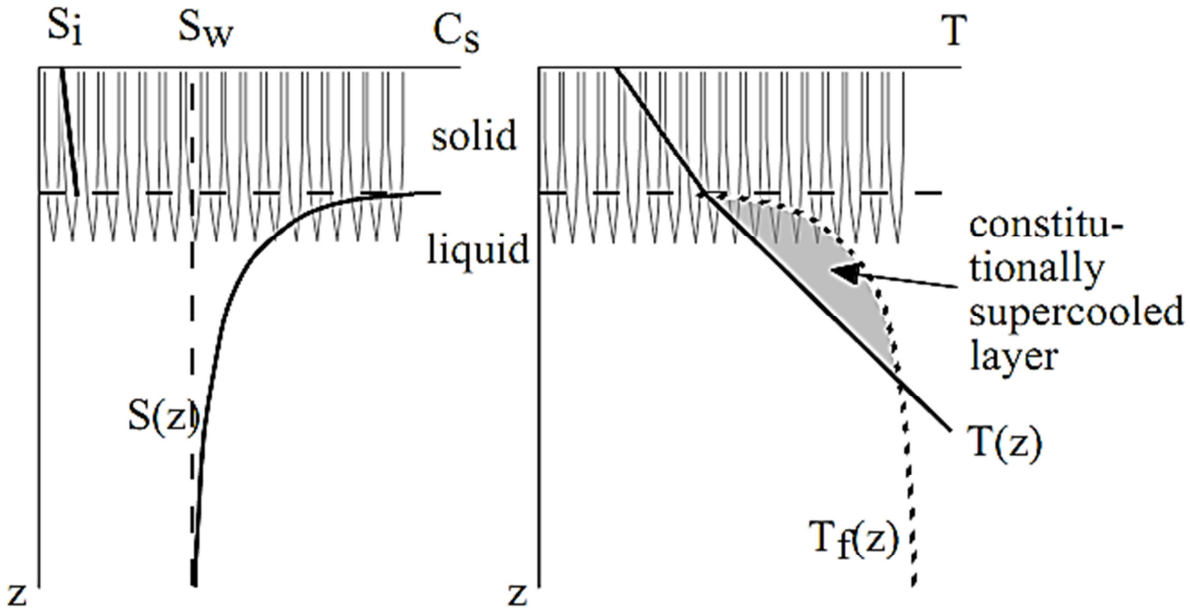

Figure I.3.9: Schematic depiction of lamellar ice-water interface (skeletal layer) and the corresponding salinity (left) and temperature (right) gradients. The freezing temperature profile is shown as a dotted line, with a constitutionally supercooled layer bounded by the actual temperature gradient and the salinity-dependent freezing-point curve [*Eicken*, 2003].

As a consequence of this constitutional supercooling, any small perturbation of a planar ice-water interface that protrudes into the constitutionally supercooled zone finds itself in a growth advantage. The salt rejected by such protrusion contributes to decrease the freezing point of the brine retained along the protrusion boundaries. Consequently, such perturbations can grow into ordered patterns of lamellar bulges at the ice-water interface. This is called dendritic growth [*Weeks and Ackley*, 1982; *Eicken*, 2003]. Its morphology is mostly reported to be lamellar or cellular rather than fully dendritic.

At the same time these diffusional processes occur, the higher density of the more saline brine in contact with the ice bottom especially promotes the transport of brine by

convection [*Niedrauer and Martin,* 1979]. Within the columnar ice zone, a crystal substructure is developed consisting of sub-millimeter thick blades of ice, interspersed with parallel layers of brine inclusions. These inclusions represent the residual brine that cannot be rejected from the freezing interface and become segregated as inclusions between the pure ice plates. Each crystal of sea ice thus contains a number of plates between which layers of brine pockets are sandwiched. The brine layer separation distance can vary from a few tenths millimeter to more than a millimeter, depending mainly on the rate of freezing [*Nakawo and Sinha,* 1981; *Perovich and Gow,* 1996]. These crystals and the attendant layers of brine become elongated in the vertical during growth.

The transitional layer, demarcated by ice volume fraction tending towards 0 at its lower end and with a transition to laterally interconnected ice lamellae at a porosity ≤ 30% at it uppers end, is commonly referred to as the "skeletal layer" [*Eicken,* 2003].

3.4.1.1. Constitutional supercooling and dendritic growth

As described above, a potentially most important factor in controlling initial ice salinity is the segregation of sea salt ions at the ice-water interface, in what is referred to as the "boundary layer". In this layer, the solute transport is thought to occur by diffusion process only and will control the initial incorporation of ionic and gaseous solutes in the ice [*Weeks and Ackley,* 1982; *Killawee et al.*, 1998; *Tison et al.*, 2002].

During progressive freezing, solutes will tend to concentrate at the ice-water interface in the boundary layer, unless removed by convection or unless the rate of freezing is slow compared to solute diffusion rates. If there is no convection, the concentration of solutes with depth in the boundary layer can be predicted by consideration of the relative magnitude of advection of the growing ice-water interface and diffusion in the water away from the interface.

The concentration of the liquid (C_L) can be expressed as:

$$C_L = C_0 + \left[1 + \left(\frac{1-k}{k}\right) exp\left(-\frac{v}{D}x\right)\right] \qquad \text{(I.3.3)}$$

where C_0 is the liquid concentration far from the interface, v is the linear rate of advance of the freezing front, D is the diffusion coefficient of the solute species (1.18, 1.61, 2.08 $\times 10^{-5}$ cm² s^{-1} for CO_2, N_2 and O_2, respectively [*Stauffer et al.,* 1985]), t is time. k is

defined as the equilibrium segregation coefficient or the ratio of concentrations of the solute in the ice (C_i), to solute in water at the ice-water interface (C_{iw}).

3.4.1.2. Chemical fractionation in the boundary layer

However, convection generally occurs, either spontaneously or mechanically due to turbulence in the water reservoir. In the case of downward freezing, as for sea ice formation, the layer in which diffusion occurs is truncated by convection at its base to form the boundary layer. If a steady-state is reached when the rejection of solutes at the ice-water interface is balanced by their removal by double diffusion across the boundary layer, Fick's first law of diffusion is applied:

$$Flux = C_{bw} v = D \frac{(C_{iw} - C_{bw})}{x} \qquad \text{(I.3.4)}$$

where x is the thickness of the boundary layer, C_{iw} and C_{bw} are the solute concentrations at the ice-water interface and in the bulk water, respectively.

One must also distinguish between the observed effective segregation coefficient, k_{eff}, and the equilibrium segregation coefficient, k_{eq}. The latter is much difficult to determine as it uses the seawater salinity at the ice-water interface, C_{iw} [*Killawee et al.*, 1998] while k_{eff} uses the salinity of the seawater, C_{bw}, far away from the interface [*Weeks and Ackley*, 1982; *Eicken*, 2003]:

$$k_{eq} = \frac{C_i}{C_{iw}} \qquad \text{(I.3.5)}$$

$$k_{eff} = \frac{C_i}{C_{bw}} \qquad \text{(I.3.6)}$$

k_{eq} is generally estimated from experimental runs where either growth occurs at very slow growth rate or the reservoir is thoroughly and actively mixed by convection at all times. For columnar ice grown from seawater, the magnitude of k_{eff} is proportional to ice-growth rate, v [*Cox and Weeks*, 1975]. From laboratory experiments and field work K_{eff} was estimated as [*Nakawo and Sinha*, 1981; *Eicken*, 2003]:

$$\begin{aligned} k_{eff} &= \frac{0.26}{0.26 + 0.74\, exp(-7243 v_i)} && v > 3.6\ 10^{-5}\ \text{cm s}^{-1} \\ k_{eff} &= 0.8925 + 0.0568\, ln\, v_i && 3.6\ 10^{-5}\ \text{cm s}^{-1} \geq v \geq 2\ 10^{-6}\ \text{cm s}^{-1} \\ k_{eff} &= 0.12 && v < 2\ 10^{-6}\ \text{cm s}^{-1} \end{aligned} \qquad \text{(I.3.7)}$$

The slower the ice growth, the less build-up of salt ahead of the ice-water interface with diffusive and convective transport capable or removing substantial amount of salt before it is trapped between ice lamellae. When the ice growth rate is small, the value of k_{eff} tends to k_{eq} [*Eicken,* 2003].

3.4.2. Desalination processes

Once the ice is formed, further desalination occurs. Salt is removed from the bulk of the ice sheet by several mechanisms. These processes are significant as they have consequences on sea ice physical properties and on sea ice-ocean interactions [*Niedrauer and Martin,* 1979]. *Eicken* [2003] highlights differences between a measured salinity profile and that predicted from the growth-rate/segregation relations (Fig. I.3.12). These deviations are mainly due to the loss of salt from the ice during the consolidation and ageing process. According to *Eicken* [2003], there are two different types of desalination mechanisms:

- Those active in “cold ice”, during the ice-growth period, driven mostly by temperature gradient established in the ice cover and the cooling of individual ice layer,
- Those dominating desalination of “warm ice”, requiring the presence of low-salinity meltwater either at the surface or at the bottom of the ice.

Among the first group of processes occurring during “cold” ice, one can discriminate brine expulsion, gravity drainage and brine pocket migration. The two first are of quantitative importance while the latter is only significant on a microscopic level. But the most effective desalination processes are confined to the summer melt season, when ice porosity and permeability are high and zero- or low-salinity, meltwater production at the surface and the bottom of the ice is capable to displacing higher salinity brine from within the ice [*Eicken,* 2003].

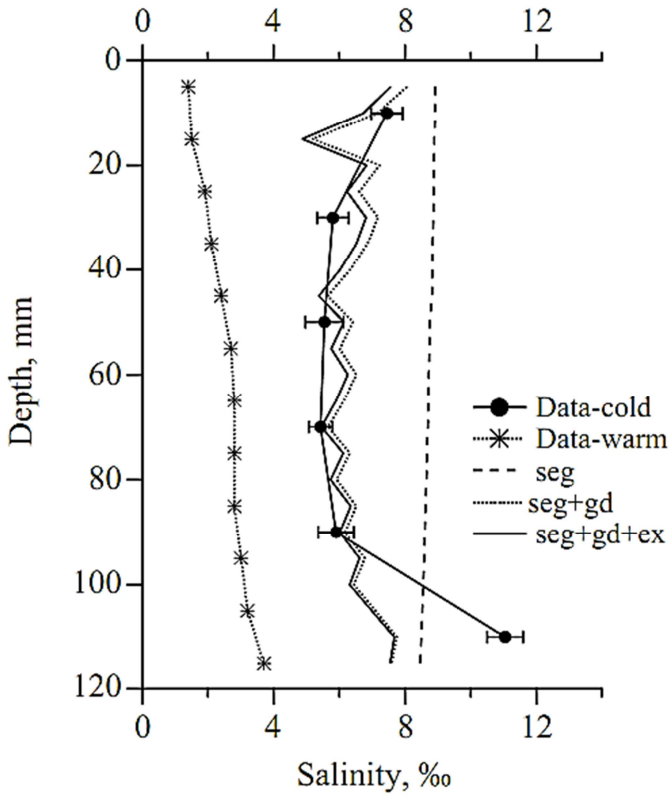

Figure I.3.12: Salinity profile for young columnar sea ice grown in a large ice tank (INTERICE experiment, Hamburg) as compared to model simulation of salinity profile evolution. "Data-cold" represents measurements of the salinity of "cold" ice (surface T ranging from -8°C to -10°C) 5 days after the start of the experiment. "Data-warm" represents measurement when the surface temperature of the ice was ranging from -1°C to -2°C, 2 weeks after the start of the experiment, following an 8 day melting period. "seg" gives the salinity of newly grown ice layers following the segregation of salts at the ice interface as predicted by the equations I.3.3 and I.3.6 based on measured growth rate. "seg+gd" represents the evolution of the salinity profile if only gravity drainage were to occur. "seg+gd+ex" represents the evolution of the salinity profile if gravity drainage and brine expulsion were to occur [*Eicken,* 2003].

3.4.2.1. Brine pocket migration

The migration of brine pocket is due to the temperature gradient present within the brine pocket. Under the influence of this gradient, the pockets freeze at their colder top side and melt at their warmer bottom, so that brine pockets migrate toward the ice bottom [*Niedrauer and Martin,* 1979]. According to *Untersteiner* [1968], salt diffusion rate limits the rate of brine pocket migration such that it is far too slow to account for the observed brine drainage. The velocity of this migration was estimated to 3.10^{-4} cm h^{-1} [*Lake and Lewis,* 1970]. This process alone is negligible [*Lake and Lewis,* 1970; *Niedrauer and Martin,* 1979; *Weeks and Ackley,* 1982; *Eicken,* 2003].

3.4.2.2. Brine expulsion

The possibility of brine expulsion being an effective desalination mechanism was first suggested by *Bennington* [1963]. Brine expulsion is driven by the cooling of the ice and is independent of the initial ice permeability [*Cox and Weeks*, 1975]. As the ice gets colder, the brine in the pockets freezes to form more ice so that the remaining brine increases its salinity, which allows the brine to remain liquid at a colder temperature. As the newly formed ice occupies more volume than the brine, the resultant pressure increases and may cause fracture along the crystallographic basal plane or lines of natural weakness. Therefore, the brine may be expelled through cracks and channels into the seawater or at the ice cover surface [*Untersteiner*, 1968; *Lake and Lewis*, 1970; *Niedrauer and Martin*, 1979].

According to *Cox and Weeks* [1975], brine expulsion plays a limited role in desalination during the periods of ice growth. However, the change in salinity is significant and cannot be neglected, especially during the periods of rapid ice growth, where the rate of change of temperature at each level is high. Brine expulsion is probably the most important desalination mechanism during the initial stages of the ice growth [*Cox and Weeks*, 1974; *Cox and Weeks*, 1975; *Eide and Martin*, 1975].

3.4.2.3. Gravity drainage

Gravity drainage includes all processes where brine, under the influence of gravity, drains out of the ice sheet into the underlying seawater [*Cox and Weeks*, 1975].

Two types of gravity drainage may occur. First, since sea ice is less dense than seawater, as the ice grows, some of the ice-trapped brine is lifted above the waterline, and the resultant hydrostatic pressure head may force the brine down out of the ice [*Eide and Martin*, 1975; *Niedrauer and Martin*, 1979]. Secondly, because density of the brine in equilibrium with ice is determined by ice temperature, an unstable vertical density distribution also exists in the brine in growing sea ice. These processes can result in a convective overturn of brine within the ice, as well as the exchange of the denser brine within the ice with the underlying less saline seawater [*Cox and Weeks*, 1975; *Eicken*, 2003], provided that the ice is permeable enough, *i.e.*, above the permeability threshold [*Golden et al.*, 1998]. This is probably where the “mushy layer” theory, in which salt transfer is mainly controlled by convection under density instability is the domain where ice is still permeable, best predicts the final equilibrium

salinity profile in the ice. Oscillations of outflowing brine and the subsequent inflow of the underlying solution have been observed by *Eide and Martin* [1975] in brine channels in the lower portion of salt ice. The pathway and exact mechanism of this convection process are however still not clearly understood.

The gravity drainage rate is depending on sea ice permeability and temperature gradient. Because of the dependency of the brine density to the temperature (Eq. I.3.7), the rate of the gravity drainage will increase at any given permeability as the temperature gradient increases [*Cox and Weeks*, 1975; *Weeks and Ackley*, 1982].

According to *Wakatsuchi and Kawamura* [1987], drainage occurs when the brine is being expelled from the brine pocket by the decreasing temperature and is then moving along the platelet boundary to join with other droplets of expelled brine at the grain boundary. The drainage of the heavier brine is augmented by gravity drainage. This suggests that, from several desalination mechanisms believed to occur in sea ice, brine expulsion and gravity drainage are the major contributors to the formation of brine channels.

3.4.2.4. Brine flushing

Flushing is a form of gravity drainage of brine above sea level. However, desalination is driven by the hydrostatic head of snow and/or ice meltwater produced on the ice surface. This meltwater percolates downward into the ice cover, driving the higher-salinity brine out of the ice cover. Therefore, flushing can only occur during spring or summer, when surface melt is possible. The other requirement for flushing is that the ice has to be permeable. The presence of significant amounts of surface meltwater also suggests that the ice is either at, or near, the pressure melting point. Such near-melting ice temperatures result in very high brine volumes for a given salinity and high brine volumes correlate with large permeability.

Flushing is the most effective mechanism for desalination in multiyear ice and is the primary mechanism that controls the form of the steady-state salinity profile. Indeed, the time when flushing starts corresponds to the time during spring and early summer when major changes occur in the salinity of sea ice. Additionally, the continual percolation of fresh water down and through sea ice should result in significant decreases in salinity [*Untersteiner*, 1968; *Cox and Weeks*, 1974; *Cox and Weeks*, 1975].

3.4.3. Brine inclusions

Within sea ice, brine is trapped in the form of brine pocket or tube, brine layer and brine channels. Above the skeletal layer, the ice bridges the platelets so that brine is isolated in pockets and tubes. The brine pocket is a bubble of brine, surrounded by ice, that has either limited or no communication with other brine masses. Brine tubes are cylindrical brine-filled hollows in the ice which are closed at one and with a bulblike cap. The size of these tubes ranges from 2 cm to 3 cm and have a diameter of about 0.5 mm. Brine pockets could be formed from the freezing of brine tubes (Fig. I.3.10) [*Niedrauer and Martin*, 1979].

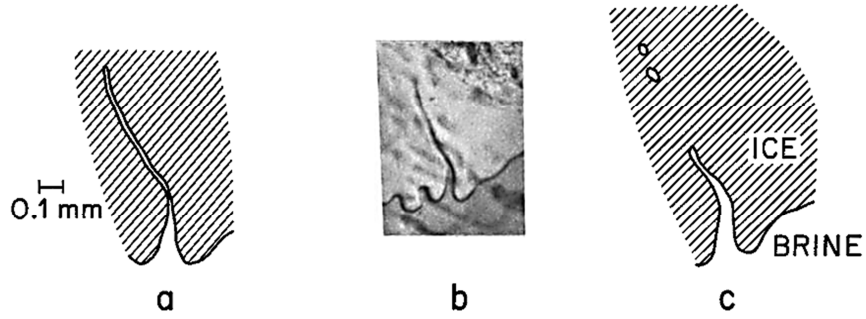

Figure I.3.10: Illustration of a brine tube pinching off into brine pockets (**a** and **c** are on the same scale, **b** is smaller). **b** is 1 hour after a situation, **c** 2 hours after a situation [*Niedrauer and Martin*, 1979].

As the ice warms, brine pockets enlarge along the boundaries between ice platelets, giving them an elongated shape. Furthermore, individual brine pockets begin to connect along these linear boundaries, resulting in additional elongation of the brine called "brine layer" [*Niedrauer and Martin*, 1979; *Perovich and Gow*, 1996].

Brine drainage channels consist of a large vertical tubular structure attended by smaller tributary tubes, the feeder channels. Figure I.3.11 is a schematic drawing of a brine drainage channel showing that the feed arms are made of inclusions forming conical patterns with apices on the main drainage channel and with semi angles between 40° and 54°.

They are distributed homogenously in space and their sizes are approximately similar but their spatial density at the initial stage of ice growth increases with increasing ice growth rate [*Tison and Verbeke*, 2001]. The predominant brine channel advances in a straight line toward the growing ice front. Although the brine channels form in the intersecting boundary areas of grains at an initial stage of ice growth, they may

subsequently advance vertically, independent of the grain orientation [*Wakatsuchi and Saito*, 1985; *Wakatsuchi and Kawamura*, 1987].

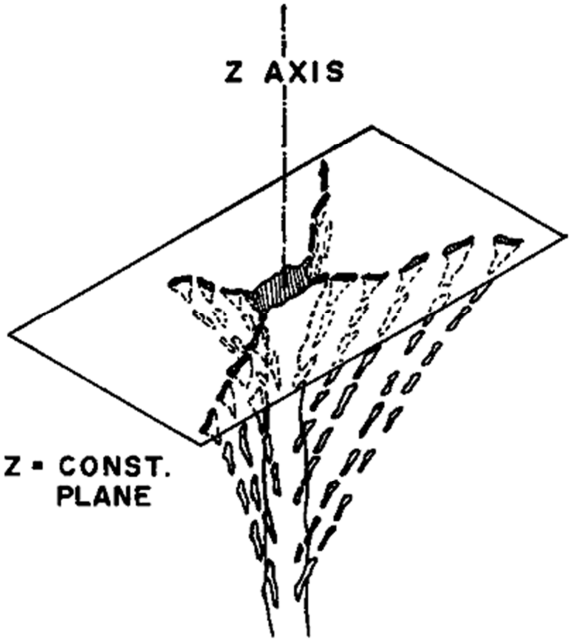

Figure I.3.11: Schematic drawing of a brine drainage channel and its feeder arms. Feeder arms are formed of inclusions inclined to the vertical at angles in the range of 40°-54° [*Lake and Lewis*, 1970].

In their theory of sea ice behaving as a "mushy layer", *i.e.*, a two-phases, two-components medium [*Feltham et al.*, 2006], *Wettlaufer et al.* [1997] associate the formation of brine channels with the initial stages of ice formation, where the increase of salt concentration in the medium drives, above a given density threshold (usually after a few centimeters of growth), the appearance of strong convective plums which emanate from channels within the ice and bring seawater back into the medium. These brine channels could persist on the full ice thickness.

3.4.4. Brine volume and brine salinity

From the *Assur* [1958] phase diagram where brine volume within sea ice is directly linked to its temperature and based on the continuity equations for a multi-phase sea ice mixture, *Cox and Weeks* [1983] derived a set of equations describing the relative brine volume fraction (V_b/V) as a function of ice temperature and salinity:

$$\frac{V_b}{V} = \left(1 - \frac{V_a}{V}\right) \frac{\rho_i S_i}{F_1(T) - \rho_i S_i F_2(T)} \qquad \text{(I.3.8)}$$

in which V, V_b, V_a is the volume of ice, brine and air, respectively, $F_1(T)$ and $F_2(T)$ are empirical polynomial functions based on the phase relations, S_i is the ice salinity and ρ_i is the density of pure ice (in g cm^{-3}), given as:

$$\rho_i = 0.917 - 1.403 \times 10^{-4} T \qquad \text{(I.3.9)}$$

with T in °C. $F_1(T)$ and $F_2(T)$ are given as:

$$F_i(T) = a_i + b_i T + c_i T^2 + d_i T^3 \qquad \text{(I.3.10)}$$

where the coefficients for different temperature intervals are listed in table I.3.3.

T (°C)	**a_1**	**b_1**	**c_1**	**d_1**
0 ≥ T > -2	-0,041221	-18,407	0,58402	0,21454
-2≥ T ≥ -22,9	-4,732	-22,45	-0,6397	-0,0174
-22,9> T ≥-30	9.899	1.309	55,27	0,7160
T (°C)	**a_2**	**b_2**	**c_2**	**d_2**
0 ≥ T > -2	0,090312	-0,016111	1,2291 x 10^{-4}	1,3603 x 10^{-4}
-2≥ T ≥ -22,9	0,08903	-0,01763	-5,330 x 10^{-4}	-8,801 x 10^{-6}
-22,9> T ≥-30	8,547	1,089	0,04518	5,819 x 10^{-4}

Table I.3.3: Coefficient for functions $F_1(T)$ and $F_2(T)$ for different temperature intervals from *Cox and Weeks* [1983] and *Leppäranta and Manninen* [1988] refitted by *Eicken* [2003].

The brine salinity, S_b, and density, ρ_b, can be approximated for temperatures above -23°C as:

$$S_b = \left(1 - \frac{54.11}{T}\right)^{-1} \times 1000 \qquad \text{(I.3.11)}$$

$$\rho_b = 1 + 8 \times 10^{-4} S_b \qquad \text{(I.3.12)}$$

with T in °C.

The volume of air, V_a, in sea ice is generally much lower than brine volume, which brings it to be ignored in many circumstances. For example, V_a is assumed to be equal to 0 in the estimation of brine volume by the equation I.3.8. However its relative amount can increase substantially in warmer ice where with the brine flushing, atmospheric air may replace brine.

According to the equation I.3.8, the brine volume is only depending on temperature and salinity. *Golden et al.* [1998] suggested that for a brine volume fraction p below a critical value $p_c \approx 5\%$, columnar sea ice is impermeable to fluid transport, while for p higher than 5%, brine or seawater can move through the ice. The relation of brine

volume to temperature and salinity implies p_c corresponds to a critical temperature $T_c \approx$ -5°C for $S \approx 5$. We refer to this critical behavior as the "law of fives". This is illustrated by the figure I.3.8 where sea ice permeability exhibits a marked transition in its fluid transport properties near T_c.

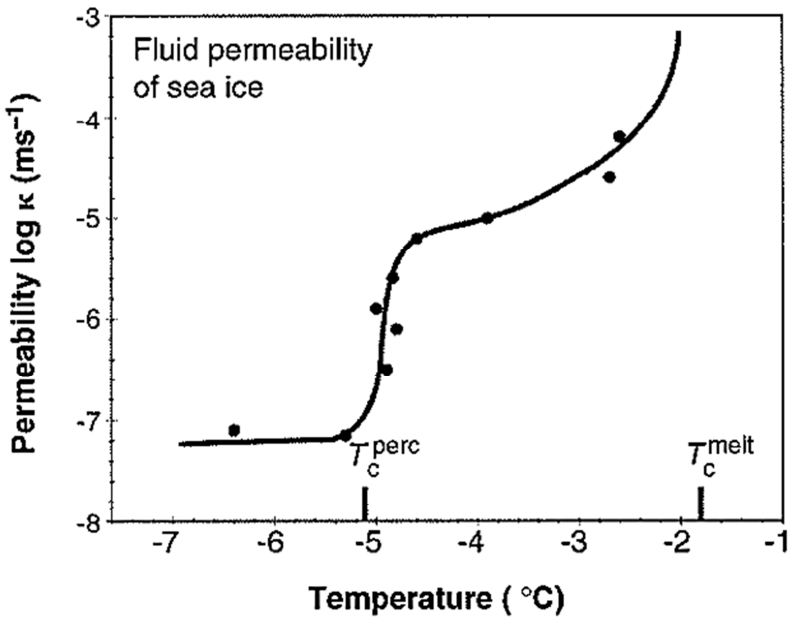

Figure I.3.8: Fluid permeability of thin young sea ice as function of surface temperature, from *Golden et al.* [1998].

According to *Weeks* [2010], the percolation threshold would be expected to vary with changes in the crystal structure of the ice, which is in agreement with recent field observations suggesting that granular ice show higher values of the percolation threshold than columnar ice [*Tison and Golden, pers. comm.*], a difference presumably caused by a more random distribution of brine inclusions.

3.4.5. Mean salinity and salinity profile

According to *Nakawo and Sinha* [1981], the salinity of freshly frozen sea ice decreases rapidly during the period after initial freezing. The major reduction in the brine content seems to occur within a week after the formation. As the freezing front moves downward, the salinity at a given depth attains a relatively stable value. Following the initial rapid desalination, the salinity of each level is quite constant but has however a tendency to further decrease slowly during the rest of the season (salinity variation of about 1 during the season).

The mean salinity results from all the desalination mechanisms integrated over the whole sea ice thickness. For first year sea ice, the mean salinity is about ~6 while it is

only about ~4 for multiyear sea ice [*Cox and Weeks*, 1974; 1975; *Nakawo and Sinha*, 1981; *Weeks and Ackley*, 1982; *Eicken*, 1992; 2003].

From the observed salinity distribution in a large number of station, *Eicken* [1992] identified 4 characteristic profile types (Fig. I.3.13):

- "C-type", shaped like a "C". This type is generally considered typical of growing young or first year ice. The high salinity in the surface layers may suggest upward brine rejection, but this feature is normally attributed to increased entrainment during rapid initial formation [*Cox and Weeks*, 1975], or incomplete drainage of the frazil layer [*Notz and Worster,* 2008]. Nevertheless, there appear to be some initial net upward transport of brine, as evidenced by observations of brine skims and high salinity frost flowers (*e.g.*, *Perovich and Richter-Menge* [1994]). The high salinity at the base is due to a higher contribution of seawater in the more porous skeletal layer.
- "S-type", similar to C-type. Salinity attains higher values at the top while stagnating or dropping to a minimum values at the bottom.
- "?-type" is the inverse of an S distribution, with a decrease in salinity toward the top. This type could be due to brine drainage above the freeboard in warmer ice.
- "I-type" is a linear salinity profile. Salinity is near-constant throughout the core or decreases steadily toward the bottom. This kind of profile may result from the brine flushing mechanism.

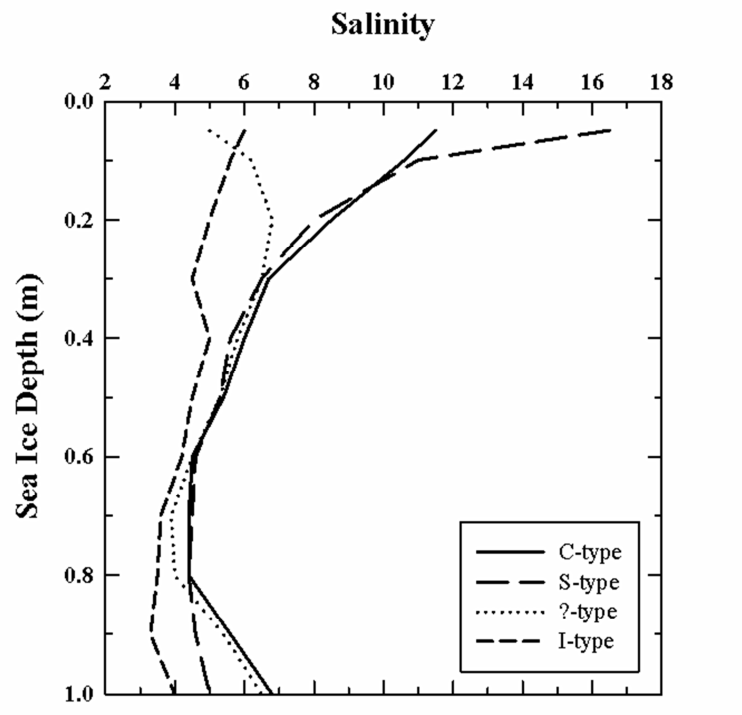

Figure I.3.13: Four characteristics salinity profile type, adapted from *Eicken* [1992]

3.5 Gas volume within sea ice

Gas volume in sea ice is generally much lower than brine volume, which bring it to be ignored in many circumstances. However its relative amount can increase substantially in warmer ice and its composition bears fundamental climatic implication. To date, there are still only very few studies dedicated to total gas content and gas composition measurements within sea ice, *e.g., Tison et al.* [2002] and *Thomas et al.* [2010]. The few gas composition measurements presently available within sea ice were obtained by *Matsuo and Miyake* [1966], *Tison et al.* [2002] and *Rysgaard et al.* [2008]. These studies were able to provide valuable estimates of total gas contents (dissolved and gaseous) in sea ice ranging from 2 to 22 mL STP[*] kg^{-1} of ice (similar that those predicted from theory of *Cox and Weeks* [1983]). These authors noted that the total gas content of their samples was lower that would be expected from instant freezing of seawater (ranging from 23 to 24 mL STP of air kg^{-1}), suggesting an expulsion of soluble gases away from the ice as it forms, through various processes such as, diffusion, enhanced solubility, bubble nucleation or convection.

The physical concentration of major and minor dissolved species in the brine pockets of sea ice has direct bearing on thermodynamic equilibrium. Salinity and temperature exert

[*] Standard temperature (0°C) and pressure (1 atm)

control on the thermodynamic parameters that describe the solubility of gases. Gas solubility increases as temperatures drops, while an increase of salinity has the opposite effect. For example, as discussed in chapter I.2, *Weiss* [1974] proposed a formulation to describe CO_2 solubility in seawater in the temperature range of 0°C and 45°C and in the salinity range of 0 to 45 (Eq. I.2.3). This is however far from the conditions encountered within sea ice where temperature and salinity reach values as high as -20°C and 150, respectively. Experimental and field data also exist for hypersaline solutions (S >> 45) but at 25°C or higher, from seawater evaporation system [*Thomas and Papadimitriou* [2003] and references therein].

In addition to the combined effect of temperature and salinity changes, the rejection of solute (gases, salts) from the consolidating ice matrix into the boundary layer leads to an increase in the concentration of dissolved gas above that of thermodynamic equilibrium of brine with air (*i.e.,* supersaturation). As result of dissolved gas supersaturation during freezing, gas bubble will nucleate and, eventually, be entrapped within the ice matrix [*Tsurikov*, 1979; *Killawee et al.*, 1998; *Tison et al.*, 2002; *Thomas and Papadimitriou*, 2003]. *Killawee et al* .[1998] and *Tison et al.* [2002] have computed gas supersaturation levels when air bubbles first appear. Gas supersaturation may indeed be calculated from the equation I.3.4 where the ratio between C_{iw} and C_{bw} (solute concentrations at the ice-water interface and in the bulk water, respectively) indicates the level of supersaturation. *Killawee et al.* [1998] found values from 2.2 to 2.5 while *Tison et al.* [2002] found values from 1.3 to 1.6. Following these authors, the amount of supersaturation appears to be controlled by the thickness of the boundary layer at the interface, itself depending on the convection regime within the reservoir. According to *Tison et al.* [2002], agitated conditions would reduce the boundary layer thickness, increase the concentration gradient therein and lower the supersaturation levels reached before bubble nucleation, all others things being equal.

According to *Tsurikov* [1979] and references therein, the processes controlling the total amount of gas entrapped in the sea ice cover can be divided into three groups: syngenetic, epigenetic and exogenetic.

3.5.1. Syngenetic processes

The syngenetic processes contain all processes connected with phenomena occurring under the ice at the time of its formation and growth.

The first of these processes was suggested by *Matsuo and Miyake* [1966]. It consists in the gas entrapment within the primary ice layer, at the time when it still consists of loose individual crystals. The gas is then presumed to be captured partly from the atmosphere and partly from the water.

A second process is the release of gas from solution during the further freezing of seawater under the combined effect of salinity increase and gas expulsion. According to the equation I.3.4, a slower freezing rate allows more time for gas diffusion across the boundary layer and hence a lesser build-up of gases at the ice-water interface. [*Killawee et al.*, 1998; *Verbeke,* 2005].

These two processes are also mentioned by *Mock et al*. [2002] and *Glud et al.* [2002] who suggested that, in their case, a major portion of the oxygen was present in the ice as gas bubble due to supersaturation as a result of increasing salinity during the freezing process.

Finally one should also consider, in areas with shallow continental shelf, the inclusion in the ice of gas bubbles which rise from the sea floor. This process was observed by *Killawee et al.*[1998] during artificial sea ice growth and by *Shakhova et al.* [2010] who observed large bubble of methane entrapped in landfast sea ice growing above the East Siberian Arctic Shelf.

3.5.2. Epigenetic processes

The epigenetic processes are all processes affecting the gas content and composition which occur within the ice cover itself.

The most important process is the release of gas from entrapped brine as the result of its further freezing. Otherwise, in the course of sea ice melt, brine can be drained downward out of the ice (see brine flushing). In this case, atmosphere air may be substituted for the brine.

On a smaller scale, the formation of water-vapor-filled pores during internal ice melting has to be considered. When melting occurs on the walls of brine pockets, the volume of meltwater that is produced is less than the volume of ice that melts. As a result, voids can be formed in the upper ends of the brine pockets. These voids are then quickly filled with vapor as the result of the partial evaporation of ice and brine. This was also observed by *Perovich and Gow* [1996] in multiyear ice.

A final process to be considered is the formation of gaseous inclusions produced through photosynthesis like suggested by, among others, *Glud et al.* [2002], *Mock et al*. [2002] and *Tison et al.* [2002].

3.5.3. Exogenetic processes

The exogenetic processes refer to all processes occurring at the upper boundary of the ice cover, leading to the entrapment of gas. It includes the capture of air during the snow ice formation and the possible migration of air inclusions from the snow cover into the underlying ice sheet. *Tsurikov* [1979] and reference therein have noted that, when a vertical temperature gradient is present in the ice cover, sublimation will occur at the warm ends of the air inclusions with the deposition of water vapor occurring at the cold ends. This causes the air bubbles to migrate in a direction opposite to the direction of heat flow.

3.5.4. Gas composition

According to *Carte* [1961], the composition of the gas phase would be controlled by diffusion processes between the water close to the interface and the air bubble.

Killawee et al. [1998] and *Tison et al.* [2002] suggested that the composition of air bubbles in the ice can be predicted by the equation I.3.3, assuming that it is determined by the ratio of composition of the gases at the ice-water interface which will differ from that in the bulk water. The initial concentrations in the sea ice bubbles, in the absence of biological bias, strongly differ from those in equilibrium with saturated seawater at 0°C [*Tison et al.,* 2002]. Therefore, diffusion should occur, according to differences in partial pressures between the air in the bubbles and the air dissolved in the interface water. Bubbles composition differs depending on the diffusion coefficient of different type of dissolved gases (1.18, 1.61, 2.08×10^{-5} cm^2 s^{-1} for CO_2, N_2 and O_2, respectively [*Stauffer et al.,* 1985]). This process occurs as long as sea ice is permeable and as bubbles are not isolated within the ice matrix. As a result, the ratio O_2: N_2 within sea ice (0.32 – 0.45) is generally lower than the ratio observed in seawater (0.56), because of the faster diffusion of oxygen [*Killawee et al.,* 1998; *Tison et al.,* 2002; *Verbeke*, 2005]. In the absence of bubble nucleation, a minimum value of 0.46 (ratio of O_2: N_2 in water) will be observed when diffusion processes are maximized, *i.e.*, when the growth rate is fast and/or the boundary layer is thick. Then, and as long as the basal part of the ice is

still permeable, gas composition will be affected by a post genetic diffusion towards the underlying seawater [*Verbeke, 2005*]. Also, the relative proportion of air bubbles (O_2: N_2 = 0.26) and of dissolved gases in the brine will affect the gas ratios, driving the latter towards even lower O_2: N_2 values.

Biological activity can also affect the gas composition within sea ice. Indeed, photosynthesis produces oxygen and consumes carbon dioxide while respiration has inverse effects.

Killawee et al. [1998] observed CO_2 concentration around 50000 ppm with a maximal value at 63000 ppm in artificial $CaCO_3$ saturated fresh water ice while the range of concentration observed by *Tison et al.* [2002] on artificial sea ice is between 18000 ppm and 57000 ppm. The first measurement on natural sea ice was provided by *Matsuo and Miyake* [1966] with a maximal value at 24000 ppm. *Tison et al.* [2002] suggested that two major biases could explain these high concentrations: (i) the precipitation of calcium carbonate observed during the experiment could promote a degassing of CO_2. (ii) an uncontrolled sustained bacterial activity could also produce CO_2.

However, more recent work has put forward a potential methodological bias in all these measurements, since these were all obtained using gas extraction under vacuum [*Tison et al.*, 2002; *Verbeke*, 2005] and at very low temperature, which surely must have profoundly affected the carbonate expulsion from the brine system. This point will be more developed in the chapter IV of this work.

3.5.5. Potential gas transport

Gas transport through such a medium as sea ice is extremely complex. Gas can move through sea ice with the brine displacement. However, gas also has the potential to move diffusively as a dissolved gas through brine and in the gaseous phase.

The diffusive transport is expected to be prevailing only when fluid transport is minimal. Besides, experimental attempts to measure gas diffusivity through sea ice cannot separate diffusive transport from convective transport caused by brine movement. Below the liquid permeability threshold [*Golden et al.*, 1998; 2007], convective liquid transport is expected to be minimal and diffusive transport maximal.

Gosink et al. [1976] presented the first measurements of gas migration through arctic pack ice at temperature ranging from -15°C to -7°C but unfortunately without reporting

on the ice salinity. Therefore, it is difficult to estimate the ice permeability during these experiments. Their results ranged from 10^{-7} cm^2 s^{-1} atm^{-1} for SF_6 at -15°C and 10^{-5} cm^2 s^{-1} atm^{-1} for CO_2 at -7°C. Their result indicates that gas migration through sea ice can still be an important factor in ocean-atmosphere winter communication, even when the surface temperature is below -10°C.

More recently, *Loose et al.* [2009] measured the rate of O_2 and SF_6 exchange, *k*, during conditions of fractional ice cover and found that gas flux through ice pack may not scale linearly with the open water area. For example, in a condition of 100% open water, $k_{100\%}$ of O_2 and SF_6 is at 1.02 and 0.83 cm h^{-1}, respectively while at 15% of the ice cover, $k_{15\%}$ was about 25% of $k_{100\%}$.

Loose et al. [2011] measured diffusion rates of O_2 and SF_6 in artificial columnar sea ice in a temperature range of -4°C to -12°C. The observed diffusivities were higher than those of *Gosink et al.* [1976] and ranged from 1.3 x 10^{-4} cm^2 s^{-1} (±40%) for SF_6 and 3.9 x 10^{-5} cm^2 s^{-1} (±41%) for O_2. These experiments provide us, with a first order of magnitude, gas diffusivities in sea ice just above the brine permeability threshold.

As ice warms, much of the brine will drain, leaving an air-filled pore space. As ice porosity increases into spring, the gas permeability is expected to increase, which is supported by field measurements of gas fluxes above the surface of sea ice [*Delille*, 2006; *Delille et al.*, 2007; *Nomura et al.*, 2010b; 2010a; *Miller et al.*, 2011; *Papakyriakou and Miller*, 2011]. Under these conditions, gas diffusion through snow and melting sea ice may be much more rapid than the rates already observed [*Loose et al.*, 2011].

According to *Gosink et al.* [1976] and *Loose et al.* [2011], the porosity threshold for gas transport may be lower than for fluid transport [*Golden et al.*, 2007]. If the gas transport threshold is at lower temperature, then diffusive transport could allow gas exchanges earlier in the spring and later in the fall or even during winter.

4. Carbon dioxide dynamics within sea ice: state of the art

According to *Verbeke* [2005] there are very few studies on sea ice gas composition and more particularly on carbon dioxide. Most carbon cycle research has not considered the possibility of either direct air-sea gas exchange in the presence of sea ice or indirect air-ice-sea gas exchange, where sea ice actively participates in CO_2 transfer [*Tison et al.*, 2002; *Bates and Mathis*, 2009]. Therefore, global and regional budgets of air-sea CO_2 exchange have ignored ice-covered regions [*Bates and Mathis*, 2009; *Takahashi et al.*, 2009; *Arrigo et al.*, 2010b], relying instead on the assumption that sea ice cover is impermeable to gases. However, recent observations using both tower-based micrometeorological approaches and chamber sampling indicate that uptake and evasion of CO_2 does occur over sea ice [*Semiletov et al.*, 2004; *Delille*, 2006; *Zemmelink et al.*, 2006; *Semiletov et al.*, 2007; *Nomura et al.*, 2010b; 2010a; *Miller et al.*, 2011; *Papakyriakou and Miller*, 2011]. The community is still uncertain about the expected magnitude of the fluxes because observed rates of exchange differ between methodologies (Table I.4.1.).

4.1 CO_2 fluxes measurements

4.1.1. Accumulation chamber vs. Eddy correlation

Two techniques are mainly used to measure the CO_2 fluxes at the ice interface with the atmosphere: the technique of the chamber of accumulation and the eddy covariance techniques.

The chamber of accumulation is usually a metal cylinder closed at the top and connected in a closed loop to a gas analyzer. The measurement of the pCO_2 is carried out in the chamber for a given time (typically 15-20 min). The flux is then computed from the slope of the linear regression of pCO_2 against time ($r^2>0.99$) according to *Frankignoulle* [1988]. The chamber technique is easy to set above the ice as it does not require much heavy equipment and the time necessary for the measurement is quite short. Flux measurements derived from chamber-based techniques have a limited spatial (0.5 – 1m^2) and temporal (minutes – hours) extent and may not be representative of the ecosystem as a whole. The measurements are potentially biased from attenuation of natural turbulent mixing, or anomalous chamber heating, or pressure gradients [*Oechel et al.*, 1998].

Eddy covariance is a widely used technique that integrates gas fluxes over large areas. A surface flux can be measured by quantifying the covariance between vertical fluctuations in wind speed, mass and energy. It relies on adequate turbulent mixing, high-frequency sensor response, high sensor sensitivity to the fluctuating components and the adequate spatial or temporal averaging. Therefore, this technique requires a more heavy and expensive material on the field and a more consistent data processing. But, all these requirements and assumptions could be compromised, for example, when in complex terrain and under periods of low turbulent mixing and stable atmospheric conditions [*Oechel et al.*, 1998; *Papakyriakou and Miller*, 2011].

As these techniques have different spatial and temporal scales, the information obtained using one measurement technique may not be quantitatively similar to the information derived from the other technique. The information gathered from each technique is complimentary and essential for understanding the spatial and temporal patterns in fluxes. However, each technique has potential weaknesses which have been thoroughly described in the literature [*Oechel et al.*, 1998] and reference therein.

There is a debate among eddy covariance users about the accuracy of the use of an open path gas analyzer instead of a closed path in winter time. Although many studies have shown excellent agreement between open-path-derived CO_2 fluxes and those derived from other eddy covariance systems, other studies have shown that open-path systems can underestimate the CO_2 flux (*i.e.*, underestimate efflux and overestimate uptake) [*Papakyriakou and Miller*, 2011] and references therein. This could be due to: (i) sensor heating during winter season applications, (ii) lens contamination with dust and water during unattended deployments or (iii) a cross-sensitivity between the open-path's concentration measurements of CO_2 and H_2O in marine applications [*Papakyriakou and Miller*, 2011]. *Burba et al.* [2008] proposed an empirical relationship and procedures to overcomes issues related to the open path analyzer heating in cold temperature conditions.

4.1.2. Published studies

There is a growing body of evidence that sea ice could play a role in CO_2 dynamics in polar oceans. Backbone idea is that there is a temperature threshold above which the ice is permeable, allowing exchanges between sea ice and atmosphere but also between sea ice and the underlying seawater. It has been demonstrated that the ice could be

considered as permeable when brine volume: ice volume ratio (usually denoted as brine volume) is above 5%. Sea ice with an average salinity of 5 reaches this threshold at -5°C [*Gosink et al.*, 1976; *Golden et al.*, 1998; 2007]. This finding has been reported as the "law of five". The brine volume can be calculated from T and S data with the equations provided by *Eicken* [2003] and references therein.

The first measurements of CO_2 flux between sea ice cover and the atmosphere were carried out by *Semiletov et al.* [2004] on melting land-fast sea ice in June, near Point Barrow. A flux ranging from -39 mmol m^{-2} d^{-1} to + 39 mmol m^{-2} d^{-1} was measured using the eddy covariance technique with an open-path gas analyzer. The chamber technique was also used to measure a flux ranging from -4 mmol m^{-2} d^{-1} to -51 mmol m^{-2} d^{-1}. He suggested that melt-ponds and open brine channels within sea ice represent a significant sink for atmospheric CO_2, without discussing the difference between the two techniques used. The magnitude of the fluxes was ascribed to the increase of the biological activity.

Zemmelink et al. [2006] also reported CO_2 flux using eddy covariance technique, with an open-path gas analyzer, on antarctic pack ice in the Weddell Sea through early summer. The fluxes were in the same order of magnitude than *Semiletov et al.* [2004] ranging from -4 mmol m^{-2} d^{-1} to -27 mmol m^{-2} d^{-1}. *Zemmelink et al.* [2006] argued as well that biological activity could explain the magnitude of the fluxes. The uncertainty of the eddy covariance measurements presented in this study was estimated to 10-30%, which is comparable to the error estimation of previous experiments conducted at sea and slightly higher than the uncertainty of land-based covariance flux measurements, which is typically of 10-15% [*Zemmelink et al.*, 2006] and reference therein. During the same survey, *Delille and co-workers* (*i.e., Delille* [2006]) measured CO_2 fluxes, ranging from -4 mmol m^{-2} d^{-1} to +2 mmol m^{-2} d^{-1} using the chamber technique. These fluxes were related to the brine pCO_2 according to the sea ice thermodynamical evolution and biological activity. This link is also suggested by *Nomura et al.* [2010b] and [2010a] who measured CO_2, from +0.7 mmol m^{-2} d^{-1} to -1 mmol m^{-2} d^{-1} in first year land-fast sea ice in Barrow (US) and from +1 mmol m^{-2} d^{-1} to -3.6 mmol m^{-2} d^{-1} in land-fast sea ice in Hokkaido (Japan). Both field measurements were carried out using the chamber technique.

In the Canadian Arctic Archipelago, *Papakyriakou and Miller* [2011] measured air-ice CO_2 fluxes using the eddy covariance from early spring to the formation of melt-ponds.

These measurements ranged from +86.4 mmol m^{-2} d^{-1} to -259 mmol m^{-2} d^{-1} and are larger than previously reported values using the chamber technique [*Semiletov et al.*, 2004; *Delille*, 2006; *Zemmelink et al.*, 2006; *Nomura et al.*, 2010b; 2010a] or for those measured using an open-path gas analyzer [*Semiletov et al.*, 2004; *Zemmelink et al.*, 2006]. It must be noted that *Semiletov et al.* [2004] and *Zemmelink et al.* [2006] did not used the correction proposed by *Burba et al.*[2008] while *Papakyriakou and Miller* [2011] did so. This correction is applied for open path in cold weather conditions, where the surface of the instrument became substantially warmer than ambient due to electronics and radiation load during daytime while at night, radiative cooling moderated temperature increases in the path. This affect heat sensible flux inside the path and then assessment of CO_2 fluxes [*Burba et al.*, 2008]. According to *Papakyriakou and Miller* [2011] uptake of CO_2 generally occurred for wind speeds larger than 6 m s^{-1} and corresponded to local maxima in temperature at the snow-ice interface and net radiation, while efflux occurred under low wind speeds and period of local minima in temperature and net radiation. *Heinesch et al.* [2009] carried out the first study on CO_2 fluxes using a closed path during the arctic winter and also suggested that wind speed can act as a trigger for effluxes. The fluxes were measured on landfast sea ice, in Barrow and ranged from -86 mmol m^2 d^{-1} to +128 mmol m^2 d^{-1}.

Hence, the ventilation of the snow pack, pressure pumping associated to wind speed and the increase of permeability acts to increase gases transfers at the ice interface with the snow and/or the atmosphere.

Miller et al. [2011] collected an integrated data set CO_2 fluxes from deep winter (December 2003) into spring (June 2004) at a single location on land-fast sea ice in the Beaufort Sea. The fluxes ranged from + 345.6 mmol m^{-2} d^{-1} to -1123 mmol m^{-2} d^{-1} using the eddy covariance technique with an open path gas analyzer. The largest fluxes in both directions often occurred during periods of high wind speed and when the temperature was at a relative maximum or increasing. The high wind speed accelerates vertical exchanges of CO_2 and ventilates the snow cover as indicated by *Papakyriakou and Miller* [2011] and *Heinesch et al.* [2009]. The relationship to temperature is consistent with the ice becoming more permeable as it warms up and brine volume increases [*Gosink et al.*, 1976; *Golden et al.*, 2007].

While all these studies document fluxes over thick slow growing or decaying ice, CO_2 fluxes were never measured on natural thin young growing sea ice, while experiments

on artificial sea ice suggest potential fluxes to the atmosphere ranging from +1 mmol m^{-2} d^{-1} to -4 mmol m^{-2} d^{-1} [*Nomura et al.*, 2006]. This is a significant gap in the current knowledge of CO_2 fluxes seasonal change over the whole growth/decay sea ice cycle.

4.1.3. Summary

Studies	Techniques	CO_2 fluxes (mmol m^2 d^{-1})	Place	Period of the year	Sea ice conditions
***Semiletov et al.* [2004]**	EC – open path	-39 to +39	Arctic - Barrow	June	Landfast sea ice, melt ponds
	chamber	-51 to -4			
***Zemmelink et al.* [2006]**	EC – open path	-27 to -5	Antarctica – Weddell Sea	Nov. – Dec.	Pack ice /slush
***Delille* [2006]**	chamber	-4 to +2	Antarctica – Weddell Sea	Nov. – Dec.	Pack ice, same area as *Zemmelink et al.* [*2006*]
***Nomura et al.* [2006]**	chamber	-4 to +1	Artificial sea ice		
***Nomura et al.* [2010b]**	chamber	-1 to +1	Arctic - Barrow	May	Landfast sea ice
***Nomura et al.* [2010a]**	chamber	-4 to +1	Japan – Bay of Hokkaido	Feb. - March	Landfast sea ice
***Heinesch et al.* [2009]**	EC – closed path	-0.8 to +1.4	Arctic - Barrow	March - April	Landfast sea ice
***Papakyriakou and Miller* [*2011*]**	EC – open path*	-259 to +86	Arctic – center of the Arctic Archipelago	May - June	Landfast sea ice
***Miller et al.* [2011]**	EC – open path*	-1123 to +346	Arctic – Beaufort Sea	Dec. to June	Landfast sea ice

Table I.4.1: Synthesis of current knowledge about CO_2 fluxes at sea ice interface with the atmosphere.

* designed studies using the correction proposed by *Burba et al.* [*2008*]

4.2 Brine pCO_2

Delille and co-workers (*i.e., Delille* [2006]) and *Nomura et al.* [2010b], [2010a] established the link between CO_2 fluxes and CO_2 dynamics within brines. Inorganic carbon dynamics in sea ice is controlled by a mixture of biotic and abiotic processes interacting in complex ways that change as the season's progress. The biogeochemical processes that ultimately control the fate of carbon in sea ice are still poorly understood [*Thomas and Dieckmann*, 2010].

4.2.1. Biotic processes

Primary production could play a significant role in brine pCO_2 dynamics as spring progresses [*Delille*, 2006; *Delille et al.*, 2007]. *Delille et al.* [2007] observed undersaturated brine pCO_2 in landfast sea ice in the coastal area of Adélie Land, Antarctica. The high biological activity promoted the decrease of the brine pCO_2. *Delille and co-workers* (*i.e., Delille* [2006]) and *Delille et al.* [2007] provide tentative estimate of sea ice primary production by using temporal changes of oxygen or biomass of autotrophic cells to in antarctic sea ice and found that primary production account for the same magnitude of CO_2 decrease than the increase of temperature and related brine dilution or calcium carbonate dissolution.

Heterotrophic remineralization by bacteria [*Deming*, 2010] could promote to the high pCO_2 values in sea ice brine [*Miller et al.*, 2011]. Some studies showed evidence that significant bacterial activity can occur in sea ice during the winter [*Junge et al.*, 2004; *Wells and Deming*, 2006]. Nevertheless, respiration, like bacteria growth, is a temperature-dependent process [*Deming*, 2010]. Therefore, increase of the temperature might promote the respiration and therefore the increase of the pCO_2.

At the interface of the ice with the atmosphere, surface communities may develop, benefitting of high light levels and nutriments from seawater flooding. Melting snow, ice and flooding seawater covering sea ice is known to accommodate highly productive algae community and might be responsible for the majority of sea surface productivity in antarctic sea ice [*Legendre et al.*, 1992]. These surface communities can exchange CO_2 directly with the atmosphere. As they can be highly productive, the uptake of CO_2 may be significant. Indeed, *Semiletov et al.* [2004], *Zemmelink et al.* [2006] and

Nomura et al. [2010b] reported significant CO_2 fluxes over melt ponds and related theses fluxes to surface communities primary production.

4.2.2. Abiotic processes

As sea ice forms and grows, sea ice impurities (*e.g.*, gases, ionic species, particles) are partly rejected from the sea ice and partly trapped within the sea ice structure (*cf.*, Ch. I.3). Rejection of DIC and CO_2 was documented during sea ice growth in experimental ice tank studies [*Killawee et al.*, 1998; *Papadimitriou et al.*, 2004]. It can also be exported from the ice to the underlying water with draining ice brines [*Rysgaard et al.*, 2007; *Loose et al.*, 2009; *Rysgaard et al.*, 2009]. *Gibson and Trull* [1999] and *Rysgaard et al.* [2007; 2009] observed CO_2 supersaturation and high DIC concentration below antarctic and arctic sea ice that can be due to CO_2 rich brines. Decrease of the temperature of brine trapped within sea ice reduces the solubility of CO_2 and pCO_2 (thermodynamic effect). However, increase in brine salinity related to temperature decrease leads to significant increase in DIC and pCO_2 that outweighs the thermodynamic effect (*cf.*, Ch. I.2). This is what *Delille and co-workers* (*i.e.*, *Delille* [2006]) called the concentration effect.

Associated to this temperature decreases and salinity increases, significant changes in the mineral-liquid thermodynamic equilibrium can occur, leading to a sequential mineral precipitation. Ikaite[3], a hexahydrate polymorph of calcium carbonate ($CaCO_3.6H_2O$), begins to precipitate at -2.2°C, mirabilite ($Na_2SO_4.\ 10H_2O$) below -8°C. Hydrohalite ($NaCl.2H_2O$) precipitates below -26°C, while potassium and magnesium salts precipitate below -34°C [*Assur*, 1958; *Richardson*, 1976; *Marion*, 2001].

Discovery of ikaite within natural sea ice were reported in Antarctica [*Dieckmann et al.*, 2008] and then in arctic sea ice [*Dieckmann et al.*, 2010]. The authigenesis of ikaite in natural sea ice is poorly understood. Little is known about the spatial and temporal occurrence of ikaite precipitates in sea ice, but recent discovery of ikaite in sea ice from both hemispheres indicates that ikaite precipitation is not a localized phenomenon.

According to *Selleck et al.* [2007], precipitation of ikaite is limited by its stability field to near-freezing temperatures , lower than +3°C [*J L Bischoff et al.*, 1993a]. Ikaite was

[3] Ikaite is a monoclinic crystal structure, its density is about 1.8 g cm^{-3} [*Bischoff et al.*, 1993a]

mainly found in anoxic marine sediments of cold-climate shelves and estuaries or in deeper oceanic basins and in lacustrine and terrestrial spring systems [*Kennedy et al.*, 1987; *J L Bischoff et al.*, 1993b; *Whiticar and Suess*, 1998; *Selleck et al.*, 2007] indicating that ikaite can precipitate from a wide range of water chemistries.

Nevertheless, ikaite precipitation in a natural environment requires several conditions other than low temperature. Indeed, seawater is undersaturated with respect to ikaite at temperate temperatures but seawater rapidly approaches saturation near 0°C. Nevertheless, ikaite cannot form directly by the cooling of seawater [*J L Bischoff et al.*, 1993a]. The solution from which it forms must, at least temporarily, be supersaturated with respect to ikaite. This supersaturation is most likely to occur near 0°C but even then, external additions of either Ca^{2+} or HCO_3^- are required [*J L Bischoff et al.*, 1993a]. Furthermore, natural occurrence of ikaite requires conditions which also inhibit the precipitation of more stable anhydrous forms of calcium carbonate. Calcite ($CaCO_3$) is the most stable polymorph of calcium carbonate. The other polymorphs are the minerals aragonite and vaterite. Calcite, aragonite and vaterite forms are much less soluble than ikaite and are supersaturated in solutions saturated with respect to ikaite. Ikaite will be stabilized under conditions that inhibit the nucleation and growth of the anhydrous forms of $CaCO_3$. Conversely, under conditions favorable to crystallization of anhydrous forms, ikaite will not precipitate [*J L Bischoff et al.*, 1993a]. Orthophosphate is a well-known inhibitor of both crystal growth and dissolution of calcite and aragonite [*Walter and Hanor*, 1979; *J L Bischoff et al.*, 1993a; *Lin and Singer*, 2006], at concentrations of orthophosphate above 5 µM [*J L Bischoff et al.*, 1993a], but it does not interact with ikaite [*J L Bischoff et al.*, 1993a; *Buchardt et al.*, 2001]. Accordingly, high phosphate concentration have been linked to ikaite precipitation in antarctic and arctic sediments [*Kennedy et al.*, 1987; *Whiticar and Suess*, 1998] and others various environments [*J L Bischoff et al.*, 1993b; *Buchardt*, 2004; *Selleck et al.*, 2007].

Therefore, precipitation of ikaite is promoted by alkaline conditions and elevated phosphate concentrations and its stability field seems to be limited to near-freezing temperatures. Indeed, *Whiticar and Suess* [1998] and *Dieckmann et al.* [2010] found that samples of natural ikaite disintegrate within minutes to hours into a mush of water and small whitish crystals of vaterite and/or calcite when exposed to atmospheric conditions.

$CaCO_3$ precipitation receives a growing attention as *Rysgaard et al.* [2007; 2009] suggested that calcium carbonate precipitation in sea ice could act as a significant sink for atmospheric CO_2. This abiotic pump would result from the high DIC: TA ratio of brine expelled from sea ice during the ice growth and brine drainage as a consequence of $CaCO_3$ precipitation. Precipitation of 1 mole of $CaCO_3$ transfers HCO_3^- to the CO_2 pool, decreasing DIC by 1 mole and TA by 2 moles (Eq. I.2.48). According to *Rysgaard et al.* [2007], this pump could represent a downward transport of 0.2 - 0.5 PgC yr^{-1} out of the surface ocean. However, according to *Delille and co-workers* (*i.e., Delille* [2006]), the role and significance of the $CaCO_3$ formation in sea ice with regard to atmospheric CO_2 depend on sea ice permeability and therefore on conditions and timing of this precipitation. Indeed, *Munro et al.* [2010] suggested that the precipitation of calcium carbonate could drive CO_2 fluxes to the atmosphere. Laboratory and field experiments using carbon isotope fractionation to trace calcium carbonate precipitation were inconclusive [*Papadimitriou et al.*, 2004; *Munro et al.*, 2010] due to contradictory impacts of calcium carbonate precipitation compared to the impact of the biology.

The figure I.4.1 illustrates the different possible interactions between calcium carbonate precipitation and sea ice physics scenarios and how they relate to air-sea CO_2 fluxes. Calcium carbonate could precipitate in high salinity and low temperature conditions, in late fall or winter, in the upper layers of sea ice, while brines channels are closed (Fig. I.4.1, case A). The CO_2 produced could not be released to the atmosphere or migrated through the ice structure. During spring and summer, the $CaCO_3$ is dissolved by the melting sea ice and consumes CO_2 in the same proportion as it was produced. The balance of both processes is nil in term of air-ice CO_2 fluxes. The precipitation of $CaCO_3$ could also occur at relatively low salinity and high temperature, when the ice is still permeable, or in the skeletal layer (Fig. I.4.1, case B). In this case, the fate of the carbonate minerals appears to be crucial to assess CO_2 transfer. (i) The precipitate remains trapped in the ice while the CO_2 is released to the water column. This segregation of the impurities enhances CO_2 concentration at the ice-water interface [*Killawee et al.*, 1998] and acts as a source of CO_2 for the underlying seawater and the atmosphere.(ii) But if only the brine enriched in pCO_2 is expelled into the water column and trapped under the pycnocline, the dissolution of the carbonate minerals in spring and summer would consume CO_2 and drive a net CO_2 uptake within the ice. (iii) The precipitate and the CO_2 produced are both released in the underlying seawater. The

impact on air-sea CO_2 fluxes will then depend on the ratio of the amount of entrained dissolved CO_2 compared to the amount of sinking carbonate mineral. (iv) The carbonate precipitate sinks while the salt remains trapped in the sea ice brine. In spring and summer, the CO_2 is released to the atmosphere so that the ice acts as a source of CO_2 to the atmosphere.

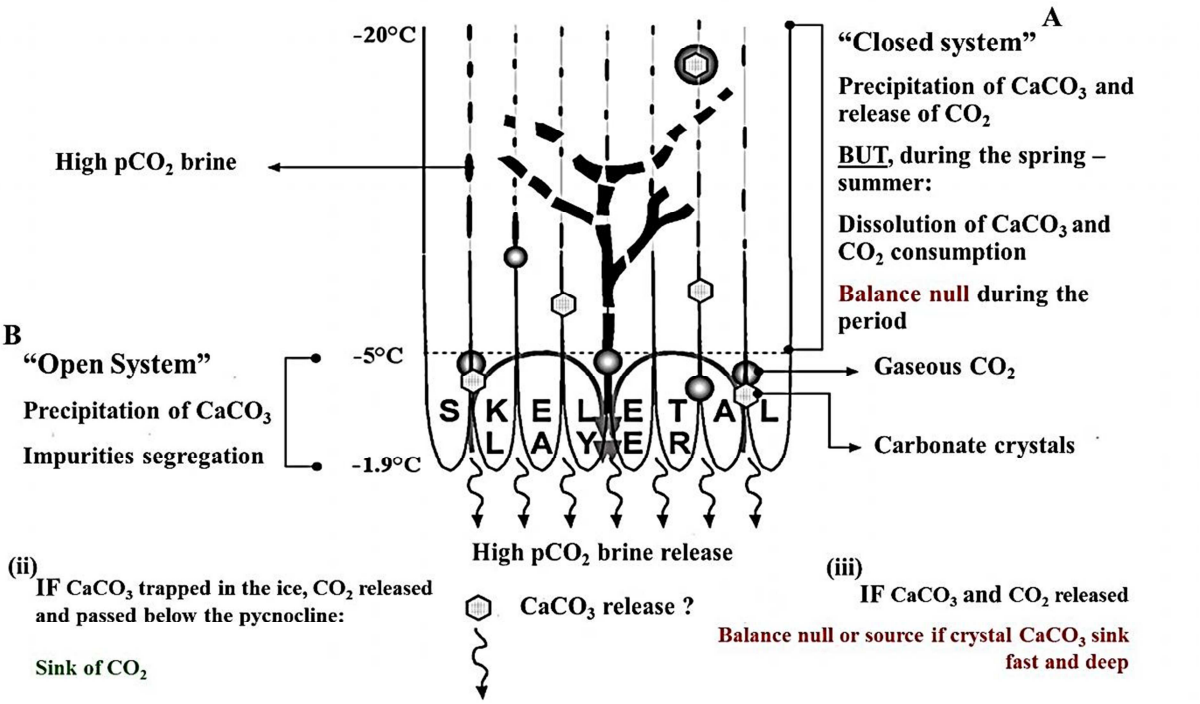

Figure I.4.1: Fate of carbonate minerals precipitated within sea ice [*Delille*, 2006].

As sea ice melts during spring and summer, the carbonate minerals trapped within sea ice dissolved as the temperature increases and the salinity decreases within sea ice or in the underlying seawater. This dissolution of carbonate minerals in spring and summer was observed in Arctic by *Jones et al.* [1983] and *Rysgaard et al.* [2007; 2009], and leads to a decrease of pCO_2 that may act as a significant sink of CO_2.

Rejection of CO_2 rich brines into the underlying layer, as a result of brine concentration and drainage, or/and $CaCO_3$ precipitation can be an efficient pump of CO_2 from the atmosphere. Indeed, the brine expulsion associated to sea ice formation leads to the formation of dense water [*Shcherbina et al.*, 2003; *Skogseth et al.*, 2004]. The sinking of dense water is the main driver of deep-water formation [*Bonisch and Schlosser*, 1995]. Nevertheless, the efficiency of CO_2-rich brines rejection as a sink of CO_2 for the atmosphere depends on the fraction of brine (denoted α) that passed below the pycnocline [*Rysgaard et al.*, 2007]. Assessment of α is therefore crucial to assess the

efficiency of the abiotic processes as sink for the atmospheric CO_2. However, α is still poorly constrained and assessment of α is proven difficult [*Rysgaard et al.*, 2007].

4.3 Synthesis

The figure I.4.2 illustrates the sequence of events controlling the dynamics of inorganic carbon within sea ice. In the late summer and fall, during the initial growth of sea ice and the subsequent decrease of ice temperature, impurities are partly rejected from the sea ice and partly trapped within brine. Brine salinity increases significantly and becomes supersaturated in CO_2 with respect to the atmospheric concentration [*Papadimitriou et al.,* 2004] while the brine expulsion causes the increase in salinity and DIC concentration in the underlying seawater [*Rysgaard et al.*, 2007; 2009]. However, none CO_2 fluxes were reported during the initial sea ice growth, excepted *Nomura et al.* [2006] who carried out artificial sea ice experiment that suggests potential fluxes of CO_2 to the atmosphere, associated to an increase in DIC concentration and a potential precipitation of $CaCO_3$.

The superposition of a snowpack above the initial brine-enriched layer creates a new situation which prevails for most of the winter season. Brine may come into equilibrium with the atmosphere and outgassing could occur through the snowpack. This period might be characterized by episodic CO_2 release driven by wind pumping events [*Heinesch et al.*, 2009; *Miller et al.*, 2011; *Papakyriakou and Miller*, 2011].

During winter, as the air and ice temperature decreases, the brine volume of surface sea ice reduce and the sea ice permeability decreases, hampering ice-atmosphere gas exchanges. In addition to the brine volume contraction, brine salinity, pCO_2 increases and then precipitation of calcium carbonate could occur. This precipitation will promote high level of pCO_2 within sea ice brine [*Miller et al.*, 2011].

In early spring, as temperature rises, sea ice melt and brine volume increases, so that the ice becomes permeable [*Golden et al.*, 2007]. Thereafter, brine at the surface of the ice can exchange gases with the atmosphere. Nevertheless, the rate of gas exchange may be controlled by the snowpack. During the first episodes of warming, brine could be supersaturated in CO_2 compared to the atmosphere and CO_2 outgassing from the ice to the atmosphere could therefore occur [*Delille*, 2006]. However, brines are quickly diluted by meltwater as the ice temperature increases, promoting pCO_2 decreases and dissolution of carbonate minerals trapped in sea ice. In addition to the increase of ice

temperature, light availability and brine transport trigger sympagic algae bloom and related increase of primary production. Therefore, brines become strongly undersaturated [*Delille*, 2006; *Delille et al.*, 2007]. Influx of CO_2 from the atmosphere to the ice could then be observed [*Semiletov et al.*, 2004; *Delille*, 2006; *Zemmelink et al.*, 2006; *Delille et al.*, 2007; *Nomura et al.*, 2010b; 2010a; *Papakyriakou and Miller*, 2011].

Under the ice, sea ice melting leads to the stratification of the water column. This meltwater is depleted in DIC and potentially enriched in TA due to the dissolution of calcium carbonate. Therefore supply of meltwater to the water column will results in an increase in TA and a decrease in pCO_2 of the top of the water column. This enhances air-sea CO_2 fluxes [*Rysgaard et al.*, 2009; *Shadwick et al.*, 2011]. *Jones et al.* [*1983*], *Rysgaard et al.* [2007; 2009] observed TA excess in the Arctic while *Jones et al.* [2010] reported TA excess in surface waters of the Southern Ocean.

As sea ice break-up, light availability increases in the surface waters triggers pelagic primary production [*Arrigo et al.*, 2010a], and promote enhanced decreases of pCO_2 of the surface water (*e.g.*, *Shadwick et al.* [2011]).

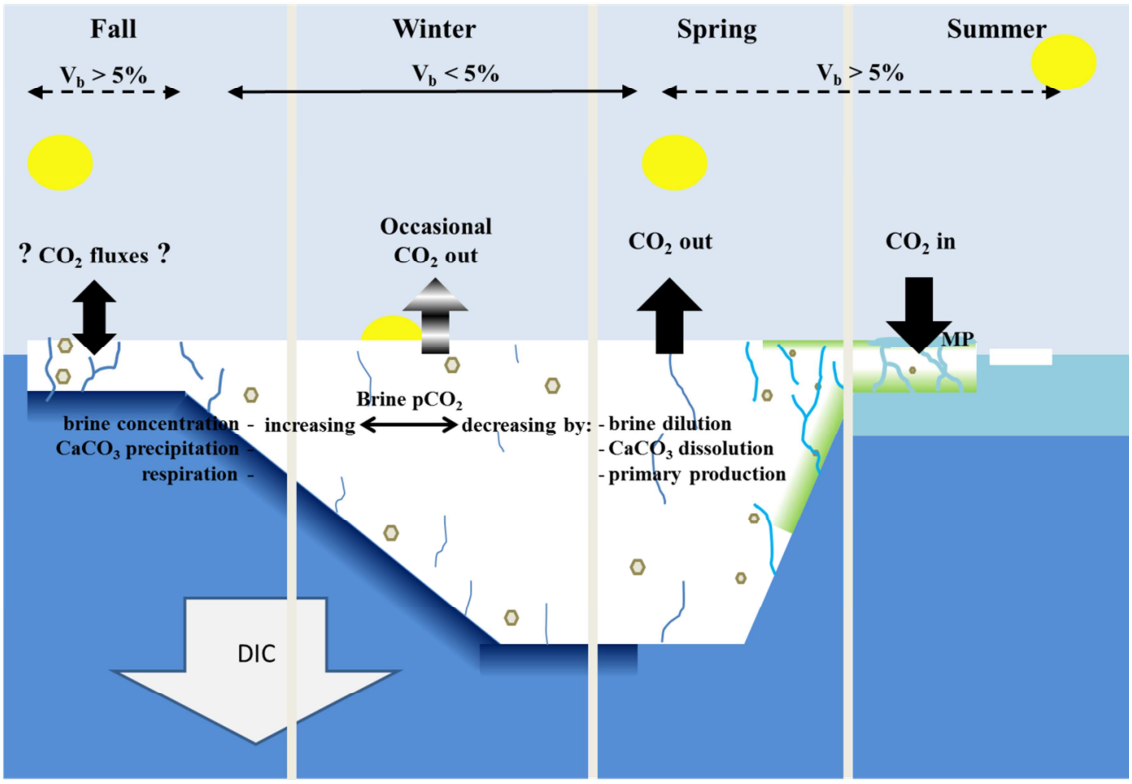

Figure I.4.2: Sequential evolution of several processes affecting the pCO_2 dynamics within sea ice. The green area corresponds to the sympagic communities, **MP** corresponds to melt ponds and the brown diamonds correspond to ikaite crystals.

5. Aims

As discussed before, to our best knowledge, only few studies of inorganic carbon dynamic within natural sea ice were carried out [*Gleitz et al.*, 1995; *Rysgaard et al.*, 2007; 2009; *Munro et al.*, 2010; *Nomura et al.*, 2010b; *Miller et al.*, 2011] and only two reported direct measurements of pCO_2 [*Delille*, 2006; *Delille et al.*, 2007].

Hence, we aim to contribute to a better understanding of the dynamics of inorganic carbon within sea ice. We intend to describe the influence of biotic and abiotic processes in relation to physical properties of sea ice (temperature, salinity) on the inorganic carbon dynamic and to assess the impacts in term of air-ice CO_2 fluxes.

The pCO_2 dynamics within sea ice was investigated by direct *in situ* measurement on brine and on bulk sea ice. Sea ice brine pCO_2 was measured with a system developed by *Delille and co-workers* (*i.e., Delille* [2006]) and *Delille et al.* [2007], based on the equilibration method. Measurement was carried out directly *in situ* rather than computed from TA and pH measurement which require to use the dissociation constants of the carbonate system which might not be valid in the range of temperature and salinity encountered in sea ice (*cf.*, Ch. I.2). However, since the measurements were carried out on brines, this method cannot capture vertical variability precisely and it was not possible to measure pCO_2 at the air-ice interface, a prerequisite to assess consistently air-ice pCO_2 gradients. Then, we aimed to develop a new method of measurement of pCO_2 on bulk ice with high vertical resolution that could (i) achieve a higher vertical resolution of pCO_2 measurement than the sackholes technique and (ii) measure the CO_2 concentration at the ice interface with the atmosphere. This new technique of measurement is also based on the equilibration method and is explained in further details in the chapter IV.

Among the few studies carried out on CO_2 fluxes between sea ice and the atmosphere, only two reported fluxes during winter and these studies did not relate the fluxes to direct measurements of pCO_2 dynamics within sea ice although *Delille and co-workers* (*i.e., Delille* [2006]) and *Nomura et al.* [2010b] suggested a link between brine pCO_2 and the magnitude of the fluxes. To our best knowledge, no studies of pCO_2 dynamics were carried out in fall, during the initial sea ice growth and only one was performed in winter [*Miller et al.*, 2011]. In order to bridge the gap in current knowledge of sea ice

pCO_2 variability over the entire growth and decay cycle, we aimed to carry out measurement of pCO_2 and related air-ice CO_2 fluxes during sea ice growth.

A special attention was focused on the precipitation of calcium carbonate ($CaCO_3$) since *Rysgaard et al.* [2007; 2009] suggested that $CaCO_3$ precipitation could act as a significant sink for atmospheric CO_2 and since *Dieckmann et al.* [2008; 2010] reported the discovery of $CaCO_3$ precipitation as ikaite within sea ice. We intended to document favorable conditions for such precipitation. In addition we aimed to determine the role of this precipitation on the dynamic of the inorganic carbon within sea ice and its possible role as sink or source for atmospheric CO_2.

This work was carried out in the frame of two arctic surveys. First survey was the Circumpolar Flaw Lead (CFL) system study. It was the largest International Polar Year (IPY) initiative led by Canada that gathered over 350 participants from 27 countries. The CFL study was 293 days in duration and involved the overwintering of the Canadian research icebreaker *CCGS Amundsen* in the Cape Bathurst flaw lead (Amundsen Gulf) throughout the annual sea-ice cycle of 2007-2008 [*Barber et al.*, submitted]. In the chapter III, presented the evolution of the pCO_2 dynamics from the end of the winter to the decay of arctic sea ice (from April to June 2008).

The second survey was carried out in Barrow, Alaska, from January to June 2009, in the frame of the project “Year round follow up of air-ice-ocean carbon dioxide exchanges for arctic sea ice: a contribution to the International Polar Year”. During this field trip, CO_2 exchanges were measured continually until the ice break up in June. We had the opportunity to carry out first pCO_2 measurement on young growing sea ice that are presented in chapter II. We also carry out first measurement of CO_2 fluxes at the ice interface with the atmosphere, over young growing thin ice.

Chapter II: First estimates of the contribution of $CaCO_3$ precipitation to the release of CO_2 to the atmosphere during young sea ice growth

Sampling of thin ice in Barrow, Alaska.

Foreword

This study estimates the release of CO_2 related to the precipitation of calcium carbonate in young growing sea ice at Barrow, Alaska. We confirmed that the presence of calcium carbonate as ikaite precipitates within arctic sea ice and we presented the first quantitative estimation of this precipitation according to total alkalinity and pH measurements. This estimate was compared to the first *in situ* measurement of CO_2 fluxes carried out on young thin ice. This represents an important step in our understanding of CO_2 exchange over the annual growth/decay sea ice cycle.

This chapter has been submitted to the Journal of Geophysical Research, Oceans:

Geilfus, N. –X., Carnat, G., Dieckmann, G. S., Halden, N., Nehrke, G., Papakyriakou, T. N., Tison, J. –L. and Delille B., First estimates of the contribution of $CaCO_3$ precipitation to the release of CO_2 to the atmosphere during young sea ice growth.

Abstract

We report measurements of pH, total alkalinity, air-ice CO_2 fluxes (chamber method) and $CaCO_3$ content of frost flowers (FF) and thin (20 cm, less than 1 week old) landfast sea ice near Barrow, Alaska. As the temperature decreases, concentration of solutes in the brine skims (BS) increases. Along this gradual concentration process, some salts reach their solubility threshold and start precipitating. The precipitation of ikaite ($CaCO_3.6H_2O$) was confirmed in the FF and throughout the ice by Raman spectroscopy and X-ray analysis. The amount of ikaite precipitated was estimated to be 25 µmol kg^{-1} in the FF and shown to decrease from 19 µmol kg^{-1} in the upper part of the ice to 15 µmol kg^{-1} at the bottom of the ice. CO_2 release due to precipitation of $CaCO_3$ is estimated at 54 µmol kg^{-1}. The dissolved inorganic carbon (DIC) normalized at a salinity of 10 exhibits significant depletion in the upper layer of the ice and in the FF. This loss of DIC is estimated to be 2069 µmol kg^{-1} and corresponds to an average CO_2 flux ranging from 18 mmol m^{-2} d^{-1} to 35 mmol m^{-2} d^{-1}. This estimate is consistent with chamber flux measurements of air-ice CO_2 exchange. Our measurements confirm previous laboratory findings that growing young sea ice acts as a source of CO_2 to the atmosphere. $CaCO_3$ precipitation promotes release of CO_2 to the atmosphere. At this point we believe that its contribution to the overall release by newly formed ice is minor.

1. Introduction

Most carbon cycle researches had not considered the possibility of either direct air-sea gas exchange in the presence of sea ice or indirect air-ice-sea gas exchange, where sea ice actively participates in CO_2 transfer. Therefore, global and regional budgets of air-sea CO_2 exchange have ignored ice-covered regions [*Bates and Mathis,* 2009*; Takahashi et al.,* 2009], relying instead on the assumption that a sea ice cover is impermeable to gases. However, recent observations using both tower-based micrometeorological approaches and chamber sampling indicate that uptake and evasion of CO_2 does occur over sea ice [*Semiletov et al.,* 2004; *Delille,* 2006; *Zemmelink et al.,* 2006; *Semiletov et al.,* 2007; *Nomura et al.,* 2010b; 2010a; *Miller et al.,* 2011; *Papakyriakou and Miller,* 2011].

Observations of gas exchange have been attributed to numerous processes in sea ice, both physiochemical and biological, but the community is both uncertain of the amount

of CO_2 that sea ice can exchange with its surrounding, and the exact nature of the sea ice, and possibly upper ocean, CO_2 source or sink. Complicating the situation are observations of gas exchange that vary in magnitude by several factors associated with chamber [*Delille et al.*, 2007; *Nomura et al.*, 2010b; 2010a] and eddy covariance methodologies [*Semiletov et al.*, 2004; *Zemmelink et al.*, 2006; *Miller et al.*, 2011; *Papakyriakou and Miller*, 2011]. *Semiletov et al.* [2004] reported that melt ponds and open brine channels within sea ice represent a sink for atmospheric CO_2, of up to -39.3 mmol m^{-2} d^{-1}. *Papakyriakou and Miller* [2011] observed CO_2 fluxes over seasonal sea ice in the Canadian Arctic Archipelago to be highly variable, ranging between hourly peak exchanges of +86.4 mmol m^{-2} d^{-1} and -259 mmol m^{-2} d^{-1}, in respectively the cold and warm phases of the spring transition. The large, but short-lived, late-spring spike in uptake corresponded, in time, to a rapid increase in brine volume and associated opening of the brine channels leading the authors to speculate that the downward flux was in part driven by photosynthesis at the ice base. With chambers, *Delille and co-workers* (*i.e., Delille* [2006]) measured CO_2 fluxes, ranging from -4 mmol m^{-2} d^{-1} to +2 mmol m^{-2} d^{-1} on antarctic pack ice and related these fluxes to the seasonal differences in brine pCO_2 relative to atmospheric levels. *Nomura et al.* [2010b] who, also with chambers, measured CO_2 fluxes that increased from +0.7 mmol m^{-2} d^{-1} to -1 mmol m^{-2} d^{-1} in warming first year land-fast sea ice in Barrow in the late spring. Both ascribed flux direction to the difference in air-sea ice brine pCO_2.

The studies cited here document fluxes over mature slow growing or decaying seasonal sea ice. Fluxes over growing artificial sea ice have been reported by *Nomura et al.* [2006], however comparative field measurements of fluxes over thin rapidly growing sea ice do not exist, representing a significant gap in our understanding of CO_2 exchange over the annual growth/decay sea ice cycle.

As mentioned above, we remain uncertain on the exact drivers of the CO_2 exchange, although several processes have been identified as possibly important. As sea ice forms and grows, salts are partly rejected from the sea ice and partly trapped within the sea ice structure. Brine within the sea ice is concentrated into brine pockets, tubes and channels [*Weeks and Ackley*, 1982]. Cooling of brine therefore promotes not only an increase in brine salinity, but also an increase of brine pCO_2 through a decrease in brine CO_2 solubility [*Papadimitriou et al.*, 2004]. Significant changes in the mineral-liquid thermodynamic equilibrium can occur on temperature change, leading to a sequential

mineral precipitation [*Marion*, 2001]. Ikaite, a hexahydrate polymorph of calcium carbonate ($CaCO_3.6H_2O$), begins to precipitate at -2.2°C, mirabilite ($Na_2SO_4.\ 10H_2O$) below -8°C. $NaCl.2H_2O$ precipitates below -26°C, while potassium and magnesium salts precipitate below -34°C [*Assur*, 1958; *Rankin et al.*, 2000; *Marion*, 2001]. The precipitation of calcium carbonates from the brines [*Papadimitriou et al.*, 2004; *Dieckmann et al.*, 2008; 2010] would also serve to increase pCO_2. Sea ice hosts a complex biological system [*Thomas et al.*, 2010] and carbon is cycled through processes of photosynthesis and respiration associated with seasonally large algal communities [*Arrigo et al.*, 2010a] and bacterial communities that are thought to function throughout and annual cycle [*Deming*, 2010]. CO_2 can be exchanged among sea ice brine, seawater and atmosphere, as long as the ice remains permeable [*Nomura et al.*, 2006; *Rysgaard et al.*, 2007; *Loose et al.*, 2009].

The possible role of $CaCO_3$ precipitation on sea ice carbonate biochemistry has received growing attention. *Rysgaard et al.* [2007; 2009] suggested that calcium carbonate precipitation in sea ice could act as a significant sink for atmospheric CO_2. An abiotic pump would result from the high DIC: TA ratio (TA being defined as the total alkalinity) of brine expelled from sea ice during the ice growth and brine drainage as a consequence of $CaCO_3$ precipitation which is described by:

$$2HCO_3^- + Ca^{2+} \leftrightarrow CaCO_3 + H_2O + CO_2 \qquad \text{(II. 1)}$$

Precipitation of 1 mole of $CaCO_3$ transfers HCO_3^- to the CO_2 pool, decreasing DIC by 1 mole and TA by 2 moles. According to *Rysgaard et al.* [2007], this pump could represent a downward transport of 0.2 - 0.5 PgC yr^{-1} out of the surface ocean. However, the role and significance of $CaCO_3$ formation/dissolution in sea ice on atmospheric CO_2 depends on rates of mineral production and sea ice permeability; the latter depending on conditions and timing of precipitation [*Delille*, 2006].

The authigenesis of ikaite in natural sea ice is not yet fully understood. Little is known about the spatial and temporal occurrence of ikaite precipitates in sea ice, but recent discovery of ikaite in sea ice from both hemispheres indicates that ikaite precipitation is not a localized phenomenon [*Dieckmann et al.*, 2008; 2010]. Ikaite stability field is limited to near-freezing temperatures and is apparently favored by alkaline conditions, elevated phosphate concentrations and by presence of certain additives like amino acids

[*J L Bischoff et al.*, 1993a; *Whiticar and Suess*, 1998; *Buchardt et al.*, 2001; *Selleck et al.*, 2007].

In addition to the potential uptake of atmospheric CO_2, $CaCO_3$ precipitation at the top of sea ice is thought to play a role in atmospheric chemistry as a trigger for the transformation of inert sea-salt bromide to reactive bromine monoxide and the occurrence of tropospheric ozone depletion events (ODEs) at high latitudes [*Sander et al.*, 2006]. It was suggested that this conversion was possibly due to a decrease of the alkalinity [*Sander et al.*, 2006]. However, *Morin et al.* [2008] pointed out that the alkalinity decrease required for such transformation may not occur in sea ice and that further work is needed to resolve this issue. *Piot et al.* [2008] showed that the precipitation of calcium carbonate ($CaCO_3$) in sea ice brine is a key process allowing the rapid acidification of aerosols originating from frost flowers (FF), highlighting potential importance of FF for ozone chemistry in the Arctic. Their work supports earlier suggestions that FF and their accompanying brine skim may play an important role as a salt aerosols source for the atmosphere [*Rankin et al.*, 2000; 2002; *Alvarez-Aviles et al.*, 2008]. FF mainly grow on newly formed sea ice [*Perovich and Richter-Menge*, 1994; *Alvarez-Aviles et al.*, 2008] and are centimeter-scale ice structures, formed by a mixture of atmospheric hoar and liquid from the brine skim, brine expelled from the ice crystals during the sea ice growth. The latter explains the observed high bulk salinity of FF. Growth is thought to proceed in three stages [*Alvarez-Aviles et al.*, 2008]: (i) development of small nodules on nilas, (ii) the initial formation of FF on the nodules, and (iii) their subsequent growth into mature structures.

To our best knowledge, field measurements of CO_2-related parameters have not yet been reported over young rapidly forming sea ice. Laboratory experiment suggest than young newly formed sea ice releases CO_2 to the atmosphere [*Nomura et al.*, 2006]. During our 2009 field work in Barrow (Alaska), we had the opportunity to sample a newly formed ice sheet and associated frost flowers. In this paper, quantitative analysis including measurement of major ions chemistry, pH, TA, DIC and amount of ikaite precipitates in FF and bulk sea ice, allowed us to identify the influence of abiotic process on the sea ice carbonate system during the early growth phase and to demonstrate calcium carbonate precipitation as ikaite. Furthermore, we report on the first arctic measurements of air-sea CO_2 fluxes over young growing ice and FF and

provide a first assessment of the contribution of $CaCO_3$ precipitation to the total observed CO_2 release to the atmosphere.

2. Methods

Individual FF, surface brine skim and young sea ice cores (20 cm thick) were collected from young shore-fast sea ice near Barrow, Alaska, on April 6, 2009 (Fig. II.1).

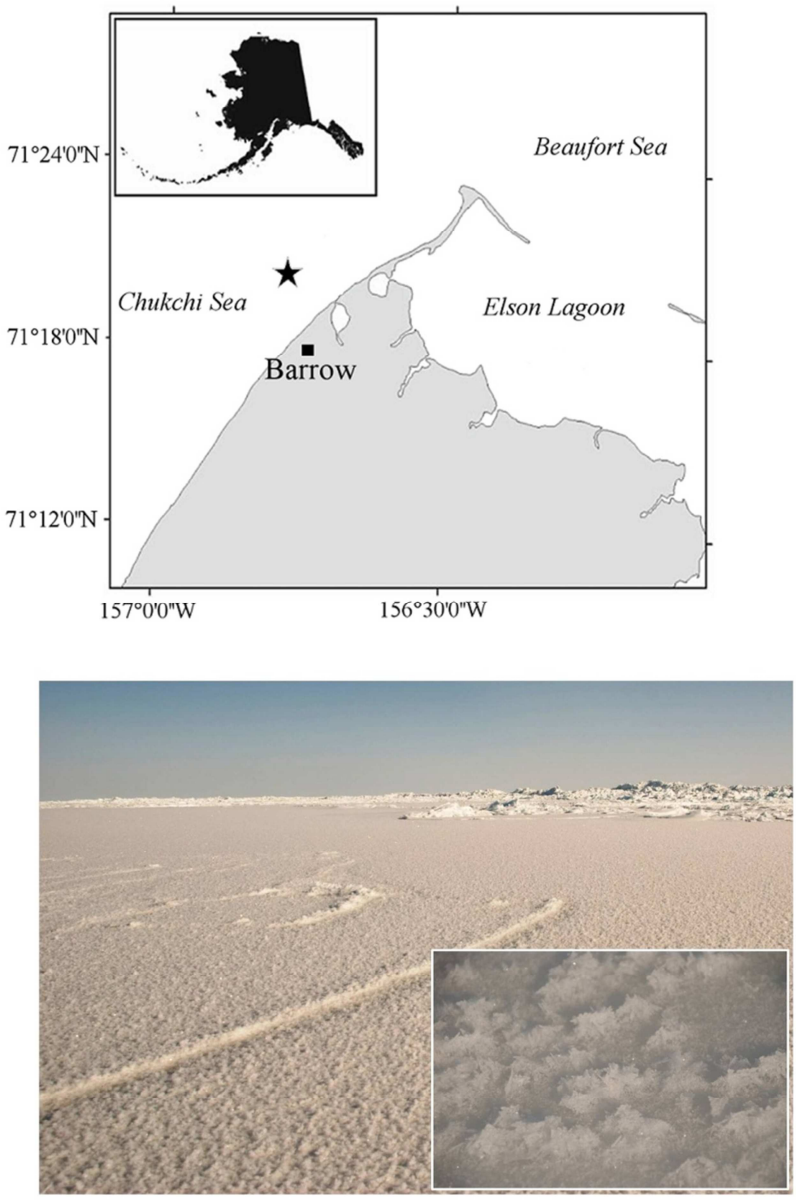

Figure II.1: Location of the sampling area (black star) at Barrow (Alaska) and pictures of the sampling site.

Several FF were sampled using a clean spatula and stored frozen in a clean plastic bag. A Teflon coated stainless steel corer with an internal diameter of 7 cm was used to sample several cores from the young ice. A total of 5 cores was sampled in an area of

1 m² with a maximum spacing between cores of 20 cm. Sea ice temperature was measured *in situ* directly after extraction of the first core, using a calibrated probe (TESTO 720) inserted in pre-drilled holes (perpendicular to core sides) at the exact diameter of the probe and with a depth resolution of 2.5 cm. Precision of the measurement was ±0.1°C (not including potential bias from the heat transfer on drilling and temperature change during temperature measurements). Sea ice cores and FF samples were kept frozen at -28°C. Back in the lab, the temperature core was cut into successive 2.5 cm thick slices. Each slice was stored in a bucket and left to melt at +4°C in the dark. Salinity of the meltwater was measured with a Thermo-Orion® portable salinometer WP-84TPS meter with a precision of ±0.1.

Vertical thin sections were performed on one of the cores following standard procedures [*Tison et al.*, 2008], in order to describe the texture of the ice. Pictures of crystal texture were taken from the thin sections using a light table and cross- and parallel- polarized sheets with a macro setting on a camera (Nikon® Coolpix S200, 7.1 mega-pixels).

Another core was cut into vertical sections at a 5 cm depth resolution. For each section, 20 g of ice were melted at room temperature to measure major ions Ca^{2+}, SO_4^{2-}, Na^+ and PO_4^{3-}. These major ions were measured by atomic absorption spectrometry using a Varian® SpectrAA-300® spectrometer, with a precision of ±3%. Phosphate was measured using standard colorimetric procedure on a Genesys® spectrophotometer [*Grasshoff et al.*, 1983].

Fluxes of CO_2 at the sea ice-atmosphere interface were measured using an accumulation chamber, West System®. The chamber is a metal cylinder closed at the top, with an internal diameter of 20 cm and an internal height of 9.7 cm. A rubber seal surrounded by a serrated edge iron ensured an air tight connection between the ice and the accumulation chamber. The chamber was connected in a closed loop to an infrared gas analyser (Li-Cor® 6262) with an air pump flow set at 3 L min^{-1}. The measurement of pCO_2 in the chamber was recorded every 30 sec for a minimum time of 5 min. The flux was then computed from the slope of the linear regression of pCO_2 against time (r^2>0.99) according to *Frankignoulle* [1988]. The uncertainty on the flux computation due to the standard error on the regression slope was on average ±3%.

Crystals of calcium carbonate were extracted from the ice cores following *Dieckmann et al.* [2008]. Ice cores were cut into 5 cm sections, which were then transferred into clean

plastic containers, sealed and melted at +4°C. Samples were processed as soon as they were melted. Meltwater temperature never rose significantly above 0°C. The meltwater was then gently swirled, in order for the crystals to settle in the central part of the container. On a first ice core, a proportion of the crystals was collected for direct observation under a binocular microscope, while the rest of the crystals were stored on 0.2 µm Millipore filters. The filters were rinsed with 75% ethanol and kept frozen at -25°C for later identification of the mineralogical phase. On a twin ice core, the same melting process was followed but the crystals were pipetted into a glass vial containing 60% ethanol and kept frozen at -18°C for the identification of the mineralogical phase.

Analyses were carried out by X-ray diffraction using a Siemens® (Bruker) D5000 Powder Diffractometer at room temperature. Bruker's DIFFRACplus software and MDI Jade + software were used to collect and analyze the data. The goniometer was configured in Bragg-Brentano (θ-2θ) geometry and used Cu radiation (Cu Kα1 λ = 1.54060). The system was equipped with computer-controlled divergence and receiving slits, a rotating sample holder, diffracted beam graphite monochromator and a scintillation detector. Scanning electron microscopy (SEM) was performed on a single crystal, from the same filter used for the X-ray (left one day at room temperature). The instrument used was a Cambridge® Stereoscan 120, running at 20 keV. Other analyses using a confocal Raman microscope (WITec®, Ulm, Germany) were performed for phase identification of the crystals extracted. The Raman was equipped with a diode laser (532 nm) and an Olympus® 20x Teflon coated water objective. The sample was transferred in a temperature controlled room into cooled (~ 1°C) glass Petri dishes and then transferred to the Raman microscope. The ikaite stayed stable for at least 15 minutes with this approach, before signs of transformation into calcite were observed. Time was sufficient for reliable phase identification of ikaite given that the measurement took only a few seconds.

The size of $CaCO_3$ crystals found in our sample ranged from <40 µm to 200 µm (Fig. IV.2), so that they could all be removed by a filtration on 0.2 µm filters. According to previous work of *Rysgaard et al.* [2007] and [2009], we assumed than dissolution of $CaCO_3$ crystals during the melting processes was not significant, and paid attention to keep the sample below 4°C at all time during melting processes, filtration and pH measurement. The overall calcium carbonate content ($\Delta CaCO_3$) was then estimated from the difference between alkalinity of none filtered sample, denoted as bulk

alkalinity (TA_b) and sample filtered on Millipore filters of 0.2 µm, denoted as filtered alkalinity (TA_f). $\Delta CaCO_3$ is computed according to:

$$\Delta CaCO_3 = \frac{1}{2} TA_b - TA_f \qquad \text{(II. 2)}$$

Additionally, ice cores and FF were melted to estimate this precipitation. Twin ice cores, cut into 5 cm segments, and FF were transferred into Tedlar® gas sampling bags, closed with a 30 cm gas tight Tygon tube. The excess air was quickly removed through the valve. The ice samples were melted in a fridge at +4°C. As soon as the ice was completely melted, samples were collected to measure pH, TA_b and TA_f. The meltwater was shaken to put back the crystals in suspension to homogenize the liquid. First, samples for TA_b were collected, then samples for TA_f. The filtration was carried out at cold temperature (+4°C) to avoid any dissolution of calcium carbonate. Then, pH was measured using Metrohm® combined electrode calibrated on the total hydrogen ion scale using TRIS (2-amino-2hydroxymethyl-1.3-propanediol) and AMP (2-aminopyridine) buffers prepared at salinities of 35 and 75 according to the formulations proposed by *DOE* [1994]. The pH measurements were carried out at low temperature (typically below +4°C). The pH electrode was calibrated at temperatures ranging from +1°C to +4°C, at salinities of 35 and 75. The accuracy of pH measurements was ±0.01 pH units. TA was measured by open-cell titration with HCl 0.1 M according to *Gran* [1952] on 50 ml of sea ice meltwater samples. Titration was stopped for 10 minutes at pH 4.2 to ensure that all $CaCO_3$ crystals were dissolved, prior to TA measurement over the pH range 3 and 4.2, required for the Gran function. The accuracy of TA measurements was ± 4 µmol kg^{-1}.

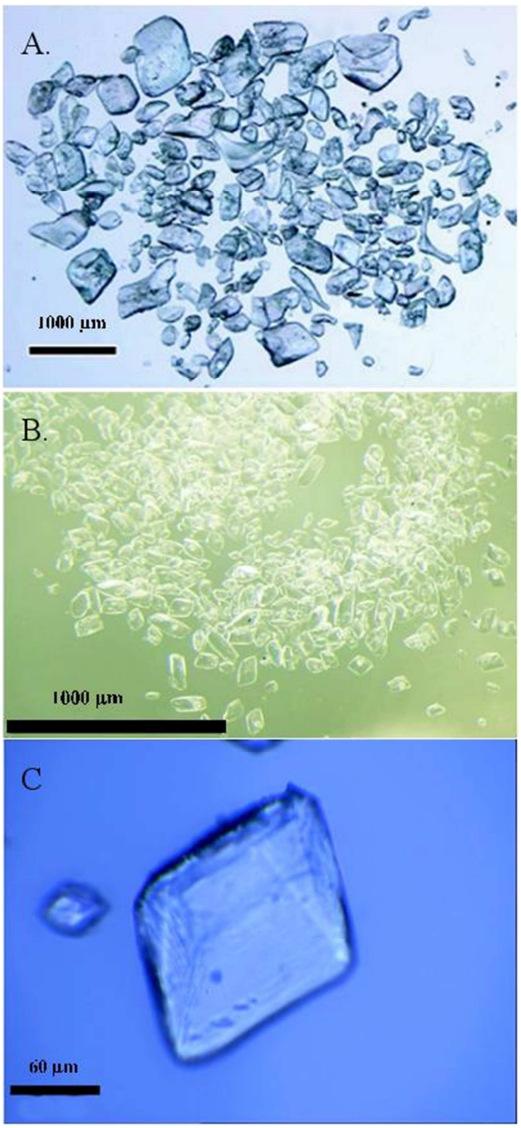

Figure II.2: Pictures of ikaite crystals. **A.** from *Dieckmann et al.* [2008], **B.** from our direct measurement under a binocular microscope, **C.** from a Raman

Data were quality checked with certified reference material acquired from Andrew Dieckson (Scripps Institution of Oceanography, University of California, San Diego). DIC_b and DIC_f were computed from TA_b and TA_f, respectively, and pH, according to CO_2 acidity constants of *Mehrbach et al.* [1973] refitted by *Dickson and Millero* [1987] and other constants advocated by *DOE* [1994]. We assumed a conservative behavior of CO_2 dissociation constants at subzero temperature. *Delille et al.* [2007] and *Marion et al.* [2001] suggested that thermodynamic constants relevant for the carbonate system can be assumed to be valid at subzero temperatures. DIC_f is not influenced by calcium carbonate dissolution after sampling. DIC_b obtained from TA_b was used in the sake of consistency with previous works of *Rysgaard et al.* [2007] and [2009].

The age of the ice was roughly estimated using the air and sea temperature records from the location of the Barrow Sea Ice Mass Balance (data available at http://seaice.alaska.edu/gi/data) at the time of the sampling [*Druckenmiller et al.*, 2009]. The time since the formation, T, was estimated by subtracting the change of the ice thickness, H_i, for each time step ΔT until $H_i = 0$ [*Lepparanta*, 1993] according to:

$$\Delta H_i = \frac{K_i}{H_i \rho_b L}(T_w - T_a)\Delta T \qquad \text{(II. 3)}$$

where ρ_b is the sea ice bulk density, K_i the thermal conductivity of the ice and T_w and T_a the seawater and air temperatures, respectively. The thermal conductivity was calculated using the exponential regression suggested by *Eicken* [2003] and references therein. The latent heat of fusion, L, was kept at 333.9 kJ kg^{-1}. We assumed that T_a and T_w observed at the mass balance site was representative for larger area and that oceanic heat flux was negligible.

3. Results

3.1 Sea ice properties

The young sea ice was about 20 cm thick (±1 cm). A strong temperature gradient was observed between the atmosphere (T = -23°C), the FF (T = -19°C) and the sea ice interface (T = -14.2°C). The salinity profile was C-shaped, with a salinity of 31.5 at the top of the ice and 11.2 at the bottom (Fig. II.3), which is typical for new arctic sea ice [*Ehn et al.*, 2007]. The brine volume fraction was calculated using the equations given in *Eicken* [2003] and references therein. The brine volume was never below 5%, hence

the sea ice was permeable [*Golden et al.*, 2007] throughout the whole thickness allowing exchanges of matter with the atmosphere or the water column.

A high salinity skim of brine (BS; S = 114) covered the ice surface and FF were observed (Fig. II.4). The brine skim is the result of the upward expulsion of brine associated with ice crystal growth, and is facilitated by the high porosity within the few centimeters of the surface layer [*Perovich and Richter-Menge*, 1994]. The upper part of the sea ice column was characterized by a distinct layer of fine-grained granular ice (FG) directly followed by a layer of granular ice (G, Fig. II.4). At 4 cm depth, there was a zone of transition of 2 cm between the granular ice and the columnar ice (G/C). The rest of the sea ice cover was formed of columnar ice, except at 8 cm depth where a very thin layer (few mm) of granular ice was present.

Using T_a and T_w at the mass balance site, calculation using equation (II. 3) suggests that sea ice reached the total thickness after only 45.5 hours. While the ice was estimated to 1 week by a local interpreters that is consistent with the degraded aspect of frost flowers [*Bowman and Deming*, 2010].

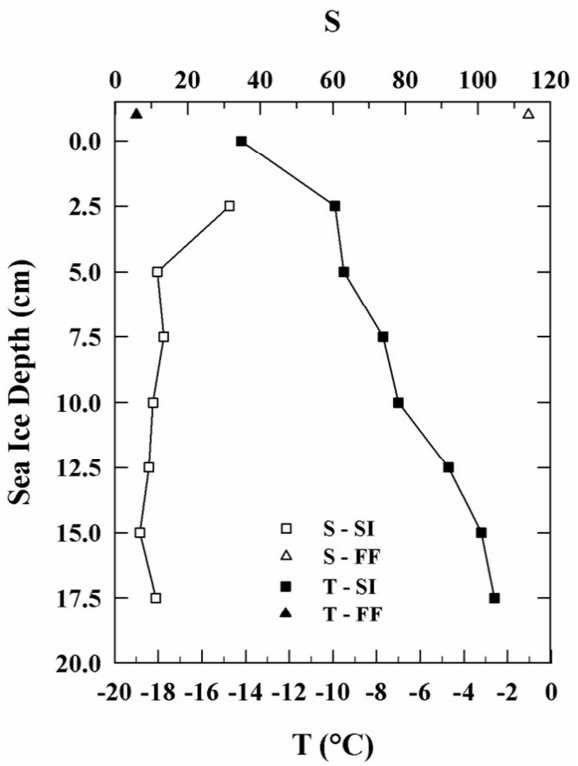

Figure II.3: Temperature and salinity profile at Barrow young ice site

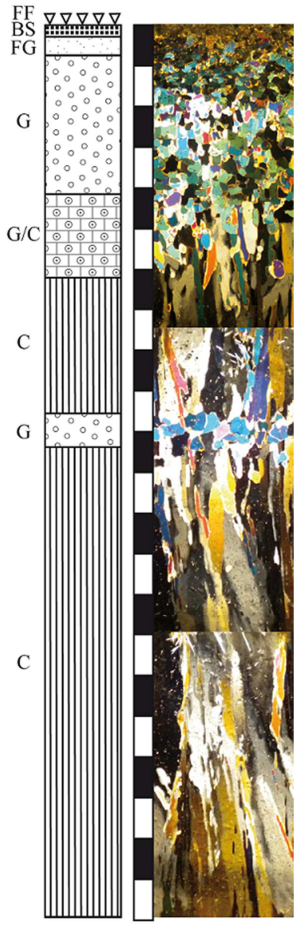

Figure II.4: Textural features of the young sea ice include: frost flowers (**FF**), brine skim (**BS**), fine-grained granular ice (**FG**), orbicular granular ice (**G**), intermediate granular/columnar ice (**G/C**) and columnar ice (**C**).

3.2 Carbonate system

The pH ranged from 8.7 to 9.5 in the upper layer of young sea ice while FF exhibited a pH of 9.0 (Fig. II.5a). The pH measured in FF or young sea ice were in the same order of magnitude than previous studies on sea ice [*Gleitz et al.*, 1995; *Delille et al.*, 2007; *Papadimitriou et al.*, 2007]. TA_f and DIC_f concentration in sea ice ranged from 492 µmol kg^{-1} to 863 µmol kg^{-1} and from 418 µmol kg^{-1} to 488 µmol kg^{-1}, respectively, while TA_f and DIC_f were much higher in FF (2586 µmol kg^{-1} and 1183 µmol kg^{-1}, respectively) (Fig. II.5b). These results were in the same order of magnitude than the observations of *Rysgaard et al.* [2007] and [2009] for arctic sea ice.

DIC_f normalized to a salinity of 10 (DIC_{10}, 10 is the mean salinity of this young sea ice), allows us to decipher variations in DIC_f (Fig. II.5c) that are independent of salinity changes. FF and the upper layer of the young sea ice showed a strong decrease in DIC_{10} while the rest of the ice column was relatively homogeneous (around 520 µmol kg^{-1}).

TA_b: DIC_b ratio in sea ice ranged from 1.12 to 1.79 in the upper layers of the young sea ice with a value peaking at 2.05 in the FF (Fig. II.5e). According to *Rysgaard et al.* [2007] and [2009], a ratio TA_b: DIC_b as high as 2 indicates that precipitates of calcium carbonate are formed. This precipitation has been estimated by the difference between the TA_b and TA_f, following the equation (II. 2). This estimation was about 25 µmol kg^{-1} in the FF and decreased from 19.4 µmol kg^{-1} in the upper part of the ice to 15 µmol kg^{-1} in the bottom of the ice (Fig. II.5f). These estimates might be underestimates as the method does not account potential $CaCO_3$ dissolution during melting of the ice prior to sub-sampling for TA measurement.

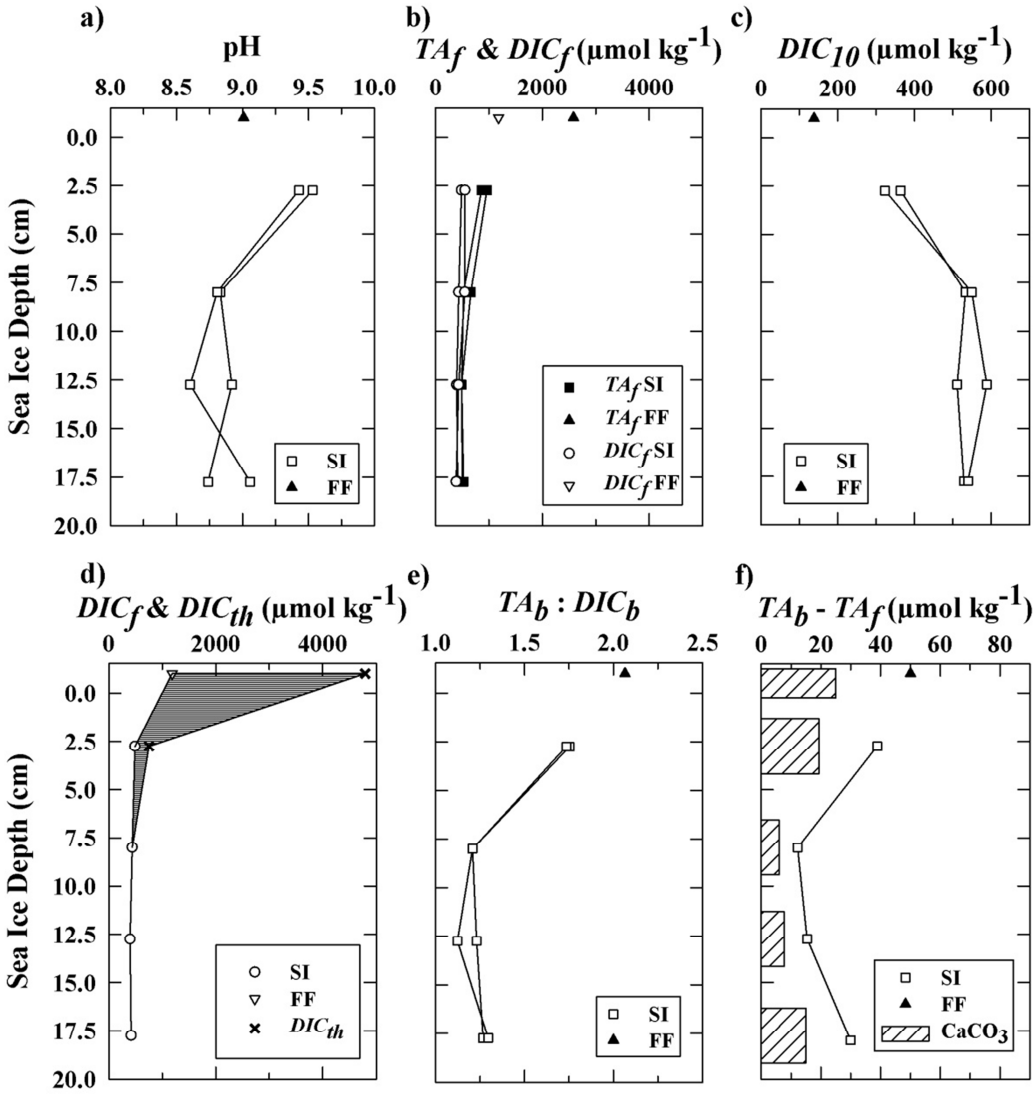

Figure II.5: Profiles of pH (**a**), TA_f and DIC_f (**b**), DIC_{10} (**c**), difference between the DIC_f and DIC_{th} (**d**), ratio between TA_b and DIC_b (**e**) and the difference between bulk and filtrated TA with the estimation of the precipitated amount of calcium carbonate (**f**).

3.3 Air-ice CO_2 fluxes

Several CO_2 fluxes measurements were taken at the sea ice surface. The fluxes ranged from 4.2 mmol m^{-2} d^{-1} to 9.9 mmol m^{-2} d^{-1} (positive flux denoting gas evasion), with an overall mean of 6.7 mmol m^{-2} d^{-1}. Flux magnitude were similar to those previously reported in spring and summer sea ice [*Delille*, 2006; *Nomura et al.*, 2010a] using the chamber method, but opposite in direction.

3.4 Precipitation of minerals

The concentrations in major ions of FF and sea ice showed significant fractionation with respect to standard seawater (Fig. II.6). Sulfates were depleted in comparison to Na^+ which is an indicator of mirabilite precipitation [*Assur*, 1958; *Rankin et al.*, 2000]. The ratio SO_4^{2-}: Na^+ in FF (0.193) was intermediate between the values observed by *Rankin et al.* [2000] or *Beaudon and Moore* [2009] and the standard mean ocean water (SMOW) value. This could be due to the sampling method. Indeed, FF were collected by scrapping the ice surface using a spatula. Therefore, the samples were a mix between FF and BS. However, considering the degraded aspect of the FF, a downward flux of brine from the FF to the BS could occur. This would reduce the fractionation between SO_4^{2-} and Na^+. The ratio observed confirmed that mirabilite could precipitate in FF and/or BS at the ice surface. Calcium was also depleted in comparison to Na^+. The ratio Ca^{2+}: Na^+ in FF (0.02) was lower than the ratio observed by *Rankin et al.*[2000] or *Beaudon and Moore* [2009]. This ratio of 0.025 could be a clue of precipitation of calcium carbonate.

Various analyses were carried out on crystals found in samples of sea ice melted at +4°C. Crystals were found at all depth of the young sea ice and in the FF. The first observation under a binocular microscope at ambient temperature revealed that crystals ranged from <40 µm to 200 µm (Fig. II.2b). Their morphology was relatively similar to that of the crystals found by *Dieckmann et al.* [2008] and [2010] but they were significantly smaller. After a few minutes under the binocular, their appearance became milky as also observed by *Whiticar and Suess* [1998] and *Dieckmann et al.* [2010]. This could be due to the transformation of ikaite ($CaCO_3.6H_2O$) into calcite, $CaCO_3$, with increasing crystal temperatures. No clear X-ray diffraction pattern could be obtained from crystals stored on Millipore filters (Fig. IV.7a, b, c) even if they had perfect crystal faces. Again, the change of phase as a result of warming during the X-ray scanning of

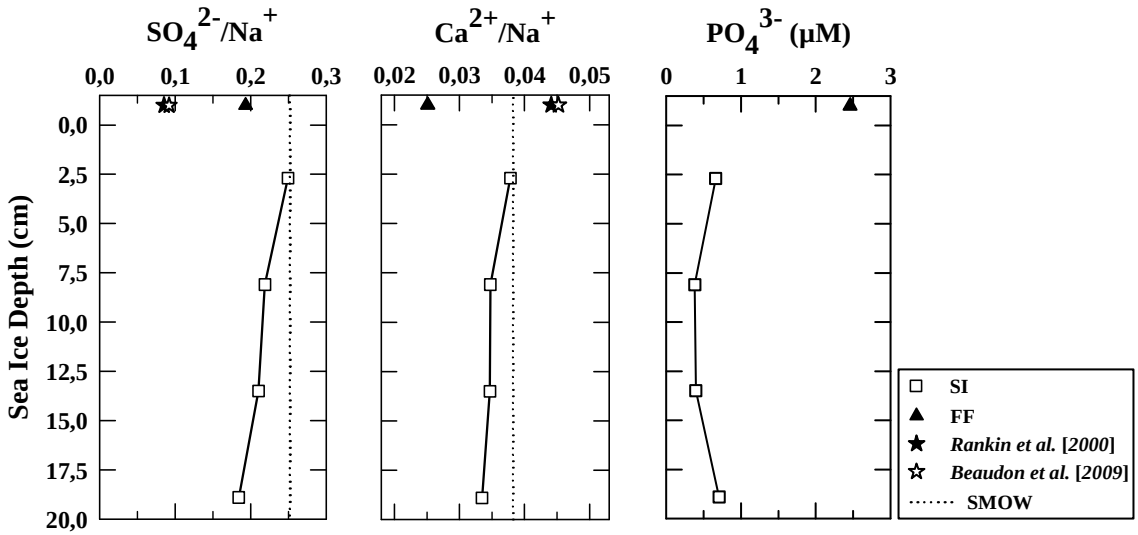

Figure II.6: Ratios of ions in frost flowers (FF) and sea ice (SI) in our study as compared with the frost flowers data from *Rankin et al.* [2000] and *Beaudon et al.* [2009] and to standard mean ocean water (SMOW). Concentration of phosphates in frost flowers (FF) and sea ice (SI)

the sample was responsible for these unidentifiable X-ray patterns. A clear X-ray pattern was finally obtained after leaving the crystals 1 day at room temperature (Fig. II.7d). In that case, calcite and halite were the two minerals identified by the X-ray scan, as illustrated by the patterns of calcite and halite shown in figure II.6e and d. A SEM performed on the same crystals confirmed the presence of calcite, with 84% of the total weight of these crystals in Ca. The Raman spectra of the precipitate and two reference samples (natural calcite and freshly precipitated ikaite) are given in figure II.8. The spectra showed the typical internal vibration modes of the symmetric stretch of the carbonate ion v_1 (1085 cm^{-1} calcite and 1075 cm^{-1} for ikaite) and its in-plane band v_4 (715 cm^{-1} calcite and 723 cm^{-1} ikaite) [*W D Bischoff et al.*, 1985]. In addition the lattice modes in the range between 100 cm^{-1} and 300 cm^{-1} were visible. The three duplets at ~150, 200, and 270 cm^{-1} in the ikaite spectra, strongly depend on its crystallographic orientation. However, the large difference in the peak positions of the internal modes v_1 and v_4 of calcite and ikaite made it possible to unambiguously distinguish between these two phases. Raman spectra determined on a set of different samples showed ikaite to be the only mineral phase present.

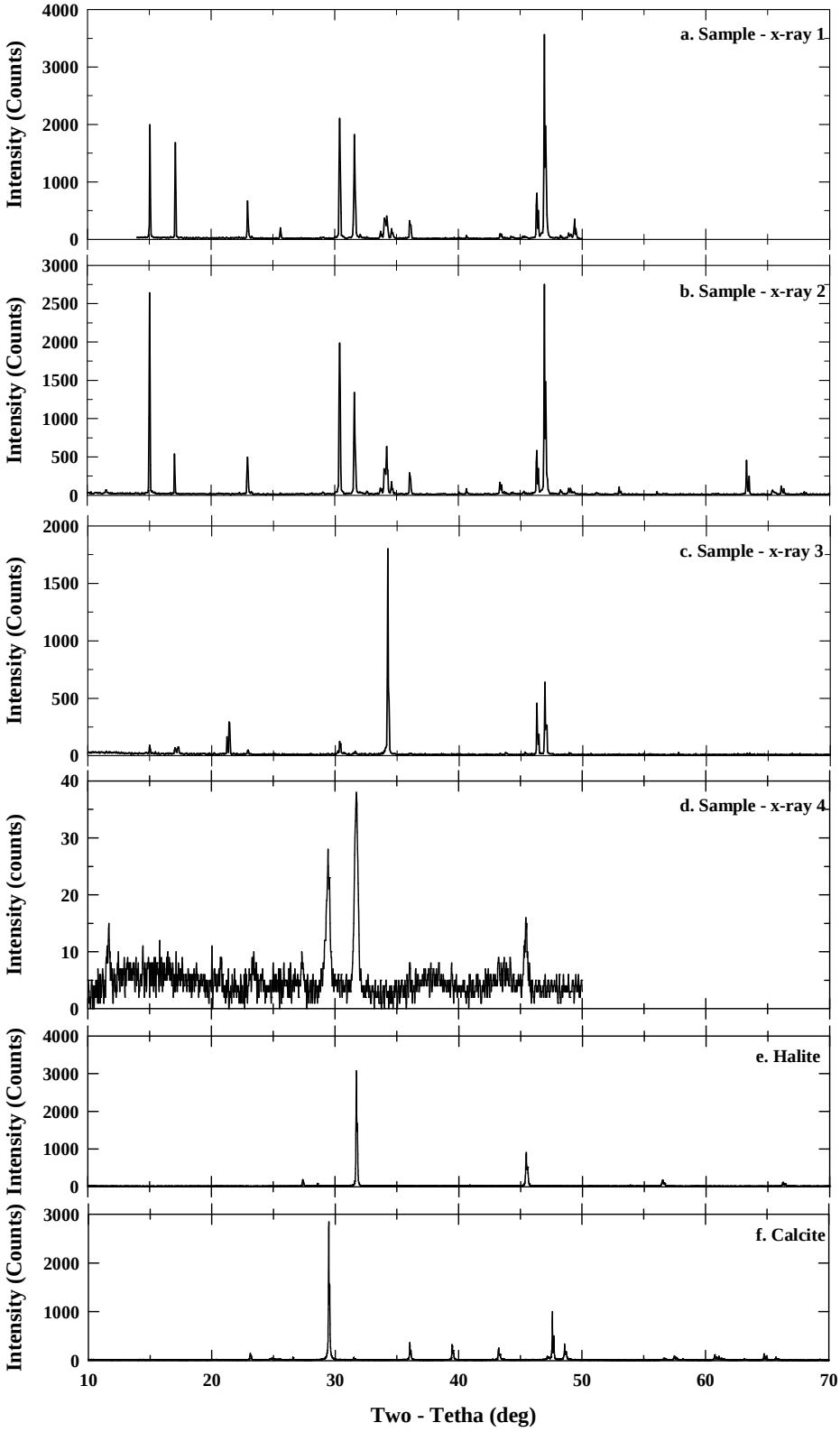

Figure II.7: Successive X-ray diffraction patterns of crystals stored on Millipore filters at -25°C (**a**, **b**, **c**), X-ray diffraction from same sample after 1 day at room temperature (**d**). Line patterns for Halite (**e**) and Calcite (**f**) from the RRUFF data base. The data base numbers are R070534 for Halite and R040070 for Calcite.

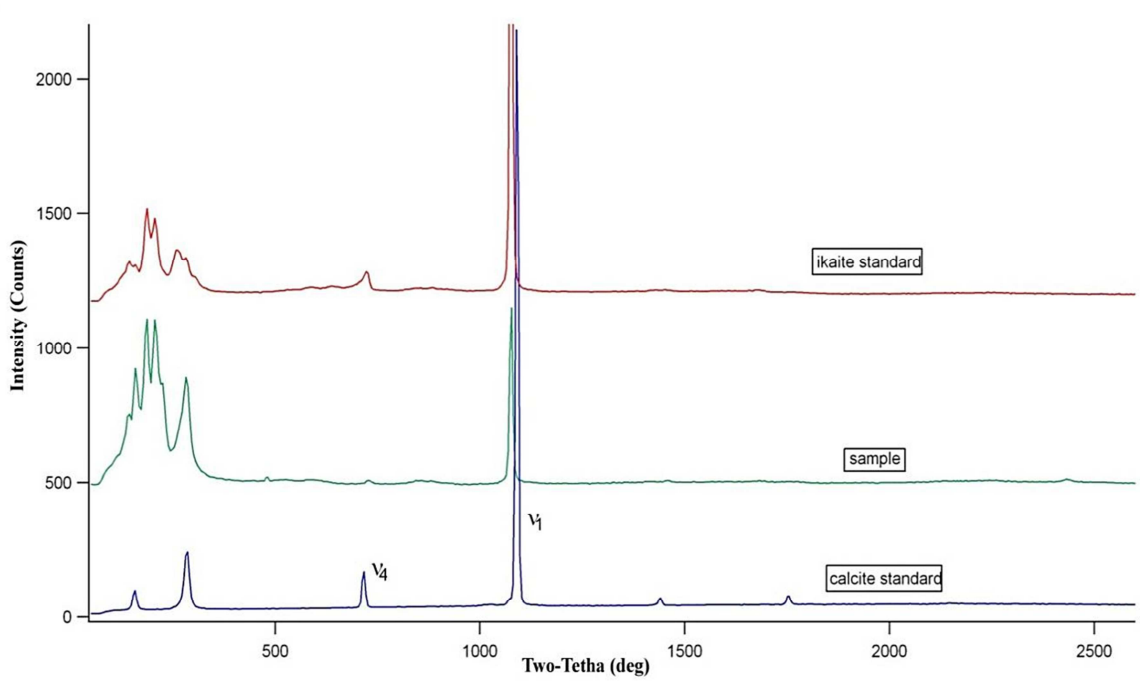

Figure II.8: Raman spectra of calcite standard (blue), ikaite (red) and sample (green).

4. Discussion

As sea ice grows, salting out process promotes buildup of a high salinity layer on top of the ice, the brine skim (BS). This BS is an active layer allowing several processes to take place. Firstly, it leads to the FF formation [*Perovich and Richter-Menge*, 1994; *Alvarez-Aviles et al.*, 2008] and favors direct exchanges with the atmosphere [*Alvarez-Aviles et al.*, 2008; *Bowman and Deming*, 2010]. Secondly, as the BS concentration increases with the decreasing temperatures, some salts can reach their solubility threshold and start precipitating.

The ratio SO_4^{2-}: Na^+ found in the FF seems to confirm the precipitation of mirabilite in the BS and the upper part of the ice cover, whereas only ikaite was found in the melted sea ice sample (see Raman spectra, Fig. II.8). The observation of halite crystals on the X-ray pattern were attributed to a storage artifact. Indeed halite only starts to precipitate at temperatures lower than -26°C [*Assur*, 1958; *Rankin et al.*, 2000; *Marion*, 2001]. The absence of mirabilite could be explained by the melting procedure. When sea ice melts the mirabilite is dissolved while ikaite remains stable, at least for temperature below +4°C.

Recent studies based on field observations [*Delille*, 2006; *Delille et al.*, 2007; *Papadimitriou et al.*, 2007; *Dieckmann et al.*, 2008; *Rysgaard et al.*, 2009; *Munro et al.*, 2010] and on laboratory freezing experiments [*Papadimitriou et al.*, 2004; *Nomura et*

al., 2006] indicate that precipitation of $CaCO_3$ occurs within sea ice. The precipitation of ikaite was found in the FF and throughout the sea ice but was not uniformly distributed with depth in the ice cores. Estimations of the amount precipitated, through the TA_b - TA_f difference, showed a maximum in the FF and then a decrease with depth (Fig. II.5). The ratio TA_b: DIC_b also showed a maximum in the FF. According to *Rysgaard et al.*[2009] and [2007], a ratio TA_b: DIC_b as high as 2 indicates the precipitation of calcium carbonate. Our results point out that this precipitation occurs with a lower TA_b: DIC_b ratio.

Ikaite precipitation in a natural environment requires several conditions. Ikaite is undersaturated at all temperatures in seawater but it rapidly approaches saturation near 0°C. Nevertheless, ikaite cannot form directly by the cooling of seawater [*J L Bischoff et al.*, 1993a]. The solution from which it forms must, at least temporarily, be supersaturated with respect to ikaite. This supersaturation is most likely to occur near 0°C but even then, external additions of either Ca^{2+} or HCO_3^- are required [*J L Bischoff et al.*, 1993a]. Furthermore, natural occurrence of ikaite requires conditions which also inhibit the precipitation of more stable anhydrous forms of $CaCO_3$. Indeed, calcite, aragonite, vaterite are much less soluble than ikaite and are supersaturated in solutions saturated in respect with ikaite. Ikaite will be stabilized under conditions that inhibit the nucleation and growth of the anhydrous forms of $CaCO_3$, and, conversely, ikaite will likely not occur under conditions which are favorable to crystallization of the anhydrous forms [*J L Bischoff et al.*, 1993a]. Orthophosphate is a powerful inhibitor of both crystal growth and dissolution of calcite and aragonite, even at concentrations as 5 µM [*J L Bischoff et al.*, 1993a]. It prevents the crystallization of the more stable anhydrous forms of $CaCO_3$ but does not interact with ikaite [*J L Bischoff et al.*, 1993a; *Buchardt et al.*, 2001]. Accordingly, high PO_4^{3-} concentration have been linked to ikaite precipitation in antarctic and arctic sediments [*Kennedy et al.*, 1987; *Whiticar and Suess*, 1998] and others various environments [*J L Bischoff et al.*, 1993b; *Buchardt*, 2004; *Selleck et al.*, 2007]. Hence, ikaite precipitation seems to be favored by the near-freezing temperature, alkaline conditions, elevated phosphate concentrations [*J L Bischoff et al.*, 1993a; *Buchardt et al.*, 2001; *Selleck et al.*, 2007] and/or by presence of certain additives like amino acid [*Whiticar and Suess*, 1998].

With a surface temperature ranging from -9.9°C to -14°C, temperature was not a limiting factor to calcium carbonate precipitation. The phosphate concentrations in the

ice column ranged from 0.38 µM to 0.7 µM while the FF concentration is 2.45 µM. These concentrations are comparable with previous studies in arctic sea ice [*Krembs et al.*, 2002; *Lee et al.*, 2008; *Mathis et al.*, 2009] except for the FF where the PO_4^{3-} concentration is significantly higher. The alkaline condition was also observed at this station with a pH of 9 in the FF. According to *Whiticar et al.* [1998], the presence of amino acids and phosphates at cold temperature allows ikaite to form preferentially over calcite or aragonite but this feature is not a universal requirement. *Bowman et al.* [2010] collected samples with us (*i.e.*, same day, same sampling site) and measured high concentrations of particulate exopolymeric substances (pEPS) up to 36.5 mg gluceq ml^{-1}, 725 mg gluceq ml^{-1} and 1420 mg gluceq ml^{-1} in, respectively, sea ice, BS and FF. They pointed out the role of bacterial activity to provide ice-nucleating particles through pEPS production. As suggested by [*Whiticar and Suess*, 1998] pEPS could also act as calcium carbonate precipitation nuclei and then high pEPS production in Barrow likely promoted ikaite formation. On the whole, lower temperature and higher phosphate and pEPS concentration where observed in the BS and FF compared to sea ice promoting ikaite formation in the surface layers.

Sander et al. [2006] proposed that calcium carbonate precipitation in brine at subzero temperature could efficiently remove most of the seawater alkalinity, hence annihilating its buffering capacity, making it easier for atmospheric acids such as HNO_3^- and H_2SO_4 to acidify it. A model used by *Piot et al.* [2008] showed that calcium carbonate precipitation out of brine is a key process which allows a more rapid acidification of aerosols originating from brine and/or FF. The alkalinity depletion rate is a critical factor for the onset and the sustainment of tropospheric ozone depletion events (ODEs). ODEs in the Arctic may not necessarily require the precipitation of HCO_3^- to take place. They may appear more frequently and more severe with haze events [*Piot and von Glasow*, 2008]. The conclusion from *Sander et al.* [2006] have been undermined by *Morin et al.* [2008]. Following the discovery of ikaite precipitation within sea ice [*Dieckmann et al.*, 2008], *Morin et al.* [2008] integrates ikaite precipitation in the FREZCHEM model to investigate the thermodynamics of seawater at subzero temperatures, with a focus on the behavior of the carbonate system. According to this model, if ikaite precipitates instead of calcite, there is no depletion of the alkalinity during freezing down to -4.9 °C, which contradict the prediction of *Sander et al.* [2006]. Still, below -4.9°C, according to run 2, figure II.5 from the work of *Morin et al.* [2008],

the FREZCHEM model predicts dramatic changes of TA with a 25% reduction of TA from -4.9°C to -9.9°C. Reduction of TA related to ikaite precipitation outweighs the increase of TA due to salinity increase. In the run 2 of *Morin et al.* [2008], decrease of temperature from -4.9°C to -9.9°C lead to a TA change from 5100 µmol.kg^{-1} to 3800 µmol.kg^{-1} (denoted as $TA_{-4.9°C}$ and $TA_{-9.9°C}$ respectively). This temperature change corresponds to a salinity change from 83 to 154 according to *Cox and Weeks* [1983] so that TA should reach 9500 µmol.kg^{-1} (denoted as $TA_{no\ CaCO3}$) if brine concentration was the only process affecting TA. We can derive the precipitation of ikaite (P_{CaCO3}) predicted by the FREZCHEM model at -9.9°C as:

$$P_{CaCO3} = \frac{TA_{no\ CaCO3} - TA_{-9.9°C}}{2} \qquad \text{(II. 4)}$$

P_{CaCO3} reach 2850 µmol.kg^{-1} of brines at -9.9°C. Assuming an ice salinity of 5 and then a brine volume of 0.027 % according to *Eicken* [2003] and taking into account brine and ice density, we derive a P_{CaCO3} of 94 µmol.kg^{-1} of sea ice. This amount is 5 times higher than the amount found in Barrow at -9.9°C in the first 5 top centimeters that is about 19 µmol.kg^{-1}. This highlights that ikaite precipitation does not follow thermodynamics constrain as predicted by FREZCHEM model and the amount of carbonate mineral in natural sea ice could be significantly lower than predicted by the FREZCHEM model even in favorable conditions (low temperature, high phosphate and pEPS concentrations). On the whole, our observations of TA and pH in top layer of ice in Barrow challenges previous hypothesis by *Sanders et al.* [2006] that a significant precipitation of $CaCO_3$ in sea ice and frost flowers, reduces significantly pH buffering capacity of sea ice and allow significant decrease in pH. Indeed, to our best knowledge, pH in sea ice ranges from 7.78 to 9.89 [*Gleitz et al.*, 1995; *Delille et al.*, 2007; *Papadimitriou et al.*, 2007] with a rather elevated higher end value for seawater and an overall range far higher than the values proposed by *Sander et al.* [2006].

In both artificial and natural sea ice, a depletion in DIC was observed in sea ice brine [*Papadimitriou et al.*, 2004] and in the ice [*Munro et al.*, 2010] that could not be ascribed to biological activity. In both cases, the authors suggest that $CaCO_3$ precipitation and CO_2 degassing may occur in sea ice without being able to decipher both processes. We observed a strong decrease of the DIC_{10} in the upper layer of the ice column and in the FF. We attempt to assess the overall depletion in the upper layer by assuming that DIC_{10} should be homogeneous over the ice column. This should be the

case, if no biogeochemical processes occur (*i.e.*, primary production, $CaCO_3$ precipitation and CO_2 transfer to the gas phase). We then take into account DIC_f at 7.5 cm ($DIC_{7.5cm}$ and compute DIC_{th} as the value of $DIC_{7.5cm}$ extrapolated to the salinity encountered in the upper part of the ice column assuming a linear relationship between DIC and salinity). DIC_{th} at a given depth *i* was then computed according to:

$$DIC_{th} = \frac{DIC_{7.5\ cm} * S_i}{S_{7.5\ cm}} \qquad \text{(II. 5)}$$

where $DIC_{7.5cm}$ holds for the DIC at 7.5 cm, $S_{7.5cm}$ and S_i hold for salinity at 7.5 cm and at a given depth *i*, respectively. The difference between the DIC_f (Fig. II.5d) and the DIC_{th} represents the loss of DIC, illustrated by the hatched area in the figure II.5d. This loss is estimated to 2069 µmol kg^{-1}. Only few studies estimate the primary production in arctic sea ice and a wide range of production may be found, from 0.03 mg C m^{-2} d^{-1} to 463 mg C m^{-2} d^{-1} [*Arrigo et al.*, 2010a]. *Gosselin et al.* [1997] advanced a rate of production of 47 mg C m^{-2} d^{-1} in an area between 70 – 75°N and 169 – 170°W during the arctic summer. Applying this rate to an ice cover of 20 cm during 7 days, we found a production of 137 µmol C. If only the upper 7.5 cm of the ice is considered, the primary production would account only for 51 µmol C. This corresponds to only 2.5 % of the DIC depletion. This is probably an overestimate as *Arrigo and Sullivan* [1992] found greatly reduced photosynthetic rates in fast ice at brine salinity higher than 50 and total photosynthetic shutdown at brine salinity higher than 100, which is the range of salinity found at this station within the upper 10 cm of ice. According to the amount of calcium carbonate precipitated in the FF and in the upper layer of the ice (top 10 cm), the CO_2 generated during this precipitation corresponds only to 50 µmol kg^{-1} of ice. The part of the precipitation process in the release of CO_2 from the BS and/or FF is therefore minor compared to the total exchanges of 2069 µmol kg^{-1} estimated by the DIC depletion. In the same way *Munro et al.* [2010] used the $\delta^{13}C_{DIC}$ to determine the fractional contributions of $CaCO_3$ precipitation and CO_2 degassing. They found that degassing seems to be solely responsible for DIC depletion. Therefore we consider that the contribution of primary production and calcium carbonate precipitation to DIC depletion are negligible. DIC depletion then mainly corresponds to a release of CO_2 from the ice to the atmosphere. According to several studies [*Rankin et al.*, 2000; 2002; *Alvarez-Aviles et al.*, 2008; *Bowman and Deming*, 2010], FF and BS facilitate salts transport (or other materials) to the atmosphere and FF increases the specific surface area of the ice of about 40% [*Domine et al.*, 2005]. Also, enhanced salt transport,

related brine concentration, and increase of specific surface area potentially promote CO_2 degassing.

If we consider the age of the ice to be between 2 and 7 days, the loss in DIC would correspond to a CO_2 flux ranging from 18 mmol m^{-2} d^{-1} to 35 mmol m^{-2} d^{-1}. An efflux in this range is approximately a factor of 4 larger than CO_2 flux measurements using the chamber method during the relatively short sampling period (4.2 mmol m^{-2} d^{-1} to 9.9 mmol m^{-2} d^{-1}).

Using the DIC depletion calculated in this study and its corresponding fluxes (ranging from 18 mmol m^{-2} d^{-1} and 35 mmol m^{-2} d^{-1}), we can make a first order estimate of annual release of CO_2 from the first year sea ice in the Arctic. The first year sea ice extension peaks at 7.10^6 km² [*Dieckmann and Hellmer*, 2010]. Assuming that the genesis of first year sea ice goes through an evolution step similar to the ice conditions observed in this study (young sea ice ranging from 2 to 7 days, with BS and FF), we integrate the flux on the maximal first year sea ice extension in the Arctic, during 1 week. We derive a flux of 0.01 PgC per single growth episode. This estimate does not consider repeated *in situ* ice formation and production that occurs when ice is advected from a region during the cold season, hence is probably a gross underestimate of the total CO_2 efflux associated with the production of $CaCO_3$ in sea ice. Considerable research is required to constrain this estimate, and to better understand the influence of external parameters, such as snow cover, on this estimate.

5. Conclusions

Raman and X-ray analysis of thin shore fast ice and frost flowers (FF) collected in Barrow, Alaska, show conspicuous evidence of calcium carbonate precipitation as ikaite in the FF and throughout the ice by. Precipitation of ikaite in sea ice is not yet fully understood. From our knowledge, ikaite precipitation seems to be favored by the near-freezing temperature, alkaline conditions, elevated phosphate concentrations and/or by presence of certain additives like amino acids [*J L Bischoff et al.*, 1993a; *Whiticar and Suess*, 1998; *Buchardt et al.*, 2001; *Selleck et al.*, 2007]. Our results suggest that all these conditions were satisfied at our sampling location. However, the amount of precipitation of calcium carbonate observed at our sampling site is significantly lower than simulation by FREZCHEM model [*Morin et al.*, 2008] based on thermodynamics considerations. This suggests that precipitation of calcium carbonate in sea ice is not

merely triggered by thermodynamic constrains (*i.e.*, oversaturation with respect to ikaite), like calcite and aragonite precipitation in open seawater. In addition, the role of sea ice as a trigger for tropospheric ozone depletion as a consequence of low pH due to $CaCO_3$ precipitation and related reduced sea ice buffer capacity should be considered with caution. Investigations are needed to further understand and budget ikaite precipitation in sea ice.

According to the amount of $CaCO_3$ precipitated in FF and in the upper layer of the ice (top 10 cm), the share of the CO_2 generated by this process is therefore minor compared to the total exchanges estimated by DIC depletion. This decrease was estimated at 2069 µmol kg^{-1} and mainly corresponds to a release of CO_2 from the ice to the atmosphere. Considering the age of the ice between 2 days and 7 days old, the loss in DIC would correspond to a CO_2 flux ranging from 18 mmol m^{-2} d^{-1} to 35 mmol m^{-2} d^{-1}. Assuming that the genesis of first year sea ice goes through an evolution step similar to the ice conditions observed in this study (young sea ice ranging from 2 to 7 days, with BS and FF), we estimate that 0.01 PgC is evaded to the atmosphere per single growth episode of sea ice. This estimate does not consider repeated *in situ* ice formation and production that occurs when ice is advected from a region during the cold season, hence is probably a gross underestimate of the total CO_2 efflux associated with the production of $CaCO_3$ in sea ice.

6. Acknowledgements

The authors warmly thank Pr. Hajo Eicken for its strong and crucial support to the project. We would like also thank Dr. Don Perovitch and the rest of the sea ice group of the Geophysical Institute of the University of Alaska Fairbanks for setting the sea ice mass balance buoy and providing data. We are indebted to the Barrow Arctic Science Consortium and the North Slope Borough for their logistical support, to Dr. Giles Marion for his help in understanding FREZCHEM model. This research was supported by the F.R.S-FNRS (contract 2.4584.09), with which BD is a research associate, the National Science Foundation, the University of Alaska Fairbanks and the Belgian Science Policy (contract SD/CA/03A). NXG received a PhD grant from the Fonds pour la Formation à la Recherche dans l'Industrie et l'Agriculture. This is MARE contribution no. XXX.

Chapter III: pCO_2 dynamics and related air-ice CO_2 fluxes in the arctic coastal zone (Amundsen Gulf, Beaufort Sea)

Recovery of the mast equipped for eddy-covariance measurements drifting through Darnley Bay (Amundsen Gulf) during CFL.

Foreword

This study was carried out in the framework of the International Polar Year Circumpolar Flaw Lead System Study (IPY-CFL). IPY-CFL project was focusing on a part of the Circumpolar Flaw Lead system located in the Amundsen Gulf (Beaufort Sea). The Cap Bathurst polynya, located at the shelf break between Amundsen Gulf and the Beaufort Sea, in the area southeast of Banks Island [*Barber and Hanesiak*, 2004], is an important feature in the dynamics of the arctic ice sheet (*e.g*,. formation of arctic deep water, highest densities of birds and mammals found anywhere in the Arctic [*Arrigo and van Dijken*, 2004]). This polynya consists of a series of flaw leads and a sensible/latent heat polynya within Amundsen Gulf.

The annual evolution of sea ice in this region is described in details by *Galley et al.* [2008] for a 25 years period (1980-2004), while *Barber et al.* [submitted] describe the ice conditions during the CFL project (2007-2008). Sea ice is formed in October in

shallow areas along the coast under the form of landfast ice, and offshore under the form of drift ice. In winter the ice is rafted and/or drifted to the edge of the landfast ice, in contact with the mobile pack ice. At this contact, it forms a zone of thick compression ridges parallel to the coast so-called "stamukhi" [*Arrigo and van Dijken*, 2004; *Barber and Hanesiak*, 2004]. Between the landfast first-year sea ice and the offshore mobile pack ice, a recurrent ice-free channel forms, the flaw lead polynya [*Barber and Hanesiak*, 2004]. To our best knowledge, until now, only few polynya have been studied in detail [*Weeks*, 2010]. Therefore, the IPY-CFL project was designed to investigate the importance of changing climate processes in the flaw lead system of the northern hemisphere on the physical, biogeochemical and biological components of the arctic marine system [*Barber et al.*, submitted]. During CFL, much of the ice in the Amundsen Gulf remained mobile due to strong easterly winds [*Barber et al.*, submitted]. As a result, landfast ice remained restricted to near-shore locations and a drift ice icescape with small leads dominated throughout the winter and spring.

This study gives an overview of pCO_2 dynamics within sea ice from late spring to summer in the arctic coastal waters of the Amundsen Gulf. We present the first vertical profiles of pCO_2 in sea ice brine and discuss the impact of sea ice physical and biogeochemical processes. Finally, we present CO_2 fluxes at the ice-atmosphere interface and discuss the link with sea ice pCO_2.

This chapter has been submitted to the Journal of Geophysical Research, Oceans in the special issue IPYCFLEXP1 – The IPY Circumpolar Flaw Lead and Arctic SOLAS Experiments: Oceanography, Geophysics and Biogeochemistry of the Amundsen Gulf and Southern Beaufort Sea:

Geilfus, N. –X., Carnat, G., Papakyriakou, T. N., Tison, J. –L., Else B., Thomas H., Shadwick E. and Delille B. – pCO_2 dynamics and related air-ice CO_2 fluxes in the arctic coastal zone (Amundsen Gulf, Beaufort Sea).

Abstract

We present an arctic seasonal survey of carbon dioxide partial pressure (pCO_2) dynamics within sea ice brine and related air-ice CO_2 fluxes. The survey was carried out from early spring to the beginning of summer in the arctic coastal waters of the Amundsen Gulf. High concentrations of pCO_2 (up to 1834 µatm) were observed in the sea ice in early April as a consequence of concentration of solutes in brines, $CaCO_3$ precipitation and microbial respiration. $CaCO_3$ precipitation was detected through anomalies in total alkalinity (TA) and dissolved inorganic carbon (DIC). This precipitation seems to have occurred in highly saline brine in the upper part of the ice cover and in bulk ice. As summer draws near, the ice temperature increases and brine pCO_2 shifts from a large supersaturation (1834 µatm) to a marked undersaturation (down to almost 0 µatm). This decrease was ascribed to brine dilution by ice meltwater, dissolution of $CaCO_3$ and photosynthesis during the sympagic algal bloom. The magnitude of the CO_2 fluxes was controlled by ice temperature (through its control on brine volume and brine channels connectivity) and the concentration gradient between brine and the atmosphere. However, the state of the ice-interface clearly affects air-ice CO_2 fluxes.

1. Introduction

For both hemispheres, sea ice cover ranges between 18 and 28 million km^2 at its maximal extension [*Comiso*, 2003] and the sea ice zone is one of the largest biomes on Earth [*IPCC*, 2007]. It has been shown that sea ice has a strong impact on the global climate system through its control on albedo, air-sea exchange of heat, moisture and momentum, production of deep-water, stratification of surface waters during the spring melt and the seeding of primary production into the marginal ice zone [*Arrigo and Thomas*, 2004; *Thomas and Dieckmann*, 2010].

Each year, 7 Pg of anthropogenic carbon (C) are released to the atmosphere. Of this carbon release, 29% is taken up by the oceans through physical and biological processes [*Sabine et al.*, 2004]. According to the pCO_2 climatology of *Takahashi et al.* [2009], high latitude areas act as sinks for atmospheric CO_2. It represents a direct pathway for CO_2 exchanges between the atmosphere and the ocean by mechanisms that are not yet fully understood [*Takahashi et al.*, 2002; *Rysgaard et al.*, 2007]. The lack of data in the polar areas, particularly with respect to sea-ice and gas exchange is therefore an

important issue in the context of the oceanic uptake of atmospheric CO_2. As pointed out by *Tison et al.* [2002], it is often assumed that sea ice prevents the atmosphere from exchanging CO_2 with the oceans. Moreover, in the pCO_2 climatology of *Takahashi et al.* [2009], the fluxes over sea ice covered areas are approximated by using pCO_2 data from underneath the ice. However, recent observations challenge this approach and suggest that sea ice could actually be a permeable medium allowing CO_2 exchanges with the atmosphere, during polar spring-summer [*Semiletov et al.*, 2004; *Delille*, 2006; *Zemmelink et al.*, 2006; *Semiletov et al.*, 2007; *Papakyriakou and Miller*, 2011] but also during the winter [*Heinesch et al.*, 2009; *Miller et al.*, 2011]. *Semiletov et al.* [2004] suggested that melt ponds and open brine channels within sea ice represent a sink for atmospheric CO_2, up to -39.3 mmol m^{-2} d^{-1}, during arctic sea ice melt in June. *Delille and co-workers* (*i.e., Delille* [2006]) measured CO_2 fluxes, ranging from an uptake of -4 mmol m^{-2} d^{-1} to an evasion of +2 mmol m^{-2} d^{-1}, on antarctic pack ice using chambers and linked these fluxes with the brine pCO_2. This link was also identified by *Nomura et al.* [2010b], who measured CO_2 fluxes ranging from -1 mmol m^{-2} d^{-1} to +0.7 mmol m^{-2} d^{-1} in first year landfast sea ice in late May 2008 in Barrow, Alaska. During winter, brine pCO_2 becomes supersaturated with respect to the atmosphere as sea ice temperature decreases and brine salinity increases [*Papadimitriou et al.*, 2004]. CO_2 can then be emitted from brine channels to the underlying water and, if the ice is permeable, to the overlying atmosphere [*Papadimitriou et al.*, 2004; *Nomura et al.*, 2006; *Rysgaard et al.*, 2007; *Loose et al.*, 2011].

During sea ice growth, most of the impurities (solutes, gases and particular matter) cannot be incorporated into the ice matrix and are rejected at the advancing ice-water interface. This brine rejection influences the release of dissolved gases and solutes into the water column [*Papadimitriou et al.*, 2004]. However, some of the impurities are retained in liquid inclusions or as gas bubbles within the solid ice matrix. This has important consequences for the microstructure and properties of sea ice, both of which being heavily influenced by the relative brine volume [*Eicken*, 2003]. Sub-ice pCO_2 has been shown to be greater than atmospheric values in both the Arctic Ocean [*Semiletov et al.*, 2004; 2007] and the Southern Ocean [*Gibson and Trull*, 1999; *Delille*, 2006]. High dissolved inorganic carbon (DIC) concentrations have also been reported below arctic sea ice [*Anderson et al.*, 2004]. Low total alkalinity (TA) and DIC concentrations, relative to surface waters, have been described in sea ice brine in Antarctica during the

summer, while high TA and DIC concentrations have been reported during the winter [*Gleitz et al.*, 1995; *Delille*, 2006; *Papadimitriou et al.*, 2007].

In addition, sea ice affects pCO_2 of the underlying water column and then the budget of air-sea CO_2 fluxes of Arctic Ocean open waters [*Bates and Mathis*, 2009; *Fransson et al.*, 2009; *Shadwick et al.*, 2011]. Air-sea CO_2 fluxes are likely to change in the context of global warming [*Cai et al.*, 2010], one of the main forcing being sea ice retreat. Collectively, these observations indicate that sea ice likely effects the vertical transport of CO_2 in the polar marine environments. It follows that, in order to predict future change of air-sea CO_2 fluxes in Arctic Ocean, the role of sea ice in the overall budget of air-sea CO_2 must be understood.

The chemical composition of sea ice is primarily a function of salinity and temperature, but is further modified by productivity of the internal microbial assemblages recruited from the surface water during sea ice formation [*Thomas and Dieckmann*, 2010]. Because of the strong influence of biological activity on the composition of natural sea ice brine, little attention has been paid to the potential contribution of abiotic processes, such as gas exchanges or mineral formation [*Papadimitriou et al.*, 2007]. The increase of salinity at low temperature in the ice induces changes in the mineral-liquid and gas-liquid thermodynamic equilibrium that could lead to a degassing and/or a mineral precipitation from the highly concentrated brine [*Killawee et al.*, 1998; *Marion*, 2001; *Papadimitriou et al.*, 2004; 2007; *Munro et al.*, 2010]. *Rysgaard et al.* [2007] suggested that precipitation of carbonate minerals within sea ice during winter growth, and associated release of CO_2 to the underlying ocean with brine rejection, could drive a significant CO_2 uptake from the atmosphere on sea ice warming in the spring. This precipitation was observed for the first time by *Dieckmann et al.* [2008] and [2010] in antarctic and arctic sea ice, respectively. Calcium carbonate was found under the form of the mineral ikaite ($CaCO_3$. $6H_2O$). According to both *Papadimitriou et al.* [2004] and *Rysgaard et al.* [2007], precipitation of $CaCO_3$ can occur during fall and winter within growing sea ice.

Precipitation of calcium carbonate in standard seawater conditions is described by:

$$Ca^{2+} + 2HCO_3^- \leftrightarrow CaCO_3 + H_2O + CO_2 \qquad \text{(III. 1)}$$

As the temperature of sea ice decreases, so does the brine volumes in the ice. This leads to an increase in concentration of calcium (Ca^{2+}) and bicarbonate (HCO_3^-) ions, which may later combine to form $CaCO_3$. This synthesis results in a release $CO_{2(aq)}$ (Eq. III. 1).

DIC is defined by the equation:

$$DIC = [HCO_3^-] + [CO_3^{2-}] + [CO_2] \qquad \text{(III. 2)}$$

Total alkalinity can be described by:

$$TA = [HCO_3^-] + 2[CO_3^{2-}] + [B(OH)_4^-] + [OH^-] - [H^+] \qquad \text{(III. 3)}$$

The precipitation of one mole of $CaCO_3$ reduces DIC by one mole and TA by two moles, and drives the system to higher pCO_2 (Fig. III.1). Dissolution of $CaCO_3$ in standard seawater conditions corresponds to the reverse of equation III. 1.

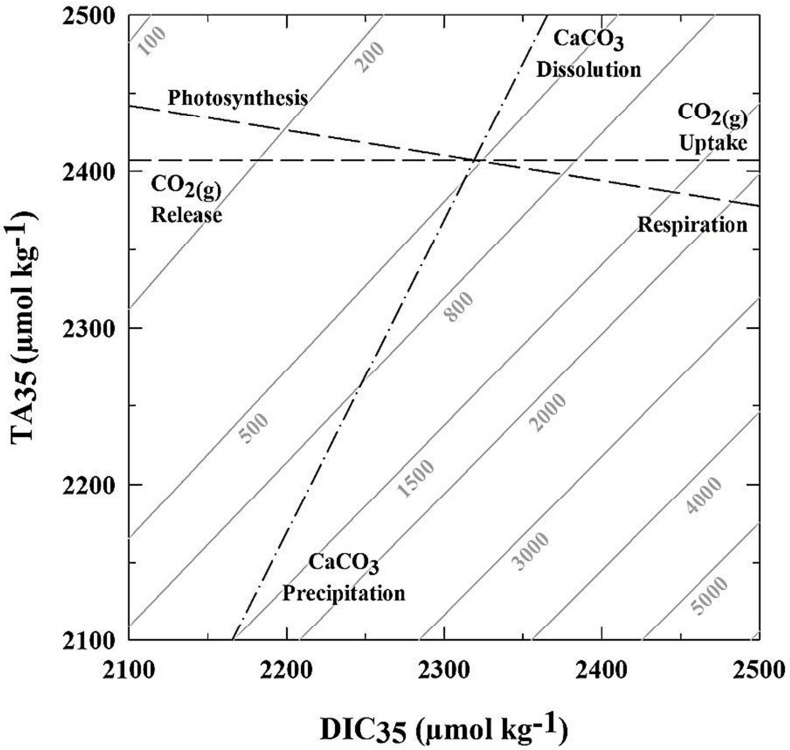

Figure III.1: Effect of various processes on DIC_{35} and TA_{35}, TA and DIC values normalized to a salinity of 35, (dashed lines). Gray lines indicate levels of constant pCO_2 (in µatm).

According to *Delille and co-workers* (*i.e.*, *Delille* [2006]), precipitation of $CaCO_3$ can occur at different depths in the ice. Depending on the physical conditions at the location where the precipitation takes place, the impact on the net budget of CO_2 fluxes from the ice to the atmosphere will be very different, depending on the timing of this precipitation and sea ice permeability. Hence, $CaCO_3$ precipitation could promote CO_2

uptake from the atmosphere [*Rysgaard et al.*, 2007; 2009] but release of CO_2 can be possible in some case [*Delille*, 2006].

In this paper, we present results from the largest survey ever performed on the pCO_2 dynamics within sea ice, from early spring to the beginning of the arctic summer. Ice cores and brine samples were analyzed for temperature, salinity, TA, DIC, chlorophyll-a (Chl a) concentrations as well as for dry-extraction measurements of pCO_2. We investigate CO_2 fluxes at the sea ice interface with the atmosphere and correlate these with the pCO_2 dynamics observed in the brine channels.

2. Study site, material and methods

Data presented in this paper were collected onboard the *CCGS Amundsen* during the International Polar Year – Circumpolar Flaw Lead system study (IPY-CFL 2008). This project was carried out in the Amundsen Gulf, Beaufort Sea, Canada (70°N, 120°W). Samples were collected at individual stations between April and June 2008, from the beginning of spring until the beginning of summer (Fig. III.2, Table III.1). It is therefore important to note that the results potentially integrate both spatial and temporal variability.

Sampling was achieved within an area of about 25 m² in order to minimize bias from spatial heterogeneity. The sample area was always located upwind of the ship to avoid any contamination from activities on the research vessel. The first part of a sampling day was dedicated to ice-core extraction after which the group collected brine from sack holes and undertook *in situ* measurements. Seawater was typically collected from the first ice core and was sampled at the ice-water interface.

A Teflon coated stainless steel corer with an internal diameter of 7 cm was used to retrieve ice cores. Cores were immediately wrapped in polyethylene (PE) bags and stored on the sampling site in an insulated box filled with individual cooling bags, pre-cooled at -70°C. This precaution served to minimize brine drainage from samples [*Tison et al.*, 2008].

A dedicated ice core for bulk ice measurements of TA and DIC was processed in the field. The top and bottom 15 cm, as well as the central part of the ice core, were cut off and placed immediately in a gas-tight laminated NEN/PE plastic bag fitted with a gas-tight Tygon tube and valve for sampling. A solution of supersaturated $HgCl_2$ was added

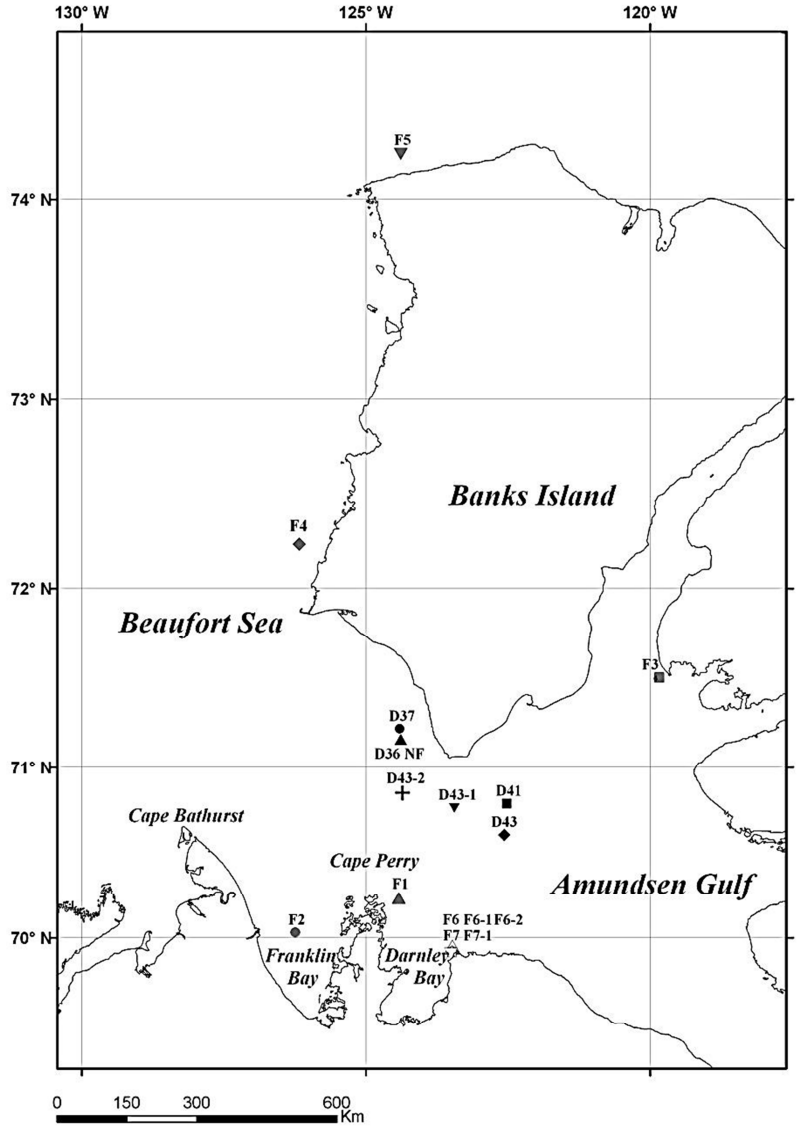

Figure III.2: Map of the CFL study area in the Amundsen Gulf (NT, Canada) indicating the locations of the sampling stations where the CO_2 data was collected.

Station	Date	Station	Date	Station	Date
D36	April 6	F1	May 9	F6	June 2
D37	April 11	F2	May 13	F6-1	June 7
D41	April 16	F3	May 20	F6-2	June 9
D43	April 26	F4	May 24	F7	June 12
D43-1	April 29	F5	May 28	F7-1	June 18
D43-2*	May 2				

* Station D43-2 was sampled in May but as it was on same location as station D43 and D43-1, we decided to regroup them in April.

Table III.1: Dates of the sampling stations. The "D" stations were sampled on drifting sea ice (pack ice) while the "F" stations were sampled on landfast sea ice.

to the plastic bag to halt biological activity. The bag was immediately closed, and excess air was removed through the tube. The ice was allowed to completely melt at +4°C in the dark, after which DIC and TA analysis were immediately undertaken. The maximum potential leakage has been estimated to less than 20 µmol kg^{-1} by *Miller et al.* [2011]. This error is consistent with our own assessment at high pCO_2 in the conditions encountered during the survey. Sackholes were drilled at different depths, ranging from about 15 cm. Brines, from adjacent brine channels and pockets, seeped into the sackholes for 10 – 60 min before being collected using a peristaltic pump (Cole Palmer, Masterflex® - Environmental Sampler) [*Gleitz et al.*, 1995]. Each sackhole remained covered with a plastic lid to minimize mixing with the free-atmosphere. Under ice sea-water was also collected using the same peristaltic pump at the ice-water interface and at 1 m depth.

Sea ice temperature was measured *in situ* directly after extraction of the core using a calibrated probe (TESTO® 720) inserted into pre-drilled holes (~3 cm depth) perpendicular to core sides. The hole diameter matched that of the temperature probe. Precision of the measurements was ±0.1°C. Bulk ice salinity was determined on board from melted ice sections with a Thermo-Orion® portable salinometer WP-84TPS meter with a precision of ±0.1. Ice sections were cut from successive 5 cm thick slices of a dedicated ice core. These sections were then melted in the dark at +4°C to perform Chl a measurements that were carried out using the extraction method described by *Parsons et al.* [1984].

DIC and TA were measured on melted bulk ice, brine and seawater samples. Brine and seawater samples were poisoned with a solution of supersaturated $HgCl_2$ and samples were stored in the dark, at +4°C until analysis. The concentration of DIC and TA in melted bulk ice, brine and seawater were all analyzed on board by coulometric and potentiometric titration, respectively, using a VINDTA® 3C (Versatile Instrument for the Determination of Titration Alkalinity, by Marianda®). A description of procedures is detailed by *Shadwick et al.* [2011]. Routine analyses of Certified Reference Materials (provided by A. G. Dickson, Scripps Institution of Oceanography) ensured that the uncertainty of the DIC and TA measurements were less than 2 µmol kg^{-1} and 3 µmol kg^{-1}, respectively.

The pCO_2 of brine and seawater from underneath the ice was measured *in situ* using a custom made equilibration system [*Delille et al.*, 2007]. The system consisted of a

membrane contractor equilibrator (Membrana®, Liqui-cell) that was connected to a non-dispersive infrared gas analyser (IRGA, Li-Cor® 6262) via a closed air loop. Brine and air flow rates through respectively the equilibrator and IRGA were approximately 2 L min^{-1} and 3 L min^{-1}. Temperature was simultaneously measured *in situ* and at the outlet of the equilibrator using Li-Cor® temperature sensors. Temperature correction of pCO_2 was applied assuming that the relation of *Copin-Montégut* [1988] is valid at low temperature and high salinity. The IRGA was calibrated soon after returning on the ship while the analyser was still cold. Data were stored on a Li-Cor® Li-1400 data logger. All the devices, except the peristaltic pump, were enclosed in an insulated box that contained a 12 V power source providing enough warming to keep the inside temperature just above 0°C.

The CO_2 fluxes at the upper sea ice surface were measured using an accumulation chamber (West system®). The chamber is a metal cylinder closed at the top, with an internal diameter of 20 cm and an internal height of 9.7 cm. A rubber seal surrounded by a serrated-edge steel ensures an air-tight connection between the ice and the chamber of accumulation. For measurement over snow, a steel tube was mounted at the base of the chamber to enclose snow down to the ice and prevent lateral infiltration of air through the snow. The chamber was connected in a closed loop to the IRGA with an air pump rate at 3 L min^{-1}. The measurement of pCO_2 in the chamber was recorded every 30 sec for at least 5 min. The flux was computed from the slope of the linear regression of pCO_2 against time ($r^2>0.99$) according to *Frankignoulle* [1988], taking into account the volume of ice or snow enclosed within the chamber. The uncertainty of the flux computation due to the standard error on the regression slope was on average ±3%.

3. Results

3.1 Background measurements

Drift sea ice was sampled in April (stations D36 to D43-2) while landfast sea ice was sampled from May to June (stations F1 to F7-1) (Fig. III.3). Our reference to Fig. III.3 is limited to the interpretation of the CO_2 data. A companion paper [*Carnat et al., this issue*] describes in details the thermodynamic evolution of the sea ice cover during the whole survey. In April, bulk ice salinity profiles (Fig. III.3b) presented a well-marked C-shape while the brine salinity exhibited a strong vertical gradient, driven by the temperature profile (Fig. III.3a). Apart from the warm bottom sea ice base, the ice was

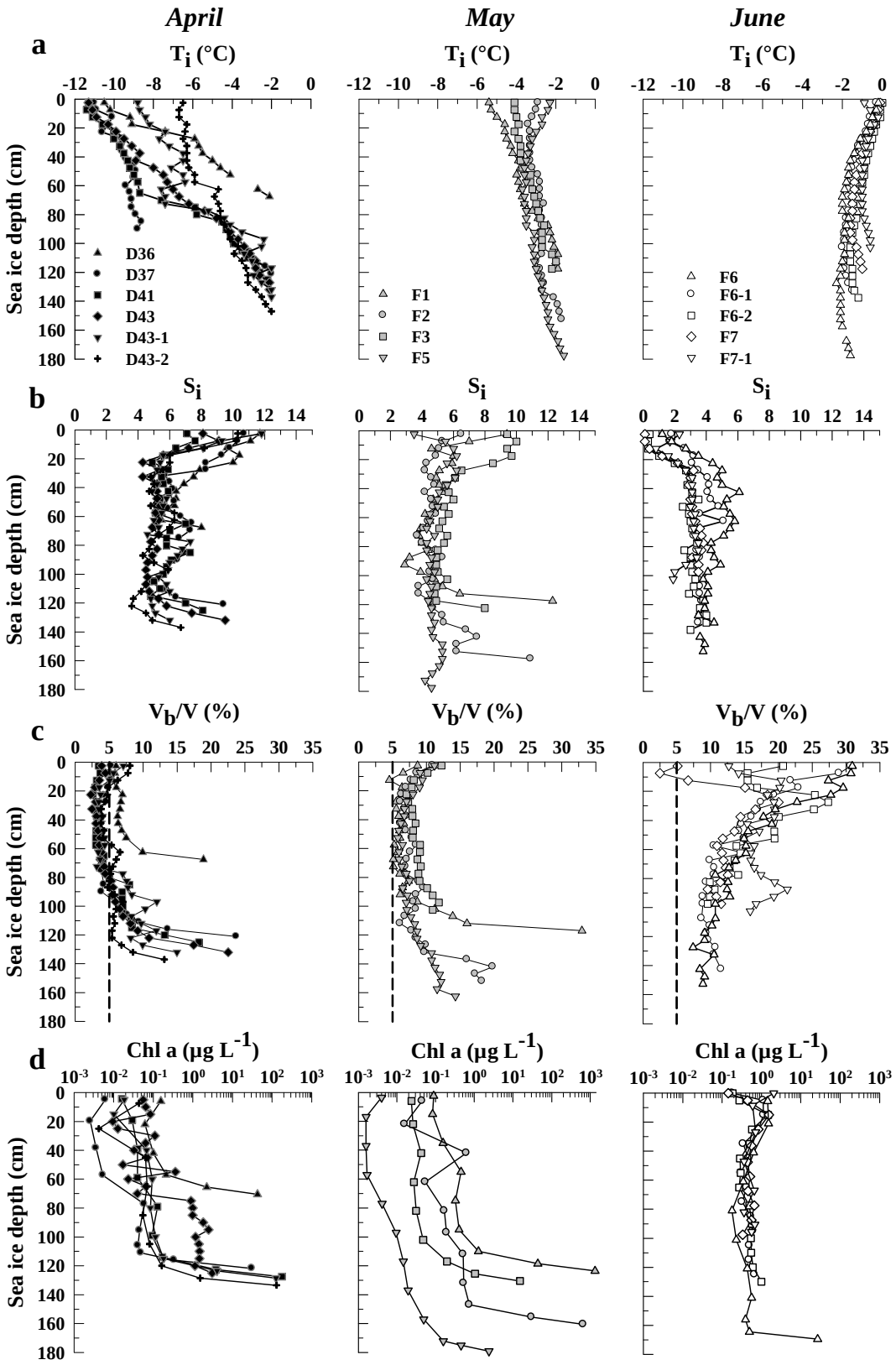

Figure III.3: Sea ice conditions for the CFL stations considered, adapted from the companion paper *Carnat et al.* [*this issue*], including (**a**) temperature profile,T_i, (**b**) salinity profile, S_i, (**c**) relative brine volume, V_b/V and (**d**) Chl a concentration.

NB: during June, the data at a depth of 0 represents the melt ponds.

mainly under the permeability threshold of 5% for columnar ice (Fig. III.3c). These stations were typical of a late winter situation. Bulk ice salinity at the surface decreased with a minimal value observed at the end of the month. The brine salinity decreased as well. The ice was beyond the permeability threshold. These stations were typical of a warming period. Finally, in June, the ice temperature profiles became isothermal, around -1°C, with a maximal temperature observed at the top of the ice. Bulk ice as well as brine salinity were marked by a minimum at the top. The ice was highly permeable. These characteristics are typical of a decaying sea ice cover.

The sea ice concentration of Chl a ranged from below 0.01 µg L^{-1} up to 1330 µg L^{-1} (Fig. III.3d). From April to May, Chl a concentration in bottom sea ice increased significantly from 130 µg L^{-1} to 1330 µg L^{-1} then decreased to 1 µg L^{-1} in June. Our Chl a concentrations are consistent with values reported by *Mundy et al.* [*this issue*] and by *Song et al.* [*this issue*] during this survey and by *Riedel et al.*[2008] in the same area in 2004.

Brine temperature for the sampling stations ranged from -8.5°C in April to 0°C in June (Fig. III.4a). By mid-May brine temperature approached that of the underlying seawater, and then stabilized around 0°C thereafter. Brine salinity decreased from 137.4 in April to 0 in June (Fig. III.4b) in response to the seasonally rise in temperature. Brine salinity actually dropped below seawater salinity in late May. Seawater salinity at the ice-water interface remained fairly constant (between 33.2 and 30.7) until late May and then decreased slightly to 26.4, with very low values of 2.9 and 6.9 observed at F6-1 and F7, respectively.

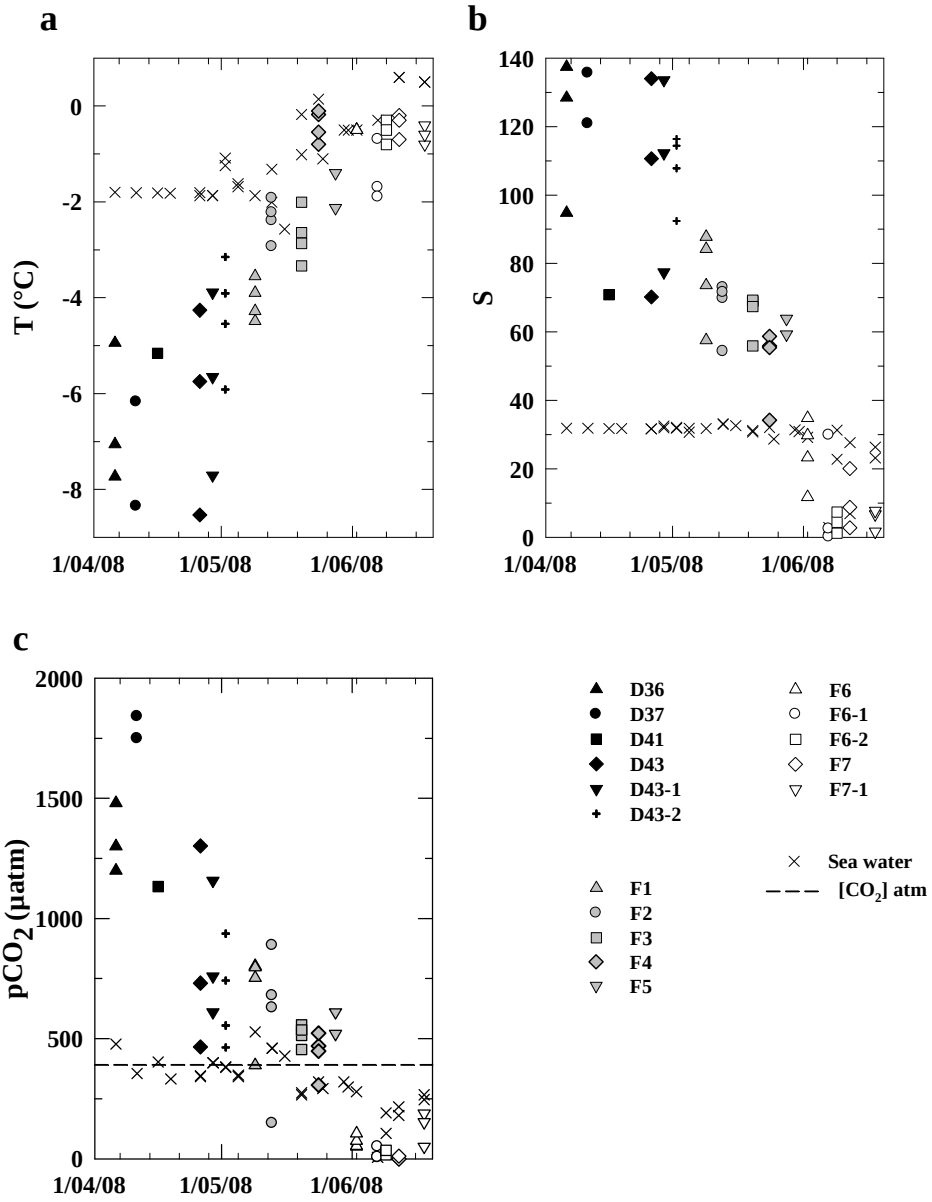

Figure III.4: Temporal evolution of brine and seawater temperature (**a**), salinity (**b**) and pCO_2 (**c**) for the CFL stations considered.

3.2 Inorganic carbon

In April, it was not possible to collect brine samples at all depths due the small volume of brine available (Fig. III.3c). Brine pCO_2 were supersaturated (relative to atmospheric concentration) throughout the sea ice, ranging between 1839 µatm to 465 µatm (Fig. III.5). The maximum brine pCO_2 was observed in the middle of the ice column. Variation in pCO_2 with depth declined in May, with pCO_2 decreasing from F1 to F4. The brine pCO_2 remained supersaturated (between 888 µatm to 389 µatm), except at the 2 bottom most brine sampling depths, where a pCO_2 of 147 µatm and 306 µatm was observed at F2 and F4 respectively. Brine pCO_2 declined significantly by June, at which

time it was highly undersaturated with respect to the atmosphere, with values ranging from 188 µatm to 0 µatm. The pCO_2 in the melt ponds ranged between 79 µatm to 348 µatm.

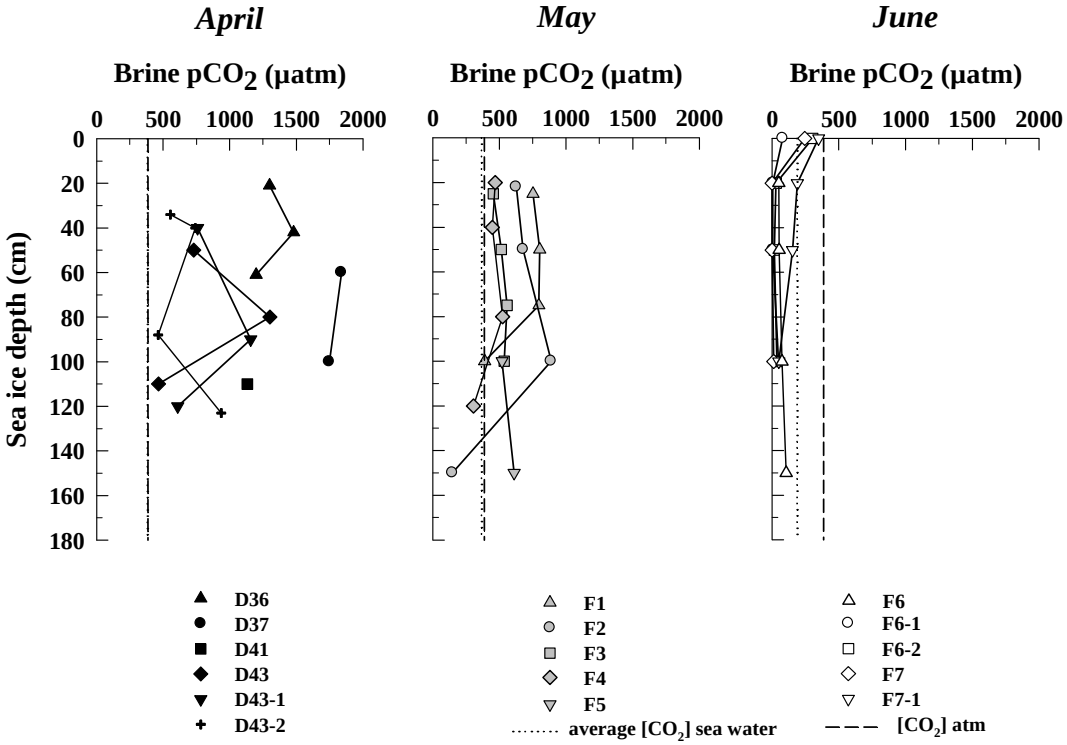

Figure III.5: Profiles of brine pCO_2 for the three groups of stations considered. The seawater pCO_2 (dotted line) is an average for the considered month.

The pCO_2 of the underlying water ranged from 528 µatm to 5 µatm (Fig. III.4c) over the sampling period. In April, seawater pCO_2 was relatively stable near to atmospheric levels (396 µatm). In early May, seawater pCO_2 increased, reaching 528 µatm, and then declined to a marked undersaturation by June, with some measurements approaching 5 µatm. The low summer seawater pCO_2 is associated with a reduction in seawater salinity (Fig. III.4c). The pCO_2 of both underlying water and brine passed below the threshold of saturation at the same time. At some time, seasonal variation of pCO_2 of the underlying water does not mimic seasonal pattern presented by *Shadwick et al.* [2011]. However, the pCO_2 values of *Shadwick et al.* [2011] are underway pCO_2 data collected water at 3 m deep and averaged both spatially (over a larger region than that presented here) and temporally (monthly), while the data presented here was discrete measurement at the ice-water interface.

TA and DIC in brine ranged from 173 µmol kg^{-1} to 8191 µmol kg^{-1} and from 165 µmol kg^{-1} to 8254 µmol kg^{-1}, respectively. TA and DIC in bulk sea ice ranged from 69 µmol

kg^{-1} to 635 µmol kg^{-1} and 177 µmol kg^{-1} to 613 µmol kg^{-1}, respectively (Fig. III.6a, b). In seawater samples, TA and DIC ranged from 331 µmol kg^{-1} to 2280 µmol kg^{-1} and 301 µmol kg^{-1} to 2210 µmol kg^{-1}, respectively. Both TA and DIC for bulk sea ice and seawater samples are of the same order of magnitude than those reported by *Miller et al.* [2011] and *Rysgaard et al*. [2007] who both presented TA and DIC measurement from landfast sea ice in Franklin Bay, Canada.

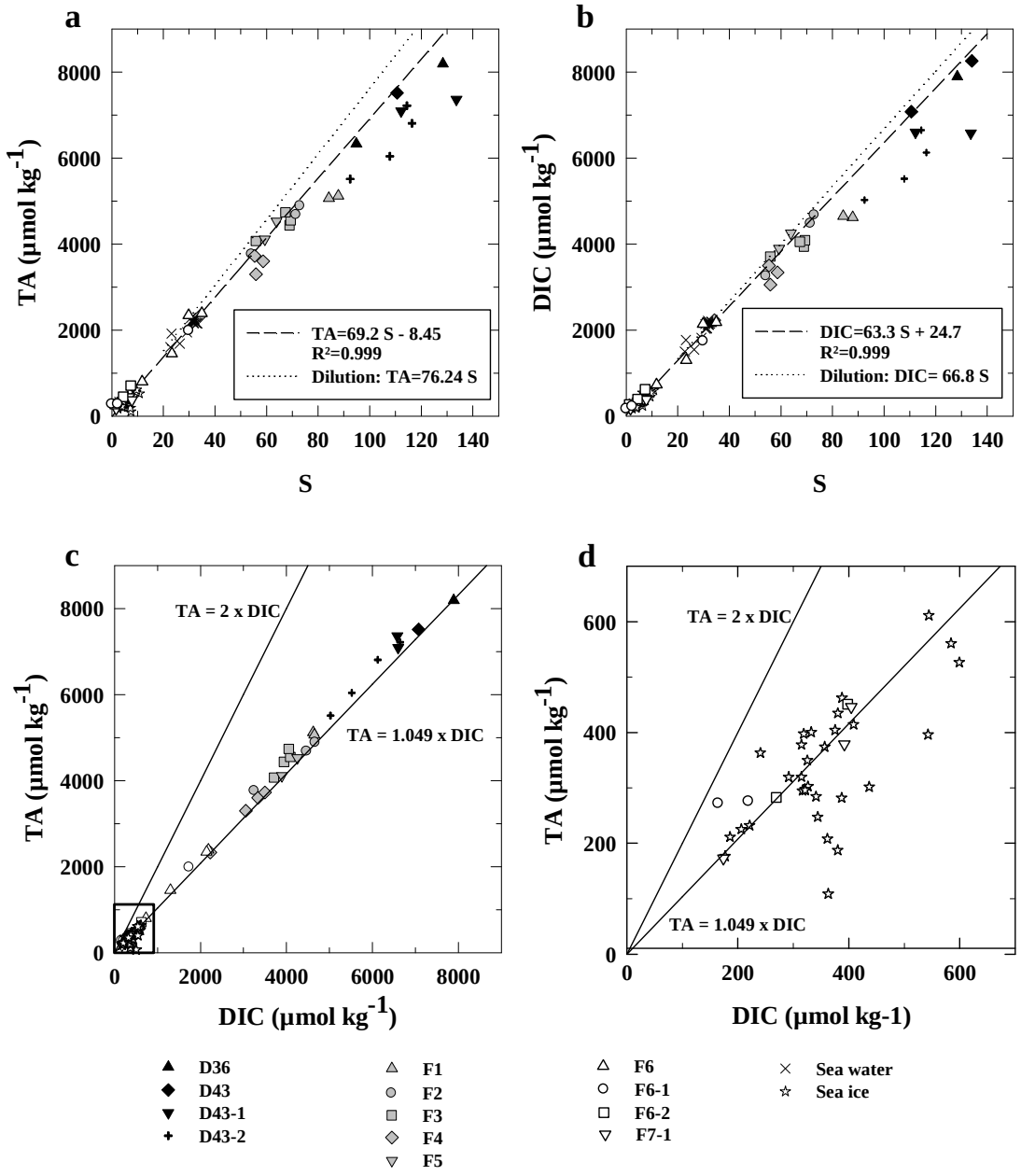

Figure III.6: Evolution of TA (**a**) and DIC (**b**) as a function of the salinity of the brine for all the CFL stations considered. The dotted line represents expected values based on dilution effect during melting while the dashed line represents the highly correlated relation between TA (or DIC) with salinity. The relation between TA and DIC for both the brine and the sea ice (stars) is shown in **c**. Figure **d** is a "zoom in" of the square from figure **c** in order to better document the relation in bulk sea ice. The two lines show the ratio TA: DIC of 2 (representing the stoichiometry of the precipitation/dissolution equilibrium in equation 1) and the TA: DIC ratio of 1.049, typical of the underlying seawater.

3.3 CO_2 fluxes

CO_2 fluxes were measured over sea ice, on sea ice, melt ponds, superimposed ice (Fig. III.7a) and on snow cover (Fig. III.7b). The CO_2 fluxes at the sea ice interface ranged from +0.84 mmol m^{-2} d^{-1} to -2.63 mmol m^{-2} d^{-1} (where a positive value indicates a CO_2 released from the ice surface to the atmosphere) while fluxes over snow cover ranged between +2.1 mmol m^{-2} d^{-1} and -1.49 mmol m^{-2} d^{-1}. No fluxes were detected on superimposed ice. Strong negative fluxes were measured over melt ponds, ranging from -0.13 mmol m^{-2} d^{-1} to -2.65 mmol m^{-2} d^{-1}. Observed fluxes over the sea ice were similar to measurements reported in Barrow (Alaska) or in the Hokkaido island (Japan) by *Nomura et al.* [2010b] and [2010a], respectively and by *Delille and co-workers* (*i.e., Delille* [2006]) in Antarctica, using similar chamber techniques. Note that fluxes were also not detected on superimposed sea ice by *Nomura et al.* [2010a] and *Delille and co-workers* (*i.e., Delille* [2006]).

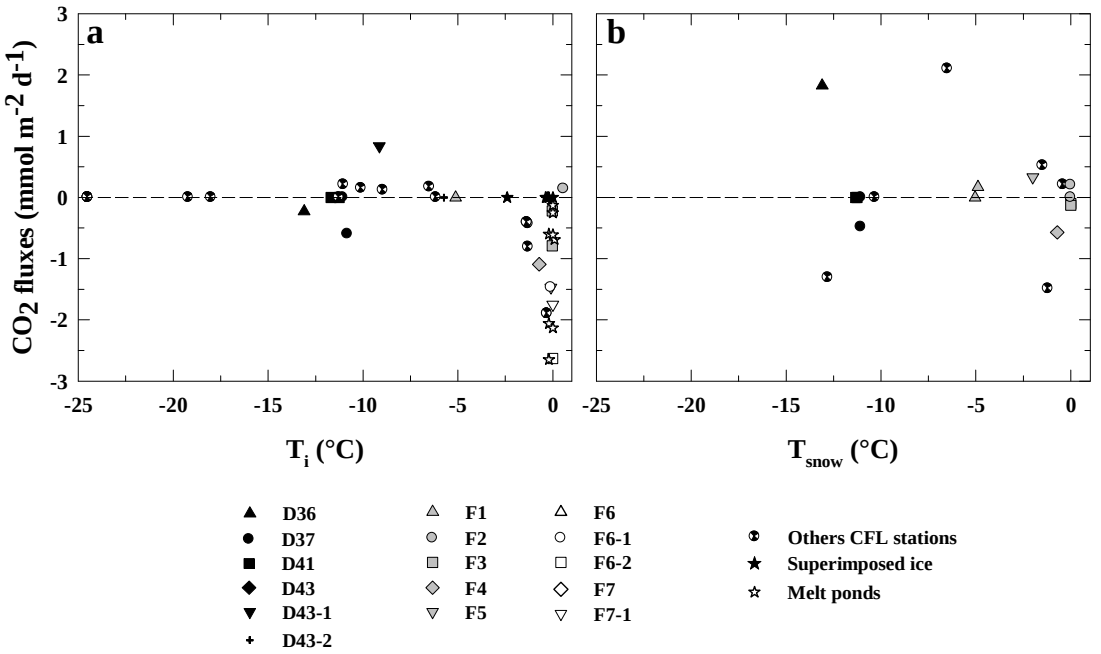

Figure III.7: CO_2 fluxes measured on sea ice, melt ponds and superimposed ice interface with the atmosphere (**a**) and on the snow (**b**). The other CFL stations represent additional sampling stations where only fluxes where measured.

No fluxes were detected for ice surface temperature below -10°C, with the exception of a small negative flux of -0.23 mmol m^{-2} d^{-1} to -0.6 mmol m^{-2} d^{-1} at stations D36 and D37, respectively. As the temperature of the ice increased from -10°C to -6°C, a positive flux was observed with a maximum value of +0.84 mmol m^{-2} d^{-1}. Finally, from -6°C to 0°C, negative fluxes with a maximum value of -2.6 mmol m^{-2} d^{-1} were

observed. On snow, flux trends were much less clear with higher temporal variability. Fluxes ranged from -1.49 mmol m^{-2} d^{-1} to +2.1 mmol m^{-2} d^{-1}. The overall pattern is similar to fluxes over the ice, but with a large number of observations showing negligible fluxes and a few outliers, with higher values than over the ice, both positive and negative, with no relationship to the air and ice temperature.

4. Discussion

Inorganic carbon dynamics in the ocean is affected by several processes, including temperature and salinity changes, precipitation or dissolution of $CaCO_3$ and biological activity [*Zeebe R.E. and Wolf-Gladrow*, 2001]. This holds true for sea ice, yet changes in temperature and salinity are enhanced compared to the water column.

4.1 Effects of primary production

Evaluating primary production within sea ice and the related impact on brine pCO_2 has been proven difficult [*Delille et al.*, 2007]. A common indicator of primary production is the change in autotrophic biomass. A rough measure of algal biomass is algal pigment concentration (Chl a). Chl a in sea ice varies by geographic region, ice type and seasons [*Arrigo et al.*, 2010a].

In April and May, while Chl a concentration values remained below 1.7 µg L^{-1} in brine, a large increase of Chl a concentration up to 1330 µg L^{-1} of bulk ice at the bottom was observed. Such build-up of Chl a suggests sustained primary production that potentially consumes CO_2, *i.e.*, reducing both sea ice DIC and brines pCO_2. An enhanced pCO_2 decrease was observed at the time of the sympagic algal bloom in April and May and corresponded, in time, to a rapid decrease of DIC at the bottom of the ice, as reported by *Shadwick et al.* [2011]. This sympagic bloom led to a sharp increase of net community production in the surface water up to 1.1 mol C m^{-2} $month^{-1}$ [*Shadwick et al.*, 2011]. However, in June, Chl a concentration decreased significantly down to 1 µg L^{-1}, likely due to brine flushing. This range of Chl a concentration was also observed at the bottom of the ice cover by *Song et al.* [*this issue*] and *Mundy et al.* [*this issue*]. At that time, brine pCO_2 continued to decrease, suggesting that processes other than the production of sympagic algae contributed to the pCO_2 decrease. Thereafter, the impact of primary production on pCO_2 appears to last only a few weeks during biomass build up prior to brine flushing.

4.2 Effects of $CaCO_3$ precipitation, dissolution

As suggested by *Delille and co-workers* (*i.e., Delille* [2006]) and *Rysgaard et al.* [2007; 2009], other processes, such as $CaCO_3$ dissolution, can potentially promote the decrease in brine pCO_2. According to equations III.1 to III.3, $CaCO_3$ precipitation reduces both DIC and TA in the brine. *Rysgaard et al.* [2007] suggested that this precipitation within sea ice could drive significant CO_2 uptake and that the TA: DIC ratio as high as 2 in melted bulk sea ice indicates that $CaCO_3$ precipitation occurs. During our survey, brine samples with salinity larger than 80 showed lower TA and DIC than expected from salinity changes (Fig. III.6a, b). In addition, plotting TA_{35} as a function of DIC_{35} (TA and DIC values being normalized to a salinity of 35 to discard concentration/dilution effects) indicates that these high salinity brine samples (D36, D43-1, D43-2, F1, F3, and F4) are well aligned (slope 0.89, $R^2 > 0.999$) on a trend between the theoretical trend for calcium carbonate precipitation and the one for CO_2 degassing (Fig. III.8). This could be expected if both $CaCO_3$ precipitations occurred in high salty brines and CO_2 degassing occurred in the sea ice (Fig. III.8). This is consistent with previous findings of *Rysgaard et al.* [2007].

In order to compare with literature, we computed none-normalized TA: DIC ratio in bulk ice that is about 0.96 (Fig. III.6c, d), *i.e.,* very close to the value of underlying water (1.049) and the value of 1.01 reported by *Miller et al.* [2011], but significantly lower than the average of values reported by *Rysgaard et al.* [2007] in Franklin Bay that is about 1.55. *Miller et al.* [2011] addressed discrepancies between their study and observations of *Rysgaard et al.* [2007] and proposed several explanations. TA_{35} and DIC_{35} of bulk ice are lower than TA_{35} and DIC_{35} from the underlying water as a result of $CaCO_3$ precipitation and subsequent release of by-products of $CaCO_3$ into the water column (Fig. III.8).

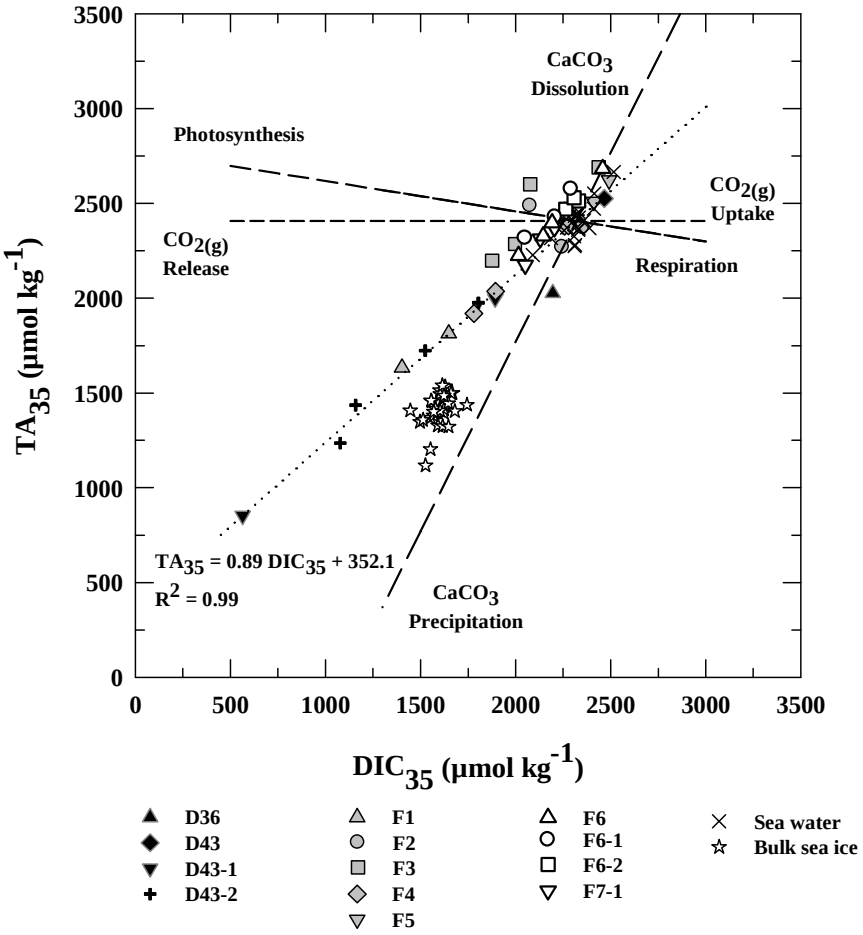

Figure III.8: DIC_{35}: TA_{35} (values normalized to a salinity of 35) relationship in brine, seawater samples and ice samples. The different dotted lines represent the theoretical evolution of DIC_{35}: TA_{35} following a precipitation/ dissolution of calcium carbonate, a release or uptake of $CO_{2(g)}$ and impacts of biology.

4.3 Effects of temperature and salinity

As the ice temperature increases, ice crystals melt and salinity decreases accordingly. We explored the relationships among brine pCO_2, temperature and salinity according to the following steps: (i) we calculated brine salinity at a given temperature according to the relationship of *Cox and Weeks* [1983]; (ii) we normalized mean TA and DIC to a salinity of 35 (TA_{35}, and DIC_{35}, respectively) for all samples with salinity < 80 (see section 4.2 for the choice of this threshold); (iii) we computed TA_t and DIC_t at a given temperature, *t* (and related salinity) assuming a conservative behavior of TA and DIC; and (iv) computed the brine pCO_2 for each temperature from TA_t and DIC_t, using CO2SYS [*Lewis and Wallace*, 1998] with the CO_2 acidity constants of *Dickson and Millero* [1987]. Here we assume that these constants are valid for the range of temperatures and salinities encountered within the sea ice [*Papadimitriou et al.*, 2004; *Delille et al.*, 2007]. The resulting pCO_2 - temperature relationship (denoted as CFL-

dilution) is shown in figure III.9. A test of root mean square deviation was carried out on the dilution curve and showed a mean dispersion of 230 µatm. This dispersion decreased in June down to 52 µatm. Scattering is due to spatial heterogeneity, superimposition of physical and biogeochemical processes that are not related together, and thermal history of the ice, among other explanations.

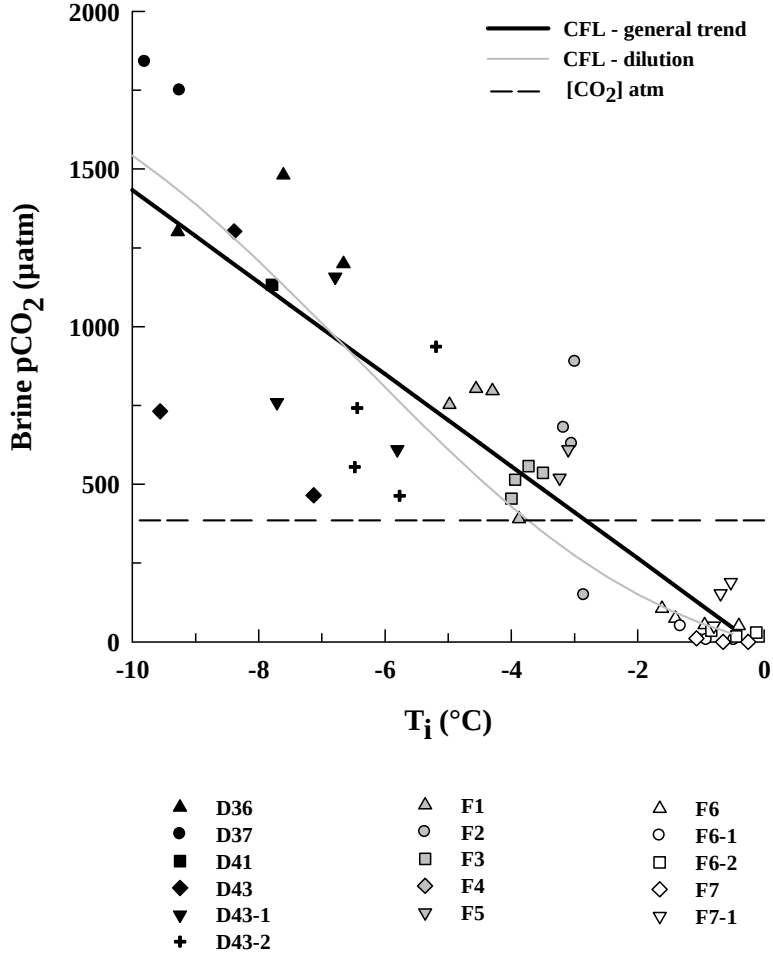

Figure III.9: The pCO_2 evolution with ice temperature. The ice temperature was integrated over the depth of ice where the brine was sampled (*i.e.,* from surface to bottom of sackholes). The solid lines represent the general trend during CFL while the dashed lines represent the pCO_2: temperature relationship computed for the dilution effect (see text for details).

The observed pCO_2 response to temperature, roughly mimics the dilution curve, highlighting a major control of melting on pCO_2 as observed in Antarctica by *Delille and co-workers* (*i.e., Delille* [2006]). In June, brine drainage significantly reduced bulk ice salinity, leading to a drastic decrease in pCO_2, down to the almost zero as a result of the melting of low-CO_2 pure ice matrix.

4.4 Under-ice melt ponds

Ice melting, brine flushing and drainage of melt pond lead to the formation of a stable fresh water layer at the ice-ocean interface. These fresh water lenses, called under-ice melt ponds by *Hanson* [1965], are usually trapped under thinner ice areas or in depressions in the bottom of thicker ice. Within this fresh water layer, we observed a marked undersaturation down to 5 µatm (Fig. III.4c). At that time, despite the increase in light availability, algal biomass remained low, probably as a consequence of nitrate + nitrite limitation [*Mundy et al., this issue*]. Our results suggest that phytoplanktonic growth can also be limited by CO_2 availability [*Riebesell et al.*, 1993; *Wolf-Gladrow and Riebesell*, 1997]. Hence, phytoplanktonic limited growth is likely to play a minor role on CO_2 undersaturation. At that time, pCO_2 of melt ponds at the top of the ice was larger than pCO_2 of under-ice melt ponds, suggesting that this low salinity-low pCO_2 water layer is originated from melted sea ice, rather than surface melt ponds that percolated through the ice.

4.5 Inter-hemisphere comparison

In Antarctica, *Delille and co-workers* (*i.e., Delille* [2006]) reported values of pCO_2 ranging from 30 µatm to 920 µatm. The range of pCO_2 observed during the survey was significantly larger than in Antarctica, with both higher and lower end values (Fig. III.9). In cold sea ice in particular, we observed significantly higher pCO_2 values in the Amundsen Gulf than in Antarctica for a given temperature. As discussed above, several processes can be responsible for the pCO_2 dynamics within the sea ice brine: temperature and salinity changes, calcium carbonate precipitation, and/or primary production. The first is unlikely to explain our Arctic-Antarctica discrepancies in cold sea ice. Also, at a given temperature, the effect of brine concentration on pCO_2 is expected to be similar in both hemispheres. The processes driving $CaCO_3$ precipitation in the brine network are also likely to be similarly controlled by temperature-driven brine concentration in sea ice from both polar regions. The discrepancy in pCO_2 between the polar regions may be related to differences in the rate that organic carbon is oxidized through ecosystem respiration.

We compared organic matter (dissolved organic carbon, DOC, and particulate organic carbon, POC) abundance in the Amundsen Gulf and antarctic open water (Table III.2). Higher level of organic matter in the Amundsen Gulf, compared to antarctic open

waters is likely due to large riverine input. The Mackenzie River, the largest river in terms of POC discharge in the Arctic, has the potential to cause strong variations in POC export from shelf to basin, and discharge directly in the Beaufort Sea [*Lalande et al.*, 2009]. According to *Magen et al.* [2010], the Mackenzie River mainly contributes to the input of organic matter. Higher organic carbon concentration in the Amundsen Gulf compared to Antarctica could potentially support higher respiration and related CO_2 production and can therefore possibly explain the generally higher pCO_2 values. Taking into account that the Arctic Ocean is a closed sea with a stronger continental organic matter input compared to Antarctica, elevated pCO_2 in cold sea ice could be a general feature in the Arctic. More pCO_2 surveys in the arctic sea ice and reliable assessment of winter respiration over the whole ice thickness are however required to settle this question.

	Studies		**POC ($\mu mol\ L^{-1}$)**	**DOC ($\mu mol\ L^{-1}$)**
Arctic	*Riedel et al.* [2008]	Pre-bloom	53.53	60.22
		Bloom	740.54	496.29
		Post-bloom	2185.93	777.34
	Song et al. [*this issue*]			563 ±434
Antarctica	*Dumont* [2009]	Bruxelles	35.34	55.2
		Liège	26.6	34.2
	Thomas et al. [2001]	SE Weddell Sea		523
		Bellingshausen Sea		109
		Weddell Sea		207

Table III.2: POC and DOC concentration in sea ice. In Arctic, *Riedel et al.* [2008] measured POC and DOC concentration in the bottom 4 cm of the ice from February 24th to June 20th in Franklin Bay, in the Amundsen Gulf in the frame of the *Canadian Arctic Shelf Exchanges Study* (CASES). *Song et al.* [*this issue*] measured DOC concentration in the bottom 10 cm of the ice between mid-March and early July 2008. *Dumont* [2009] measured POC and DOC within sea ice in the Bellingshausen Sea, Antarctica in September – October 2007. *Thomas et al.* [2001] presented data from the southeastern Weddell Sea in April – May 1992, Bellingshausen Sea in January – February 1994 and Weddell Sea in January – March 1997. Data from *Dumont et al.* [2009] are an average on the bottom 10 cm of the ice while *Thomas et al.* [2001] only shows a mean values.

4.6 Air-ice CO_2 fluxes

In cold sea ice (below -11°C), we did not detect significant air-ice CO_2 fluxes. As temperature increased, ice became permeable to gases and air-CO_2 fluxes were observed for temperature above -11°C. Effluxes of CO_2 from the ice to the atmosphere were then observed in April (Fig. III.7) while brine pCO_2 was supersaturated with respect to the atmosphere, which explains the decrease of the brine pCO_2 observed in the top layers in the vertical profiles of figure III.5. In some cases, we observed CO_2 effluxes while brine

volume was under the permeability threshold of 5% [*Golden et al.*, 2007]. According to *Gosink et al.* [1976] and *Loose et al.* [2011], the porosity threshold for gas transport may be lower than for fluid transport [*Golden et al.*, 2007]. If the gas transport threshold is lower than the threshold of permeability for liquid, then diffusive transport could allow gas exchanges earlier in the spring and later in the fall or even during winter. However, further experiments are needed to better explain and constrain gas fluxes below the permeability threshold for liquids.

In addition, the internal precipitation of calcium carbonate, at that time or earlier, could promote the release of CO_2 to the atmosphere. This is consistent with the observed trend of the DIC_{35}: TA_{35} relationship in the high salinity brine sample that suggests a release of CO_2 associated with the precipitation of $CaCO_3$ (Fig. III.8). From May, the brine pCO_2 was initially supersaturated but decreased with rising of ice temperature and passed below the threshold of the atmospheric concentration. Accordingly, negative fluxes were measured from F6 onwards down to -2.6 mmol m^{-2} d^{-1}.

This is in agreement with previous works of *Delille and co-workers* (*i.e.*, *Delille* [2006]), *Nomura et al.* [2006] and [2010b] who suggested that brine pCO_2 is an important factor controlling the air-ice CO_2 flux. The magnitude of CO_2 fluxes also depends on sea ice permeability. Since, ice temperature controls both pCO_2 and permeability through brine volume [*Golden et al.*, 2007], ice temperature therefore appears to be one of the main control of air-ice CO_2 fluxes.

Air-ice CO_2 fluxes are also affected by the state of the air-ice interface. A particular importance is the occurrence of superimposed ice that clearly impedes air-ice gas transfer (Fig. III.7a). *Nomura et al.* [2010b] suggested that snow cover was an impermeable medium, blocking CO_2 diffusion and exchange to the atmosphere. Nevertheless, this observation was made during superimposed ice formation [*Nomura et al.*, 2010a]. Our observations are agree with the work of *Delille and co-workers* (*i.e.*, *Delille* [2006]), *Nomura et al.* [2010a] and suggest that superimposed ice hamper air-ice CO_2 fluxes. However, in none-superimposed ice conditions, we observed CO_2 fluxes as previously reported over snow covered terrestrial ecosystem. In our study, air-ice CO_2 fluxes appear to be driven by air-ice pCO_2 gradient and controlled by sea ice permeability. Air-ice fluxes appear to be moderated by the snow, but the CO_2 fluxes measured in absence of snow do not translate readily into snow-air CO_2 fluxes. Snow physical and chemical properties, *e.g.*, porosity, texture, salinity, total alkalinity, among

other parameters like snow thickness, are likely to affect the magnitude of the fluxes. The impact of the snow cover on gas exchanges is still unknown. *Albert et al.* [2002] suggested that the high permeability of the snowpack allow rapid gases exchanges with the atmosphere, even with moderate winds. On the other hands, *Takagi et al.* [2005] found that CO_2 concentrations in the snowpack fluctuated significantly as wind speed varied, suggesting a strong wind-pumping effect on CO_2 movement in the snowpack. Using eddy covariance, *Papakyriakou and Miller* [2011] generally found fluxes to increase with increasing wind speed over seasonal sea ice, with the largest fluxes occurring during periods of blowing snow.

By contrast, melt ponds development appears to promote the uptake of CO_2 by the ice with observed air-ice CO_2 fluxes as low as -2.7 mmol m^{-2} d^{-1}. This magnitude is lower than what was reported by *Nomura et al.* [2010b] with values ranging from -38.6 mmol m^{-2} d^{-1} to -19.5 mmol m^{-2} d^{-1} over melt ponds in landfast ice near Barrow, Alaska. These fluxes are in the same order of magnitude than fluxes measured by *Semiletov et al.* [2004] using the chamber techniques. *Semiletov et al.* [2004] suggested a significant role of photosynthesis activity to the fluxes. However, Chl a was measured on melt ponds and exhibited low concentration (~2 µg L^{-1}) as also measured by *Mundy et al.* [*this issue*]. On the other hand, melting of low-CO_2 pure ice matrix acts to decrease pCO_2.

We attempted to assess the potential uptake of atmospheric CO_2 by melting sea ice that equilibrates with the atmosphere. In the station F6-2, we observed air-ice CO_2 fluxes around -2.6 mmol m^{-2} d^{-1}. Taking into account the brine conditions (TA= 451 µmol kg^{-1}, DIC=398 µmol kg^{-1}, S = 4.4 and T= -0.8°C), the equilibrium of such brines with the atmosphere (pCO_2 = 390 µatm) would correspond to an uptake of CO_2 of 80 µmol kg^{-1} of brines. In the same way, the equilibration of ice samples of station F6-2, or pure freshwater ice would correspond to an uptake of 40 and 32 µmol kg^{-1} of ice respectively. If we assume a complete melting, and subsequent equilibrium with the atmosphere of a 1.3 m thick ice cover within one month, this would lead to average CO_2 fluxes ranging from -1.2 to -3.1 mmol m^{-2} d^{-1} that are rather consistent with the air-ice CO_2 fluxes measured over melt ponds and decaying sea ice (-0.02 mmol m^{-2} d^{-1} to -2.65 mmol m^{-2} d^{-1}). This computation provides a potential CO_2 uptake, assuming an ideal case of complete melting without interactions with the underlying seawater.

5. Conclusions

This study gives an overview of the evolution of pCO_2 dynamics within sea ice from late spring to summer in the arctic coastal waters of the Amundsen Gulf. We present the first vertical profiles of pCO_2 in sea ice brine to demonstrate the evolution with the physical and biogeochemical parameters in the ice and their relationship to the CO_2 fluxes at the ice-atmosphere interface.

As sea ice forms and grows, and ice temperature decreases, all the impurities (including salts, organic matter and gases) are concentrated in brine leading to a significant increase of brine salinity and brine pCO_2 (up to 1839 µatm in April). As salinity increases, significant changes with respect to mineral-liquid thermodynamic equilibrium can occur and calcium carbonate can precipitate [*Dieckmann et al.,* 2008]. Indirect evidence of such precipitation was observed within highly saline brine, in the upper part of the sea ice cover and in bulk sea ice. This is in agreement with the work of *Dieckmann et al.* [2008] and *Rysgaard et al.* [2007; 2009].

As summer draws near, the ice temperature increases and, according to *Papadimitriou et al.* [2004], *Delille and co-workers* (*i.e., Delille* [2006]), *Nomura et al.* [2006] and *Delille et al.* [2007], the brine pCO_2 decreases. We measured a shift from 1834 µatm in April to almost 0 µatm in June. This decrease was mainly due to the brine dilution by fresh water coming from internal and surface melting of sea ice. Dissolution of calcium carbonate, and primary production, enhance this spring/summer pCO_2 decrease. As sea ice became more permeable to gas exchange and brine became undersaturated, strong negative CO_2 fluxes were observed (down to -2.6 mmol m^{-2} d^{-1} above sea ice and -2.7 mmol m^{-2} d^{-1} above melt ponds).

While primary production at the bottom of the ice reduces the brine pCO_2 during spring bloom, organic matter degradation by microbial communities could explain the higher pCO_2 level in the Amundsen Gulf compared to antarctic open waters in winter.

6. Acknowledgments

The authors would like to acknowledge the outstanding support and kindness of the crew members of the *CCGS Amundsen*. Funding for the Circumpolar Flaw Lead project was provided by the Canadian International Year (IPY) program office, the Canadian Natural Sciences and Engineering Research Council (NSERC), ArcticNet - a Network

of Centres of Excellence, the Canada Research Chairs (CRC) Program and the Canada Foundation for Innovation (CFI). We would also like thanks Ms. Noel from National Geographic Institute (Belgium) for her support in mapping. This research was also supported by the F.R.S-FNRS (contract 2.4649.07), with which BD is a research associate, and the Belgian Science Policy (contract SD/CA/03A). NXG received a PhD grant from the Fonds pour la Formation à la Recherche dans l'Industrie et l'Agriculture. This is MARE contribution no. XXX.

Chapter IV: Towards a method for high resolution measurements of the partial pressure of CO_2 within bulk sea ice

Sea ice temperature measured in situ during CFL.

Foreword

This method results of several years of work. Several issues have been encountered principally due to the difficulty to develop a non-destructive method allowing to have access to brine inside of the ice sample.

We decided to use this method on sample from the survey “Year round follow up of air-ice-ocean carbon dioxide exchanges for arctic sea ice: a contribution to the International Polar Year” carried out in Barrow, Alaska. To strive towards our aim, a meteorological mast equipped for eddy-covariance measurement was installed on the landfast sea ice. We hypothesized that CO_2 fluxes are driven by the gradient of concentration between sea ice. Robust assessment of the pCO_2 at the sea ice interface with the atmosphere was therefore required. However, until now, the only way to measure the pCO_2 within sea ice was to performed *in situ* pCO_2 measurement within sea ice brine collected in sackholes. Unfortunately, the sackholes method does not allow to measure robustly the pCO_2 at the sea ice interface, owing to its poor vertical resolution. Therefore, using the pCO_2 measurement on bulk sea ice was a good opportunity, especially as we were able to validate this new method by comparing our data from several depths with *in situ* brine pCO_2 measurements.

This chapter has been submitted to the Journal of Glaciology:

Geilfus, N.-X., Delille, B., Verbeke, V. and Tison, J.-L., Towards a method for high resolution measurements of the partial pressure of CO_2 within bulk sea ice.

Abstract

Fluxes of atmospheric CO_2 have been reported over sea ice during winter [*Heinesch et al.*, 2009; *Miller et al.*, 2011] and spring [*Semiletov et al.*, 2004; *Delille*, 2006; *Zemmelink et al.*, 2006; *Nomura et al.*, 2010b; 2010a; *Papakyriakou and Miller*, 2011]. According to *Delille and co-workers* (*i.e.*, *Delille* [2006]) and *Nomura et al.* [2010b], these fluxes are partly driven by the gradient of the CO_2 concentration between sea ice and the atmosphere.

In this report, we present a new non-destructive method to measure the pCO_2 of bulk sea ice at its *in situ* temperature. This method is based on an equilibration procedure between sea ice and a standard gas of known CO_2 concentration. The concentration is measured by gas chromatography (GC, Varian 3300®) with a precision of 5%. Tests were performed on artificial standard sea ice and confirmed the reproducibility of the technique in the range of precision of the gas chromatograph. To test the accuracy of this method, the first profiles of pCO_2 measured in bulk sea ice are reported and compared with direct *in situ* measurements of sackhole brine pCO_2 over depth-integrated intervals.

1. Introduction

Because of its specificities and the large variation of its seasonal extent (from 18.10^6 km^2 to 28.10^6 km^2), sea ice influences the global climate system through a suite of large-scale processes. Sea ice controls and is controlled by the albedo and the fluxes of heat and moisture across the ocean-atmosphere interface. The sea ice extent exerts control over thermohaline circulation through the production of deep water during its formation and the stratification of surface waters during the melt period [*Dieckmann and Hellmer*, 2010].

Each year, 7 Pg of carbon are released into the atmosphere as CO_2 by human activities. Oceans play a major role in the context of rising atmospheric CO_2 levels because 29% of anthropogenic CO_2 is taken up by the ocean through physical and biological processes [*Takahashi et al.*, 2009]. For decades, sea ice was assumed to be an impermeable and inert barrier to air-sea gas exchanges (*e.g.*, for CO_2), and thus, global climate models do not include CO_2 exchanges between sea ice and the atmosphere [*Tison et al.*, 2002; *Bates and Mathis*, 2009]. Nevertheless, there is growing evidence

that sea ice exchanges CO_2 with the atmosphere. *Golden et al.* [2007] showed that the columnar sea ice permeability for liquids drops by approximately two orders of magnitude below a 5% relative brine volume, which corresponds roughly to -5°C for a bulk salinity of 5 (known as the "law of fives"). Recent field observations also question the impermeability of sea ice because large fluxes of CO_2 have been reported over sea ice during winter [*Heinesch et al.*, 2009; *Miller et al.*, 2011] and spring [*Semiletov et al.*, 2004; *Delille*, 2006; *Zemmelink et al.*, 2006; *Nomura et al.*, 2010b; 2010a; *Papakyriakou and Miller*, 2011]. These fluxes must be partly driven by the gradient of the CO_2 partial pressure (pCO_2) between sea ice and the atmosphere [*Delille*, 2006; *Nomura et al.*, 2010b], which indicates the need for further investigations on pCO_2 dynamics within sea ice. To date, very few studies have been performed on the dynamics of the carbonate system within natural sea ice. These studies have generally focused on investigation of the potential precipitation of carbonate minerals using measurements of pH, total alkalinity (TA) and dissolved inorganic carbon (DIC), rather than pCO_2 directly [*Gleitz et al.*, 1995; *Papadimitriou et al.*, 2004; *Delille et al.*, 2007; *Papadimitriou et al.*, 2007; *Rysgaard et al.*, 2007; *Nomura et al.*, 2010b]. To our knowledge, only *Delille and co-workers* (*i.e.*, *Delille* [*2006*]) and *Delille et al.* [*2007*] have presented direct *in situ* measurements of brine pCO_2 in sea ice. These measurements were performed using the same principle as the equilibration method used for oceanic underway pCO_2 measurements. This method is based on employing an infrared gas analyser (Licor®) and a silicon membrane equilibrator. Seawater flows continuously through the equilibrator, where it equilibrates with a closed loop of air. A CO_2 analyser monitors the pCO_2 of the air in the closed loop. These measurements do not rely on assessment of the dissociation constants of the carbonate system (with the exception of a correction due to temperature changes between the inlet of the system and the equilibrator). However, although this method provides accurate and reliable measurements, it applies only to brines and is associated with the following potential drawbacks: (i) the impossibility of accurately tracking the origin of the brines filling the sackholes, (ii) poor vertical resolution and (iii) the difficulty of comparing measurements of dissolved compounds, such as inorganic carbon, with particulate compounds that are trapped or fixed in the ice matrix such as micro-algae. In particular, while studying inorganic carbon dynamics within sea ice, pCO_2 at the interface with the atmosphere has crucial importance because it determines the direction and the magnitude of air-sea ice CO_2 transfers. Unfortunately, due to the poor vertical

resolution of the measurements, brines cannot provide an accurate estimate of sea ice pCO_2 at the air-sea ice interface with the atmosphere (*e.g.*, in the five top centimetres).

The first measurements of CO_2 concentration in bulk sea ice were performed by *Matsuo and Miyake* [1966], with maximum values of 24000 ppmV being found. The gas concentration was measured using the melting-refreezing method coupled with Toepler pump extraction. The gas was analysed using a mass spectrometer. When the CO_2 concentration was higher than 10000 ppmV, the sample was analysed by the commonly applied mass spectrometric method. When it was lower than 10000 ppmV, however, the isotope dilution method was used.

Killawee et al. [1998] observed a CO_2 concentration of approximately 50000 ppmV in artificial $CaCO_3$-saturated fresh water ice, which is on the same order of magnitude as the concentration measured by *Tison et al.* [2002] in an artificial sea ice tank experiment. The gas composition measurements performed by *Killawee et al.* [1998] and *Tison et al.* [2002] were performed in similar ways. They applied the dry-extraction technique that was previously employed for glacial ice and described by *Raynaud et al.* [1982] and *Barnola et al.* [1983]. Gas samples were crushed at very low temperature (-55°C) under vacuum (10^{-2} torr, 1.333 Pa), so that the technique measured the gas composition from both gas bubbles and gas dissolved in the brines of the sea ice. An extraction line was used in conjunction with a Varian 3300® gas chromatograph.

Tison et al. [2002] had suggested that two major biases could explain the high CO_2 concentrations measured in their sea ice tank experiments. First, the calcium carbonate precipitation observed during the experiment could have promoted a degassing of CO_2, according to the following equation:

$$2HCO_3^- + Ca^{2+} \Leftrightarrow CaCO_3 + H_2O + CO_2 \qquad \text{(IV.1)}$$

Second, uncontrolled sustained bacterial activity would also act as a CO_2 source. However, more recent work has suggested a potential methodological bias in these types of measurements [*Verbeke*, 2005], as they were obtained using gas extraction under vacuum at low temperature, the carbonate system was significantly disturbed, leading to the release of CO_2 in the headspace in larger quantities than those that were effectively initially dissolved within the brine. In seawater, as well as in brine, most CO_2 is dissociated in carbonates and bicarbonates [*Zeebe R.E. and Wolf-Gladrow*, 2001]. Brine pCO_2 depends on the equilibrium between CO_2, HCO_3^- and CO_3^{2-}, which

is governed by the dissociation constants of the carbonate system (K_1, K_2), as illustrated in the equation IV.2:

$$CO_{2(aq)} + H_2O \Leftrightarrow H_2CO_3 \overset{K_1}{\Leftrightarrow} HCO_3^- + H^+ \overset{K_2}{\Leftrightarrow} CO_3^{2-} + 2H^+ \quad \text{(IV.2)}$$

These constants are strongly affected by changes in salinity and temperature [*Zeebe R.E. and Wolf-Gladrow*, 2001]. According to *Papadimitriou et al.* [2004], a decrease of temperature promotes an increase of the brine concentration and, consequently, an increase of pCO_2. Additionally, the vacuum in the vessel forces the transfer of CO_2 from the liquid phase to the headspace. In turn, removal of CO_2 forces the displacement of the equilibrium so that the CO_2 removed from the liquid phase is rapidly replaced by CO_2 converted from the pool of CO_3^{2-} and HCO_3^-. As a result, measuring the CO_2 concentration in the headspace of the vessel leads to a value that is not related to the *in situ* pCO_2 or DIC because the total extraction of DIC cannot be achieved without acidification. Overall, the CO_2 concentration in the headspace under a vacuum is useless in constraining the carbonate system.

The common method for measuring the pCO_2 of a liquid phase is to measure the concentration in a headspace in equilibrium with the liquid phase at a pressure close to the atmospheric pressure. We applied this rationale to sea ice and developed a method for determination of the pCO_2 of bulk sea ice that can be performed with a vertical resolution of 5 cm. This resolution allows the accurate assessment of the pCO_2 gradients in the ice and at the air-sea ice interface and better comparisons of pCO_2 with crucial biogeochemical parameters. Measurements were performed in standard artificial sea ice samples synthesised in a laboratory with reproducible properties to test the accuracy and the reproducibility of the method. The method was then validated against direct *in situ* brine pCO_2 measurements performed according to the method proposed by *Delille et al.* [2007].

2. Materials and methods

The method used in this study was first tested on standard sea ice with homogeneous properties, such as its salinity, texture and pCO_2 content, to assess the method's reproducibility and the precision of the measurements. Then the method was applied in natural sea ice samples to produce high-resolution profiles and compare them with *in situ* brine pCO_2 measurements to assess the accuracy of the measurements. Samples

were collected from January 2009 to June 2009 (Table IV.1) on first-year landfast sea ice offshore from Niksiuraq at the end of the road to Point Barrow, Alaska (71.37055°N, 156.51363°W).

Station #	Date	Station #	Date	Station #	Date
1	Jan. 29	5	Apr. 3	9	May 12
2	Feb. 2	6	Apr. 7	10	June 5
3	Mar. 27	7	Apr. 10		
4	Mar 31	8	May 8		

Table IV.1: Sampling date during the 2009 field experiment in Barrow (Alaska)

2.1 General principle of the pCO_2 analytical procedure

The method described below was inspired by *Weiss* [1981], *DOE* [1994] and *Neill et al.* [1997], who proposed procedures to measure oceanic pCO_2 in discrete water samples. The general principle of our method is as follows: a sea ice sample of known volume is equilibrated at the observed *in situ* temperature with a mixture of nitrogen and CO_2 of known concentration (the so-called standard gas); once the ice sample is equilibrated, the air phase is injected into a gas chromatograph (GC), Varian 3300® to measure the CO_2 concentration.

2.2 Synthesis of standard artificial sea ice

Jacka and Lile [1984] proposed a method to create artificial fresh water ice by mixing fresh water at the freezing point with individual ice crystals. The principle underlying this technique is simple. The fresh water-ice crystal mix is compresses under a mechanical press. As the pressure increases, the freezing point of the water decreases, and the liquid water is expelled from the container. Upon sudden release of the pressure, the freezing point of the water increases and allows bulk freezing of the mixture. According to *Jacka and Lile* [1984], this method is reproducible and provides ice samples with constant physical-chemical properties. Moreover, the ice crystals comprising this kind of ice do not show preferential orientation.

In this study, this technique was adapted for sea ice production. Seawater (deep seawater from the Bay of Biscay) was stored in an ice cream maker in a -20°C cold room to bring it to its freezing point. The continuous rotation of the blades of the ice cream maker allowed avoidance of the formation of large sea ice crystals and prevention of salt segregation due to the rejection of impurities as sea ice forms [*Weeks and Ackley*, 1982] by mixing the newly formed slush continually. When the slush

density became high enough to hamper the rotation of the blades, the slush was transferred to a dedicated vessel and squeezed to a pressure of approximately 20 bars, and the pressure was then released. Directly after sea ice formation, the block was stored in a freezer at -30°C for at least 48 h before further treatment.

The seawater used to produce this standard sea ice was ageing seawater for the purpose of limiting CO_2 production from biological activity. According to *Takahashi et al.* [1993], a decrease of 1°C acts to reduce pCO_2 by approximately 4.1%. To maintain a constant and known value of the pCO_2 of the seawater before ice formation, despite the decrease in temperature, air with an atmospheric CO_2 concentration (approximately 385 ppmV) was bubbled continuously in the solution for 24 h prior to ice formation and subsequently throughout the process of standard sea ice formation. The bubbled air was cooled down using a cooling coil before being injected into the seawater reservoir.

To assess the homogeneity of the properties of the standard sea ice, a set of salinity profiles and examination of ice thin sections were performed.

2.2.1. Salinity of artificial ice

The ice sample must have a rectangular parallelepiped shape of 4 x 4 x 4.4 cm to fit tightly in the analysis vessel. Sample was cut from the centre of the standard sea ice block to avoid any contamination from the squeezed salty water or from brine rejection during the storage of the ice at -30°C. The ice sample was then cut into slices with a thickness of approximately 1 cm (slice 1, 2,…, n), and each slice was cut into 4 identical pieces (A, B, C and D). The ice was melted in a closed receptacle at ambient temperature, and salinity was measured using a TitraLab TIM 870® with a cell of conductimetry CDC 565 from radiometer Analytical®. A Heto® thermostatic bath was used to maintain the temperature at a constant 25°C, with a precision of approximately ±0.1°C. The constant of the cell of conductimetry was calibrated before each set of analyses using a standard Merck® KCl solution at 0.01 M with known conductivity at 25°C.

2.2.2. Thin sections

Vertical and horizontal thin sections were produced following standard procedures [*Tison et al.*, 2008] to describe the texture of the ice. Images of the texture of the crystals were collected from the thin sections using a light table and cross- and parallel-

polarised sheets with a macro setting on the camera (Nikon® Coolpix S200, 7.1 mega-pixels).

2.3 Natural sea ice sampling

An electro-polished stainless steel corer with an internal diameter of 14 cm was used to retrieve ice cores. Cores were immediately wrapped in polyethylene (PE) bags and stored on the sampling site in an insulated box filled with individual cooling bags that were pre-cooled at -70°C. This precaution served to minimise brine drainage from the samples [*Tison et al.*, 2008].

The sea ice temperature was measured *in situ* directly after the extraction of the core using a calibrated probe (Testo 720®) inserted into pre-drilled holes (~3 cm depth) perpendicular to the sides of the core. The diameter of the hole matched that of the temperature probe. The precision of the measurements was ±0.1°C. This "temperature core" was cut into successive slices with a thickness of 5 cm in the lab. Each slice was stored in a bucket at 4°C in the dark to melt it, and the salinity was measured with a Thermo-Orion® portable salinometer WP-84TPS meter with a precision of ±0.1.

2.4 Ice pCO_2

2.4.1. Dedicated container for pCO_2 measurements in sea ice samples

A special sample container was designed for performing pCO_2 measurements in the sea ice samples. The ice sample was required to precisely fit into this container to minimise the headspace. The container also had to be thermally conductible to maintain the ice sample temperature during the equilibration procedure at the field *in situ* temperature. The container was made of epoxy resin, which is inert and does not interact with CO_2. This resin was mixed with an aluminium powder at the proportion of 20-80% of the total weight aluminium-resin to improve heat conduction across the container walls (Fig. IV.1).

The container was equipped with a flat glass top that included a tap and a silicon joint to ensure air tightness. This top was designed to reduce the headspace above the ice sample. Several tests showed that the container could absorb a small portion of the standard gas. Therefore, the container was stored filled with the standard gas at a

pressure higher than atmospheric pressure to saturate the container adsorption sites with CO_2.

Figure IV.1: Dedicated container for the measurement of pCO_2 in solid sea ice samples, equipped with a flat glass top, silicon joint and a clamp.

2.4.2. Vacuum line and gas chromatograph

An extraction line (Fig. IV.2) was used in conjunction with a Varian 3300® Gas Chromatograph. The latter device is equipped with a Haysep column and a flame ionisation detector (FID) following catalytic transformation into methane. It allows the measurement of oxygen and argon (as a single peak), nitrogen, methane and carbon dioxide. The carrier gas is helium. The extraction line is made of stainless steel. It is equipped with a vacuum pump and a Pfeiffer® pressure indicator (with optimised sensitivity in the atmospheric range). A water trap consisting of a mixture of ethanol and liquid nitrogen at -65°C is placed just before the inlet of the GC. pCO_2 is therefore measured in dry air because the water vapour is trapped before injection.

According to *Tison et al.* [2002], the precision of the measurements made with these system settings is ± 5%. Accordingly, a mean relative error of 5.03% was obtained from 30 injections of standard gas ($[CO_2]$ = 298 ppmV), with a standard deviation of 17.15 ppmV and a variation coefficient (CV) of 5.9%.

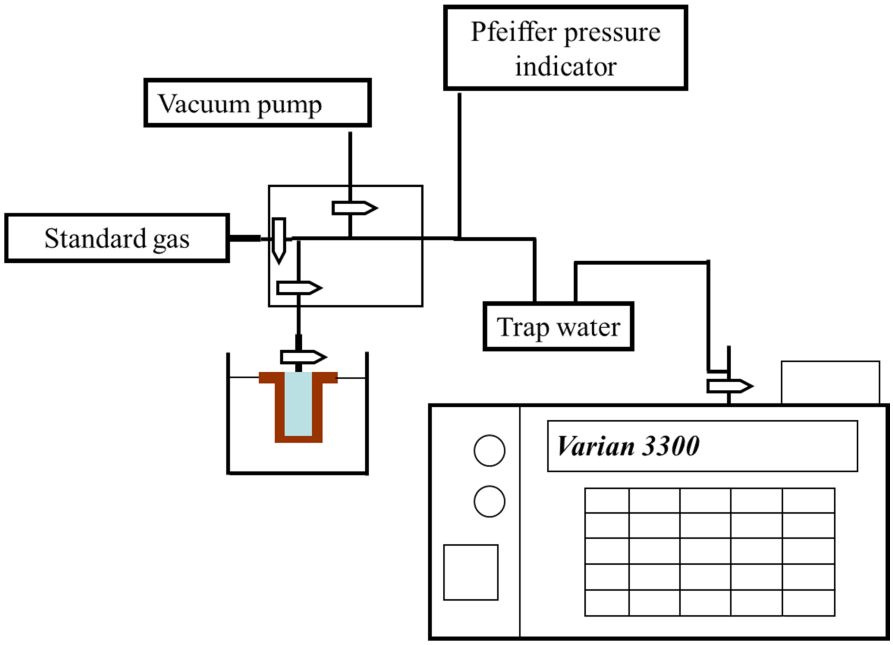

Figure IV.2: Sketch of the different components forming the extraction line, including the Varian 3300® gas chromatograph.

2.4.3. Temperature equilibrium

Temperature is a crucial parameter for pCO_2 analyses, as pCO_2 is strongly related to temperature. Additionally, temperature controls brine salinity [*Weeks and Ackley*, 1982; *Eicken*, 2003] and, thus, pCO_2 [*Delille*, 2006; 2007]. Finally, temperature controls brine volume and, consequently, permeability, which is a critical parameter for our purposes because equilibrium can be achieved only if the ice is permeable to gases. Therefore, the bulk ice pCO_2 must be measured at the *in situ* temperature (*i.e.*, the sea ice temperature measured in the field during core sampling). As the ice samples were stored in a freezer at -30°C, it was necessary to warm the sample to the *in situ* temperature during the equilibration procedure between the ice sample and the standard gas. The ice sample within the container was therefore stored in a thermostatic bath during the equilibration.

According to *Eicken* [2003] and references therein, the thermal conductivity of sea ice depends on the temperature gradient and the sea ice salinity. The specific heat capacity of sea ice, C_{si}, is expressed as follows:

$$C_{si} = C_i + 17.2 \times 10^{-3} \frac{S_i}{T^2} \qquad \text{(IV.3)}$$

where C_i is the specific heat capacity for pure ice of 2.11 J g^{-1} K^{-1}; S_i is the ice salinity; and T is the temperature in °C. According to this equation, more energy is needed to

warm a sea ice cover sample by 1°C at a temperature close to the freezing point of seawater than at a colder temperature. Therefore, to reach the *in situ* temperature more rapidly, the thermostatic bath was first set to -2°C until the ice sample reached the *in situ* temperature. When the ice sample reached the *in situ* temperature, the temperature of the bath was adjusted to the *in situ* temperature for fine adjustment of the temperature. Tests were performed on artificial sea ice to determine the time required to equilibrate the temperature of the ice with the temperature of the thermostatically controlled bath for the ice samples reach the *in situ* temperature. Tests were performed with ultrapure water with NaCl added to obtain salinities of 4, 6, 8, 10, 16 and 23. The solution was stored at -30°C for freezing. Once frozen, the ice was cut, adjusted to the pCO_2 container inner volume and a temperature probe (a calibrated Testo 720® with a precision of ±0.2°C) was inserted into its centre. The container with the ice sample was placed into a thin plastic bag and submerged in a thermostatic bath at -2°C. Temperature was recorded every 5 min until an ice temperature of -2 ± 0.5°C was reached.

2.4.4. pCO_2 analysis

According to *Golden et al.* [1998], because the ice samples were stored at -30°C, their brine volume should be less than 5%, so they can be considered impermeable to gas exchanges with the atmosphere. Therefore, the sea ice samples could be manipulated in the absence of contamination in the cold room maintained at -30°C.

The same procedure was followed for both artificial standard and natural sea ice samples. The day before the analysis, the container was filled with standard gas to saturate the potential adsorption sites of its inner surface. Thirty minutes before the beginning of the sample treatment, the container was pre-cooled in the cold room.

In the cold room, the ice sample was cut with a band saw and adjusted to the container's inner volume (4 x 4 x 4.4 cm). The sample was sanded down using fine-grained sandpaper so that it fit tightly into the container to both minimise the headspace volume and obtain a constant headspace volume. Next, the container, equipped with its glass top and the silicon joint, was placed into a dewaer filled with a mixture of ethanol-liquid nitrogen at -30°C. The container was then connected to the extraction line (tap closed). The line was first evacuated down to a pressure of 10^{-3} Torr, after which the container was evacuated for 5 min (tap open for a maximum of 5 min to

avoid drawing the absorbed CO_2 from the container due to the vacuum). The standard gas was then injected into the container at 1013 mb and the container was subsequently removed from the extraction line (tap closed), placed in a thin plastic bag and submerged in a thermostatic bath (set to -2°C). Then the equilibration process was begun. The ice sample was warmed up and equilibrated with the standard gas. Following the salinity of the sample and the appropriate abacus, 30 min before the sample was expected to reach the *in situ* temperature, the temperature of the thermostatic bath was adjusted to the *in situ* temperature. The sea ice sample was then left in the thermostatic bath for an additional 90 minutes to reach the *in situ* temperature and complete the equilibration. Subsequently, the container was placed in a dewaer filled with a mixture of ethanol–liquid nitrogen at the *in situ* temperature and reconnected to the evacuated (10^{-3} Torrs) extraction line. At the same time, a water trap consisting of a dewaer filled with an ethanol-liquid nitrogen mixture at -65°C was placed on the line just before the GC. The gas was finally injected into the GC. Immediately after completion of the injection, the ice sample temperature was measured using a calibrated temperature probe (Testo 720®).

3. Results and discussion

3.1 Standard artificial sea ice properties

3.1.1. Thin sections

In both transversal and longitudinal thin sections, the ice crystals were of millimetric size and did not show any preferential orientation, which was in good agreement with the findings of *Jacka and Lile* [1984]. These types of crystals and the absence of orientation are typical of granular ice [*Tison et al.*, 1998; *Eicken*, 2003].

3.1.2. Salinity

The salinity of each section ranged from 7.5 to 23 (Fig. IV.3), while the bulk salinities of the blocks were between 10.1 and 17. This is significantly higher than the mean salinity of natural sea ice [*Nakawo and Sinha*, 1981; *Weeks and Ackley*, 1982; *Meese*, 1989; *Eicken*, 2003]. All profiles showed a trend of increasing salinity towards the bottom of the block, suggesting that a consolidation process had occurred moving from top to bottom, with variable salt segregation from block to block.

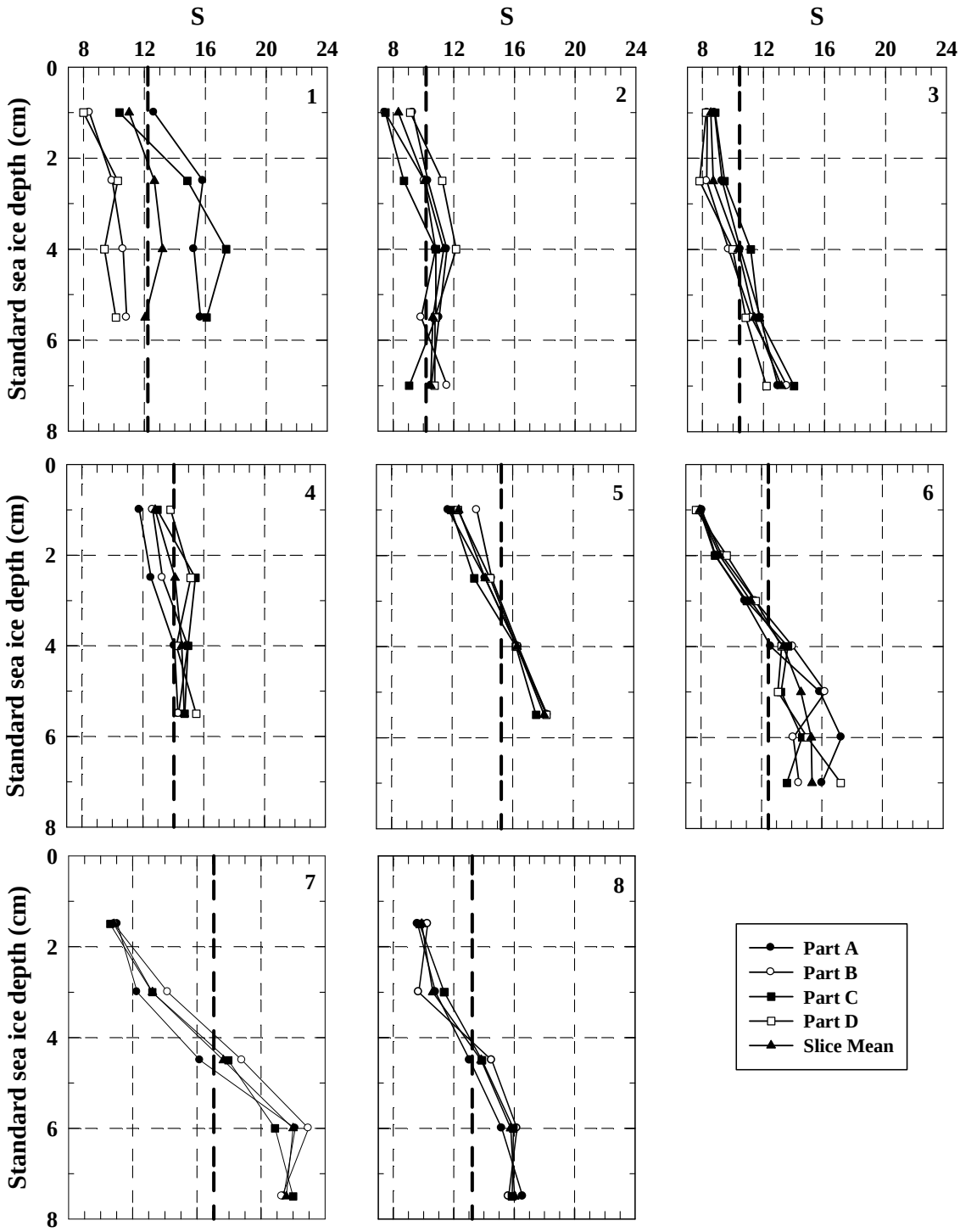

Figure IV.3: Salinity profile in 8 artificial standard sea ice blocks. The bold dashed line represents the mean salinity of the bulk block while the black triangle is the mean salinity of each slice of the block.

Only block 1 exhibited significant salinity heterogeneity at a given depth. The salinity range of block 1 was the greatest, with salinity ranging from 8.4 to 17.4, while the other blocks were more homogeneous, with a maximal dispersion of the salinity of ±4 at the same depth.

The salinity profiles of this artificial standard sea ice will be affected by several processes. First, the initial grain size should influence the porosity of the medium but thin sections did not exhibit significant differences with respect to grain sizes. The pressure applied to squeeze the slush should be constant. Nevertheless, some variations may have occurred due to the lack of precision of the pressure indicator. Second, a leak may occasionally occur at the bottom of the container used during pressurisation, and the bottom of this container was not completely watertight if not firmly screwed. Hence, as the pressure increased, most of the residual seawater was expelled at the top of the container, but on some occasions, some water was also expelled at the bottom. This could explain the range of bulk ice salinities observed. However, each block of standard sea ice was considered as reasonably homogeneous.

As a further test, in parallel with the pCO_2 tests, a thin slice was cut from the analysed sea ice block to measure its bulk salinity. We measured 36 samples and the mean salinity was 16 with a standard deviation of 1.05 (coefficient of variation of 6.5%) (Table IV.2). Therefore, 2 samples cut side by side from the same block of artificial standard sea ice were considered as similar in terms of salinity and other physical properties and, thus, in terms of pCO_2.

3.2 Time required for temperature adjustment

The warming of the ice was rapid and linear up to -5°C. Above -5°C, the rate of the temperature increase decreased steadily, tending asymptotically towards the temperature of the thermostatic bath (-2°C) (Fig. IV.4). For each salinity range, several tests were performed to assess the precision and the accuracy of this method to warm the ice to a given temperature.

Following this procedure, the *in situ* temperature could be reached within ± 1°C (Fig. IV.4), which was not fully satisfactory. To improve the reliability and precision of temperature adjustment, 30 minutes before the sample was expected to reach the *in situ* temperature (following the abacuses), the temperature of the thermostatic bath was adjusted to the *in situ* temperature and the sample was left in the bath for an additional period of 90 minutes.

Gas Standard: 298 ppmV					**Gas Standard: 1483 ppmV**				
Sample id	T (°C)	S	V_b/V (%)	pCO_2 (ppmV)	Sample id	T (°C)	S	V_b/V (%)	pCO_2 (ppmV)
A-1	-15.3	17.38	6.5	1667	**M-1**	-12.7	16.63	7.3	1775
A-2	-15.2	17.38	6.5	1490	**M-2**	-12.8	16.63	7.3	1613
B-1	-6.8	16.84	12.8	475	**O-1**	-8	15.17	9.9	1091
B-2	-7.1	16.84	12.3	500	**O-2**	-8	15.17	9.9	1153
C-1	-9.9	16.2	8.8	1075	**P-1**	-6.5	13.96	11	1066
C-2	-10.2	16.2	8.6	758	**P-2**	-6.4	13.96	11.1	885
D-1	-9.2	17.71	10.3	1102	**Q-1**	-6.5	15.74	12.4	1047
D-2	-9.5	17.71	10	1142	**Q-2**	-4	15.74	19.6	602
E-1	-10.3	16.62	8.8	1078	**R-1**	-4.3	16.04	18.6	556
E-2	-10.3	16.62	8.8	796	**R-2**	-3.9	16.04	20.5	417
F	-6.8	15.58	11.8	511	**S-1**	-3.1	14.47	23.1	332
G-1	-6.3	16.94	13.8	721	**S-2**	-3	14.47	23.9	362
G-2	-6.9	16.94	12.7	715	**T**	-1.8	16.46	47.3	211
H-1	-15.2	17.29	6.5	688	**Y-1**	-14	15.77	6.3	1478
H-2	-15.3	17.29	6.5	965	**Y-2**	-14.6	15.77	6.1	1135
I-1	-3.5	14.88	21.1	285					
I-2	-3.7	14.88	19.9	283					
J-1	-3.9	16.6	21.2	415					
J-2	-3.9	16.6	21.2	375					
K-1	-14.9	17.84	6.8	1448					
K-2	-15.2	17.84	6.7	1683					

Table IV.2: Samples “A” to “K” were analysed with a standard gas of 298 ppmV while samples “L” to “S” were analysed with a standard gas of 1483 ppmV. *T* corresponds to the temperature measured in the sample after the injection in the GC. *S* is the salinity measured on a thin slice of ice from the block of standard sea ice. V_b/V was calculated from *T* and *S*. pCO_2 is the concentration measured by the GC.

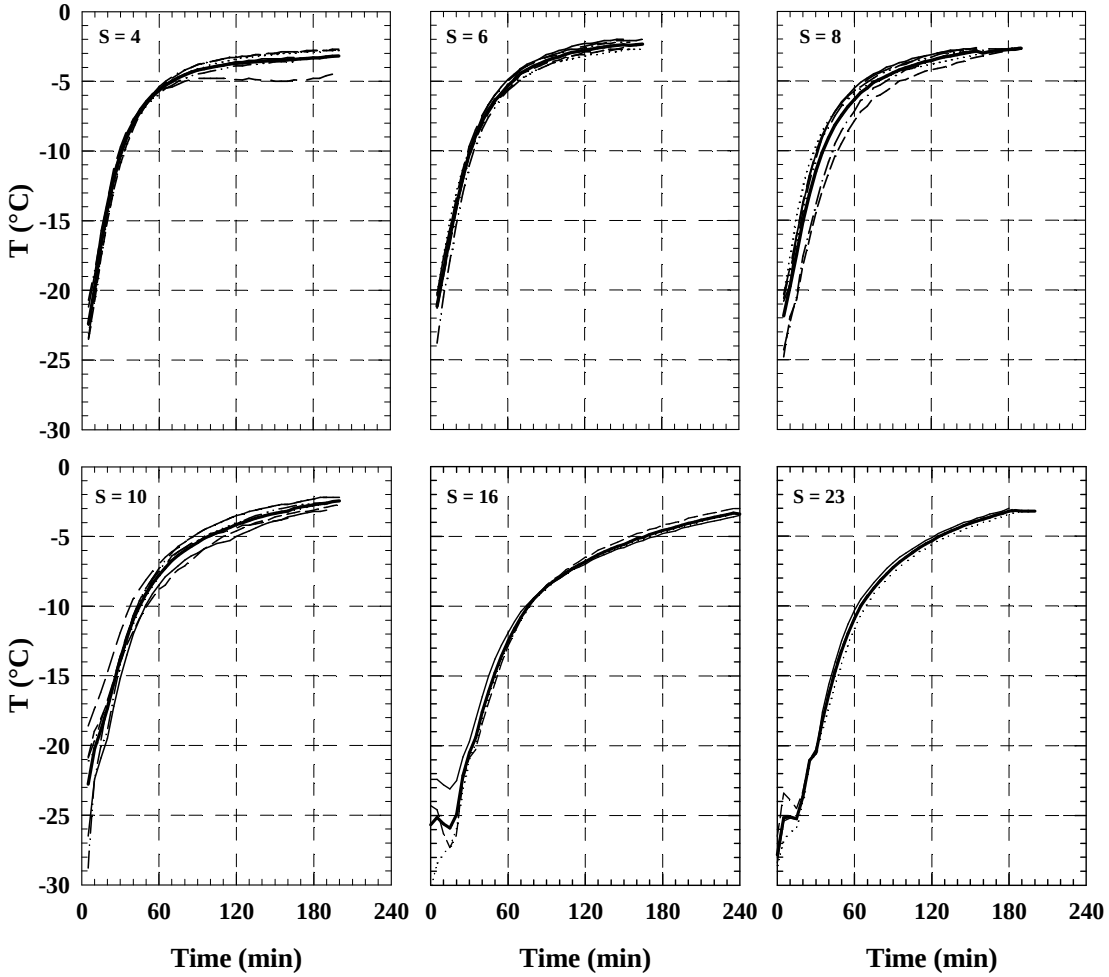

Figure IV.4: Evolution of ice temperature with time as a function of mean ice salinity for artificial ice samples immersed in a bath at -2°C. The bold line in each graphic is the mean trend.

3.3 pCO_2 measurements in standard sea ice

Sea ice brines will equilibrate with the atmosphere (or the standard gas) following the law of Henry, where K_H is the constant of Henry:

$$pCO_2 = K_H[CO_2] \qquad \text{(IV.4)}$$

A prerequisite of this equilibrium is that sea ice must be permeable to gas exchanges. According to *Golden et al.* [1998; 2007], sea ice may be considered as permeable once its relative brine volume (V_b/V) is higher than the threshold of 5%. Therefore, the relative brine volume was calculated from salinity and temperature data [*Eicken*, 2003] and was found to be above 5% for all artificial ice samples (Table IV.2).

The accuracy and precision of this method were estimated by measuring the CO_2 concentration in twin samples of artificial standard sea ice. These measurements were performed at various temperatures and with two different equilibration standard gases

with concentrations of 298 ppmV and 1483 ppmV, respectively, and the results are shown in the figure IV.5. By observing both datasets, a common general trend may be observed. pCO_2 appears to be inversely correlated with ice temperature. Using the 298 ppmV standard gas, pCO_2 ranged from 1667 ppmV at -15.3°C to 285 ppmV at -3.5°C. Down to a temperature of -9.5°C, the results exhibited good reproducibility, with a coefficient of variation (CV) of approximately 2.9 % between twin samples. Below -9.5°C, greater dispersion was observed for one of the experiments, where the CV increased to 17.6%, which is out of the range of precision calculated for the GC measurements (CV = 5.9 %). Using the 1483 ppmV standard gas, pCO_2 ranged from 1775 ppmV at -12.7°C to 211 ppmV at -1.8°C. Samples "P", "Q" and "R" were analysed at different temperatures and therefore presented pCO_2 values that were significantly different. In contrast, samples "O" and "S" were analysed at the same temperature and showed good reproducibility, with a CV close of the range of precision of the GC measurements. Samples analysed below -10°C showed a larger dispersion, with CVs of approximately twice the precision of the GC.

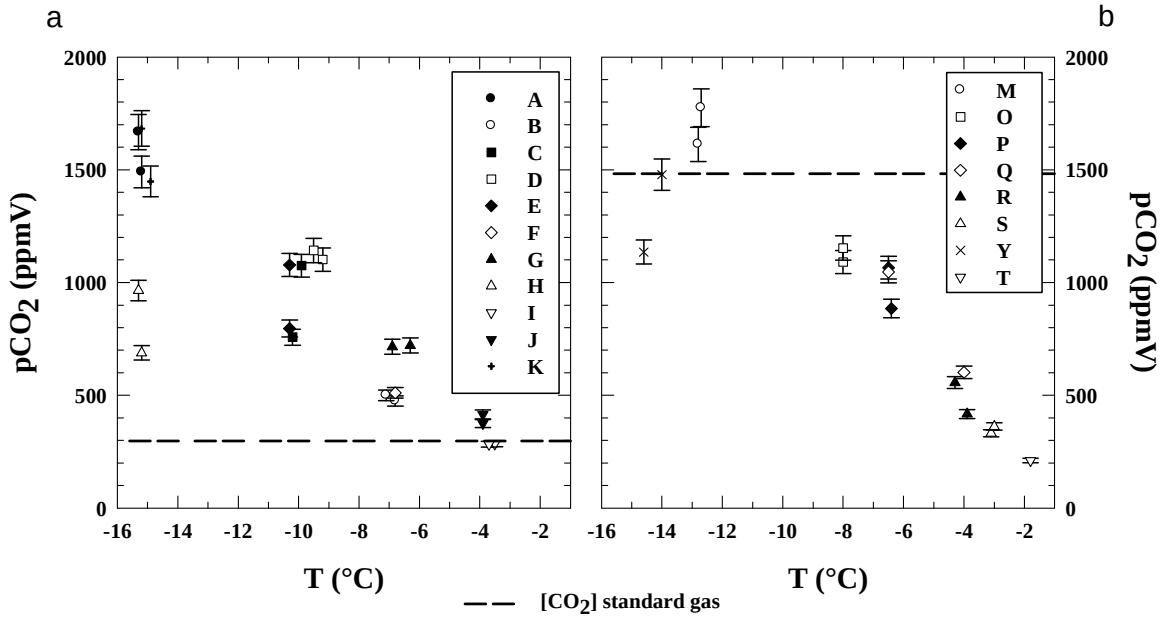

Figure IV.5: pCO_2 of bulk sea ice using equilibration standard gas of 298 ppmV (**a**) and 1483 ppmV (**b**). The standard gas concentration is represented as a dashed line. Each couple of point represents twin samples from the same block of standard sea ice. The error bar represents the GC precision (5.9%).

The general trend of decreasing pCO_2 as ice temperature increases was previously described by *Delille and co-workers* (*i.e., Delille* [2006]). As ice temperature increases, the melt water from the ice crystals dilutes the brine and, therefore, the pCO_2 decreases. Associated with the brine dilution, potential precipitates of calcium carbonate within

sea ice [*Dieckmann et al.*, 2008; 2010] may dissolve, promoting pCO_2 decreases. In the figure IV.6, we compare the results of our artificial standard sea ice to natural sea ice data from *Delille and co-workers* (*i.e., Delille* [2006]) and *Delille et al.* [2007], who measured the pCO_2 of sackhole brines *in situ*. The range of concentrations measured using this new method is consistent with the natural sea ice dataset. Our results are also in agreement with findings from brine pCO_2 sampled in the Arctic in Barrow, Alaska, (data not shown) and during the "Circumpolar Flaw Lead system study" (CFL) field trip, in which brine pCO_2 values were measured from April to June 2008 following the same procedure as used by *Delille et al.* [*2007*] and *Geilfus et al.* [submitted]. It should be noted that, in comparing the artificial sea ice pCO_2 values obtained with the two different standards, it was observed that the pCO_2 values equilibrated with the 298 ppmV standard were systematically lower than those measured with the 1483 ppmV standard, suggesting a potential bias due to the choice of the standard used for equilibration.

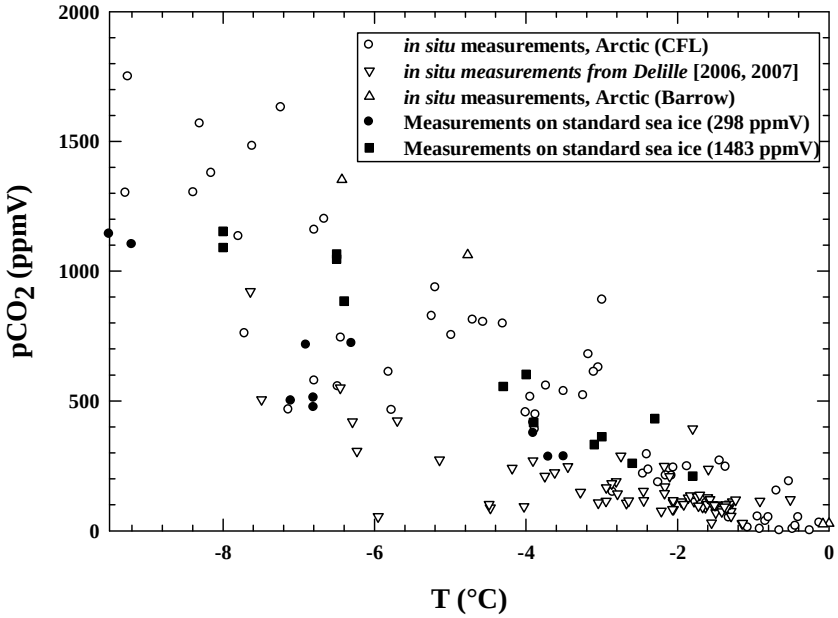

Figure IV.6: Comparison between pCO_2 measurements on bulk standard sea ice and *in-situ* measurements of brine pCO_2.

3.4 Influence of the headspace volume:ice volume ratio

The number of moles exchanged between the standard gas and the brine medium must be negligible compared to the number of moles initially present within the brine to ensure that the equilibration procedure between the ice sample and the standard gas does not affect the initial brine pCO_2. This requires that the volume of brine must be sufficiently large compared with the volume of the standard gas and that the

concentration of the standard gas used for the measurements should be as close as possible to the expected concentration of the ice sample. *DOE* [*1994*] suggests an air-seawater volume ratio of 0.087 to achieve a precision of 2.5%. In the procedure applied in the present study, the sample size was 4 x 4 x 4.4 cm (70.4 ml). The internal volume of the container equipped with the glass top and silicon joint was 83.39 ml. Hence, the air volume:ice volume ratio was 0.18. However, only the brine equilibrated with the headspace. Considering a minimum relative brine volume of 5% (permeability threshold), the brine volume was 3.52 ml. This lead to a ratio headspace volume:brine volume ratio of 3.69 (12.99 ml/3.52 ml), which should be compared to the ratio of 0.087 advocated by the *DOE* [1994]. However, it should be noted that the DIC of brines can be significantly higher than the DIC of seawater [*Rysgaard et al.*, 2007; 2009; *Miller et al.*, 2011] as a result of brine concentration, so the air volume:liquid volume ratio for seawater and brines cannot be readily compared. The existence of a high air volume:brine volume ratio emphasises the fundamental need for specific dedicated tests to ensure the accuracy and reproducibility of the method.

Brine volume depends on temperature, salinity and ice volume. To increase the headspace volume:brine volume ratio, it is necessary to increase the headspace volume:ice volume ratio as much as possible. We attempted to assess the bias related to various headspace volume:ice volume ratios and various differences between standard gases and the pCO_2 values of brines with a simple model (Fig. IV.7). The model iteratively computes the amount of CO_2 exchanged between brines at a given pCO_2 ($pCO_{2,i}$) and the headspace with a given standard to reach an equilibrium, taking into account the total alkalinity of the brines and the CO_2 dissociation coefficients. CO_2 speciation was calculated using numerical routines for the calculation of carbonate system parameters from *Zeebe and Wolf Gladrow* [2001], the CO_2 acidity constants of *Mehrbach et al.* [1973] refitted by *Dickson and Millero* [1987], the CO_2 solubility coefficient of *Weiss* [1974], the SO_4^{2-} dissociation constant of *Dickson* [1990a] and the borate acidity constant of *Dickson* [1990b], while the total borate molality was calculated using the *Uppström* [1974] ratio to chlorinity. We assumed conservative behaviour of the CO_2 dissociation constants at subzero temperatures. *Marion et al.* [2001] and *Delille et al.* [2007] suggested that thermodynamic constants relevant for the carbonate system can be assumed to be valid at subzero temperatures. The difference of the pCO_2 at equilibrium and $pCO_{2,i}$ is the error of the measurement due to

the exchange of CO_2 between the sample and the headspace. It is obvious that the error increases significantly both when the chosen standard shows an increasing difference from the real value and when the headspace volume:ice volume ratio increases. It should also be noted that the results of these calculations further suggest that there are no geometrical constrains on the equilibrium process.

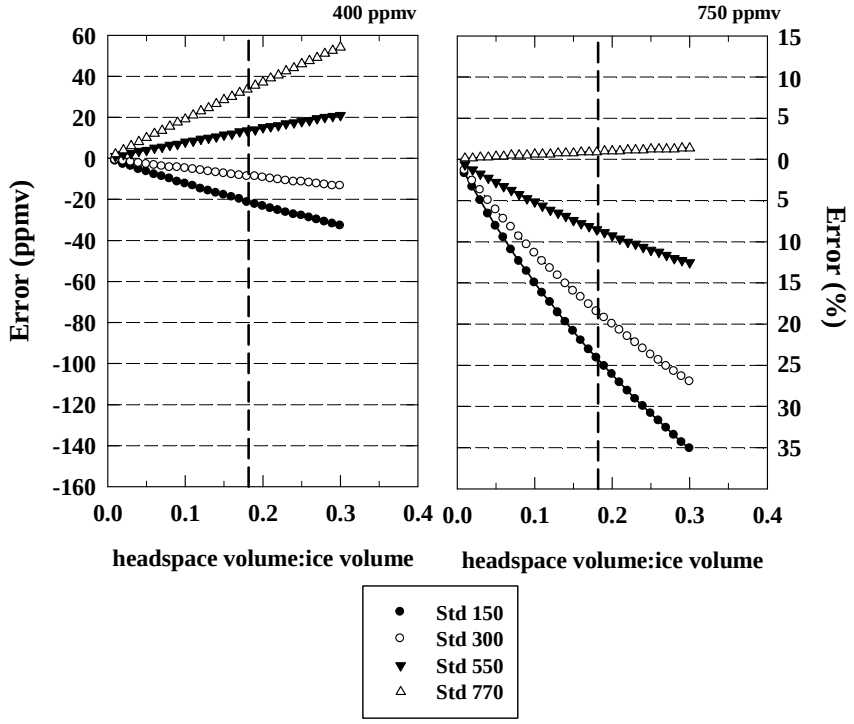

Figure IV.7: Error of the method following different ratio headspace volume:ice volume and different concentration of standard gas. The initial conditions at the computation were: T = -5°C, S = 6, TA = 2400 µmol kg^{-1} and brine pCO_2 = 400 ppmV (**a**) and 750 ppmV (**b**).

3.5 pCO_2 measurement in arctic sea ice

Ensuring that sea ice is permeable to gas exchange is a prerequisite to apply this new method and to measure the pCO_2 of bulk ice under *in situ* conditions. Therefore, the brine volume was calculated from temperature and salinity data collected in the field according to the formula of *Eicken* [2003].

The brine volume was generally lower than 5% until reaching station 8, where the threshold of 5% was exceeded. Therefore, bulk pCO_2 measurements was first applied to station 9, where the larger diameter of the ice core provided the opportunity to measure twin samples, allowing us to check the reproducibility and the precision of the natural sea ice samples. Station 10 was then analysed to compare the results from this method to direct *in situ* measurements of the brine pCO_2 available at that station. These data were obtained following the protocol of *Delille et al.* [2007]. This provided a test of the

accuracy of the method. Finally, station 7 was analysed. This station presented a brine volume below the permeability threshold and the limits of the method were tested in this respect. All of the samples were analysed using a 318 ppmV standard gas.

The pCO_2 profile of station 9 was mainly undersaturated, with concentrations ranging from 40 ppmV up to 442 ppmV (Fig. IV.8). A first pCO_2 minimum was observed at the 5 cm depth, with a pCO_2 of approximately 103 ppmV. Below this value, pCO_2 increased to its maximal concentration at the depth of 25 cm. Between depths of 30 cm and 110 cm, pCO_2 remained relatively constant, ranging from 250 ppmV to 350 ppmV. Below the 110 cm depth, pCO_2 decreased to 40 ppmV at the bottom of the ice core. Profiles from replicates ice samples, exhibited the same general trend, excepted for 3 values at 50 cm, 70 cm and 80 cm depths.

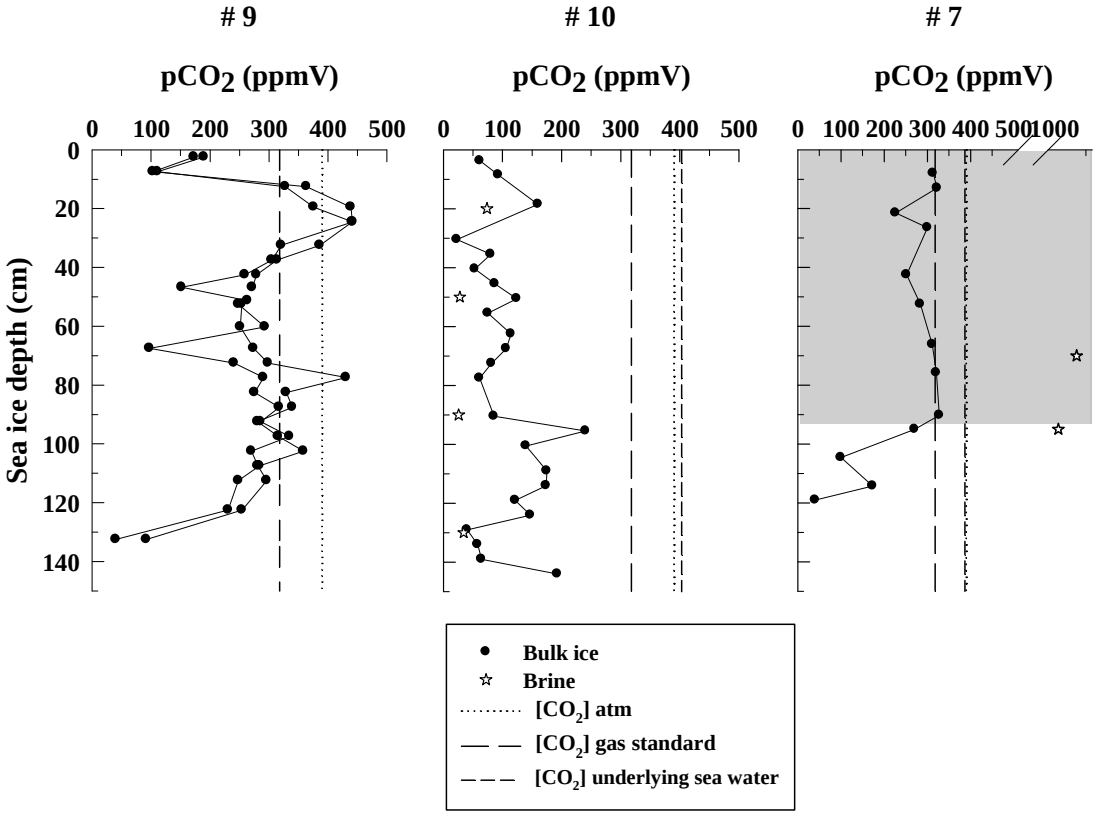

Figure IV.8: High resolution pCO_2 profiles on natural sea ice sampled in Barrow (Alaska). Station 9, 10 and 7 are shown. The dashed line represents the standard gas concentration (318 ppmV) while the dotted line represents the atmospheric CO_2 concentration. The *in situ* measurements of brine pCO_2 are plotted as white stars. The gray area in station 7 is the impermeable part of the ice, as determined from the relative brine volume threshold of 5%, according to *Golden et al.* [2007] and [1998].

The pCO_2 profile at station 10 was undersaturated throughout the thickness of the ice sample, with concentrations ranging from 23 ppmV up to 240 ppmV. pCO_2 at the ice interface with the atmosphere was 61 ppmV. It increased slightly to 160 ppmV at the 20 cm depth and then decreased to 22 ppmV at 30 cm depth. Below 30 cm, the general

trend of the profile was an increase of pCO_2 with increasing ice depth, up to 193 ppmV at the bottom of the ice sample. This profile can be compared to the *in situ* measurements of brine pCO_2, which ranged from 26 ppmV to 74 ppmV. Both measurements were on the same order of magnitude, although the *in situ* measurements presented slightly lower values than the measurements in bulk sea ice.

The pCO_2 of station 7 ranged from 40 ppmV up to 327 ppmV. The top 90 cm of the ice exhibited a brine volume below the permeability threshold. In this region, with a few exceptions, the pCO_2 was stable, presenting values around the concentration of the standard gas (318 ppmV). Below the depth corresponding to the threshold of permeability, the pCO_2 dropped from 327 ppmV to 40 ppmV at the bottom of the ice sample. *In situ* measurements of brine pCO_2 were also performed, with values ranging from 1352 ppmV to 1063 ppmV. These values were significantly higher than the results for pCO_2 in bulk sea ice. However, this apparent discrepancy can be explained by taking into account that sackhole brine collects material from the entire sea ice cover above the bottom level of the sackhole. Therefore, its pCO_2 can easily be biased by the signal of the colder upper layers.

The reproducibility and precision of this method were confirmed by the results from station 9. The same general trend as in station 7 was observed and a CV of 8.8 % was calculated. This was slightly higher than the CV of the GC (5.9 %) measurements. Nevertheless, according to *Eicken et al.* [1991], sea ice is a very heterogeneous medium, even at a high resolution, depending on the brine channel location. Therefore, considering the difficulty of ensuring homogeneous samples within sea ice, we consider this range of reproducibility to be acceptable.

The comparison between the pCO_2 measured in the bulk ice and the *in situ* brine pCO_2 represents a measure of the accuracy of our new method. Brine samples were collected in sackholes [*Gleitz et al.*, 1995], which is currently considered to be the best available method to sample brine for chemical studies [*Papadimitriou et al.*, 2004]. However, as noted above, sackholes do not enable us to track the origin of the brine and they provide a record that could be biased due to a dominant input from a given level into the sea ice cover. This characteristic may explain the moderate difference observed between the two methods. Another possibility is the potential bias towards higher pCO_2 values resulting from the choice of the standard at 318 ppmV. However, the high resolution profile still presents features inherited from the previous profile of station 9, such as the

relatively broad minimum between 30 and 80 cm and the relatively broad maximum between 90 cm and 130 cm. At this stage, the generally good agreement between the *in situ* brine measurements and the pCO_2 determined in bulk sea ice suggests that this new method is reasonably accurate.

Using the bulk ice salinity, the ice temperature and the total alkalinity of the brines at the 4 sackhole levels of station 10, it was possible to assess the error in the pCO_2 values measured with our new method as a function of the headspace volume:ice volume ratio and for various equilibration standards used. This is plotted in the figure IV.9. Note that the carbonate equilibrium constants used for these calculations are only strictly valid for higher temperatures and generally lower salinity conditions.

Using the headspace volume:ice volume ratio in our settings and the concentration of the standard gas (300 ppmV), the error due to the injection of a standard gas with a given CO_2 concentration in the sample ranged from 2 ppmV (Br 3) to 8 ppmV (Br 1). This error increases dramatically when a standard gas with a higher concentration is used, while the inverse is true, when the chosen standard gas has a concentration closer to that of the brine pCO_2. In our case, the use of a standard gas with a CO_2concentration of 150 ppmV would have provided an error less than the precision of the GC measurements. Therefore, it is essential to make a first assessment of the expected pCO_2 levels, either by measuring the brine pCO_2 *in situ* or using the brine pCO_2-ice temperature relationship reported in the literature by *Delille and co-workers* (*i.e., Delille* [2006]).

The measurement of the pCO_2 of the bulk sea ice at station 7 clearly demonstrated the limitation of our method when the ice is impermeable. The equilibration process between the standard gas and the ice sample is hampered in such cases, resulting in measured pCO_2 values close to that of the standard gas used. This was confirmed by the concentrations obtained in the impermeable portion of the ice from station 7. As the ice became permeable again in the lower portion of station 7, coherent changes in pCO_2 were detected again. The detailed profiles shown in the figure IV.8 certainly call for further analysis of the processes that controls pCO_2 dynamics. This will be discussed in a dedicated paper with the assistance of the full suite of ancillary physical and biogeochemical parameters collected during the Barrow 2009 experiments.

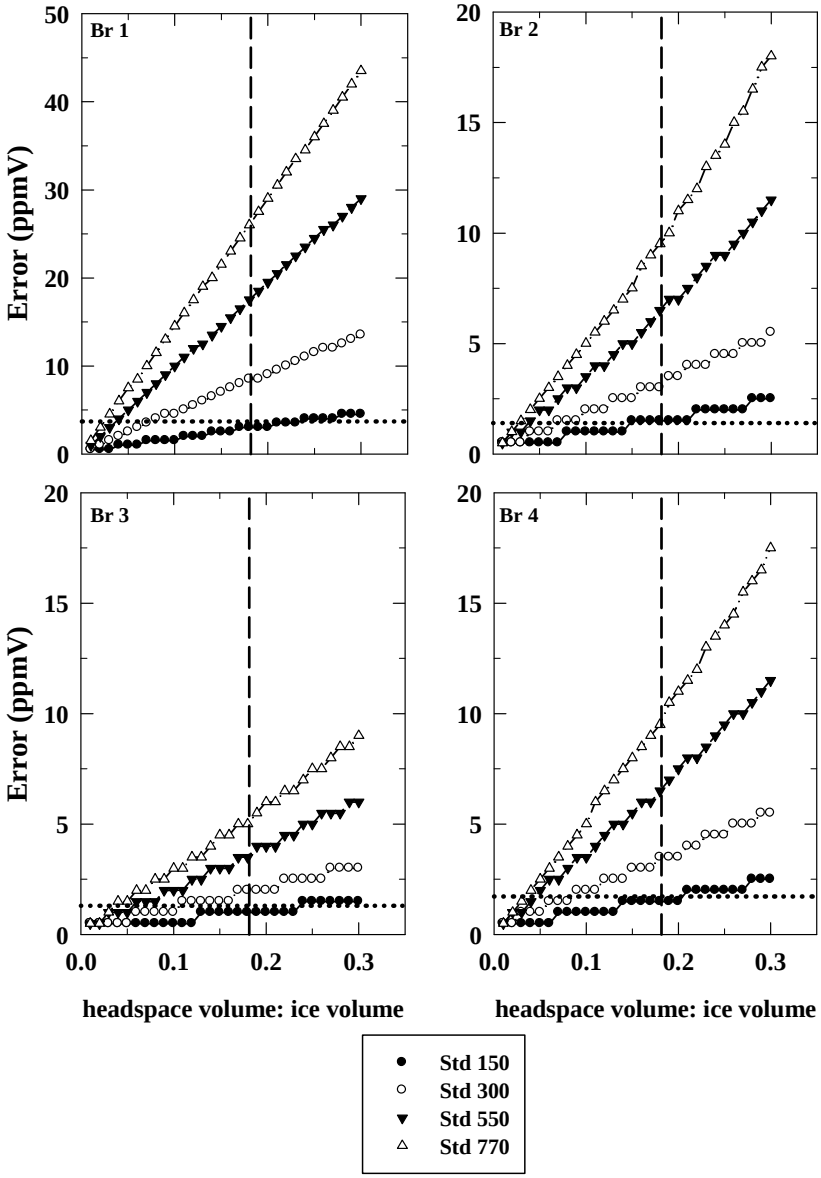

Figure IV.9: Error estimated following the chemical conditions measured in brines from station 10. **Br 1**: T = -0.08°C, S = 2.7, pCO2 = 73, TA = 319 µmol kg^{-1}. **Br 2**: T = -0.29°C, S = 5.1, pCO_2 = 28, TA = 474 µmol kg^{-1}. **Br 3**: T = -0.54°C, S = 3.4, pCO_2 = 26.1, TA = 344 µmol kg^{-1}. **Br 4**: T = -0.09°C, S = 2.3, pCO_2 = 34.4, TA = 276 µmol kg^{-1}. The dashed line represents the headspace volume:ice volume ratio from this method, the dotted line is the precision of the GC.

4. Conclusions

A novel method for obtaining high-resolution pCO_2 profiles in bulk sea ice was proposed and tested with respect to its accuracy and reproducibility, both in artificially produced and natural sea ice samples. The measurements made in artificial standard sea ice demonstrated good reproducibility of the method when compared to a large dataset of brine pCO_2 values from Antarctica and Arctic natural environments for temperatures above -9°5C.

Applying our pCO_2 equilibration method in natural sea ice samples from Barrow, Alaska, provided, to our knowledge, the first ever published high-resolution pCO_2 profiles in sea ice. Both precision and accuracy were demonstrated for the method, provided that the ice is permeable at its *in situ* temperature, *i.e.,* with relative brine volumes above 5%. Below this threshold, repeated measurement of the equilibration standard gas values showed the limitation of the method.

The choice of the equilibration standard value is a crucial parameter for obtaining a reasonable accuracy of the measurements. It is suggested that this choice should be based on either an *in situ* value of brine pCO_2 as a first approximation or on the pCO_2-temperature relationship proposed in the literature. Alternatively, if there is sufficient material available, the sample can be measured in triplicate, beginning with an atmospheric standard and refining the choice of the subsequent standards used on the basis of the equilibration pCO_2 value from the previous measurements.

This method offers the opportunity of working at a high resolution with small ice volumes. It allowed us to document small-scale pCO_2 gradients and rapid pCO_2 variations within the sea ice cover. It also provides access to a measure of the bulk ice pCO_2 at the interface with the atmosphere. Until now, it was extremely difficult to reconstruct the pCO_2 of the upper layer of the sea ice cover using the sackhole technique. However, this information is crucial for better understanding the CO_2 fluxes between sea ice and the atmosphere. Nevertheless, as the method is only valid if the ice is permeable, it is currently limited to use in young ice or autumn-spring-summer sea ice.

5. Acknowledgments

The authors would like to acknowledge the help of Alan Willame and France Deleuze who extensively tested the method. This research was supported by the F.R.S-FNRS (contract 2.4649.07 and 2.4584.09), in which BD is a research associate, and the Belgian research program Action de Recherche Concerté “Sea Ice Biogeochemistry in a CLIMate change perspective” (ARC-SIBCLIM) financed by the Belgian French Community under contract no. ARC-02/7-287. NXG received a PhD grant from the Fonds pour la Formation à la Recherche dans l’Industrie et l’Agriculture. This is MARE contribution no. XXX.

Chapter V: Conclusions

Midday sunset on landfast sea ice in Barrow, Alaska.

1. Context

The Arctic Ocean sustains rapid environmental changes of which the loss of sea ice is one of the best quantified since the late 1970s [*Comiso et al.*, 2008]. The perennial[4] sea ice cover declined of about 10% per decade while the full ice cover (perennial sea ice + seasonal sea ice) decreased of about 3% per decade [*Comiso*, 2003; *Stroeve et al.*, 2007; *Parkinson and Cavalieri*, 2008]. This reduction has been linked to a combination of factors, including increased advection of warm water into the Arctic Ocean, atmospheric circulation patterns that favour advection of sea ice out of the Arctic Ocean through Farm Strait and increased arctic temperatures [*Serreze et al.*, 2007; *Arrigo et al.*, 2008; *Serreze et al.*, 2009; *Steele et al.*, 2010; *Tivy et al.*, 2011]. Arctic Ocean contributes to the global oceanic uptake of CO_2 by about 5% to 14% in taking up from 66 to 199 TgC yr^{-1} [*Bates and Mathis*, 2009]. However, *Bates and Mathis* [2009] ignored the role of the cryosphere in the overall balance of CO_2. Indeed, sea ice is mainly considered as an impermeable barrier, impeding the gas exchanges between the ocean and the atmosphere [*Tison et al.*, 2002; *Bates and Mathis*, 2009; *Takahashi et al.*, 2009; *Papakyriakou and Miller*, 2011].

Our aims were to contribute to a better understanding of the inorganic carbon dynamics within sea ice, to describe the influence of biotic and abiotic processes in relation to sea ice physical properties and to assess the impacts in term of air-ice CO_2 fluxes.

Until now, only a few studies reported inorganic carbon dynamics within sea ice as well as CO_2 fluxes over sea ice. These studies were mainly based on TA and DIC measurements on brine and melted bulk ice samples [*Gleitz et al.*, 1995; *Papadimitriou et al.*, 2004; *Rysgaard et al.*, 2007; 2009; *Munro et al.*, 2010; *Nomura et al.*, 2010b; *Miller et al.*, 2011]. Only *Delille and co-workers* (*i.e.*, *Delille* [2006]) and *Delille et al.* [2007] reported direct measurement of brine pCO_2 within sea ice. In addition, CO_2 fluxes were only reported over spring-summer sea ice in Antarctica [*Delille*, 2006; *Zemmelink et al.*, 2006] and Arctic [*Semiletov et al.*, 2004].

To our best knowledge, no data were reported during the initial sea ice growth and during fall and winter. The sea ice growth was supposed to act as a source of CO_2 to the atmosphere since the work of *Nomura et al.* [2006] on artificial sea ice where the role

[4] Perennial ice is the ice cover that remains during minimum ice extent and consists mainly of thick multiyear ice floes [*Comiso et al.*, 2008].

of sea ice during winter was mainly suggested as nil according to the sea ice impermeability [*Golden et al.*, 2007]. Recently, a first glimpse was revealed by our survey in Barrow [*Heinesch et al.*, 2009] and by *Miller et al.* [2011] who measured an efflux of CO_2 from arctic sea ice to the atmosphere during winter. These effluxes were related with wind speed but the magnitude of the fluxes was very different, depending on the method used for the measurement (*cf.*, Ch. I.3).

In this work, we reported measurements of pCO_2 dynamics within sea ice brine and related air-ice CO_2 fluxes carried out during two arctic coastal seasonal surveys in the framework of the International Polar Year (IPY). We first reported a snapshot of the initial sea ice growth that was carried out in the framework of the project "Year round follow up of air-ice-ocean carbon dioxide exchanges for arctic sea ice: a contribution to the International Polar Year" in Barrow, Alaska. Then, we reported pCO_2 dynamics from early spring to beginning of summer during the IPY – Circumpolar Flaw Lead system study (IPY-CFL) in the Amundsen Gulf.

As part of this work, we also developed a new analytical method to measure pCO_2 on bulk sea ice sample with a vertical resolution that allow to both further investigate CO_2 dynamics and to assess pCO_2 at the air-ice interface. Indeed, similar measurement developed for continental ice using gas extraction under vacuum and at low temperature cannot be used for sea ice due to the interaction of the carbonate system [*Tison et al.*, 2002; *Verbeke*, 2005]. Hence, we developed a new method based on the equilibration techniques widely used in oceanography.

2. Summary of processes controlling sea ice inorganic carbon dynamics

In the figure V.1, we propose the following sequence of events. In late summer and fall, during the initial sea ice growth and the subsequent decrease of ice temperature, impurities are partly rejected from the sea ice and partly trapped within brine. As the temperature decreases, brines are concentrated and become supersaturated in CO_2 in respect with the atmospheric concentration [*Papadimitriou et al.*, 2004; *Delille*, 2006]. The brine expulsion could occur downwards, into the underlying sea water, causing an increase in salinity and DIC concentration [*Rysgaard et al.*, in prep.]. During the first stage of sea ice growth, when the ice is thin, young and permeable, brine could also be rejected upwards, at the sea ice interface with the atmosphere. The upward rejection of

brine may form a brine skim and/or frost flower at the sea ice surface [*Perovich and Richter-Menge*, 1994]. By increasing the surface exchange owing to dendritical structure, frost flowers formation promotes CO_2 exchanges. In the same way, brine skim and associated frost flowers continuous exchange surface with the atmosphere (rather than localized brine channel pore) promoting gas transfers. Therefore, effluxes of CO_2 to the atmosphere were observed.

Moreover, associated with the increase of brine salinity, significant changes in mineral-liquid thermodynamic equilibrium can occur and calcium carbonate can precipitate, promoting the increase of pCO_2 of brines. If this precipitation of calcium carbonate occurs in this young ice, it will promote degassing of CO_2. Such fluxes were measured on thin (20 cm, less than 1 week old) landfast sea ice in Barrow (Alaska).

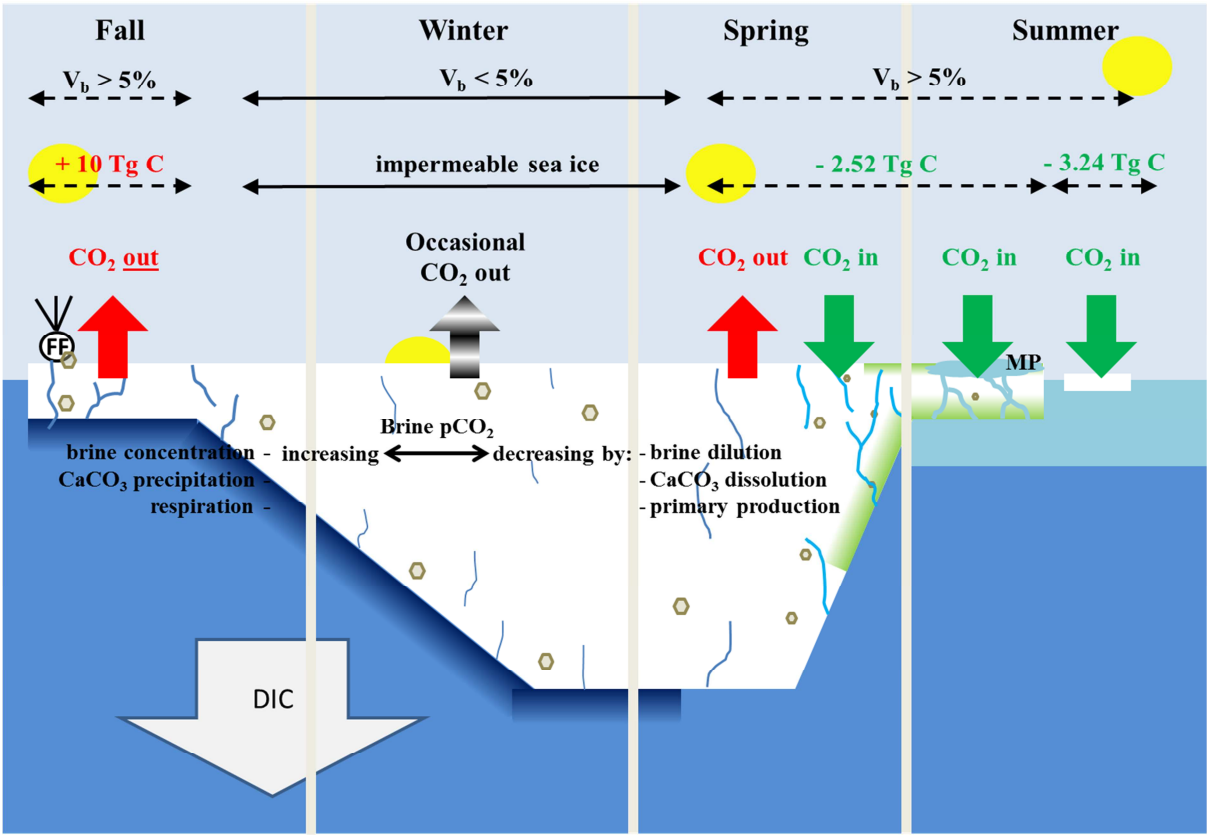

Figure V.1: Sequence of processes driving the inorganic carbon dynamics within sea ice. **FF** corresponds to frost flowers while **MP** corresponds to melt ponds. The brown diamonds represent the ikaite crystals and the green area represents sympagic communities. The red narrows are the information reported by this work.

During winter, as the air and ice temperature decrease, the brine volume of surface sea ice decreases and sea ice permeability decreases accordingly, hampering ice-atmosphere gas exchanges. In addition to the brine volume contraction and increase of brine salinity, pCO_2 increases and then precipitation of calcium carbonate can

potentially occur. This precipitation promotes high level of pCO_2 within sea ice brine. A supersaturation within brine was measured during CFL with value up to 1839 µatm (*cf.*, Ch. III). However, brine may be in contact with the atmosphere and occasionally outgassing can occur through the snowpack during high wind speed events. Wind pumping events was suggested by *Heinesch et al.* [2009], *Miller et al.* [2011] and *Papakyriakou and Miller* [2011] who observed episodic CO_2 release correlated to high wind speed events.

In early spring, as temperature rises, sea ice melts and brine volume increases, so that the ice becomes permeable [*Golden et al.*, 2007] and brine at the surface of the ice can exchange CO_2 with the atmosphere. The snowpack may control the rate of gas exchange but its influence is still poorly understood (*cf.*, Ch. III). At the beginning of the warming episodes, brine can be supersaturated in CO_2 compared to the atmosphere and CO_2 outgassing from the ice to the atmosphere can therefore occur (*cf.*, Ch. III, *Delille and co-workers, i.e., Delille* [2006]). As the summer draws near, brines are diluted by meltwater, promoting pCO_2 decreases. In addition, dissolution of calcium carbonate and primary production enhance the decrease of brine pCO_2. Thereby, a marked undersaturation was measured during CFL with value down to almost 0 µatm and influx of CO_2 from the atmosphere to the ice was measured, up to -2.6 mmol m^{-2} d^{-1} (*cf.*, Ch. III).

As the sea ice surface temperature increases, snowpack disappears and melt ponds develop. Brines are completely flushed out of sea ice and the brine channels act as conduits for meltwater migrating through to the underlying seawater. Since the meltwater is essentially fresh water, the melt ponds and the draining meltwater exhibit a low pCO_2 (*cf.*, Ch. III). The constant flushing of meltwater from ponds acts to keep pCO_2 low in the ponds as new meltwater replaces the drained water. CO_2 exchange at the interface between melt ponds and the atmosphere exhibits a net uptake of CO_2, up to -2.7 mmol m^{-2} d^{-1}.

Overall, the main factor controlling inorganic carbon dynamics within sea ice appears to be the temperature. Indeed, as the temperature decreases (or increases) the pCO_2 shift to a supersaturation (or undersaturation). Then additional processes come along, enhancing the variation of pCO_2 due to temperature change. Indeed, as observed during CFL survey, minimum of brine pCO_2 (almost 0 µatm) was observed when Chl a measurements were already low (< 1 µg L^{-1}), suggesting that other processes

contributed to the pCO_2 decrease. This idea was already suggested by *Delille and co-workers* (*i.e., Delille* [2006]).

As an additional process, the precipitation of calcium carbonate has been suggested to play a role on the inorganic carbon dynamics. During the sea ice formation, its precipitation promotes an increase of the brine pCO_2 while during the sea ice melt its dissolution promotes the decreasing of the brine pCO_2. However, we think that the role of sea ice precipitation of $CaCO_3$ as a sink for atmospheric CO_2 as suggested by *Rysgaard et al.* [2007; 2009], is not fully established.

Conditions promoting ikaite precipitation are not fully understood. Ikaite precipitates at near-freezing temperature, under alkaline conditions with elevated phosphates concentrations and/or in the presence of some additives like amino acids [*J L Bischoff et al.*, 1993a; *Whiticar and Suess*, 1998; *Buchardt et al.*, 2001; *Selleck et al.*, 2007; *Dieckmann et al.*, 2008; 2010]. Our results suggest that all these conditions were encountered during Barrow survey (*cf.*, Ch. II). Some parameters are missing for CFL where we found only indirect evidences of $CaCO_3$ precipitation in the upper part of the ice cover, within highly saline brine. According the figure V.2 who represents the different scenarios possible for calcium carbonate precipitation, an additional scenario was found as ikaite also precipitates in frost flowers and/or brine skim and in the upper layer of the ice cover. This could lead to a direct release of CO_2 to the atmosphere if this precipitation occurs within thin permeable sea ice (*cf.*, Ch. II). The indirect evidences of precipitation of calcium carbonate observed during CFL suggested that we were in the situation A during this work.

3. New analytical method

The new analytical method is based on the equilibration between an ice sample and a standard gas. It was developed and successfully applied on both artificial and natural sea ice. The precision was tested on artificial sea ice and is lower than 5%. The accuracy was successfully tested by comparing results from this method with direct *in situ* brine measurements using the sackholes techniques as reported by *Delille et al.* [2007]. However, the limitation of this method is that the sea ice has to be permeable otherwise the ice sample cannot equilibrate with the standard gas. According to *Golden et al.* [2007], the brine volume content within sea ice must be at least at 5%, which limits the use of this method to spring or summer sea ice. For impermeable sea ice (*i.e.*,

winter sea ice), the sackholes technique as used by *Delille and co-workers* (*i.e., Delille* [2006]) and *Delille et al.* [2007] as the peepers method developed by *Miller et al.* [2011] are available. Of course, indirect measurements of TA, DIC are also possible on melted bulk ice [*Rysgaard et al.*, 2007; 2009; *Munro et al.*, 2010; *Miller et al.*, 2011].

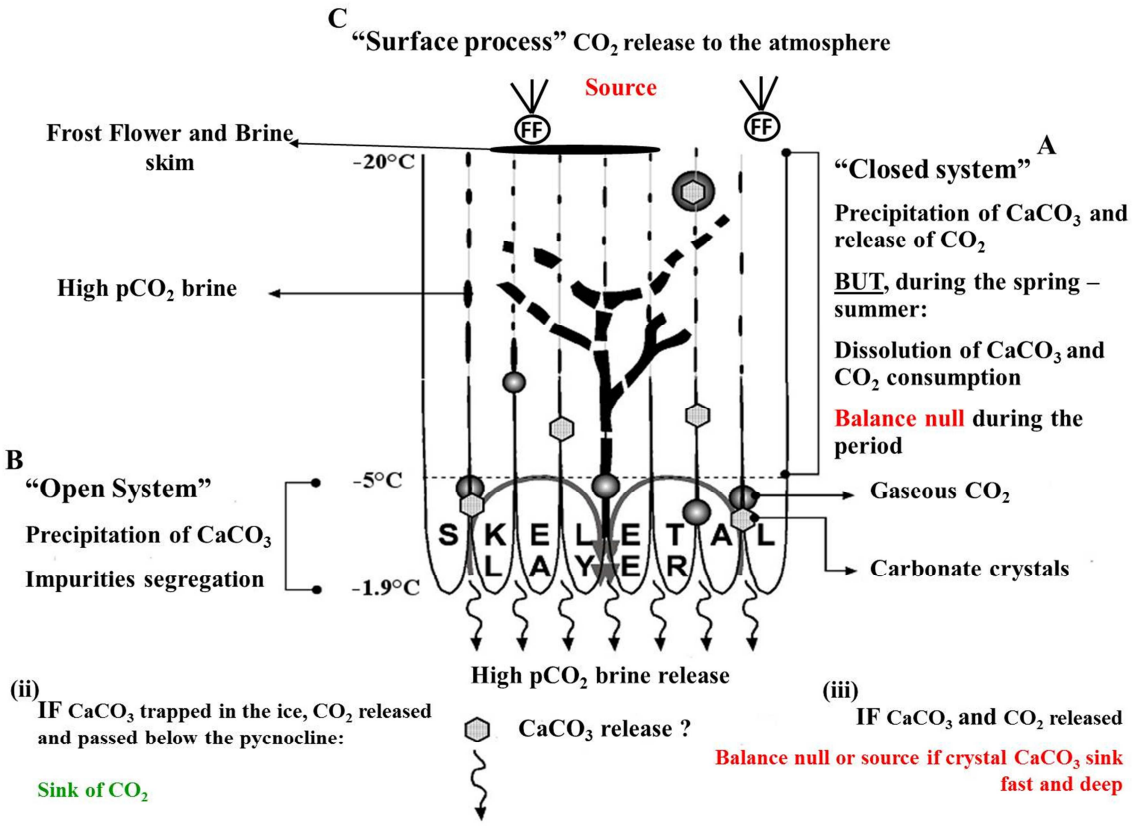

Figure V.2: Fate of carbonate minerals precipitated within sea ice, adapted from *Delille and co-workers* (*i.e., Delille* [2006]).

All of these methods have advantages and disadvantages. Process melted bulk ice sample is easy to carry out. But by melting the ice, the equilibrium of inorganic carbon within sea ice is disturbed and is not representative of the initial state. In addition, until now, the equilibrium constants of the carbonate system are still unknown for the temperature and salinity encountered within sea ice. *Miller et al.* [2011] developed a new *in situ* method based on silicone exchange chambers, the peepers. Holes are drilled into the ice cover and these peepers are frozen inside at different depth and are supposed to reach the equilibrium with their surroundings, even at low temperature. Gas samples were drawn from the peeper with a syringe and then injected into a gas chromatograph. The main issue of this technique is that we do not really know what is in equilibrium with the peeper. As the peeper is frozen into the ice we do not know if the ice surrounding the peeper equilibrates or if it is the brine, already enriched in CO_2

that frozes around the peeper. This could lead to the large supersaturation (*i.e.*, > 5000 µatm) reported by *Miller et al.* [2011] in Arctic. *Delille and co-workers* (*i.e.*, *Delille* [2006]) report pCO_2 of brines ranging from 30 µatm to 920 µatm in antarctic sea ice while we reported values ranging from 0 µatm to 1800 µatm in arctic sea ice, with the *in situ* equilibration method applied on brines extracted from sackholes. Direct *in situ* pCO_2 measurements yield values much lower than the values reported by *Miller et al.* [2011]. Direct *in situ* pCO_2 measurements have some limitations. Indeed, by drilling sackholes through the ice cover, it is not possible to track the brine origins or to collect brine from the surface layer of the ice. However, this information is crucial as the direction and the magnitude of the CO_2 fluxes are driven by the gradient of concentration between sea ice and the atmosphere [*Delille*, 2006; *Nomura et al.*, 2010b].

4. Annual cycle

Surveys carried out in the Arctic allow to derive a rough budget of the CO_2 fluxes over sea ice. The initial ice growth of the arctic sea ice leads to CO_2 release to the atmosphere. This trend was suggested by *Nomura et al.* [2006] and is confirmed by our measurement of CO_2 fluxes over a young growing thin ice in Barrow. Considering the maximal extension of arctic first year sea ice of 7.10^6 km^2 [*Dieckmann and Hellmer*, 2010] and that all the first year sea ice passe through the state of "thin ice" during 1 week, an efflux of +10 TgC was proposed (*cf.*, Ch. II).

In the chapter III, we attempted to assess the potential uptake of CO_2 by melting sea ice that equilibrates with the atmosphere. Considering the sea ice conditions (TA, DIC, S) from station F6-2, the uptake of CO_2 was estimated to 40 µmol kg^{-1} of ice. Therefore, taking into account the maximal extension of arctic first year sea ice of 7.10^6 km^2 [*Dieckmann and Hellmer*, 2010] and an average thickness of 1.06 m [*Kwok et al.*, 2009], the first year sea ice accounts for 6.7 10^{15} kg. Taking into account the uptake of CO_2 of 40 µmol kg^{-1} of ice, we assess that melting sea ice would uptake 3.24 TgC of atmospheric CO_2.

In order to complete the global budget of CO_2, we need to estimate the CO_2 fluxes from the winter to the summer. As describe in the chapter III and in the work of *Delille and co-workers* (*i.e.*, *Delille* [2006]), the CO_2 fluxes depend on sea ice temperature. For temperature below -10°C, we considered that sea ice was impermeable and we did not

account fluxes during this period. We considered this situation as the "winter situation". Then, as the ice temperature increases, a flux from the ice to the atmosphere is observed and as the brine becomes undersaturated, an uptake of CO_2 is reported. We computed the relationship between the ice temperature and the CO_2 fluxes (Fig. V.3) using measurements carried out during CFL and reported by *Nomura et al.* [2010b].

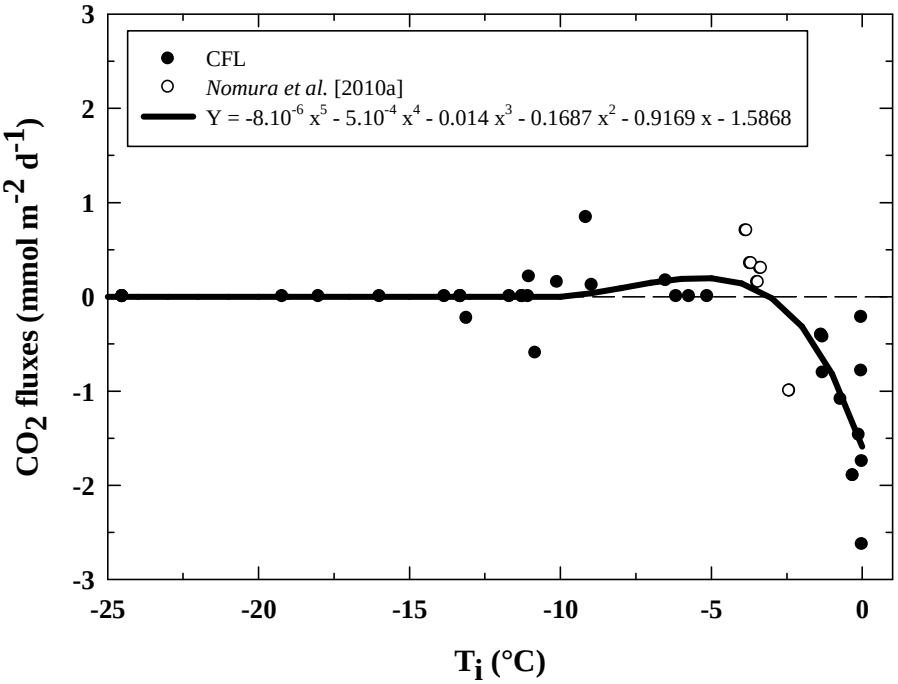

Figure V.3: Relationship between sea ice temperature and CO_2 fluxes. Black dots represents measurement from CFL (*cf.*, Ch. III) while the white dots represent measurements from *Nomura et al.* [2010b] using a chamber of accumulation in Barrow, AK.

Then, we used the sea ice temperature data recorded from the location of the Barrow Sea Ice Mass Balance (data available at http://seaice.alaska.edu/gi/data) for the years 2008 – 2009 [*Druckenmiller et al.*, 2009] to compute a mean flux on the arctic sea ice of -2.52 TgC on the all first year sea ice in the Arctic. We consider that this temperature records are representative for the all arctic sea ice.

Bates and Mathis [2009] estimated the global uptake of the Arctic Ocean from -66 to -199 TgC yr^{-1}. This estimation is consistent with the data from *Takahashi et al.* [2009] (-121 TgC yr^{-1}) (Table V.1). *Delille and co-workers* (*i.e.*, *Delille* [2006]) estimated a mean uptake of -29 TgC for the antarctic sea ice during the spring-summer. This uptake is significantly higher than the -2.5 TgC estimated for the Arctic. However, the first year sea ice cover is two times larger in Antarctica (15.5 10^6 km^2) than in Arctic (7.10^6 km^2) [*Dieckmann and Hellmer*, 2010]. In addition, as suggested in the chapter III, the brine pCO_2 appears to be higher in Arctic than in Antarctica. Then while in Antarctica

sea ice shifts rapidly from a source to a sink of atmospheric CO_2, in Arctic early release of CO_2 lasts much longer than in Antarctica. Then, CO_2 uptake at higher temperature only slightly outweighs early release and the overall uptake in Arctic is then lower than in Antarctica. Finally, we must bear in mind the large uncertainty due to the small number of measurement compared to the size of the considered area.

	Studies	**Period**	**CO_2 fluxes (TgC yr^{-1})**	
Arctic	*This work*	winter	+10	**Sea ice**
		spring – summer	-2.52	
		summer	-3.24	
		balance	+4.24	
	Bates and Mathis [2009]	annual	-66 to -199	**Water column**
	Computed from *Takahashi et al.* [2009], North of 66°N	annual	-121	
Antarctica	*Delille and co-workers* (*i.e., Delille* [2006])	spring-summer	-29	**Sea ice**

Table V.1: Estimation of the global uptake by the arctic sea ice in our study, compared to the estimation from *Bates and Mathis* [2009], calculation from data of *Takahashi et al.* [2009] and the estimation of the CO_2 uptake by antarctic sea ice from *Delille and co-workers* (*i.e., Delille* [2006]).

Robust budget of air-ice CO_2 fluxes during sea ice growth needs to address temporal and spatial variability of air-ice CO_2 fluxes. Unfortunately, due to the small number of sampling carried out on growing ice, it is not possible yet to address both spatial and temporal variability. However, air-ice CO_2 fluxes presented in the chapter II confirm that growing sea ice releases CO_2 to the atmosphere during first days of ice formation as it was suggested by laboratory work [*Nomura et al.*, 2006]. In addition, tentative budget, derived in chapter II, highlights that air-ice CO_2 fluxes can be significant and might counterbalance spring and summer uptake, so that assessment of air-ice CO_2 fluxes over growing ice is crucial to provide a robust annual budget of air-ice CO_2 fluxes.

5. Impact of sea ice changes to the overall uptake of CO_2 by the Arctic Ocean

In the context of global warming and the overall decreases of the summer arctic sea ice extent, it is crucial to determine the role of the marine cryosphere on the global budget of CO_2. This information needs to be included in models predicting the climate evolution in the next century.

Arctic Ocean uptake of atmospheric CO_2 depends of the gradient of concentration between the atmosphere and the other medium (*i.e.,* sea ice or seawater). Predicted decreases of the arctic sea ice [*Stroeve et al.,* 2007] or changes from perennial to first year sea ice will affect the overall budget of CO_2 in different ways. The reduction of the summer arctic sea ice has been associated with significant increase of ocean primary production [*Arrigo et al.,* 2008] that should drive a decrease of the pCO_2 of the arctic surface waters. However, surface water pCO_2 in the Arctic Ocean depends on several other processes, including mixing of various source waters (*i.e.,* seawater, river water, melt ice water), temperature change, air-sea gas exchange, biological CO_2 fixation and microbial recycling of organic matter [*Bates and Mathis,* 2009; *Cai et al.,* 2010]. And sea ice melting will have profound impacts on these processes.

Sea ice melt was suggested to promote phytoplanctonic bloom (*e.g., Shadwick et al.* [2011]). But as the sea ice melt is earlier, the subsequent release of ice algal communities into the water column occurred when the zooplankton abundance is relatively low. Indeed, surface waters are cold and at that time, the zooplankton growth rate is low [*Hunt Jr et al., 2002*]. Therefore, the grazing losses are reduced, increasing the export of organic matter [*Michel et al., 2006*] and the increasing primary production should keep a low pCO_2 in the mixed layer.

In addition, sea ice melting promotes stratification of the water column. This stratification may also limit the nutrient availability in the mixed layer that corollary limits the water column productivity but also ice-algal productivity [*Gradinger,* 2009*; Manes and Gradinger,* 2009]. This stratification was suggested by *Cai et al.* [2010] as a reason for higher than expected pCO_2 in surface water. Without ice cover, the wind could lead to upwelling formation and mixing of nutrient and CO_2 rich subsurface. In addition, the reduction of the arctic sea ice cover will result in higher gas exchange

rates. Assuming that gas transfer is more rapid through open water than most ice types, the increased ice free area will lead to higher gas exchange.

According to *Cai et al.* [2010], the uptake of CO_2 due to the sea ice melt in the Arctic would quickly weaken because surface-water pCO_2 will equilibrate rapidly with the atmosphere. However, the effects on climate change on the carbon cycle are less clear and need further investigations.

6. Perspectives

Our work identified some current gaps in the understanding of CO_2 dynamics within sea ice and related air-ice CO_2 fluxes. Robust assessment of the overall budget of air-ice CO_2 fluxes over sea ice is hampered by the lack of data of brine pCO_2 and CO_2 fluxes over sea ice. Improving annual assessment requires further measurements to account spatial heterogeneity, inter-seasonal and inter-annual variability. Attention must be paid to the assessment of fluxes during the first step of the sea ice growth since the magnitude of the fluxes might potentially outweigh the spring and summer atmospheric CO_2 uptake.

Understanding of air-ice CO_2 fluxes observed during the winter is also a major issue. Indeed, in our assessment of the overall CO_2 fluxes, we assumed that during the winter the fluxes are nil. By doing that, we ignored previous work from *Heinesch et al.* [2009] and *Miller et al.* [2011] who measured episodic fluxes during the arctic winter. More investigations are needed to understand how these fluxes occur while sea ice is supposed to be impermeable, according to *Golden et al.* [1998; 2007]. From this point of view, the role of the snowpack is still unknown and is probably playing a significant control on the magnitude of the fluxes observed during the winter. Moreover, the gas transport through sea ice should be further investigated as the parameterization of sea ice permeability are only defined for liquid and not gases [*Gosink et al.*, 1976; *Golden et al.*, 1998].

In addition, more investigations on biogeochemical processes within sea ice are also required as the magnitude of some processes (*e.g.*, photosynthesis, precipitation of calcium carbonate) remain uncertain. Precipitation of $CaCO_3$ has been confirmed and estimated within thin growing arctic sea ice. But more investigation is needed regarding when, where and in what conditions this precipitation occurs. Indeed, assessing the role of precipitation of $CaCO_3$ on the overall budget of CO_2 within sea ice is crucial (*cf.*,

Fig. V.2). In this work, we suggested that the air-ice CO_2 fluxes due to the $CaCO_3$ precipitation can be negligible or even a source of CO_2 for the atmosphere. This challenges previous finding of *Rysgaard et al.* [2007; 2009] who suggested that this precipitation could be a significant sink for atmospheric CO_2. But we think that our current work is not settling the question and that the role played by $CaCO_3$ precipitation as a sink or source of CO_2 for the atmosphere is still an open debate that deserves further investigation.

References

Arctic palm tree (made of whalebone plate) along the road to Point Barrow, Alaska.

Albert, M. R., A. M. Grannas, J. Bottenheim, P. B. Shepson, and F. E. Perron (2002), Processes and properties of snow-air transfer in the high Arctic with application to interstitial ozone at Alert, Canada, *Atmos. Environ.*, *36*(15-16), 2779-2787.

Alvarez-Aviles, L., W. R. Simpson, T. A. Douglas, M. Sturm, D. Perovich, and F. Domine (2008), Frost flower chemical composition during growth and its implications for aerosol production and bromine activation, *J. Geophys. Res.-Atmos.*, *113*(D21).

Anderson, L. G., E. Falck, E. P. Jones, S. Jutterstrom, and J. H. Swift (2004), Enhanced uptake of atmospheric CO_2 during freezing of seawater: A field study in Storfjorden, Svalbard, *Journal of Geophysical Research-Oceans*, *109*(C6).

Arrigo, K. R., and C. W. Sullivan (1992), The influence of salinity and temperature covariation on the photophysiological characteristics of Antarctic sea ice microalgae, *J. Phycol.*, *28*(6), 746-756.

Arrigo, K. R., and D. N. Thomas (2004), Large scale importance of sea ice biology in the Southern Ocean, *Antarctic Science*, *16*(4), 471-486.

Arrigo, K. R., and G. L. van Dijken (2004), Annual cycles of sea ice and phytoplankton in Cape Bathurst polynya, southeastern Beaufort Sea, Canadian Arctic, *Geophysical Research Letters*, *31*(L08304).

Arrigo, K. R., G. van Dijken, and S. Pabi (2008), Impact of a shrinking Arctic ice cover on marine primary production, *Geophysical Research Letters*, *35*.

Arrigo, K. R., T. Mock, and P. M. Lizotte (2010a), Primary producers and sea ice, in *Sea Ice - second edition*, edited by Wiley-Blackwell, pp. pp. 283 - 326, Oxford.

Arrigo, K. R., S. Pabi, G. L. van Dijken, and W. Maslowski (2010b), Air-sea flux of CO_2 in the Arctic Ocean, 11998-2003, *Journal of Geophysical Research*, *115*(G04024).

Assur, A. (1958), Composition of sea ice and its tensile strength, in *Arctic Sea Ice*, edited by N. A. o. S.-N. R. Concil, Easton, Maryland.

Barber, D. G., and J. M. Hanesiak (2004), Meteorological forcing of sea ice concentrations in the southern Beaufort Sea over the period 1979 to 2000, *Journal of Geophysical Research*, *109*(C06014).

Barber, D. G., M. G. Asplin, Y. Gratton, J. V. Lukovich, R. Galley, R. L. Raddatz, and D. Leitch (submitted), The International Polar Year (IPY) Circumpolar Flaw Lead (CFL) System Study: overview and the physical system, *Atmos.-Ocean*, *48*(4).

Barnola, J., D. Raynaud, A. Neftel, and H. Oeschger (1983), Comparison of CO_2 measurements by two laboratories on air from bubbles in polar ice, *Nature*, *303*(5916), 410-413.

Bates, N. R., and J. T. Mathis (2009), The Arctic Ocean marine carbon cycle: evaluation of air-sea CO_2 exchanges, ocean acidification impacts and potential feedbacks, *Biogeosciences*, *6*(11), 2433-2459.

Beaudon, E., and J. Moore (2009), Frost flower chemical signature in winter snow on Vestfonna ice cap, Nordaustlandet, Svalbard, *Cryosphere*, *3*(2), 147-154.

Bennington, K. O. (1963), Some crystal growth features of sea ice, *Journal of Glaciology*, *4*(36), 669 - 687.

Benson, B. B., and J. D. Krause (1984), The concentration and isotopic fractionation of oxygen dissolved in freshwater and seawater in equilibrium with the atmosphere, *Limnology and Oceanography*, *29*(3), 620-632.

Berelson, W. M., W. M. Balch, R. Najjar, R. A. Feely, C. Sabine, and K. Lee (2007), Relating estimates of CaCO3 production, export, and dissolution in the water column to measurements of CaCO3 rain into sediment traps and dissolution on the sea floor: A revised global carbonate budget, *Global Biogeochemical cycles*, *21*(1).

Bischoff, J. L., J. A. Fitzpatrick, and R. J. Rosenbauer (1993a), The solubility and stabilization of ikaite ($CaCO_3.6H_2O$) from 0°C to 25°C environmental and paleoclimatic implications for Thinolite Tufa, *J. Geol.*, *101*(1), 21-33.

Bischoff, J. L., S. Stine, R. J. Rosenbauer, J. A. Fitzpatrick, and T. W. Stafford (1993b), Ikaite precipitation by mixing of shoreline springs and lake water, Mono Lake, California, USA, *Geochimica Et Cosmochimica Acta*, *57*(16), 3855-3865.

Bischoff, W. D., S. K. Sharma, and F. T. Mackenzie (1985), Carbonate ion disorder in synthetic and biogenic magnesian calcites: a Raman spectral study, *American Mineralogist*, *70*, 581-589.

Bonisch, G., and P. Schlosser (1995), Deep-water formation and exchange-rates in the Greenland Norwegian Seas and the Eurasian Basin of the Arctic-Ocean derived from tracer balances, *Progress in Oceanography*, *35*(1), 29-52.

Bowman, J. S., and J. W. Deming (2010), Elevated bacterial abundance and exopolymers in saline frost flowers and implications for atmospheric chemistry and microbial dispersal, *Geophysical Research Letters*, *37*(L13501).

Buchardt, B. (2004), Ikaite geochemistry and formation of submarine tufas in Greenland, *Geochimica Et Cosmochimica Acta*, *68*(11), A348-A348.

Buchardt, B., C. Israelson, P. Seaman, and G. Stockmann (2001), Ikaite tufa towers in Ikka Fjord, southwest Greenland: Their formation by mixing of seawater and alkaline spring water, *Journal of Sedimentary Research*, *71*(1), 176-189.

Burba, G. G., D. K. McDermitt, A. Grelle, D. J. Anderson, and L. Xu (2008), Addressing the influence of instrument surface heat exchange on the measurements of CO_2 flux from open-path gas analysers, *Global Change Biology*, *14*(8), 1854-1876.

Cai, W. J., L. Q. Chen, B. S. Chen, Z. Y. Gao, S. H. Lee, J. F. Chen, D. Pierrot, K. Sullivan, Y. C. Wang, X. P. Hu, W. J. Huang, Y. H. Zhang, S. Q. Xu, A. Murata, J. M. Grebmeier, E. P. Jones, and H. S. Zhang (2010), Decrease in the CO_2 Uptake Capacity in an Ice-Free Arctic Ocean Basin, *Science*, *329*(5991), 556-559.

Carnat, G., N. X. Geilfus, B. Delille, F. Brabant, T. N. Papakyriakou, M. Vancoppenolle, R. Galley, and J. L. Tison (this issue), Year-round survey of Arctic sea ice physical properties during the CFL project, *Journal of Geophysical Research*.

Carte, A. E. (1961), Air bubbles in ice, *Proceedings of the Physical Society*, *77*(495), 757-768.

Chisholm, S. W. (2000), Oceanography: Stirring times in the Southern Ocean, *Nature*, *407*(6805), 685-687.

Comiso, J. C. (2003), Large-scale characteristics and variability of the global sea ice cover, in *Sea ice: An introduction to its physics, chemistry, biology and geology*, edited by B. Science, pp. pp. 112 - 142, London.

Comiso, J. C. (2010), Variability and trends of the global sea ice cover, in *Sea Ice, second edition*, edited by D. N. Thomas and G. S. Dieckmann, pp. 205-246, Wiley- Blackwell, Oxford.

Comiso, J. C., C. L. Parkinson, R. Gersten, and L. Stock (2008), Accelerated decline in the Arctic Sea ice cover, *Geophysical Research Letters*, *35*(1).

Copin Montégut, C. (1988), A new formula for the effect of temperature on the partial pressure of carbon dioxide in seawater, *Marine Chemistry*, *25*, 29-37.

Cox, G. F. N., and W. F. Weeks (1974), Salinity variations in sea ice, *Journal of Glaciology*, *13*(67), 109 - 120.

Cox, G. F. N., and W. F. Weeks (1975), Brine drainage and initial salt entrapment in sodium chloride ice*Rep.*, 85 pp.

Cox, G. F. N., and W. F. Weeks (1983), Equations for determining the gas and brine volumes in sea-ice samples, *Journal of Glaciology*, *29*(102), 306 - 316.

Delille, B. (2006), Inorganic carbon dynamics and air-ice-sea CO_2 fluxes in the open and coastal waters of the Southern Ocean, pp. 296 pp, Université de Liège, Liège.

Delille, B., B. Jourdain, A. V. Borges, J. L. Tison, and D. Delille (2007), Biogas (CO_2, O-2, dimethylsulfide) dynamics in spring Antarctic fast ice, *Limnology and Oceanography*, *52*(4), 1367-1379.

Deming, J. W. (2010), Sea ice bacteria and viruses, in *Sea Ice, second edition*, edited by D. N. Thomas and G. S. Dieckmann, pp. 1-22, Wiley- Blackwell, Oxford.

Dickson, A. G. (1981), An exact definition of total alkalinity and a procedure for the estimation of alkalinity and total inorganic carbon from titration data, *Deep-Sea Res. A, Oceanogr. Res. Pap.*, *28*(6A), 609-623.

Dickson, A. G. (1984), pH scales and proton-transfer reactions in saline media such as sea water, *Geochimica Et Cosmochimica Acta*, *48*, 2299-2308.

Dickson, A. G. (1990a), Standard potential of the reaction - $AgCl_{(s)}+1/2H_{2(g)}=Ag_{(s)}+HCl_{(aq)}$ and the standard acidity constant of the ion HSO_4^- in synthetic sea water from 273.15 K TO 318.15K, *J. Chem. Thermodyn.*, *22*(2), 113-127.

Dickson, A. G. (1990b), Thermodynamics of the dissociation of boric acid in synthetic seawater from 273.15 K to 318.15 K, *Deep Sea Research Part I*, *37*, 755-766.

Dickson, A. G. (1993), pH buffers for sea-water media based on the total hydrogen-ion concentration scale, *Deep-Sea Research Part I-Oceanographic Research Papers*, *40*(1), 107-118.

Dickson, A. G., and F. J. Millero (1987), A comparison of the equilibrium constants for the dissociation of carbonic acid in seawater media, *Deep Sea Research*, *I*(34), 1733-1743.

Dieckmann, G. S., and H. H. Hellmer (2010), The importance of Sea Ice: An Overview, in *Sea Ice, second edition*, edited by D. N. Thomas and G. S. Dieckmann, pp. 1-22, Wiley- Blackwell, Oxford.

Dieckmann, G. S., G. Nehrke, C. Uhlig, J. Göttlicher, S. Gerland, M. A. Granskog, and D. N. Thomas (2010), Brief communication: Ikaite ($CaCO_3.6H_2O$) discovered in Arctic sea ice, *The Cryosphere*, *4*, 227-230.

Dieckmann, G. S., G. Nehrke, S. Papadimitriou, J. Gottlicher, R. Steininger, H. Kennedy, D. Wolf-Gladrow, and D. N. Thomas (2008), Calcium carbonate as ikaite crystals in Antarctic sea ice, *Geophysical Research Letters*, *35*(8).

DOE (Ed.) (1994), *Handbook of methods for the analysis of the various parameters of the carbon dioxide system in sea water*.

Domine, F., A. S. Taillandier, and W. R. Simpson (2005), Specific surface area, density and microstructure of frost flowers, *Geophysical Research Letters*, *32*(L13502).

Druckenmiller, M. L., H. Eicken, M. A. Johnson, D. J. Pringle, and C. C. Williams (2009), Toward an integrated coastal sea-ice observatory: System components and a case study at Barrow, Alaska, *Cold Regions Science and Technology*, *56*(2-3), 61-72.

Dumont, I. (2009), Interactions between the microbial network and the organic matter in the Southern Ocean: impacts on the biological carbon pump, 202 pp, Université Libre de Bruxelles, Bruxelles.

Ehn, J. K., B. J. Hwang, R. Galley, and D. G. Barber (2007), Investigations of newly formed sea ice in the Cape Bathurst polynya: 1. Structural, physical, and optical properties, *Journal of Geophysical Research-Oceans*, *112*(C5).

Eicken, H. (1992), Salinity Profiles of Antarctic Sea Ice - Field Data and Model Results, *Journal of Geophysical Research-Oceans*, *97*(C10), 15545-15557.

Eicken, H. (2003), From the microscopic to the macroscopic to the regional scale, growth, microstrucutre and properties of sea ice, in *Sea Ice - An introduction to its physics, biology, chemistry and geology*, edited by B. Science, pp. pp. 22 - 81, London.

Eicken, H., and M. A. Lange (1989), Development and properties of sea ice in the coastal regime of the Southeastern Weddell Sea, *Journal of Geophysical Research-Oceans*, *94*(C6), 8193-8206.

Eicken, H., M. A. Lange, and G. S. Dieckmann (1991), Spatial variability of sea ice properties in the Northwestern Weddell Sea, *Journal of Geophysical Research-Oceans*, *96*(C6), 10603-10615.

Eide, L. I., and S. Martin (1975), The formation of brine drainage features in young sea ice, *Journal of Glaciology*, *14*(70), 137 - 154.

Feltham, D. L., N. Untersteiner, J. S. Wettlaufer, and M. G. Worster (2006), Sea ice is a mushy layer, *Geophysical Research Letters*, *33*(14).

Frankignoulle, M. (1988), Field-Measurements of Air Sea CO_2 Exchange, *Limnology and Oceanography*, *33*(3), 313-322.

Frankignoulle, M., and A. V. Borges (2001), Direct and indirect pCO_2 measurements in a wide range of pCO_2 and salinity values (the Scheldt estuary), *Aquatic Geochemistry*, *7*(4), 267-273.

Fransson, A., M. Chierici, and Y. Nojiri (2009), New insights into the spatial variability of the surface water carbon dioxide in varying sea ice conditions in the Arctic Ocean, *Continental Shelf Research*, *29*, 1317-1328.

Friis, K., A. Kortzinger, and D. W. R. Wallace (2003), The salinity normalization of marine inorganic carbon chemistry data, *Geophysical Research Letters*, *30*(2), 4.

Fritsen, C. H., S. F. Ackley, J. N. Kremer, and C. W. Sullivan (1998), Flood-freeze cycles and microalgal dynamics in Antarctic pack ice, in *Antarctic Sea Ice: Biological Process, Interactions, and Variability*, edited, pp. 1-21, Amer Geophysical Union, Washington.

Galley, R. J., E. Key, D. G. Barber, B. J. Hwang, and J. K. Ehn (2008), Spatial and temporal variability of sea ice in the southern Beaufort Sea and Amundsen Gulf: 1980-2004, *Journal of Geophysical Research-Oceans*, *113*(C5).

Geilfus, N. X., G. Carnat, T. N. Papakyriakou, J. L. Tison, B. Else, H. Thomas, E. H. Shadwick, and B. Delille (submitted), pCO2 dynamics and related air-ice CO2 fluxes in the Arctic coastal zone (Amundsen Gulf, Beaufort Sea).

Gibson, J. A. E., and T. W. Trull (1999), Annual cycle of fCO_2 under sea-ice and in open water in Prydz Bay, East Antarctica, *Marine Chemistry*, *66*(3-4), 187-200.

Gleitz, M., M. R. vd Loeff, D. N. Thomas, G. S. Dieckmann, and F. J. Millero (1995), Comparison of summer and winter inorganic carbon, oxygen and nutrient concentrations in Antarctic sea ice brine, *Marine Chemistry*, *51*(2), 81-91.

Glud, R. N., S. Rysgaard, and M. Kuhl (2002), A laboratory study on O-2 dynamics and photosynthesis in ice algal communities: quantification by microsensors,O-2 exchange rates, C-14 incubations and a PAM fluorometer, *Aquatic Microbial Ecology*, *27*(3), 301-311.

Golden, K. M., S. F. Ackley, and V. I. Lytle (1998), The percolation phase transition in sea ice, *Science*, *282*(5397), 2238-2241.

Golden, K. M., H. Eicken, A. L. Heaton, J. Miner, D. J. Pringle, and J. Zhu (2007), Thermal evolution of permeability and microstructure in sea ice, *Geophysical Research Letters*, *34*(16).

Gosink, T. A., J. G. Pearson, and J. J. Kelly (1976), Gas movement through sea ice, *Nature*, *263*, 41 - 42.

Gosselin, M., M. Levasseur, P. A. Wheeler, R. A. Horner, and B. C. Booth (1997), New measurements of phytoplankton and ice algal production in the Arctic Ocean, *Deep Sea Research II*, *44*(8), 1623 - 1644.

Gow, A. J., S. F. Ackley, J. W. Govoni, and W. F. Weeks (1998), Physical and structural properties of land-fast sea ice in McMurdo Sound, Antarctica, *Antarctic Research Series*, *74*, 355 - 374.

Gradinger, R. (2009), Sea-ice algae: major contributors to primary production and algal biomass in the Chukchi and Beaufort Seas during May/June 2002, *Deep-Sea Res. II, Top. Stud. Oceanogr.*, *56*(17), 1201-1212.

Gran, G. (1952), Determination of the equivalence point in potentiometric titration, *Analyst, Part II*(77), 661-671.

Grasshoff, K., M. Ehrhardt, and K. Kremling (1983), Methods of sea water analysis, *Verlag Chemie*.

Haas, C., D. N. Thomas, and J. Bareiss (2001), Surface properties and processes of perennial Antarctic sea ice in summer, *Journal of Glaciology*, *47*(159), 613-625.

Hanson, A. M. (1965), Studies of the mass budget of arctic pack-ice floes, *Journal of Glaciology*, *5*(41), 701-709.

Heinesch, B., M. Yernaux, M. Aubinet, N. X. Geilfus, T. Papakyriakou, G. Carnat, H. Eicken, J. L. Tison, and B. Delille (2009), Measuring air-ice CO_2 fluxes in the Arctic, *FluxLetter, The Newsletter of FLUXNET*, *2*(2), 9-10.

Hunt Jr, G. L., P. Stabeno, G. Walters, E. Sinclair, R. D. Brodeur, J. M. Napp, and N. A. Bond (2002), Climate change and control of the southeastern Bering Sea pelagic ecosystem, *Deep Sea Research Part II: Topical Studies in Oceanography*, *49*(26), 5821-5853.

IPCC (2007), Intergovernmental Panel on Climate Change, Fourth Assessment Report: Climate Change 2007 (AR4)*Rep.*, Geneva, Switzerland.

Jacka, T. H., and R. C. Lile (1984), Sample preparation techniques and compression apparatus for ice flow studies, *Cold Regions Science and Technology*, *8*, 235 - 240.

Jacobs, S. S., H. H. Helmer, C. S. M. Doake, A. Jenkins, and R. M. Frolich (1992), Melting of Ice Shelves and the Mass Balance of Antarctica, *Journal of Glaciology*, *38*(130), 375-387.

Jeffries, M. O., and W. F. Weeks (1992), Structural characteristics and development of sea ice in the western Ross Sea, *Antarctic Science*, *5*(1), 63-75.

Jones, E. M., D. C. E. Bakker, H. J. Venables, M. J. Whitehouse, R. E. Korb, and A. J. Watson (2010), Rapid changes in surface water carbonate chemistry during Antarctic sea ice melt, *Tellus B*, *62*(5), 621-635.

Jones, E. P., A. R. Coote, and E. M. Levy (1983), Effect of sea ice meltwater on the alkalinity of seawater, *Journal of Marine Research*, *41*, 43-52.

Junge, K., H. Eicken, and J. W. Deming (2004), Bacterial activity at-2 to-20 degrees C in Arctic wintertime sea ice, *Applied and Environmental Microbiology*, *70*(1), 550-557.

Kennedy, G. L., D. M. Hopkins, and W. J. Pickthorn (1987), Ikaite, the glendonite precursor, in estuarine sediments at Barrow, Arctic Alaska, *Geological Survey of Alaska Annual Meeting, Abstract, Programme 9*, 725.

Killawee, J. A., I. J. Fairchild, J. L. Tison, L. Janssens, and R. Lorrain (1998), Segregation of solutes and gases in experimental freezing of dilute solutions: Implications for natural glacial systems, *Geochimica Et Cosmochimica Acta*, *62*(23-24), 3637-3655.

Kortzinger, A., L. Mintrop, D. W. R. Wallace, K. M. Johnson, C. Neill, B. Tilbrook, P. Towler, H. Y. Inoue, M. Ishii, G. Shaffer, R. F. T. Saavedra, E. Ohtaki, E. Yamashita, A. Poisson, C. Brunet, B. Schauer, C. Goyet, and G. Eischeid (2000), The international at-sea intercomparison of fCO_2 systems during the R/V Meteor Cruise 36/1 in the North Atlantic Ocean, *Marine Chemistry*, *72*(2-4), 171-192.

Krembs, C., H. Eicken, K. Junge, and J. W. Deming (2002), High concentrations of exopolymeric substances in Arctic winter sea ice: implications for the polar ocean carbon cycle and cryoprotection of diatoms, *Deep-Sea Research Part I-Oceanographic Research Papers*, *49*(12), 2163-2181.

Kwok, R., G. F. Cunningham, M. Wensnahan, I. Rigor, H. J. Zwally, and D. Yi (2009), Thinning and volume loss of the Arctic Ocean sea ice cover: 2003-2008, *Journal of Geophysical Research*, *114*.

Lake, R. A., and E. L. Lewis (1970), Salt rejection by sea ice during growth, *Journal of Geophysical Research*, *75*(3), 583 - 597.

Lalande, C., A. Forest, D. G. Barber, Y. Gratton, and L. Fortier (2009), Variability in the annual cycle of vertical particulate organic carbon export on Arctic shelves: Contrasting the Laptev Sea, Northern Baffin Bay and the Beaufort Sea, *Continental Shelf Research*, *29*(17), 2157-2165.

Lange, M. A., S. F. Ackley, P. Wadhams, G. S. Dieckmann, and H. Eicken (1989), Development of sea ice in the Weddell Sea, *Annals of Glaciology*, *12*, 92-96.

Lange, M. A., P. Schlosser, S. F. Ackley, P. Wadhams, and G. S. Dieckmann (1990), O-18 Concentrations in sea ice of the Weddell Sea, Antarctica, *Journal of Glaciology*, *36*(124), 315-323.

Lee, S. H., T. E. Whitledge, and S. H. Kang (2008), Spring time production of bottom ice algae in the landfast sea ice zone at Barrow, Alaska, *Journal of Experimental Marine Biology and Ecology*, *367*(2), 204-212.

Legendre, L., S. F. Ackley, G. S. Dieckmann, B. Gulliksen, R. Horner, T. Hoshiai, I. A. Melnikov, W. S. Reeburgh, M. Spindler, and C. W. Sullivan (1992), Ecology of sea ice biota. 2 Global significance, *Polar Biol.*, *12*(3-4), 429-444.

Lepparanta, M. (1993), A review of analytical models of sea-ice growth, *Atmos.-Ocean*, *31*(1), 123-138.

Leppäranta, M., and T. Manninen (1988), The brine and gas content of sea ice with attention to low salinities and high temperatures*Rep.*, Helsinki.

Lewis, E., and D. W. R. Wallace (1998), Program Developed for CO_2 system Calculations, , in *Rep. ORNL/CDIAC-105*, edited, Carbon Dioxide Inf. Anal. Cent., Oak Ridge Natl. Lab., Oak Ridge, Tenn.

Lin, Y.-P., and P. C. Singer (2006), Inhibition of calcite precipitation by orthophosphate: Speciation and thermodynamic considerations, *Geochimica Et Cosmochimica Acta*, *70*(10), 2530-2539.

Loose, B., W. R. McGillis, P. Schlosser, D. Perovich, and T. Takahashi (2009), Effects of freezing, growth, and ice cover on gas transport processes in laboratory seawater experiments, *Geophysical Research Letters*, *36*(5), L05603.

Loose, B., P. Schlosser, D. Perovich, D. Ringelberg, D. T. Ho, T. Takahashi, J. Richter-Menge, C. M. Reynolds, W. R. McGillis, and J. L. Tison (2011), Gas diffusion through columnar laboratory sea ice: implications for mixed-layer ventilation of CO_2 in the seasonal ice zone, *Tellus B*, *63*(1), 23-39.

Luthi, D., M. Le Floch, B. Bereiter, T. Blunier, J.-M. Barnola, U. Siegenthaler, D. Raynaud, J. Jouzel, H. Fischer, K. Kawamura, and T. F. Stocker (2008), High-resolution carbon dioxide concentration record 650,000-800,000[thinsp]years before present, *Nature*, *453*(7193), 379-382.

Magen, C., G. Chaillou, S. A. Crowe, A. Mucci, B. Sundby, A. G. Gao, R. Makabe, and H. Sasaki (2010), Origin and fate of particulate organic matter in the southern Beaufort Sea - Amundsen Gulf region, Canadian Arctic, *Estuar. Coast. Shelf Sci.*, *86*(1), 31-41.

Manes, S. S., and R. Gradinger (2009), Small scale vertical gradients of Arctic ice algal photophysiological properties, *Photosynth. Res.*, *102*(1), 53-66.

Marion, G. M. (2001), Carbonate mineral solubility at low temperatures in the Na-K-Mg-Ca-H-Cl-SO_4-OH-HCO_3-CO_3-CO_2-H_2O system, *Geochimica Et Cosmochimica Acta*, *65*(12), 1883-1896.

Mathis, J. T., N. R. Bates, D. A. Hansell, and T. Babila (2009), Net community production in the northeastern Chukchi Sea, *Deep-Sea Research Part Ii-Topical Studies in Oceanography*, *56*(17), 1213-1222.

Matsuo, S., and Y. Miyake (1966), Gas composition in ice samples from Antarctica, *Journal of Geophysical Research*, *71*(22), 5235-5241.

Meese, D. A. (1989), The chemical and structural properties of sea ice in the southern Beaufort Sea, *CRREL Report*, *89*(25).

Mehrbach, C., C. H. Culberson, J. E. Hawley, and R. M. Pytkowicz (1973), Measurements of the apparent dissociation constants of carbonic acid in seawater at atmospheric pressure, *Limnology and Oceanography*, *18*, 897-907.

Michel, C., R. G. Ingram, and L. R. Harris (2006), Variability in oceanographic and ecological processes in the Canadian Arctic Archipelago, *Progress in Oceanography*, *71*(2-4), 379-401.

Miller, L., T. Papakyriakou, R. E. Collins, J. Deming, J. Ehn, R. W. Macdonald, A. Mucci, O. Owens, M. Raudsepp, and N. Sutherland (2011), Carbon Dynamics in Sea Ice: A Winter Flux Time Series, *Journal of Geophysical Research-Oceans*, *116*(C02028).

Mock, T., G. S. Dieckmann, C. Haas, A. Krell, J. L. Tison, A. L. Belem, S. Papadimitriou, and D. N. Thomas (2002), Micro-optodes in sea ice: a new approach to investigate oxygen dynamics during sea ice formation, *Aquatic Microbial Ecology*, *29*(3), 297-306.

Morin, S., G. M. Marion, R. von Glasow, D. Voisin, J. Bouchez, and J. Savarino (2008), Precipitation of salts in freezing seawater and ozone depletion events: a status report, *Atmos. Chem. Phys.*, *8*(23), 7317-7324.

Mundy, C. J., M. Gosselin, J. K. Ehn, C. Belzile, M. Poulin, E. Alou, S. Roy, H. Hop, S. Lessard, T. N. Papakyriakou, and D. G. Barber (this issue), Characteristics of two distinct high-light acclimated algal communities during advanced stages of sea ice melt, *Journal of Geophysical Research*.

Munro, D. R., R. B. Dunbar, D. A. Mucciarone, K. R. Arrigo, and M. C. Long (2010), Stable isotope composition of dissolved inorganic carbon and particulate organic carbon in sea ice from the Ross Sea, Antarctica, *Journal of Geophysical Research-Oceans*, *115*.

Nakawo, M., and N. K. Sinha (1981), Growth rate and salinity profile of first-year sea ice in the high Arctic, *Journal of Glaciology*, *27*(96), 315 - 330.

Neill, C., K. M. Johnson, E. Lewis, and D. W. R. Wallace (1997), Accurate headspace analysis of fCO2 in discrete water samples using batch equilibration, *Limnology and Oceanography*, *42*(8), 1774-1783.

Nghiem, S. V., I. G. Rigor, D. K. Perovich, P. Clemente-Colón, J. W. Weatherly, and G. Neumann (2007), Rapid reduction of Arctic perennial sea ice, *Geophysical Research Letters*, *34*.

Nicolaus, M., C. Haas, and J. Bareiss (2003), Observations of superimposed ice formation at melt-onset on fast ice on Kongsfjorden, Svalbard, *Phys. Chem. Earth*, *28*(28-32), 1241-1248.

Nicolaus, M., C. Haas, and S. Willmes (2009), Evolution of first-year and second-year snow properties on sea ice in the Weddell Sea during spring-summer transition, *J. Geophys. Res.-Atmos.*, *114*.

Niedrauer, T. M., and S. Martin (1979), An experimental study of brine drainage and convection in young sea ice, *Journal of Geophysical Research*, *84*(C3), 1176 - 1186.

Nomura, D., H. Yoshikawa-Inoue, and T. Toyota (2006), The effect of sea-ice growth on air-sea CO_2 flux in a tank experiment, *Tellus Series B-Chemical and Physical Meteorology*, *58*(5), 418-426.

Nomura, D., H. Yoshikawa-Inoue, T. Toyota, and K. Shirasawa (2010a), Effects of snow, snow-melting and re-freezing processes on air-sea ice CO_2 flux, *Journal of Glaciology*.

Nomura, D., H. Eicken, R. Gradinger, and K. Shirasawa (2010b), Rapid physically driven inversion of the air-sea ice CO_2 flux in the seasonal landfast ice off Barrow, Alaska after onset surface melt, *Continental Shelf Research*, *30*(19), 1998-2004.

Notz, D., and M. G. Worster (2008), In situ measurements of the evolution of young sea ice, *Journal of Geophysical Research-Oceans*, *113*(C3).

Notz, D., and M. G. Worster (2009), Desalination processes of sea ice revisited, *Journal of Geophysical Research*, *114*.

Oechel, W. C., G. L. Vourlitis, S. Brooks, T. L. Crawford, and E. Dumas (1998), Intercomparison among chamber, tower, and aircraft net CO_2 and energy fluxes measured during the Arctic System Science Land-Atmosphere-Ice Interactions (ARCSS-LAII) Flux Study, *J. Geophys. Res.-Atmos.*, *103*(D22), 28993-29003.

Papadimitriou, S., H. Kennedy, G. Kattner, G. S. Dieckmann, and D. N. Thomas (2004), Experimental evidence for carbonate precipitation and CO_2 degassing during sea ice formation, *Geochimica et Cosmochimica Acta*, *68*(8), 1749-1761.

Papadimitriou, S., D. N. Thomas, H. Kennedy, C. Haas, H. Kuosa, A. Krell, and G. S. Dieckmann (2007), Biogeochemical composition of natural sea ice brines from the Weddell Sea during early austral summer, *Limnology and Oceanography*, *52*(5), 1809-1823.

Papakyriakou, T., and L. Miller (2011), Springtime CO_2 exchange over seasonal sea ice in the Canadian Arctic Archipelago, *Annals of Glaciology*, *52*(57).

Parkinson, C. L., and D. J. Cavalieri (2008), Arctic sea ice variability and trends, 1979-2006, *Journal of Geophysical Research-Oceans*, *113*(C7).

Parsons, T. R., Y. Maita, and C. M. Lalli (1984), A Manual of Chemical and Biological Methods for Seawater Analysis,, 173 pp.

Pelletier, G., E. Lewis, and D. Wallace (1998), CO_2sys.xls: A calculator for the CO_2 system in seawater for microsoft Excel/VBA, edited, Olympia, WA, Washington State Departement of Ecology.

Perovich, D. K., and J. A. Richter-Menge (1994), Surface characteristics of lead ice, *Journal of Geophysical Research-Oceans*, *99*(C8), 16341-16350.

Perovich, D. K., and A. J. Gow (1996), A quantitative description of sea ice inclusions, *Journal of Geophysical Research-Oceans*, *101*(C8), 18327-18343.

Piot, M., and R. von Glasow (2008), The potential importance of frost flowers, recycling on snow, and open leads for ozone depletion events, *Atmos. Chem. Phys.*, *8*(9), 2437-2467.

Rankin, A. M., V. Auld, and E. W. Wolff (2000), Frost flowers as a source of fractionated sea salt aerosol in the polar regions, *Geophysical Research Letters*, *27*(21), 3469-3472.

Rankin, A. M., E. W. Wolff, and S. Martin (2002), Frost flowers: Implications for tropospheric chemistry and ice core interpretation, *J. Geophys. Res.-Atmos.*, *107*(D23).

Raynaud, D., R. Delmas, M. Ascencio, and M. Legrand (1982), Gas extraction from polar ice cores: a critical issue for studying the evolution of atmospheric CO_2 and ice-sheet surface elevation, *Annals of Glaciology*, *3*, 265-268.

Redfield, A. C., B. H. Ketchum, and F. A. Richards (1963), The influence of organisms on the composition of sea-water, *In: Hill, M.N. (Ed), The composition of sea-water and comparative and descriptive oceanography Wiley-Intersciences, NEw York*, 26-87.

Richardson, C. (1976), Phase relationships in sea ice as a function of temperature, *Journal of Glaciology*, *17*(77), 507-519.

Riebesell, U., D. A. Wolf-Gladrow, and V. Smetacek (1993), Carbon dioxide limitation of marine phytoplankton growth rates, *Nature*, *361*, 249-251.

Riedel, A., C. Michel, M. Gosselin, and B. LeBlanc (2008), Winter-spring dynamics in sea-ice carbon cycling in the coastal Arctic Ocean, *Journal of Marine Systems*, *74*(3-4), 918-932.

Rothrock, D. A., D. B. Percival, and M. Wensnahan (2008), The decline in arctic sea-ice thickness: Separating the spatial, annual, and interannual variability in a quarter century of submarine data, *Journal of Geophysical Research*, *113*(C05003).

Rysgaard, S., R. N. Glud, M. K. Sejr, J. Bendtsen, and P. B. Christensen (2007), Inorganic carbon transport during sea ice growth and decay: A carbon pump in polar seas, *Journal of Geophysical Research-Oceans*, *112*(C3).

Rysgaard, S., R. N. Glud, M. K. Sejr, M. E. Blicher, and H. J. Stahl (2008), Denitrification activity and oxygen dynamics in Arctic sea ice, *Polar Biol.*, *31*, 527-537.

Rysgaard, S., J. Bendtsen, L. T. Pedersen, H. Ramlov, and R. N. Glud (2009), Increased CO_2 uptake due to sea ice growth and decay in the Nordic Seas, *Journal of Geophysical Research*, *114*(C09011).

Rysgaard, S., J. Bendtsen, B. Delille, G. Dieckmann, R. N. Glud, H. Kennedy, J. Mortensen, S. Papadimitriou, D. N. Thomas, and J. L. Tison (in prep.), Sea ice drives the air-sea CO_2 exchange in the Arctic and Southern Oceans.

Sabine, C. L., R. A. Feely, N. Gruber, R. M. Key, K. Lee, J. L. Bullister, R. Wanninkhof, C. S. Wong, D. W. R. Wallace, B. Tilbrook, F. J. Millero, T. H. Peng, A. Kozyr, T. Ono, and A. F. Rios (2004), The oceanic sink for anthropogenic CO_2, *Science*, *305*(5682), 367-371.

Sander, R., J. Burrows, and L. Kaleschke (2006), Carbonate precipitation in brine - a potential trigger for tropospheric ozone depletion events, *Atmos. Chem. Phys.*, *6*, 4653-4658.

Selleck, B. W., P. F. Carr, and B. G. Jones (2007), A Review and Synthesis of Glendonites (Pseudomorphs after Ikaite) with New Data: Assessing Applicability as Recorders of Ancient Coldwater Conditions, *Journal of Sedimentary Research*, *77*(11), 980-991.

Semiletov, I. P., A. Makshtas, S. I. Akasofu, and E. L. Andreas (2004), Atmospheric CO_2 balance: The role of Arctic sea ice, *Geophysical Research Letters*, *31*(5).

Semiletov, I. P., I. Pipko, I. Repina, and N. E. Shakhova (2007), Carbonate chemistry dynamics and carbon dioxide fluxes across the atmosphere-ice-water interfaces in the Arctic Ocean: Pacific sector of the Arctic, *Journal of Marine Systems*, *66*(1-4), 204-226.

Serreze, M. C., M. M. Holland, and J. Stroeve (2007), Perspectives on the Arctic's shrinking sea ice cover, *Science*, *315*, 1533-1536.

Serreze, M. C., A. P. Barrett, J. C. Stroeve, D. N. Kindig, and M. M. Holland (2009), The emergence of surface-based Arctic amplification, *The Cryosphere*, *3*, 11-19.

Shadwick, E. H., H. Thomas, M. Chierici, B. Else, A. Fransson, C. Michel, L. A. Miller, A. Mucci, A. Niemi, T. N. Papakyriakou, and J. E. Tremblay (2011), Seasonal variability of the inorganic carbon system in the Amundsen Gulf region of the southeastern Beaufort Sea, *Limnology and Oceanography*, *56*(1), 303-322.

Shakhova, N., I. Semiletov, I. Leifer, A. Salyuk, P. Rekant, and D. Kosmach (2010), Geochemical and geophysical evidence of methane release over the East Siberian Arctic Shelf, *Journal of Geophysical Research-Oceans*, *115*.

Shcherbina, A. Y., L. D. Talley, and D. L. Rudnick (2003), Direct observations of North Pacific ventilation: Brine rejection in the Okhotsk Sea, *Science*, *302*(5652), 1952-1955.

Sigman, D. M., and E. A. Boyle (2000), Glacial/interglacial variations in atmospheric carbon dioxide, *Nature*, *407*(6806), 859-869.

Sigman, D. M., M. P. Hain, and G. H. Haug (2010), The polar ocean and glacial cycles in atmospheric CO_2 concentration, *Nature*, *466*(7302), 47-55.

Skogseth, R., P. M. Haugan, and J. Haarpaintner (2004), Ice and brine production in Storfjorden from four winters of satellite and in situ observations and modeling, *Journal of Geophysical Research-Oceans*, *109*(C10).

Song, G., H. Xie, C. Aubry, Y. Zhang, M. Gosselin, C. J. Mundy, B. Philippe, and T. N. Papakyriakou (this issue), Spatiotemporal variations of dissolved organic carbon and carbon monoxide in first-year sea ice in the western Canadian Arctic, *Journal of Geophysical Research*.

Stauffer, B., A. Neftel, H. Oeschger, and J. Schwander (Eds.) (1985), *CO_2 concentration in air extracted from Greenland ice samples*, 85-89 pp., Geophysical Monograph Washington DC.

Steele, M., J. Zhang, and W. Ermold (2010), Mechanisms of summertime upper Arctic Ocean warming and the effect on sea ice melt, *Journal of Geophysical Research-Oceans*, *115*.

Stroeve, J., M. M. Holland, W. Meier, T. Scambos, and M. Serreze (2007), Arctic sea ice decline: Faster than forecast, *Geophysical Research Letters*, *34*(9).

Takagi, K., M. Nomura, D. Ashiya, H. Takahashi, K. Sasa, Y. Fujinuma, H. Shibata, Y. Akibayashi, and T. Koike (2005), Dynamic carbon dioxide exchange through snowpack by wind-driven mass transfer in a conifer-broadleaf mixed forest in northernmost Japan, *Global Biogeochemical cycles*, *19*(2), GB2012.

Takahashi, T., J. Olafsson, J. Goddard, D. Chipman, and S. Sutherland (1993), Seasonal variation of CO_2 and nutrients in the high-latitude surface oceans: a comparative study, *Global Biogeochemical cycles*, *7*(4), 843-878.

Takahashi, T., S. C. Sutherland, C. Sweeney, A. Poisson, N. Metzl, B. Tilbrook, N. Bates, R. Wanninkhof, R. A. Feely, C. Sabine, J. Olafsson, and Y. Nojiri (2002), Global sea-air CO_2 flux based on climatological surface ocean pCO_2, and seasonal biological and temperature effects, *Deep-Sea Research Part Ii-Topical Studies in Oceanography*, *49*(9-10), 1601-1622.

Takahashi, T., S. C. Sutherland, R. Wanninkhof, C. Sweeney, R. A. Feely, D. W. Chipman, B. Hales, G. Friederich, F. Chavez, C. Sabine, A. Watson, D. C. E. Bakker, U. Schuster, N. Metzl, H. Yoshikawa-Inoue, M. Ishii, T. Midorikawa, Y. Nojiri, A. Kortzinger, T. Steinhoff, M. Hoppema, J. Olafsson, T. S. Arnarson, B. Tilbrook, T. Johannessen, A. Olsen, R. Bellerby, C. S. Wong, B. Delille, N. R. Bates, and H. J. W. de Baar (2009), Climatological mean and decadal change in surface ocean pCO_2, and net sea-air CO_2 flux over the global oceans, *Deep-Sea Research Part Ii-Topical Studies in Oceanography*, *56*(8-10), 554-577.

Thomas, D. N., and G. S. Dieckmann (2003), Sea Ice - An introduction to its physics, biology, chemistry and geology, in *Sea Ice - An introduction to its physics, biology, chemistry and geology*, edited by B. Science, London.

Thomas, D. N., and S. Papadimitriou (2003), Biogeochemistry of sea ice, in *Sea Ice - An introduction to its physics, biology, chemistry and geology*, edited by B. Science, London.

Thomas, D. N., and G. S. Dieckmann (2010), Sea Ice - An introduction to its physics, biology, chemistry and geology, in *Sea Ice - second edition*, edited by B. Science, p. 621, London.

Thomas, D. N., S. Papadimitriou, and C. Michel (2010), Biogeochemistry of sea ice, in *Sea Ice - second edition*, edited by B. Science, p. 621, London.

Thomas, D. N., G. Kattner, R. Engbrodt, V. Giannelli, H. Kennedy, C. Haas, and G. S. Dieckmann (2001), Dissolved organic matter in Antarctic sea ice, in *Annals of Glaciology, Vol 33*, edited by M. O. Jeffries and H. Eicken, pp. 297-303, Int Glaciological Soc, Cambridge.

Tison, J. L., and V. Verbeke (2001), Chlorinity/salinity distribution patterns in experimental granular sea ice, in *Annals of Glaciology, Vol 33*, edited, pp. 13-20.

Tison, J. L., C. Haas, M. M. Gowing, S. Sleewaegen, and A. Bernard (2002), Tank study of physico-chemical controls on gas content and composition during growth of young sea ice, *Journal of Glaciology*, *48*(161), 177-191.

Tison, J. L., R. Lorrain, A. Bouzette, M. Dini, A. Bondesan, and M. Stiévenard (1998), Linking landfast sea ice variability to marine ice accretion at hells gate ice shelf, Ross Sea, *Antarctic Research Series*, *74*, 375 - 407.

Tison, J. L., A. Worby, B. Delille, F. Brabant, S. Papadimitriou, D. Thomas, J. de Jong, D. Lannuzel, and C. Haas (2008), Temporal evolution of decaying summer first-year sea ice in the Western Weddell Sea, Antarctica, *Deep-Sea Research Part Ii-Topical Studies in Oceanography*, *55*(8-9), 975-987.

Tivy, A., S. E. L. Howell, B. Alt, S. McCourt, R. Chagnon, G. Crocker, T. Carrieres, and J. J. Yackel (2011), Trends and variability in summer sea ice cover in the Canadian Arctic based on the Canadian Ice Service Digital Archive, 1960-2008 and 1968-2008, *Journal of Geophysical Research*, *116*(C03007).

Tsurikov, V. L. (1979), The formation and composition of the gas content of sea ice, *Journal of Glaciology*, *22*(86), 67 - 81.

UNESCO (1978), Eight report of the joint panel on oceanographic tables and standards, *Technical papers in Marine Science*, *28*.

Untersteiner, N. (1968), Natural desalination and equilibrium salinity profile of perennial sea ice, *Journal of Geophysical Research*, *73*(4), 1251 - 1257.

Uppstrom, L. R. (1974), The boron/chlorinity ratio of deep-sea water from the Pacific Ocean, *Deep-Sea Res.*, *21*(2), 161-162.

Verbeke, V. (2005), Concentrations en gaz dans la glace de mer: développements techniques et implications environnementales, pp. 305 pp, Université Libre de Bruxelles, Bruxelles.

Wakatsuchi, M., and T. Saito (1985), On brine drainage channels of young sea ice, *Annals of Glaciology*, *6*, 200 - 202.

Wakatsuchi, M., and T. Kawamura (1987), Formation Processes of Brine Drainage Channels in Sea Ice, *Journal of Geophysical Research-Oceans*, *92*(C7), 7195-7197.

Walter, L. M., and J. S. Hanor (1979), Orthophosphate: effect on the relative stability of aragonite and magnesian calcite during early diagenesis, *Journal of Sedimentary Petrology*, *49*(3), 937-944.

Wanninkhof, R., E. Lewis, R. A. Feely, and F. J. Millero (1999), The optimal carbonate dissociation constants for determining surface water pCO_2 from alkalinity and total inorganic carbon, *Marine Chemistry*, *65*(3-4), 291-301.

Weeks, W. F. (Ed.) (2010), *On sea ice*, 664 pp., Fairbanks, Alaska.

Weeks, W. F., and S. F. Ackley (1982), *The growth, structure, and properties of sea ice.*, 117 pp., CRREL Monograph.

Weiss, R. F. (1974), Carbon dioxide in water and sea water: the solubility of a non-ideal gas, *Marine Chemistry*, *2*, 203-215.

Weiss, R. F. (1981), Determination of carbon dioxide and methane by dual catalyst flame ionization chromatography and nitrous oxide by electron capture chromatography, *Journal of Chromatographic Science*, *19*, 611-616.

Weiss, R. F., and B. A. Price (1980), Nitrous oxide solubility in water and seawater, *Marine Chemistry*, *8*, 347-359.

Wells, L. E., and J. W. Deming (2006), Modelled and measured dynamics of viruses in Arctic winter sea-ice brines, *Environ. Microbiol.*, *8*(6), 1115-1121.

Wettlaufer, J. S., M. G. Worster, and H. E. Huppert (1997), The phase evolution of young sea ice, *Geophysical Research Letters*, *24*(10), 1251-1254.

Wettlaufer, J. S., M. G. Worster, and H. E. Huppert (2000), Solidification of leads: Theory, experiment, and field observations, *Journal of Geophysical Research-Oceans*, *105*(C1), 1123-1134.

Whiticar, M. J., and E. Suess (1998), The cold carbonate connection between Mono Lake, California and the Bransfield Strait, Antarctica, *Aquatic Geochemistry*, *4*(3-4), 429-454.

Wiesenburg, D. A., and N. L. Guinasso Jr. (1979), Equilibrium solubility of methane, carbon monoxide and hydrogen in water and seawater, *Journal of Chemical and Engineering data*, *24*(4), 356-360.

Wolf-Gladrow, D., and U. Riebesell (1997), Diffusion and reactions in the vicinity of plankton: A refined model for inorganic carbon transport, *Marine Chemistry*, *59*, 17-34.

WorldMeteorologyOrganization (1985), WMO sea-ice nomenclature, terminology, codes and illustrated glossary, in *WMO/DMM/BMO*, edited by 259-TP-145, Secretariat of the World Meteorol. Org., Geneva.

Zeebe R.E., and D. Wolf-Gladrow (2001), CO_2 in seawater: Equilibrium, Kinetics, Isotopes, *Elsevier*.

Zemmelink, H. J., B. Delille, J. L. Tison, E. J. Hintsa, L. Houghton, and J. W. H. Dacey (2006), CO_2 deposition over the multi-year ice of the western Weddell Sea, *Geophysical Research Letters*, *33*(13).

List of publications

CO_2 fluxes measurements over sea ice (using chamber of accumulation), CCGS Amundsen in the background

1. Publications

- **Geilfus, N.-X.**, Carnat, G., Dieckmann, G.S., Halden, N., Nehrke, G., Papakyriakou, T.N., Tison, J.-L. and Delille, B., *First estimates of the contribution of $CaCO_3$ precipitation to the release of CO_2 to the atmosphere during young sea ice growth*, submitted (January, 2011) to the Journal of Geophysical Research, Oceans.
- **Geilfus, N.-X.**, Carnat, G., Papakyriakou, T.N., Tison, J.-L., Else, B., Thomas H., Shadwick E. and Delille, B., *pCO_2 dynamic and related air-ice CO_2 fluxes in the arctic coastal zone (Amundsen Gulf, Beaufort Sea)*, submitted (March, 2011) to the Journal of Geophysical Research, Oceans, in the special issue IPYCFLEXP1-The IPY Circumpolar Flaw Lead and Arctic SOLAS Experiments: Oceanography, Geophysics and Biogeochemistry of the Amundsen Gulf and Southern Beaufort Sea.
- **Geilfus, N.-X.**, Delille, B., Verbeke, V. and Tison, J.-L., *Towards a method for high resolution measurements of the partial pressure of CO_2 within bulk sea ice*, submitted (April, 2011) to the Journal of Glaciology.
- Carnat, C., **Geilfus, N.-X.**, Delille, B., Brabant, F., Papakyriakou, T.N., Vancoppenolle, M. and Tison, J.-L., *Year-round survey of arctic sea ice physical and structural properties during the CFL project*, in preparation for the special issue IPYCFLEXP1-The IPY Circumpolar Flaw Lead and Arctic SOLAS Experiments: Oceanography, Geophysics and Biogeochemistry of the Amundsen Gulf and Southern Beaufort Sea, deadline May 31, 2011.

2. Others

- Heinesch, B., Yernaux, M., Aubinet, M., **Geilfus, N.-X.**, Papakyriakou, T.N., Carnat, G., Eicken, H., Tison, J.-L. and Delille, B. (2009), Measuring air-ice CO_2 fluxes in the Arctic, *FluxLetter*, *The Newsletter of FLUXNET*, *2*(2), 9-10. *See Annexe*

  Other several papers related to Barrow, CFL and other Antarctic surveys are currently in preparation but not advanced enough to be included in this list.

Annexe

Barrow, Top of the World!

Measuring air-ice CO_2 fluxes in the Arctic

Heinesch B, Yernaux M, Aubinet M, Geilfus N-X, Papakyriakou T, Carnat G, Eicken H, Tison J-L, B.Delille

Sea ice covers about 7% of Earth's surface at its maximum seasonal extent, representing one of the largest biomes on the planet. For decades, sea ice has been considered by the scientific community and biogeochemical modellers involved in assessing oceanic CO_2 uptake as an inert and impermeable barrier to air-sea exchange of gases. However, this assumption is not supported by studies of the permeability of ice to gases and liquids, which show that sea ice is permeable at temperatures above -10°C. Recently, uptake of atmospheric CO2 over sea-ice cover has been reported (Delille et al., 2007; Semiletov et al., 2004; Zemmelink et al., 2006) supporting the need to further investigate pCO_2 dynamics in the sea-ice realm and related CO_2 fluxes. The processes by which the CO_2 exchange between the ocean and the atmosphere can take place are the following. While CO_2-enriched brines are expelled from the ice, carbonate minerals could remain trapped in the brine tubes and channels until spring and summer, when they would dissolve within the sea ice or in the underlying water. Such dissolution consumes CO_2 and therefore acts as a sink for atmospheric CO_2. Other processes can potentially act as sinks of CO_2. First, sea ice hosts algae communities, which imply primary production. Second, during sea-ice growth, most of the impurities (solutes, gases,

Figure 1: Set up of the mast with sonic anemometer, air intake of the CO_2 analyser and radiometer over sea ice near Barrow (Alaska) in January 2009. The temperature was -35°C.

cont. on page 10

Measuring air-ice CO_2 fluxes in the Arctic

cont. from page 9

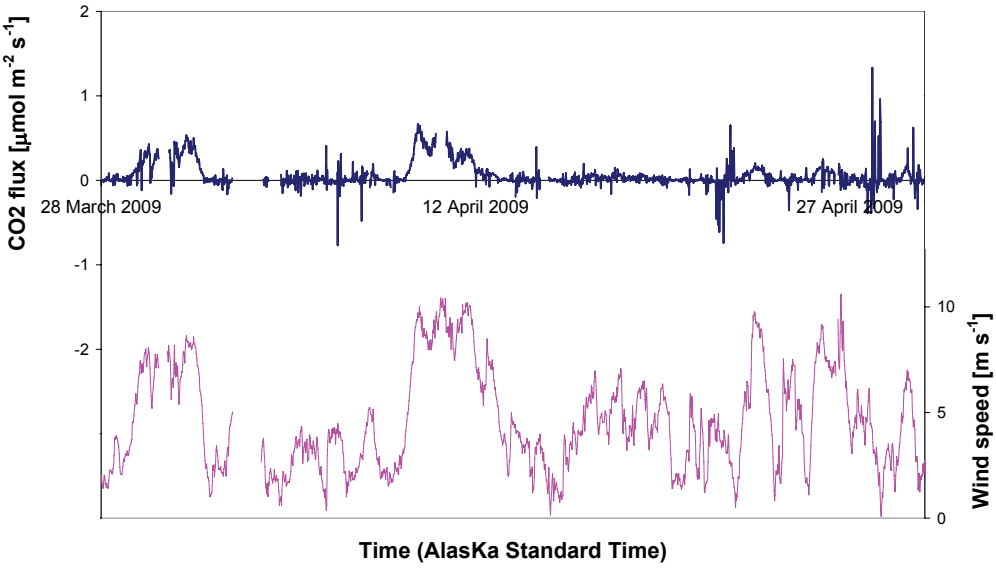

Figure 2 : CO_2 flux and wind speed in April 2009 over sea-ice in Barrow (Alaska).

particulate matter) are expelled from the pure ice crystals at the ice-water interface. The CO_2 rejected into the boundary layer will either diffuse or be convectively driven downward into the underlying water, removing CO_2 from the surface water. During spring, melting of CO_2-depleted sea ice would decrease pCO_2 of surface waters. Such a mechanism would act as a sink for atmospheric CO_2. On the whole, spring sea ice appears to act as a CO2 sink that may be significant in the budget of CO_2 fluxes in the Polar Oceans (Delille et al., 2007; Zemmelink et al., 2006). However, previous studies are sparse, and limited in term of spatial and temporal coverage.

In January 2009, we started a study that aims to robustly follow up CO_2 exchange between land fast sea-ice and the atmosphere during the winter and spring season. To this aim, a meteorological mast equipped for eddy-covariance measurements was installed on landfast sea-ice near Barrow (Alaska), 1 km off the coast, from end of January 2009 to beginning of June 2009, before ice break-up. There is some concerns about using open-path analyzer in cold environment (Burba et al., 2008) so the mast was equipped with a CO_2 closed-path analyser together with a C-SAT 3D sonic anemometer. These data were supported by continuous measure of solar radiation, snow depth, ice thickness and temperature profile in the ice. Biogeochemical data necessary for the understanding of the CO_2 dynamics in sea-ice were obtained through regular ice coring.

First results coming from this campaign show that the resolution of the eddy-covariance technique in these conditions is high enough to measure CO_2 fluxes that are typically below 1 mmol m^{-2} s^{-1}. Despite low temperature at the ice-snow interface (-14°C), we observe in April some effluxes from the ice to the atmosphere (see figure 2). This is consistent with the CO_2 oversaturation of sea-ice brines observed at the site. The fluxes are triggered by wind speed over 7 m s^{-1} suggesting that wind pumping trough the snow (snow thickness was about 20 cm) is one of the main process controlling the air-ice fluxes at that time.

As the sea ice is warming up, the partial pressure of sea ice brines is expected to decrease significantly and to pass the threshold of saturation. Sea ice would then shift from a source to a sink for atmospheric CO_2. In addition, increase of temperature will increase the permeability of sea ice, promoting the increase of the magnitude of fluxes. The system deployed in Barrow should allow us to follow these processes and to budget the net CO_2 transfer from the atmosphere to the ice over winter and spring.

This project is supported by the Fonds de la Recherche Scientifique, the National Science Foundation and the University of Alaska Fairbanks. We are indebted to the Barrow Arctic Science Consortium and the North Slope Borough for their logistical support.

contact:
Bernard Heinesch
Heinesch.b@fsagx.ac.be

References

Burba, G.G., McDermitt, D.K., Grelle, A., Anderson, D.J. and Xu, L.K., 2008. Addressing the influence of instrument surface heat exchange on the measurements of CO2 flux from open-path gas analyzers. Global Change Biology, 14(8): 1854-1876.

Delille, B., Jourdain, B., Borges, A.V., Tison, J.L. and Delille, D., 2007. Biogas (CO2, O-2, dimethylsulfide) dynamics in spring Antarctic fast ice. Limnology and Oceanography, 52(4): 1367-1379.

Semiletov, I., Makshtas, A., Akasofu, S.I. and Andreas, E.L., 2004. Atmospheric CO2 balance: The role of Arctic sea ice - art. no. L05121. Geophysical Research Letters, 31(5): 5121-5121.

Zemmelink, H.J. et al., 2006. CO2 deposition over the multi-year ice of the western Weddell Sea - art. no. L13606. Geophysical Research Letters, 33(13): 13606-13606.

Inorganic carbon dynamics in coastal arctic sea ice and related air-ice CO_2 exchanges

Arctic Ocean contributes to the global oceanic uptake of CO_2 by about 5% to 14% in taking up from 66 to 199 TgC yr^{-1}. However, the role of the marine cryosphere was ignored because it is considered as an impermeable barrier, impeding the gas exchanges between the ocean and the atmosphere [*Bates and Mathis*, 2009]. However, a growing body of evidence suggests that gases exchange could occur between sea ice and the atmosphere. In this context, two arctic surveys were carried out in the framework of the International Polar Year (IPY). From there, we present a snapshot of the partial pressure of CO_2 (pCO_2) dynamics firstly during the initial sea ice growth and secondly from early spring to the beginning of the summer.

We confirmed previous laboratory measurement findings that growing young sea ice acts as a source of CO_2 to the atmosphere by measuring CO_2 efflux from the ice (4 to 10 mmol m^{-2} d^{-1}). We also confirmed the precipitation of calcium carbonate as ikaite in the frost flowers and throughout the ice and its negligible role on the effluxes of CO_2. In early spring, supersaturations in CO_2 (up to 1834 µatm) were observed in sea ice as consequence of concentration of solutes in brines, $CaCO_3$ precipitation and microbial respiration. As the summer draw near, brine shifts to a marked undersaturation (down to almost 0 µatm) because of the brine dilution by ice meltwater, dissolution of $CaCO_3$ and photosynthesis during the sympagic algal bloom. Out of the winter, soon as the ice becomes permeable, CO_2 fluxes were observed: (i) from the ice to the atmosphere, as the brine were supersaturated, (ii) from the atmosphere to the ice, as brine shift to an undersaturation. Temperature appears to be the main driver of the pCO_2 dynamics within sea ice. It mainly controls the saturation state of the brine (where others processes may be added, *e.g.*, $CaCO_3$ precipitation, primary production) and thus, the concentration gradient of CO_2 between sea ice and the atmosphere. It also controls the brine volume and so the brine connectivity, allowing the gas exchanges between sea ice and the atmosphere.

We also present a new analytical method to measure the pCO_2 of the bulk sea ice. This method, based on equilibration between an ice sample and a standard gas, was successfully applied on both artificial and natural sea ice. However, this method is only applicable for permeable sea ice (*i.e.*, brine volume > 5% [*Golden et al.*, 1998; 2007]) to allow the equilibration between the ice and the standard gas.